Use of Novel Distributed Instrumentation in Ionospheric Research

Lo, Sam

Award date:
2022

Awarding institution:
University of Bath

Use of Novel Distributed Instrumentation for Ionospheric Research

submitted by

Yui Sum Sam Lo

for the degree of Doctor of Philosophy

of the

University of Bath

Department of Electronic and Electrical Engineering

June 2021

Acknowledgements

I would like to express my deepest gratitude to Prof Cathryn Mitchell for her expertise and her invaluable support in supervising my PhD studies. Similarly, I would like to acknowledge her decision making on refining the details of my research area and strengthening my interest in developing my research career. Her insightful suggestions on developing my research skills cannot be underestimated. In addition, I would also like to acknowledge her profound belief in my work and in my abilities to finish the thesis and the research. This thesis would not be successful without her invaluable contributions and guidance.

I am extremely grateful to Dr Talini Pinto Jayawardena for the academic support with her technical knowledge and precise assistance in analysing the results. She was instrumental in developing and refining my discussion opinions.

I would like to extend my gratitude to Dr Ben Witvliet for his academic support and his expertise in building the radio equipment and antenna. He was instrumental in developing and refining my research methods.

Thanks also to Dr Nikola Rankov for his numerous discussions on the research.

Finally, I gratefully acknowledge the effort of my family and friends for their personal support and their entertainment to encourage me to finish my thesis, especially during the pandemic period, as the thesis would not be possible without them.

I would like to acknowledge the radio amateurs ('HamSci') for providing the WSPR radio communications and their hard work and dedication to the atmospheric and ionospheric radio propagation field. This research would not have been successful without their data and shared experience.

Special thanks to Dr Manuel Cervera (manuel.cervera@dsto.defence.gov.au) for his permission on using his ray-tracing toolbox (PHaRLAP) to carry on my research. This toolbox is available by request from its author.

Finally, many thanks to Prof Dieter Bilitza (dbilitza@gmu.edu) for developing the International Ionosphere Reference Model (IRI2016).

Abstract

In recent years, a new globally distributed data source has become available using software radio. These new, configurable devices have been adopted by many radio amateurs across the world and provide a rich source of radio propagation information that can be used in scientific research.

Long-distance HF radio communication links can show clustering around the terminator times from a phenomenon known as greyline propagation. The reason for this sunrise/sunset propagation poses a long-standing research question. Interest in greyline propagation has lasted for over a century but it has mainly been reported on in recent years by the amateur radio community. These reports have included records of long-distance communications between, for example, the UK and New Zealand, often being made in the UK early morning close to sunrise. Such reports provided a motivation to look to see whether the statistical evidence from the Weak Signal Propagation Reporter (WSPR) network supported these reports.

The WSPR network data contains a range of discrete radio frequencies. For this research 7 MHz was chosen because it propagates well during the lower periods of the sunspot cycle and is also a popular choice for WSPR equipment across the world. The year 2017 was chosen which was the most recent full year of data at the start of the research.

The results show that HF communication links at 7 MHz show clustering around the terminator times throughout most of the year for communication between Europe and Australia/New Zealand. They also show that between the regions of Europe and the USA there is a preference for night-time propagation when the absorption of the signals is lower. This is also shown for the links between the USA and Australia/New Zealand regions. A surprising additional result emerged from the study where directional asymmetry was found during the European summer sunset time for radio links between Europe and Australia/New Zealand.

Possible explanations for the results were explored using the simulation tool PHaRLAP (Provision of High-Frequency Raytracing Laboratory for Propagation) with the IRI2016 (International Referenced Ionosphere 2016) model. Some of the temporal propagation patterns were explained by night-time propagation paths, but the directional asymmetry during the European summer sunset time was not explained. Further investigation of the directional asymmetry can be supported in the future through enhancements to the observational capabilities of the WSPR network and other additional instrumentation. These enhancements include HF noise observations and angle-of-arrival and polarisation discrimination capabilities.

Amateur radio instrumentation can provide useful information about HF radio propagation. This research project should encourage further use of amateur radio observations for ionospheric radio research.

Table of Contents

List of Figures

List of Tables

List of Equations

List of Abbreviations

AUS	Australia
CSV	Comma Separated Value
EM	Electromagnetic
EUV	Extreme Ultraviolet
FSK	Frequency Shift Keying
GCP	Great Circle Path
HF	High-Frequency
IGRF	International Geomagnetic Reference Field
IRI	International Reference Ionosphere
ITADR	Italy and the Adjacent Regions?
ITU	International Telecommunication Union
LF	Low Frequency
MUF	Maximum Usable Frequency
NZ	New Zealand
OfCom	Office of Communications
PHaRLAP	Provision of High-Frequency Raytracing Laboratory for Propagation
PSK	Phase Shift Keying

RF	Radio Frequency
RTW	Round-The-World
SAA	South Atlantic Anomaly
SDR	Software-Defined Radio
SNR	Signal-to-Noise Ratio
TEC	Total Electron Content
TEP	Trans-Equatorial Propagation
TIR	Total Internal Reflection
UK	United Kingdom
USA	United States of America
UTC	Coordinated Universal Time
VHF	Very High Frequency
WMM	World Magnetic Model
WSPR	Weak Signal Propagation Report

List of Symbols

q_e	Ion production rate
L_e	Recombination loss rate
$div(Nv)$	Transport of electrons
N	Electron density
t	Time
hv	Solar radiation
q_{m0}	Maximum production rate
z	Reduced height
χ	Solar zenith angle
h	Height of production rate
h_{m0}	Height of maximum production rate
H	Scale height
α	Recombination coefficient of α-Chapman layer
N_{m0}	Maximum plasma density
β	Recombination coefficient of β-Chapman layer
ε_0	Permittivity of free space
e	Charge of electron
m	Electron mass
f_p	Plasma frequency
f_c	Critical frequency
I	Inclination angle

Bz	Vertical component of Earth's magnetic field
D	Declination angle
X	Plasma frequency ratio
Y_T	The effect of transverse component of the magnetic field
Y_L	The effect of longitudinal component of the magnetic field
Z	Effect of electron collision on signal propagation
Y	Total magnetic field
ω	angular plasma frequency
μ	Real component of the complex refractive index
K	Imaginary refractive component of the complex refractive index
B	Magnetic flux density
v	Collision frequency
ω_N	Angular plasma frequency
n	Complex refractive index
E_o	Original signal strength
E	Signal strength
κ	Absorption coefficient
L_a	Power loss due to absorption
c	Speed of light
ω_L	Gyrofrequency
μ'	Group refractive index
θ	Incident angle
φ	Elevation angle
$L\ (m)$	Length of antenna

f	Radio Frequency (Hz)
L_t	Transmission loss
θ_c	Critical angle
e^-	Free electrons
P_n	Noise Power
P_t	Transmitter power

1. Introduction

The ionosphere is a stratified atmospheric layer containing a plasma of ions and free electrons. It is formed from the ionisation of the neutral atmosphere by solar radiation and is situated between approximately 60 km to over 800 km from the Earth's surface.

The ionosphere is dynamic, and the plasma density is influenced by solar radiation, particularly by extra-ultraviolet radiation (EUV), which is variable with diurnal, seasonal cycles, solar activity and geographic and geomagnetic locations. The photo-ionisation process starts with the solar radiation interacting with the neutral atmosphere causing the neutral atoms to release free electrons into the neutral atmosphere. As a result, the neutral atoms themselves are ionised and this creates a region in the upper atmosphere, which is known as the ionosphere. The ionised atoms and the free electrons in the ionosphere generate an ionospheric plasma, which is a medium consisting of an approximately equal number of ionised atoms and free electrons. The density of the plasma is influenced by the number of ionised atoms and free electrons in the ionosphere, and therefore, its density is called plasma density. The plasma density in the ionosphere is mainly influenced by solar radiation, which is related to the solar position in different seasons. The plasma density increases when solar radiation intensity increases, which excites the ionisation in the ionospheric layer. Similarly, the plasma density decreases when solar radiation diminishes during the night. This causes the ionosphere to have a day and night ionosphere, which has distinct differences.

In the high-latitude regions of the Earth the ionosphere is closely driven by the solar wind and the magnetosphere. This region is often subdivided into the auroral ionosphere and the polar cap ionosphere. In these regions, the ionosphere is governed by the solar drivers, such as the interplanetary magnetic field and the solar wind. Ionisation can be from solar photons but also from impact ionisation from incoming particles.

The ionosphere acts as a dispersive medium for radio signals that propagate through it. This dispersive medium is influenced by multiple parameters, such as the plasma density, the radio frequency and the magnetic field (Appleton, 1925). An important property of the ionosphere for high-frequency radio waves (HF, 3-30 MHz) is the refractive index.

A radio wave transmitted from the ground may be refracted from the ionosphere back down to the Earth’s ground surface. The ionospheric variations, such as geomagnetic variations, generate an uneven plasma density distribution across the world. These variations will govern when and where over-the-horizon propagation occurs and causes effects on the propagating radio signals, such as absorption. Therefore, the ionosphere and its behaviour are important to radio communications because they can either help or hinder HF propagation. For this reason, understanding the ionospheric interaction with HF signals is useful to radio users.

HF propagation is a form of radio propagation that often uses the ionosphere as a 'reflector' to refract the signals and allow communication over long distances. HF signals have wavelengths approximately between 10 m and 100 m and a frequency range approximately between 3 MHz and 30 MHz. HF propagation also allows the signals to be reflected from the ionosphere multiple times, which is known as multiple hop propagation (McNamara, 1991). As a result, it enhances long-distance communications.

There are many properties of HF propagation that make it useful for radio communications between radio stations for military, commercial and recreational purposes. Examples of applications are recreational communications between radio amateurs, aviation-to-ground communications and emergency services in remote locations. Therefore, it is critical to study and understand the effects of the ionosphere on HF propagation.

A method that is used by radio amateurs to communicate using HF uses a digital protocol called Weak Signal Propagation Reporter (WSPR). It is a protocol that was established by Prof Joe Taylor at Princeton University (Taylor, 2019) and was designed to communicate using weak radio signals through keying encoded messages. It allows radio amateurs to record links propagating at different radio frequencies between known locations through the WSPR database.

The data source from WSPR includes information about the radio signals, such as the location, time, operating frequency, signal-to-noise at reception and the signal strength from the transmitter. It identifies the established links made between users and gives information about the radio signal. It is straightforward to set up, only requiring the protocol, a computer, an antenna and radio equipment. WSPR is used by many radio amateurs worldwide, resulting in a global network whose locations can be easily identified from the comprehensive database maintained by the Maidenhead Grid Locator System, which can be converted to geographic coordinates. In addition, the radio amateurs can identify themselves with an identification marker known as the radio callsigns. The identification process is simple because the radio amateurs' callsigns follow the International Telecommunications Union (ITU) format, therefore, radio amateurs can identify themselves through their callsigns in the WSPR database. This makes WSPR an ideal source to observe HF propagation between radio stations around the world.

The availability of the radio stations makes the WSPR database a rich source of data that can be used to study HF propagation in the ionosphere. The objective of using HF propagation is to investigate the effects of ionisation on HF radio propagation. WSPR provides sufficient data to observe the time propagation patterns of HF radio signals by analysing the radio links recorded in the WSPR database. However, care must be taken in processing the data because it is a global network run on a volunteer basis and is not overseen at the equipment end by scientific researchers.

The research presented in this thesis uses recent data from the WSPR database to investigate HF propagation. There have been increasing scientific studies using radio amateur observations for systematic scientific research, which have been encouraged through HamSci (HamSCI), a group of scientists and radio amateurs bringing together scientific research and radio amateur activities. In recent years, with the proliferation of

low-cost equipment and automation of data collection using systems like WSPR, this opportunity has increased (Frissell *et al.*, 2014, 2019). This research project is therefore starting during a new phase in ionospheric research where the utilisation of a different type of instrumentation can be explored for the betterment of the ionospheric scientific community and radio users.

The research in this thesis focuses on one sub-element of the WSPR data – the year 2017 and the frequency of 7 MHz. The year was chosen due to the volume of data available at the start of the research. The frequency of 7 MHz is a popular choice and propagates well at long distances at the time under consideration – just past the solar minimum in the solar cycle.

There are of course advantages and disadvantages to using WSPR data and care must be taken. There are possible errors in the information that is input by the users, such as transmitter location, power and callsign. The same problems could arise on the receiver side. To mitigate this, multiple observations between different sites are used in aggregate to infer information from the database. The strength of WSPR is that there are many more instruments and observations than would be cost-effective to set up for a scientific experiment and the long duration of records. This means that the quantity of observations and the wealth of information they hold is unprecedented for the ionospheric community and therefore, should be used.

It is anticipated that the results from the analysis of this data will help inform radio hobbyists (known as radio amateurs) as well as professional scientists and engineers about HF propagation characteristics and patterns. In addition to being beneficial to HF communications, the study of WSPR data is expected to contribute to the field of ionospheric science. This is because HF propagation characteristics are strongly dependent on the electron density in the ionosphere that has daily, monthly, and yearly variation cycles, and which will inherently transform into different preferential times in the day, month and year. Therefore, this allows the investigation of the effect of ionospheric dynamics on radio communications, and consequently aid ionospheric research.

The structure of the thesis is as follows:

Chapter 2 introduces the ionosphere to explain its structure and application to radio propagation. Chapter 3 introduces the WSPR database and how data is extracted and processed for this thesis. It also outlines the complexities, strengths and weaknesses of the WSPR data source and suggests a method to approach these challenges. In addition to the WSPR data, Chapter 3 also introduces Provision of High-frequency Raytracing Laboratory for Propagation studies (PHaRLaP) – the ray-tracing software for HF signals that can simulate propagation paths based on locations, ionospheric conditions and time of day. The ray-tracing software PHaRLAP is used to analyse the results shown in WSPR through observing the effects of ionisation on the propagation paths using the ionospheric model IRI2016 (Bilitza *et al.*, 2017).

Chapter 4 presents the results of HF propagation data recorded in the WSPR database, particularly radio propagation between NZ and the UK at 7 MHz in the year 2017.

The objective of Chapter 5 is to see if there is any evidence of local noise affecting the propagation link patterns. The WSPR data contains the transmitter power and the signal-to-noise at reception, and these are investigated.

The objective of Chapter 6 is to observe whether the propagation predictions from PHaRLAP with the IRI2016 correlate with the observations made in WSPR, in order to try to explain the time propagation pattern and the asymmetry in successful propagation links found in Chapter 4.

Chapter 7 provides a discussion of the results from the previous chapters, in particular the results, seen in the comparison between WSPR and PHaRLAP.

Chapter 8 concludes the thesis and proposes further work to investigate HF propagation using amateur radio signals.

2. Literature Review

2.1. Introduction

The ionosphere, an ionised layer in the upper atmosphere, acts as a dispersive medium for electromagnetic signals that propagate the region. This means that the refractive index of the ionosphere is dependent on the frequency of the signal. Furthermore, the refractive index of the ionosphere is also a function of the electron density in the region, which varies in both space and time. The refractive index impacts the path and direction of a propagating electromagnetic signal as it causes the signal to refract as it travels through different plasma densities in the ionosphere. In addition to refraction, the ionosphere also has other effects on the signal, such as absorption, scattering, Faraday rotation and scintillation. These effects can distort the radio signal, which can result in an unexpected loss of radio communications over a given time or location.

The propagation range of High Frequency (HF) signals can be affected by the ionospheric density in the propagation path. As a result, understanding the interaction of the ionosphere with HF signals is essential to radio users, as they can use this knowledge to transmit and receive HF signals at appropriate time with an appropriate signal strength. In addition, analysing HF propagation can produce beneficial knowledge for ionospheric research that can advance the field of ionospheric science.

This literature review chapter explores the theory of the ionosphere, its impact on HF propagation and its application in HF radio communications. Section 2.2 describes the ionosphere. HF propagation is addressed in Section 2.3 followed by ionospheric radio links, described in Section 2.4. The chapter is concluded with a summary of the literature review in Section 2.5.

2.2. The Ionosphere

This section discusses the structure and morphology of the ionosphere.

The ionosphere refers to the ionised layers in the upper atmosphere between approximately 60 km to over 800 km from the Earth's surface (Gilmor, 1976; McNamara, 1991). The main source of ionisation in the region is solar radiation, which ionises the neutral atmosphere to form a plasma of ions and free electrons. It is influenced by extreme ultraviolet (EUV) radiation and X-rays in solar radiation (Hargreaves, 1979). In addition, particle precipitation in the high-latitude regions also contributes to the plasma in the ionosphere through the coupling of the solar wind with open geomagnetic fields.

Research on the ionosphere commenced in the 1900s after Guglielmo Marconi obtained clear experimental evidence on ionospheric propagation through his

successful experiment on his radio communication link from Poldhu, England, to Newfoundland, Canada, in 1901 (Marconi, 1922). In the upcoming years, many researchers studied the formation of these ionospheric layers and their effects on radio propagation (Kennelly, 1902; Larmor, 1924; Appleton and Barnett, 1925; Hulburt, 1927). For example, Kennelly and Heaviside (Heaviside, 1902; Kennelly, 1902) hypothesised that an electrified layer in the upper atmosphere reflected radio waves, later known as the 'Kennelly-Heaviside's layer' (Heaviside, 1902; Kennelly, 1902). Other early contributions to this field included Eccles (1912), who suggested that the atmospheric layer is a metallic reflector, and Larmor (1924), who suggested that the atmospheric layer is dielectric. The theories on the formation of ionospheric layers were solidified in the late 1920s and early 1930s with the contribution of Sir Edward Appleton. In his research, the ionospheric layers were named D, E and F layers, with the Appleton-Hartree equation, establishing calculation of the refractivity of the ionosphere, and the absorption in the ionosphere (Appleton, 1925, 1932; Appleton and Barnett, 1925).

Later in 1931, Sir Sydney Chapman (1931) suggested that solar radiation varies the plasma density exponentially with ionospheric height (Chapman, 1931; Chapman, 1931). Chapman (1931) also suggested that the solar radiation is absorbed in proportion to the electron concentration in the ionosphere, assuming that the solar radiation is monochromatic (Chapman, 1931a; Chapman, 1931b). Chapman (1931) presented this as a mathematical model that predicts the plasma density of the ionospheric layer and the rate of production during the day. The formula is also known as the Chapman Theory (Chapman, 1931). These contributions to ionospheric research have built our early understanding of the ionosphere's structure and morphology that acts as the basis for much of ionospheric research up to this day.

2.2.1. Structure of the Ionosphere

A fundamental contribution to the theory of the ionosphere is from Appleton in collaboration with other researchers from 1925 who named the ionospheric layers as D, E and F with increasing height (Appleton and Beynon, 1940; Appleton and Beynon, 1947). The ionospheric nomenclature as a function of altitude is presented in Figure 2.1, which is taken from the work of Hargreaves (1992).

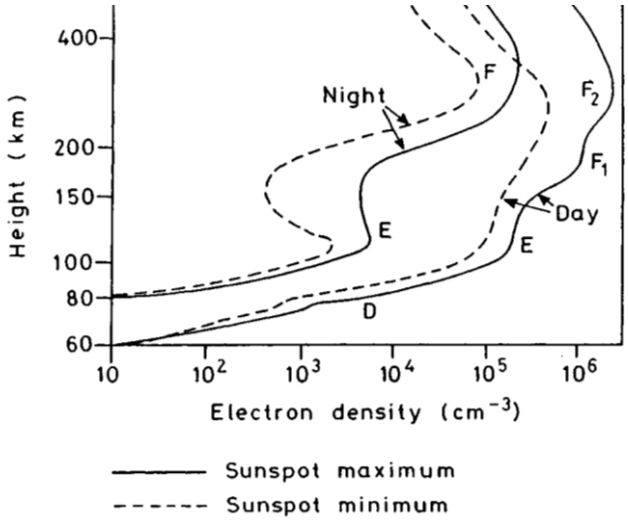

ical vertical profiles of electron density in the mid-latitude ionospher
ider, Wallchart *Aerospace Environment*, US Air Force Geophysics Lal

iour of the terrestrial ionosphere indicates that it can be consid
responding to the two principal regimes of magnetospheric

Figure 2.1 – Typical vertical profiles of electron density in the mid-latitude ionosphere with the maximum and minimum sunspot numbers (Hargreaves, 1992)

Figure 2.1. shows the layers of the ionosphere. The solar radiation increases ionisation in the ionosphere, which also influences the plasma density of the ionospheric layers in the day ionosphere. This increases the ionisation in the ionospheric layers. The F layer has two significant peak plasma densities. For this reason, the F region for the day ionosphere is divided into the F1 and F2 region, which will be described in Section 2.2.1.3.

Solar radiation decreases at sunset, which leads to weaker ionisation in the ionospheric layers. This leads to the D, E, and F1 layers being significantly weakened (Mohler, 1940; McNamara, 1991). McNamara (McNamara, 1991) states that the D layer disappears at night, while the E layer is weakened, and the F1 layer recombines with the F2 layer forming a single F layer. As the F region consists of the peak plasma density and it exists throughout the day and night, it is, therefore, considered the most critical layer for ionospheric radio propagation.

The ionosphere is in a constant state of change. The plasma density at a given time is subject to the production $\mathrm{q_e}$, loss rate of recombination $\mathrm{L_e}$ and transport of plasma and free electrons $\mathrm{div(Nv)}$, which can be expressed through the continuity equation, as shown in Equation 2.1, where v is the drift velocity of the electrons, N is the electron density, and t is time (Hargreaves, 1992).

$$\frac{\partial \mathrm{N}}{\partial \mathrm{t}} = \mathrm{q_e} - \mathrm{L_e} - \mathrm{div(Nv)} \qquad \text{Equation 2.1}$$

Production $(\mathrm{q_e})$ occurs mainly through photo-ionisation the caused by incident solar radiation, only occurring during the daytime. When solar radiation hits neutral atoms in

the atmosphere, it energises an electron to escape from a neutral atom causing the neutral atom to be ionised as a positively charged ion, as shown in Equation 2.2.

$$A + hv \rightarrow A^+ + e^- \qquad \text{Equation 2.2}$$

The removed electron now becomes a free electron in the ionosphere, contributing to the electron density in the region. This combination of positive ions and a balancing number density of free electrons results in an ionospheric plasma that is electrically neutral (Davies, 1965; McNamara, 1991).

The Loss term (L_e) describes the loss of free electrons from the plasma due to recombination. Recombination is the reverse process of photo-ionisation (Davies, 1965; McNamara, 1991). Here, a free electron recombines with a positively charged ion to form a neutral atom. Unlike photo-ionisation, recombination always takes place, both throughout the day and night and in all regions of the ionosphere. There are two types of recombination in the ionosphere – radiative and dissociative recombination (Davies, 1965; McNamara, 1991). During radiative recombination, the electron e^- combines directly with the positively charged ions A^+ forming a neutral atom A, and releases radiated energy (hv) as shown in Equation 2.3.

$$A^+ + e^- \rightarrow A + hv \qquad \text{Equation 2.3}$$

In contrast, dissociative recombination occurs as a two-stage process between positively charged ions, electrons and neutral atoms. The first stage is a reaction between a positively charged ion X and a neutral molecule A_2, such as oxygen (O_2) or nitrogen (N_2). Here, an atom from the neutral molecule is replaced with the positively charged ion forming a positively charged molecule, as shown in Equation 2.4 (Davies, 1965; McNamara, 1991).

$$X^+ + A_2 \rightarrow AX^+ + A \qquad \text{Equation 2.4}$$

The second stage of dissociative reaction combines the electron with the positively charged molecule to give two neutral atoms, as shown in Equation 2.5.

$$AX^+ + e^- \rightarrow A + X \qquad \text{Equation 2.5}$$

The difference between radiative recombination and dissociative recombination is the reaction rate. Radiative recombination is a slower process compared to dissociative recombination, with dissociative recombination 10^5 times faster than radiative recombination. Dissociative recombination is mainly seen in the E and F layers, while the D layer is influenced by both radiative and dissociative recombination. Regardless of which process dominates a given region, both recombination processes decrease the plasma density of the ionosphere.

The transport term $\mathrm{div}(\mathrm{Nv})$ of the continuity equation is the loss of electrons due to plasma motion. This term describes the transport of electrons due to the processes in the ionosphere, such as interaction with electric and magnetic fields, diffusion and interacting with plasmasphere. The transport of electrons occurs in all ionospheric layers but is most significant in the F2 layer. The transport process specific to the F2 layer is discussed in Section 2.2.1.3.

2.2.1.1. D layer

The D layer is the lowest layer in the ionosphere, which lies from approximately 60 km to 90 km above the Earth's surface (Hargreaves, 1992). It mainly ionises O, O_2 and N_2 atoms into ${\mathrm{O}_2}^+$, ${\mathrm{N}_2}^+$, and NO^+ ions (Hargreaves, 1992). The NO^+ ions are formed mainly through ionisation by solar X-rays, as presented in Equation 2.2 where A represents the O, O_2 , or N_2 atoms and $\mathrm{h\nu}$ is the energy from the solar radiation. The D layer disappears at night as the solar energy is no longer available.

2.2.1.2. E layer

The E layer is an ionised layer that spans from approximately 90 km - 160 km (Hargreaves, 1992) above the Earth's surface and is ionised by solar radiation, particularly soft X-rays and extreme ultraviolet (EUV) radiation (Mohler, 1940). The ionisation mainly ionises O, O_2 and N_2 atoms forming ${\mathrm{O}_2}^+$, ${\mathrm{O}}^+$, and ${\mathrm{N}_2}^+$ similar to the D layer using Equation 2.2. The recombination process in the E layer involves molecular ions, such as ${\mathrm{N}_2}^+$, ${\mathrm{O}_2}^+$ and NO^+ (McNamara, 1991; Hargreaves, 1992), mainly through dissociative recombination. The two stages of the dissociative recombination to form two neutral oxygen atoms are shown in Equation 2.6 and Equation 2.7 as an example.

$$\mathrm{O}^+ + \mathrm{O}_2 \rightarrow {\mathrm{O}_2}^+ + \mathrm{O} \qquad \text{Equation 2.6}$$

$${\mathrm{O}_2}^+ + \mathrm{e}^- \rightarrow \mathrm{O} + \mathrm{O} \qquad \text{Equation 2.7}$$

2.2.1.3. F layer

The F layer is the most important layer in the ionosphere since it has the bulk of the plasma situated in this region. The F layer spans approximately between 160 km and 600 km above the Earth's surface (Rishbeth, 1967; Hargreaves, 1979). It plays a significant role as a refractive medium for radio communications. As the F layer is situated at higher altitudes from the Earth's surface, it will experience stronger solar radiation. The region is mostly ionised by EUV radiation.

The F layer mainly ionises O atoms, forming O ions as shown in Equation 2.8.

$$O_2 + hv \rightarrow O_2^+ + e^- \qquad \text{Equation 2.8}$$

The ionisation processes and dynamics in the F layer result in the region having a distinct difference in its structure between the day and night. The F layer is divided into two layers in the dayside ionosphere: the F1 layer at approximately 160 km – 200 km and the F2 layer at approximately 200 km – 600 km. Both F1 and F2 layers ionize O atoms forming O_2^+ ions, as shown in Equation 2.8. However, the difference between these two layers is that the F2 layer experiences a higher ionisation rate in comparison to the F1 layer due to its higher altitude. This means the electron density in the F2 layer is significantly higher (Rishbeth, 1967; Rishbeth and Garriott, 1969b; McNamara, 1991; Hargreaves, 1992).

The plasma density in the F1 layer is proportional to the intensity of the solar radiation and behaves as a Chapman layer (Chapman, 1931; Chapman, 1931; Hargreaves, 1979). This means that the F1 layer will disappear at night due to the lack of solar radiation to ionise the medium. In contrast, the F2 layer is influenced by plasma transport and the Earth's magnetic field, as well as solar radiation. Therefore, the layer does not disappear during the night (Hargreaves, 1992).

During night-time, dissociative recombination occurs in the F layer because the recombination in the F layer involves reactions with molecules, such as O_2 (McNamara, 1991; Hargreaves, 1992), as shown in Equation 2.9.

$$O^+ + e^- + O_2 \rightarrow O + O + O \qquad \text{Equation 2.9}$$

As mentioned before, the F1 layer behaves like a Chapman layer, where its plasma density is proportional to solar radiation. This means that during night-time the rate of recombination increases significantly and the F1 layer disappears, resulting in a single F-layer mainly made from the F2-layer (Chapman, 1931; Mohler, 1940; Rishbeth & Garriott, 1969; Rishbeth, 1988).

The region above the F2 layer is known as the topside ionosphere, which reaches an approximate altitude of 800 km and then merges into the plasmasphere. As mentioned before, the F layer has a significant contribution from the transport term and electrons can be lost due to this as the topside ionosphere interacts with the plasmasphere. The ionisation in the F2 layer is therefore influenced by both recombination and the transport term. This results in the plasma density of the F2 layer being weakened during night-time. Table 2.1 gives a summary breakdown of ion production and loss processes in the different ionospheric layers, as identified by Chamberlain (1978).

Table 2.1 – The properties of each ionospheric layer (Chamberlain, 1978)

Ionospheric layers		**Maximum Electron Density (**cm^{-3})	**Ion Production Process**	**Loss of electron Process**
D		15 x 10^3	Ionisation by EUV and solar X-rays	Radiative recombination
		0		
E		0.15 x 10^6 (day)	Ionisation by EUV and solar X-rays	Dissociative recombination
		10 x 10^3 (night)		
F	F1	0.25 x 10^6 (day)	Ionisation by EUV and solar X-rays	Dissociative recombination Transport of electrons
		0 (night)		
	F2	10^6 (day)		
		10^5 (night)		

2.2.2. Chapman Theory

The rate of ionisation on each layer is influenced by solar radiation, particularly by EUV and X-rays, with the peak rate of ionisation occurring in the region which has the maximum solar radiation. Chapman (1931) developed a prediction method to determine the maximum ionisation rate and the peak plasma density for each ionospheric layer.

Chapman (1931a; 1931b) developed a formula to predict the rate of ionisation in the ionosphere using the rate of electron production. It predicts the diurnal variations of the ionospheric layers with the formula given in Equation 2.10, where q is the production rate, $\mathrm{q_{m0}}$ is the maximum production rate, z is the reduced height of the maximum ionisation production, and χ is the solar zenith angle (sun overhead is χ equals 0). The term $\mathrm{e^{-z}}$ is an exponential term indicating that the ionosphere is in an exponential atmosphere, where the production rate is influenced exponentially with the expression $\mathrm{e^{(1-z-\sec\chi e^{-z})}}$ (Hargreaves, 1992).

This is now known as the Chapman Theory (Chapman, 1931), and is commonly used to predict the rate of ionisation and the variations of the plasma density. Two main assumptions are made in this theory: 1) solar radiation is monochromatic, and 2) solar radiation is absorbed in proportion to the concentration of atoms (Chapman, 1931a; Chapman, 1931b).

$$\mathrm{q_e} = \mathrm{q_{m0}}\,\mathrm{e^{(1-z-\sec\chi e^{-z})}} \qquad \text{Equation 2.10}$$

The Chapman production function given in Equation 2.10 states that the ionisation is dependent on the sun's position with the solar zenith angle χ that leads to dependency on the intensity of solar radiation. The reduced height z is the height ratio for the neutral

gas between the scale height H for normalisation and the difference between the height of the production rate h and the height of the maximum ionisation h_{m0} as shown in Equation 2.11.

$$z = (h - h_{m0})/H \qquad \text{Equation 2.11}$$

The height of the maximum rate h_{m0} occurs when the solar zenith angle is zero. When the ionospheric height h is the same as the height of the maximum production rate h_{m0}, the reduced height z will also be zero. This is also known as the equilibrium of peak ionospheric height which gives the peak plasma density (Hargreaves, 1979, 1992; Hargreaves and Hunsucker, 2003), as it will give the maximum rate of ionisation production q_{m0} as shown in Equation 2.12, where q is equal to q_{m0} at equilibrium.

$$q_e = q_{m0} \cos\chi \qquad \text{Equation 2.12}$$

The variation of the reduced height with normalised production rate and solar zenith angle is shown in Figure 2.2 (Hargreaves, 1992).

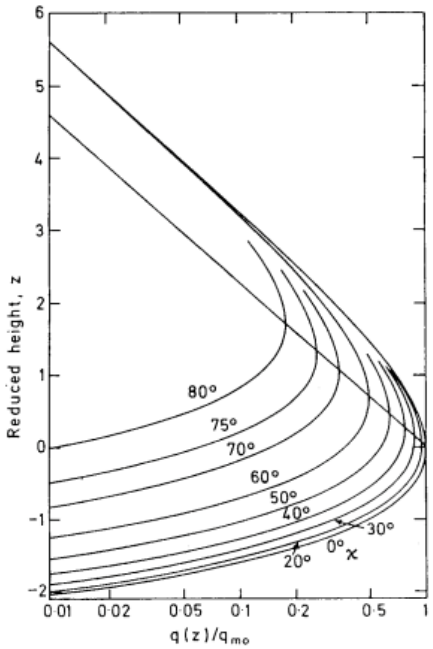

Figure 2.2 – Chapman Production Function (Hargreaves, 1992)

Figure 2.2 shows that the ratio of the production rate to the reduced height of the peak production rate varies with the sun's position, represented by the solar zenith angle χ.

The Chapman production function determines the ionisation rate of the ionospheric layers, which also determines the rate of electron production. This also influences the plasma density, which depends on production, loss and transport of electrons, as mentioned in Section 2.2.1. Therefore, the Chapman production function is also related to the loss of electrons through the recombination process. The recombination process in the Chapman production function consists of two types: chemical recombination and attachment. The process will lose electrons, which will influence the plasma density.

Chemical recombination is a process where the electrons e^- directly recombine with positive ions A^+ forming neutral atoms A as given in Equation 2.13.

$$A^+ + e^- \rightarrow A \qquad \text{Equation 2.13}$$

As the rate of chemical recombination reaches the equilibrium of peak ionisation rate, the recombination rate will be equivalent to the maximum electron production rate. As a result, the Chapman production function can be expressed in terms of the recombination rate as shown in Equation 2.14.

$$q_e = \alpha[A^+]N \qquad \text{Equation 2.14}$$

In this case, the process is shown in Equation 2.15, where α is the recombination coefficient. An ionospheric layer with this process of ionisation is called the α-Chapman layer. In addition, the term A^+ is the concentration of ions, which is equivalent to the plasma density N, therefore, combining Equation 2.12 and Equation 2.15 gives Equation 2.16 where N_{mo} is the maximum plasma density, and dividing the recombination coefficient gives Equation 2.17, which shows that the square root of the ionisation rate is proportional to the electron density in the α-Chapman layer.

$$q_e = \alpha N^2 \qquad \text{Equation 2.15}$$

$$\alpha N^2 = \alpha {N_{mo}}^2 e^{(1-z-\sec\chi e^{-z})} \qquad \text{Equation 2.16}$$

$$N = N_{m0} \cos^{1/2}\chi \qquad \text{Equation 2.17}$$

The attachment reaction is a process where the electrons e directly attach with neutral atoms M forming the negative ions M^- shown in Equation 2.18.

$$M + e^- \rightarrow M^- \qquad \text{Equation 2.18}$$

When considering loss through attachment, the reaction rate is considered linear as the number of neutral atoms in peak height is significantly higher than the electrons (Hargreaves, 1992; Hargreaves and Hunsucker, 2003). Here, β is the recombination coefficient (when attachment reaction is involved), and an ionospheric layer with this process is known as a β-Chapman layer. This is shown in Equation 2.19.

$$q_e = \beta N \qquad \text{Equation 2.19}$$

By combining Equation 2.12 and Equation 2.19, it can be shown that the ionisation rate in the β-Chapman layer is proportional to the electron density (Equation 2.20), and dividing with β coefficient gives Equation 2.21.

$$\beta N = \beta N_{m0} e^{(1-z-\sec\chi e^{-z})} \quad \text{Equation 2.20}$$

$$N = N_{m0} \cos\chi \quad \text{Equation 2.21}$$

From Equation 2.17 and Equation 2.21, it can be seen that the common factor which influences both types of ion production rate is the solar zenith angle χ. It shows that the incident solar radiation intensity changes the production rate of ions on both types of layers and therefore the electron density in the plasma.

Free electrons in a conducting medium, such as plasma, undergo rapid oscillations, also called Langmuir waves. These oscillations have a specific frequency based on the properties of the medium, known as the plasma frequency. For an electrically neutral, 'cold' ionosphere in equilibrium, the plasma (angular) frequency is given by Equation 2.22, where ω_P is the angular plasma frequency, ε_0 is the permittivity, e is the charge of the electron, m is electron mass, and N is the plasma density.

$$\omega_P{}^2 = \frac{Ne^2}{\varepsilon_0 m} \quad \text{Equation 2.22}$$

As can be seen from Equation 2.22, the angular plasma frequency of the ionosphere is directly influenced by the electron density of the region. Substituting the parameters with the relevant constants gives the plasma frequency of the ionosphere as Equation 2.23.

$$f_p{}^2 \approx 81N \quad \text{Equation 2.23}$$

The plasma frequency, f_p, of the ionosphere is an important concept for ionospheric radio propagation. This is because f_p determines if radio signals could propagate through the ionosphere or be refracted back towards the Earth. Signal frequencies greater than f_p experience trans-ionospheric propagation, while signals below the plasma frequency, such as HF signals, get refracted back to Earth. As the electron density of the ionosphere determines the plasma frequency of the medium, it, therefore, has a strong impact on the propagation of radio signals in the ionosphere.

The critical frequency is associated with the maximum electron density. The maximum electron density of each ionospheric layer will affect the critical frequency f_c relative to each ionospheric layer. Substituting the relevant parameters with the constants yields the f_c stated in Equation 2.24, where N_{max} is the maximum electron density of the ionospheric layer and f_c is the critical frequency in MHz.

$$f_c = 9 \times 10^{-6}\sqrt{N_{max}} \quad \text{Equation 2.24}$$

As a result, the ionospheric layers' electron densities affect the HF radio propagation as they will affect the propagating path (Appleton, 1925, 1932; Appleton and Barnett, 1925; Chapman, 1931; McNamara, 1991).

2.2.3. Ionospheric Anomalies

Anomalies in the ionospheric plasma density can significantly impact radio propagation. Past studies have investigated the effects of anomalies such Sporadic-E (Moser-T', Ezque and Jadu, 2000; Saito, Yamamoto and Maruyama, 2018), F-region anomaly (Oryema *et al.*, 2015), equatorial anomaly (Kelleher and Röttger, 1973; Balan, Nanan, Liu and Le, 2018) and geomagnetic variations (Tsunoda *et al.*, 2016) on radio communication. More recent publications such as Kurkin et al. (2000), Vilella et al. (2008), Stocker, Warrington and Siddle (2013), and Alsina-Pagès *et al.* (2016) have shown the effects of ionospheric conditions on the ionospheric radio links. This section will discuss several of these anomalies that are of relevance to the topic of the thesis. These are: sporadic – E, F – region winter anomaly, geomagnetic variations, equatorial anomaly and South Atlantic Anomaly (SAA).

2.2.3.1. Sporadic – E

Sporadic-E is an anomaly in the E region of the ionosphere, commonly contained within an area known as the Es layer. The Es layer is made up of clouds of electrons and occurs between 90 km and 130 km from the Earth's surface. It is caused by the variation of neutral atmospheric wind speed with height in the presence of the geomagnetic field. This is known as a wind shear, which acts to compress the ionisation in the E region (McNamara, 1991; Hargreaves, 1992). This causes the plasma density in the Es layer to be higher than that in the E region, consequently increasing the region's plasma frequency. As a result, the signal can be prematurely reflected from the Es region towards the Earth's surface at a propagation distance shorter than is reflected through the F-region. Similarly, if the signal, which is reflected from the F region, is propagating towards the Es region, the signal can be reflected from the top side of the Es layer. Sporadic-E is therefore a region that affects HF propagation as it can act as a mirror to radio signals prematurely reflecting the links over a shorter skip distance(McNamara, 1991; Hargreaves, 1992).

2.2.3.2. F- region winter anomaly

Since the F-region has the greatest concentration of electrons, it is the main refractive layer for HF radio propagation enabling long-distance radio communication. As mentioned earlier, the rate of ionisation of this region is influenced by solar radiation (Chapman, 1931), which means that the electron concentration during the summer is expected to be higher than that in winter. However, the plasma density in the F region is anomalous (Hargreaves, 1992), with terms describing this such as winter anomaly, seasonal anomaly, and annual anomaly. For this reason, the ionospheric variations in

the F layer are difficult to predict. Furthermore, the features of the anomaly are dependent on diurnal variation and seasonal variation. The most common anomaly in the F-region is the F-region winter anomaly. The winter anomaly is an anomaly in the F region during the winter season, described by the plasma density in the F region being greater in the winter than in the summer, (Hargreaves, 1992; Yadav *et al.*, 2009; Karia *et al.*, 2019). In addition, the plasma density of the F-region at noon during winter is greater than during summer. This behaviour contradicts the principles mentioned in the Chapman Theory, as a result, winter anomaly is also known as seasonal anomaly (Hargreaves, 1992). Furthermore, another anomalous result is that the overall plasma density in December is 20 % denser than that in June (Hargreaves, 1992). This is called the annual anomaly (Hargreaves, 1992). These disturbances then lead to unpredictable behaviour of radio communication channels.

2.2.3.3. Geomagnetic Variation

The ionosphere and HF propagation are influenced by the Earth's geomagnetic field (McNamara, 1991). The geomagnetic field is generated by a near-dipole magnet located in the Earth's core. The geomagnetic axis is tilted by approximately 11° from the geographic axis, resulting in an offset of the geomagnetic coordinates from the geographic coordinates. Since the geomagnetic field is not a perfect dipole, local variations of the field may be observed depending on the location on Earth, which can impact radio propagation.

Of importance are (Chulliat *et al.*, 2015; *World Magnetic Model | NCEI*, 2019) :

- Inclination angle (I) indicating the direction of the magnetic field in the north-south direction known as the magnetic dip angle. The positive angles indicate that the inclination angle is at the northerly direction, whereas the negative angles indicate that the inclination angle is at the southerly direction.
- Vertical component (Bz) of the magnetic field indicates the vertical intensity. A positive Bz indicates that the total magnetic field is dominated by the vertical intensity pointing towards the northerly direction, whereas a negative Bz indicates that the total magnetic field is dominated by the vertical intensity pointing towards the negative inclination angle, which is the southerly direction.
- Declination angle (D) indicates the direction of the magnetic field in the east-west direction. The positive angles indicate that the declination angle is pointing towards the east direction, whereas the negative angles indicate that the declination angle is pointing towards the west direction.

The reason to consider these parameters (I, Bz and D) is that these parameters define the global structure of the magnetic field. The variation of these parameters with location can be obtained through models such as the World Magnetic Model (WMM) (Chulliat et al., 2015) and International Geomagnetic Reference Field (IGRF). The distribution of the inclination angles (I), the vertical component (Bz), and the declination

angle (D) of the magnetic field as modelled by WMM is given in Figure 2.3, Figure 2.4 and Figure 2.5.

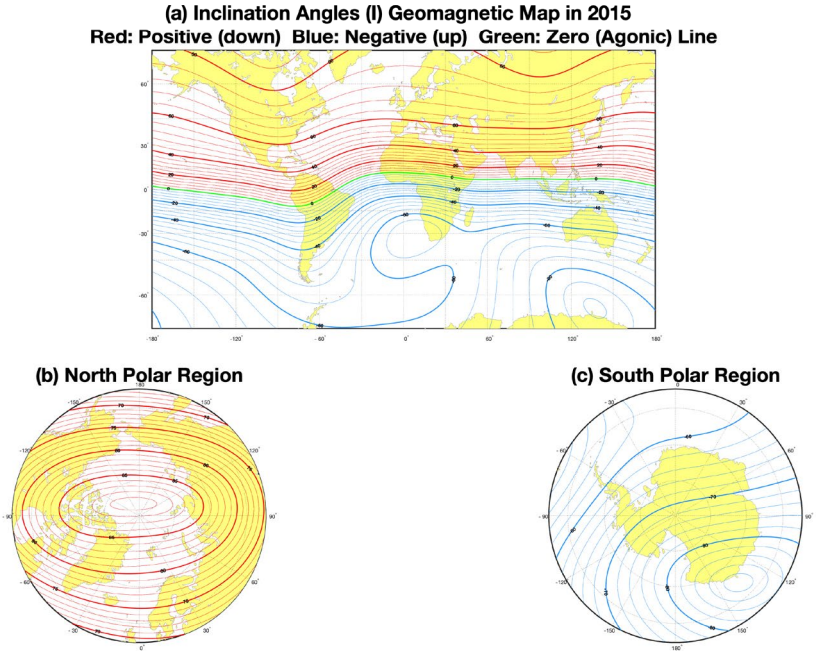

Figure 2.3 – World Magnetic Model simulation on the inclination angles (I) of the magnetic field in degrees. The positive and negative values show the geomagnetic field in the north and south hemisphere are opposed to each other (World Magnetic Model | NCEI, 2019). Note: The WMM source code is in the public domain and not licensed or under copyright. The information and software may be used freely by the public.

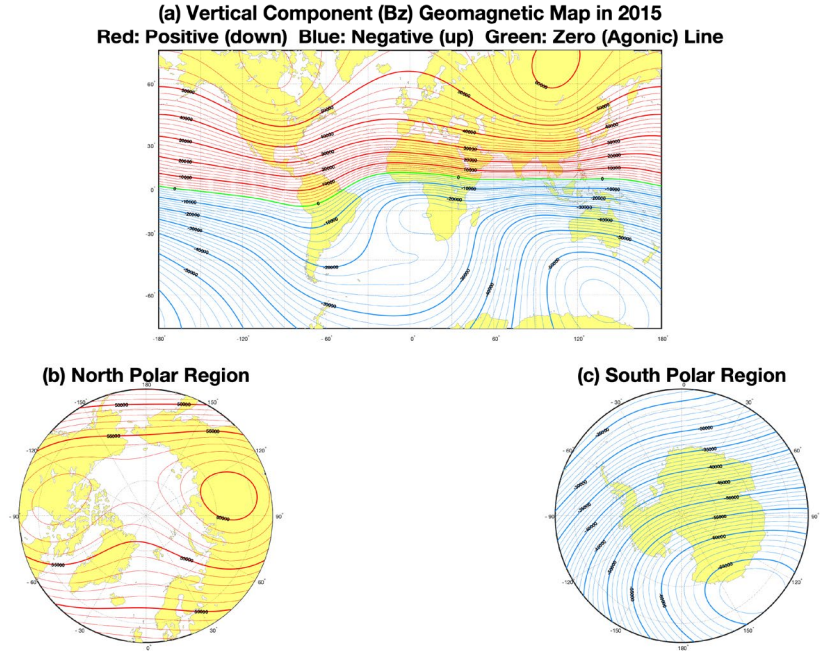

Figure 2.4 – World Magnetic Model simulation on the vertical intensity (Bz) of the magnetic field in nanotesla (nT). The positive and negative values show the geomagnetic field in the north and south hemisphere are opposed to each other (World Magnetic Model | NCEI, 2019).

Based on the geomagnetic field, the global ionosphere can be considered to have 3 distinct geomagnetic latitudinal regions – equatorial (0° - 20° N or 0° - 20° S), mid-latitude (20° N - 60° N or 20° S - 60° S) and polar (> 60° N or > 60° S) (McNamara, 1991).

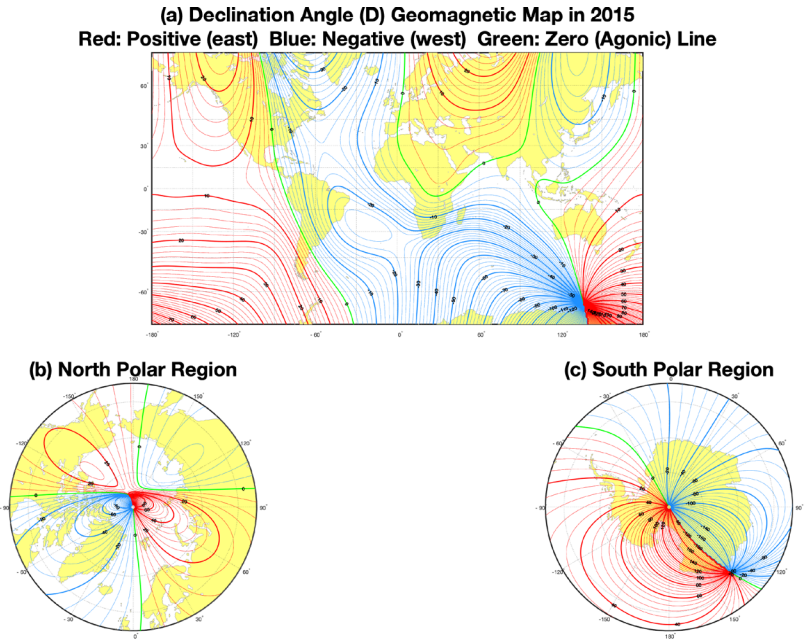

Figure 2.5 – World Magnetic Model simulation on the declination angles (D) of the magnetic field in degrees. The positive and negative values show the geomagnetic field in the east and west direction are opposed to each other (World Magnetic Model | NCEI, 2019).

The declination angles, as illustrated in Figure 2.5, shows the direction of the magnetic fields in the east-west direction. It indicates the direction where the geomagnetic axis is tilting from the geographic poles (World Magnetic Model | NCEI, 2019). This is important in the long term, as the change in the magnetic poles influence the direction and the intensity of the magnetic fields, such as the inclination angles (I) and the vertical component (Bz). This will influence the geomagnetic variations causing ionospheric disturbances in the ionosphere (McNamara, 1991).

The geomagnetic field impacts the ionosphere and HF propagation, particularly in the regions along the magnetic poles and the magnetic equator (McNamara, 1991). The motion of electrons affects the plasma density in the ionosphere; this in turn, affects HF propagation. One anomaly that the geomagnetic variations in low-latitude regions have caused is known as the equatorial anomaly (McNamara, 1991).

2.2.3.4. Equatorial Anomaly

The ionosphere in the equatorial region is influenced by solar radiation, where the solar zenith angle is much smaller (Sun's position is almost overhead) than at mid-latitude and high-latitude regions. If ionisation in the equatorial region obeys the Chapman Theory (Chapman, 1931), as mentioned in Section 2.2, then the plasma density at the equatorial region should be denser than that at mid-latitude and high-latitude regions (Hargreaves, 1979; McNamara, 1991; Balan, Liu and Le, 2018) and peak at the equator. However, in the equatorial ionosphere, the peak densities are observed +/-20º of the geomagnetic equator (called the tropics). This is known as the equatorial anomaly (Hargreaves, 1979; McNamara, 1991; Balan, Liu and Le, 2018).

Solar radiation of the ionosphere in the equatorial region causes daytime heating. This increases the plasma density causing the plasma to rise vertically in the ionosphere. When the plasma reaches higher altitudes, the plasma becomes increasingly influenced by the geomagnetic field causing an E x B drift (McNamara, 1991). As a result, the plasma flows along the magnetic field lines in low-latitude regions at around 10 and 20 º from the geomagnetic equator. The free electrons are also redistributed from the geomagnetic equator to the low-latitude regions forming large clumps of electrons, known as crests. The crests are mostly developed during the late afternoon and early evening (post-sunset), which influences HF propagation causing strong refraction and diffraction of the radio signals (McNamara, 1991). This ionisation is known as the fountain effect (Hargreaves, 1979; McNamara, 1991; Balan, Liu and Le, 2018). The equatorial anomaly can also enable signal propagation across the equator due to refraction off of the crests on either side of the geomagnetic equator. This is known as Trans-Equatorial Propagation (TEP) and is mainly observed during afternoon/post-sunset hours when the fountain effect process occurs. TEP is discussed in more detail in Section 2.4.

2.2.3.5 South Atlantic Anomaly (SAA)

The geomagnetic field in the South Atlantic region is weaker than those in other regions, such as the mid-latitude region, causing the gyrofrequency in the South Atlantic Region to be lower (McNamara, 1991). The anomaly is known as the South Atlantic Anomaly (SAA). The lower gyrofrequency causes the plasma density in the South Atlantic Region to be higher than in other regions. This affects the refractive indices of its ionospheric layers. It is a major anomaly that impacts HF propagation, such as refraction, polarisation (Faraday rotation), absorption, scattering and scintillation. The effects of varying the gyrofrequency because of SAA on the refractive index will be discussed in more detail in Section 2.3.

2.2.4. Solar Activity

Solar radiation, in particular the EUV and X-ray, influences the plasma density of the ionosphere. It is known that solar radiation varies on a daily, monthly and yearly basis (McNamara, 1991). However, solar radiation is also influenced by the solar activity, which can be observed through analysing the solar sunspot number on the Sun's surface (Hargreaves, 1992). It has been observed that the solar activity goes through an approximately 11-year cycle, which in turn produces the maximum and minimum sunspot number at the solar maximum and solar minimum respectively (Hargreaves, 1992). The solar radiation reaches its maximum during the solar maximum, and similarly, at its minimum during the solar minimum (Hargreaves, 1992). Therefore, the plasma density of the ionosphere also corresponds to the variations of the solar activity

As the solar activity varies the plasma density, the refractive indices of the ionospheric layers are also affected. This means that the most common impact of solar activity on the radio signal is refraction and absorption (Davies, 1965; Hargreaves, 1992). The signals can be prematurely reflected to the Earth's ground surface due to high plasma density. In addition, the solar activity also influences the absorption of the radio signals the increased plasma density causing the signals to be attenuated. More details will be mentioned in Section 2.3.2.

2.3. Radio Propagation in the Ionosphere

Electromagnetic (EM) waves propagating through the ionosphere are affected by the free electrons in the ionised plasma as well as the geomagnetic field. As a result, there are various ionospheric effects on the propagation of EM waves. These include refraction, polarisation (Faraday rotation), absorption, scattering and scintillation. One of the most significant ionospheric effects on HF is refraction, as the ionosphere acts as a refractive medium to propagating EM waves. As a result, this effect can be defined through the ionospheric refractive index, as described by the Appleton-Hartree theory. The refractive index in the Appleton-Hartree Equation is a complex refractive index, which has a real component μ and an imaginary component $i\chi$ (Davies, 1965, 2008). The real component μ indicates the refraction of the signal, and it is the component used to determine the phase velocity of the signal. The imaginary component $i\chi$ indicates the attenuation of the signal, which is a type of absorption. This section explores this theory with a particular focus on the propagation effects experienced by HF signals.

2.3.1. Appleton-Hartree Theory

The Appleton-Hartree equation describes the refractive index for EM waves that propagate through a cold magnetised plasma such as the ionosphere (Appleton & Beynon, 1940; Appleton & Beynon, 1947; Davies, 1965; Hargreaves, 1979). It is a complex term influenced by the electron density, the magnetic field and the electron collision frequency in the ionosphere. The equation is defined in Equation 2.25. The parameters X, Y_T, Y_L and Z in Equation 2.25 are the plasma ratio, the transverse component and longitudinal component of the magnetic field, and the ratio of collision frequency and the operational frequency and will be explained below in Equation 2.26 to Equation 2.30.

$$n^2 = 1 - \frac{X}{1 - jZ - \left[{Y_T}^2/2(1 - X - jZ)\right] \pm \left\{\left[{Y_T}^4/4(1 - X - jZ)^2\right] + {Y_L}^2\right\}^{1/2}} \quad \text{Equation 2.25}$$

The parameter X is influenced by the electron density and the angular radio frequency (Davies, 1965), and affects refraction and absorption of the RF signal where ω is the angular plasma frequency, e is the electron charge, N is the plasma density, ϵ_0 is the permittivity and m is the electron mass.

$$X = Ne^2/\epsilon_0 m\omega^2 \quad \text{Equation 2.26}$$

Parameter Y relates to the magnetic field effects that cause Faraday rotation and polarisation of an EM signal (Section 2.3.1.2). It is considered in two parts corresponding to the transverse and longitudinal magnetic field components, where the subscripts T and L refer to the transverse and longitudinal components of the Earth's magnetic field with reference to the propagation direction (Davies, 1965), B is the Earth's magnetic field, m is the electron mass and ω is the angular radio frequency.

$$Y_T = \frac{e\,B_T}{m\omega} \quad \text{Equation 2.27}$$

$$Y_L = \frac{e\,B_L}{m\omega} \quad \text{Equation 2.28}$$

The total magnetic field intensity (Y) is then obtained by both transverse and longitudinal magnetic field components, as shown in Equation 2.29.

$$Y = \sqrt{{Y_T}^2 + {Y_L}^2}$$ Equation 2.29

Parameter Z in the Appleton-Hartree equation refers to the effect of electron collision on signal propagation as shown in Equation 2.30, where ν is the collision frequency between the electrons and the neutrons (Davies, 1965; Rishbeth and Garriott, 1969a; Hargreaves, 1979; McNamara, 1991).

$$Z = \frac{\nu}{\omega}$$ Equation 2.30

2.3.1.1 Signal refraction

If the magnetic field and the collision frequency are considered to be negligible, then the refractive index is influenced by the plasma ratio alone, as shown in Equation 2.31, where ${\omega_N}^2$ is the angular plasma frequency can be expressed in Equation 2.32

$$n^2 = 1 - X = 1 - \frac{{\omega_N}^2}{\omega^2} = 1 - \frac{Ne^2}{\epsilon_0 m\omega^2} \approx 1 - \frac{81N}{\omega^2}$$ Equation 2.31

$${\omega_N}^2 = \frac{Ne^2}{\epsilon_0 m} \approx 81N$$ Equation 2.32

The refractive index, as described by the full Appleton-Hartree equation, is a complex number, which has a real component and an imaginary component. However, if the refractive index is solely influenced by the plasma ratio, i.e. the parameter X in Equation 2.26, and not by the magnetic field and the collision frequency (parameters Y and Z in Equation 2.30) then the index will be a purely real quantity. This simplified formula can now be used to describe three distinct effects of the index on propagating signal, based on the value of the square of the index (i.e. n^2):

- $n^2 > 0$ – this occurs when the angular radio frequency is greater than the angular plasma frequency. Under these conditions, the signal that propagates vertically will be refracted through the ionospheric layer
- $n^2 < 0$ – this occurs when the angular radio frequency is lesser than the angular plasma frequency. Here, a signal that propagates vertically will be reflected vertically towards the Earth's surface
- $n^2 = 0$ – this can occur when the angular radio frequency is equal to the angular plasma frequency.

The critical frequency for radio communications can therefore be determined as shown in Equation 2.33.

$$\omega \approx 9\sqrt{N}$$ Equation 2.33

2.3.1.2. The Magnetic Field, Faraday Rotation and Polarisation

The EM wave consists of an electric field and a magnetic field, which are perpendicular to each other. They are transverse waves propagating in a direction perpendicular to both the electric and magnetic fields. As mentioned earlier, the (external) magnetic field, which gives rise to Faraday rotation and polarisation, is described by parameter Y in the Appleton-Hartree Equation. The sign found in the numerator indicates that this magnetic field causes the ionosphere to be birefringent (Davies, 1965), with ordinary and extraordinary ray propagation.

The equation also defines the transverse and longitudinal components of the magnetic field individually. This is because EM waves are transverse waves and the transverse component of the magnetic field will have a greater influence than the longitudinal component of the magnetic field. As a result, the square of the transverse component will be significantly greater than the square of the longitudinal component, The Y component can therefore be approximated to that of Y_T, and the contribution from Y_L can be considered negligible. Furthermore, for HF frequencies (the subject of this thesis), the signal frequency is generally significantly higher than the collision frequency, meaning that the Z term can be ignored. The reduced form of the Appleton-Hartree Equation for HF propagation can now be expressed in Equation 2.34.

$$n^2 \approx 1 - \frac{X}{1 - \left[\frac{Y^2}{2(1-X)}\right] \mp \left[\frac{Y^2}{2(1-X)}\right]}$$ Equation 2.34

Polarisation of EM waves describes the plane in which the electric field oscillates (McNamara, 1991; Hargreaves, 1992). For example, a vertically polarised EM wave means that the electric field oscillates in the vertical direction which is perpendicular to the propagating direction. Similarly, a horizontally polarised EM wave means that the electric field oscillates in the horizontal direction which is perpendicular to the propagation direction (McNamara, 1991; Hargreaves, 1992). When the EM wave interacts with the ionised medium, which is the ionosphere, and the magnetic field, the polarisation will be rotated by the magnetic field. This is known as Faraday rotation.

Faraday rotation is a rotation of the plane of polarisation by the magnetic field. Faraday Rotation occurs in the ionosphere due to the interaction between the radio wave, the ionosphere, and the earth's magnetic field (McNamara, 1991; Hargreaves, 1992). The existence of the earth's magnetic field causes the ionosphere to be birefringent, which means that the rotation is influenced by polarisation and the propagation direction of the radio wave (McNamara, 1991; Hargreaves, 1992). In addition, the rotation can be in either the clockwise or anti-clockwise direction depending on the orientation of the

wave to the direction of the magnetic field (McNamara, 1991). As a result, the electric field rotates in a direction corresponding to Faraday rotation (McNamara, 1991) giving two different characteristic waves, which are polarised in opposite rotations. These are known as ordinary (O) and extraordinary (X) waves (Davies, 1965; McNamara, 1991). Quoting from Bust et al. (2021) *"In the northern hemisphere for a radio wave propagating along the field line toward the direction of the magnetic north pole, the O-mode is left hand circularly polarized because by definition it rotates in the opposite direction to the electrons. This arises from the electron gyration which is the circular motion of an electron in the plane perpendicular to the magnetic field and rotates along the direction given by the right hand toward the direction of the magnetic north pole, i.e. in the direction of the magnetic field. Conversely, the X-mode is right-hand polarized for a radio wave propagating along the field line toward the direction of the magnetic north pole".*

The magnitude of the Faraday rotation is influenced by the strength of the magnetic field and the plasma density, causing the electric field and the magnetic field to be out of phase while being perpendicular to each other. As a result, both O and X waves are elliptically polarised because the maximum amplitude of the electric field does not occur when the amplitude of the magnetic field is at its maximum (McNamara, 1991; Hargreaves, 1992). Nevertheless, if the maximum amplitude of the electric field occurs when the amplitude of the magnetic field is at its maximum, then both the electric field and the magnetic field are in phase. The radio wave on this occasion is classified as circularly polarisation (McNamara, 1991; Hargreaves, 1992).

The difference between the O and X waves is the direction of the rotation and the plane of the electric field. The O wave occurs when the polarisation of the wave is unchanged and the electric charges are rotating in the same direction as the electric field, parallel to the magnetic field. Whereas X wave occurs when the polarisation of the wave is polarised in the opposite rotation and the electric field is perpendicular to the magnetic field (McNamara, 1991; Hargreaves, 1992).

As electrons in the O wave rotate in the same direction as the electric field and parallel to the geomagnetic field, the effect of the magnetic field in the refractive index will be absent. Then, the Appleton-Hartree Equation uses the $+$ sign to represent the refractive index for O-wave propagation and only considers the refractive effects from the plasma ratio as shown in Equation 2.35.

$$n^2 \approx 1 - X \qquad \text{Equation 2.35}$$

In contrast, electrons in the extraordinary wave rotate in a direction perpendicular to the geomagnetic field. (Davies, 1965; McNamara, 1991; Hargreaves, 1992) The refractive index of the extraordinary wave is therefore influenced by the magnetic component, as a result, the extraordinary wave will not be refracted as if the magnetic field is absent, and the magnetic field has an additive contribution to the refractive index. The Appleton-Hartree Equation then has the $-$ sign in the denominator to represent the refractive index as shown in Equation 2.36 (Davies, 1965, 2008). As the propagation of the extraordinary wave is influenced by the magnetic field, the refractive index will

also be a function of the Y component. Therefore, the plasma ratio X can be expressed in terms of the Y component, as shown in Equation 2.37 when the refractive index n^2 is set to zero, as shown in Equation 2.38 (Davies, 1965, 2008).

$$n^2 \approx 1 - \frac{X}{1 - \left[\frac{Y^2}{2(1-X)}\right] - \left[\frac{Y^2}{2(1-X)}\right]} \approx 1 - \frac{X}{1 - \frac{Y^2}{1-X}} \quad \text{Equation 2.36}$$

$$X = 1 - Y \quad \text{Equation 2.37}$$

$$n^2 \approx 1 - \frac{X}{1 - \left[\frac{Y^2}{2(1-X)}\right] - \left[\frac{Y^2}{2(1-X)}\right]} \approx 1 - \frac{1-Y}{1 - \frac{Y^2}{1-(1-Y)}} = 0 \quad \text{Equation 2.38}$$

Equation 2.35 to Equation 2.38 show that the refractive index of the O wave is greater than the X wave, since the O wave refracts off the ionosphere as if it is in the absence of the magnetic field. This means that the X wave refracts more into the subsequent layers than the O wave. For this reason, the X wave will be reflected off from the ionosphere earlier than the O wave. This, in turn, affects the propagation distance of the radio waves. This will be explained further in Chapter 3.

2.3.2. Absorption

When a radio signal is transmitted towards the ionosphere from Earth, it will first approach the D layer. As the signal propagates through this region, the radio frequency makes the electrons oscillate at the radio frequency and the medium absorbs the energy. This energy is then re-radiated in the form of radio waves and the signal propagates through the medium. When the electrons collide with neutral atoms, the EM wave energy carried by the electrons is lost to heat and electromagnetic noise. As a result, the energy that the electrons absorbed from the radio signal is lost and it reduces the signal strength of the radio signal. This process is known as ionospheric absorption.

Ionospheric absorption affects the signal strength, as the signal will be attenuated when it is absorbed. The signal strength E_o will be reduced by the absorbed power L in decibels. The amplitude of the signal E, which is also its signal strength, decays exponentially with distance s measured in kilometres and the rate of the exponential decay is called the absorption coefficient κ, measured in decibels per kilometre (Davies, 1965, 2008). The absorption coefficient κ signifies the absorption loss per kilometre and integrating with distance s gives the absorption loss of the signal's strength. This is shown in Equation 2.39.

$$E = E_o \exp\left(-\int \kappa \, ds\right)$$ Equation 2.39

As a result, the integral of the distance and the absorption coefficient is measured in Nepers. The integral is required to be converted to decibels. A Neper Np is equivalent to 8.68 decibels, as shown in Equation 2.40.

$$1 \text{ Np} = 20 \log_{10} e \approx 8.68 \text{ dB}$$ Equation 2.40

With the distance of absorption given as s and the absorption coefficient given as κ, the absorption loss can be represented as shown in Equation 2.41 (Davies, 1965, 2008).

$$L_a = -8.68 \int \kappa \, ds$$ Equation 2.41

The Appleton-Hartree Equation describes signal attenuation through ionospheric absorption through the imaginary component of Equation 2.42. This means that the complex refractive index influences absorption (Davies, 1965, 2008). The complex refractive index with the real (μ) and imaginary (K) components are shown in Equation 2.42 and the expression in Appleton-Hartree Equation is shown in Equation 2.43.

$$n^2 = (\mu - iK)^2$$ Equation 2.42

$$(\mu - iK)^2 = 1 - \frac{X}{1 - jZ - \left[{Y_T}^2/2(1 - X - jZ)\right] \pm \left\{\left[{Y_T}^4/4(1 - X - jZ)^2\right] + {Y_L}^2\right\}^{1/2}}$$ Equation 2.43

There are two types of absorption described by the Appleton-Hartree equation - non-deviative and deviative absorption. The main difference between non-deviative and deviative absorption is the trajectory of the radio wave.

2.3.2.1. Non-Deviative Absorption

Refraction is the most common effect of deviation of a radio wave from the trajectory path. However, if, assuming, that the refractive index in Equation 2.49 is predicted in the absence of the magnetic field and collision frequency, then the refractive index will be solely influenced by the plasma density. If the plasma density of the regions gives a plasma frequency, which is significantly lower than the operational frequency, then the effect of refraction on its trajectory path is minimal. As a result, the refractive index is close to unity, meaning that the radio wave is not significantly refracted from its original trajectory path (Davies, 1965; McNamara, 1991). The absorption that occurs in regions

where the refractive index is close to unity is classified as non-deviative absorption. Non-deviative absorption occurs in the D layer because the plasma frequency of the D layer is significantly lower than the radio signals operating within the HF range. Therefore, the HF signals will not be significantly refracted from their original trajectory path when propagating through the D layer.

In addition, this type of absorption occurs in regions where the product of electron density and collision frequency Nv is large. This is the type of absorption that occurs in the D layer (Davies, 1965, 2008). This is because the D layer is situated at lower ionospheric altitudes, where the solar radiation is weaker. Therefore, when the D layer exists in the ionosphere, the electron density is significantly increased causing the product Nv to be large (Davies, 1965; McNamara, 1991).

Non-deviative absorption can be calculated both in the absence and in the presence of the magnetic field. In the absence of the magnetic field, then the complex refractive index n is significantly dominated by μ (Davies, 1965, 2008). This means the signal will be influenced by the plasma ratio and the collision frequency, as mentioned in Section 2.3.1. As a result, the refractive index in Equation 2.42 can be expressed in Equation 2.44:

$$(\mu - iK)^2 = 1 - \frac{X}{1 - jZ} = 1 + \frac{XZ}{1 + Z^2} - \frac{iXZ}{1 + Z^2} \qquad \text{Equation 2.44}$$

Equation 2.44 shows that the real refractive component μ is not zero, and therefore it shows non-deviative absorption. However, the parameter Z is negligible because the collision frequency v is significantly lower than the HF angular radio frequency ω (Davies, 1965, 2008). For this reason, the refractive component μ is close to unity. Thus, the absorption coefficient can be expressed in Equation 2.45 and by substituting the coefficients ε_o, c, e can be expressed by Equation 2.46:

$$\kappa = \frac{\omega XZ}{2c\mu(1 + Z^2)} = \frac{e^2}{2\varepsilon_o mc\mu} \frac{Nv}{(\omega^2 + v^2)} \qquad \text{Equation 2.45}$$

$$\kappa = \frac{\omega XZ}{2c\mu(1 + Z^2)} = 4.6 \times 10^{-2} \frac{Nv}{(\omega^2 + v^2)} \qquad \text{Equation 2.46}$$

In the case where the angular radio frequency is significantly greater than the collision frequency, such as in the HF band, ω^2 is significantly greater than v^2. As a result, the sum of $\omega^2 + v^2$ is approximately equal to ω^2, as shown in Equation 2.47. With the angular frequency ω being equal to $2\pi f$, where f is the operational frequency, Equation 2.47 can be expressed as shown in Equation 2.48.

$$\kappa = 4.6 \times 10^{-2} \frac{Nv}{(\omega^2 + v^2)} \approx 4.6 \times 10^{-2} \frac{Nv}{\omega^2} \qquad \text{Equation 2.47}$$

$$\kappa = \frac{4.6}{4\pi^2} \times 10^{-2} \frac{Nv}{f^2} = = 1.15 \times 10^{-3} \frac{Nv}{f^2}$$ Equation 2.48

Equation 2.48 shows that the absorption is inversely proportional to the square of the operational frequency. As a result, the absorption of a radio signal decreases with increasing frequency (Davies, 1965, 2008).

However, the motion of the electrons is influenced by the earth's magnetic field, and therefore, absorption also has its effects on the ordinary and extraordinary waves. For this reason, the operational frequency needs to include the radio frequency ω and the gyrofrequency ω_L , which corresponds to the parallel component of the magnetic field. This is expressed as the term $\omega \pm \omega_L$, where $\omega + \omega_L$ is the operational frequency for the O wave, and $\omega - \omega_L$ is the operational frequency for the X wave.

The radio wave will first approach the D layer, where the operational frequency of the signal is generally higher than the plasma frequency of the layer and the gyrofrequency. As a result, the signal refraction in the D layer is minimal. Therefore, the radio wave will not deviate from its trajectory path, and it encounters non-deviative absorption. Equation 2.49 shows the non-deviative absorption in the presence of the magnetic field (Davies, 1965).

$$\kappa = 4.6 \times 10^{-2} \frac{Nv}{(\omega \pm \omega_L)^2 + v^2}$$ Equation 2.49

As mentioned in Section 2.3.1.2, the $\pm$ sign indicates that Equation 2.49 applies to both ordinary and extraordinary waves, where $+$ is for the ordinary wave, and $-$ is for the extraordinary wave. In a case where the sum of the radio frequency ω and the gyrofrequency ω_L is significantly greater than the collision frequency v, then the product $(\omega \pm \omega_L)^2$ will be significantly greater than v^2. As a result, the denominator in Equation 2.49 will be approximately $(\omega \pm \omega_L)^2$, as shown in Equation 2.50 (Davies, 1965).

$$\kappa = 4.6 \times 10^{-2} \frac{Nv}{(\omega \pm \omega_L)^2}$$ Equation 2.50

Equation 2.50 shows that the absorption of the extraordinary wave is greater than that of the ordinary wave. The sum of the frequencies in an extraordinary wave $(\omega - \omega_L)$ is lower than the sum of the frequencies in an ordinary wave $(\omega + \omega_L)$. For this reason, if the radio frequency ω is less or equal to the gyrofrequency ω_L, then the whole signal can be heavily absorbed. The gyrofrequency range is approximately between 1 MHz and 1.6 MHz (McNamara, 1991). This means that the gyrofrequency range is approximately within the MF frequency range, which is between 0.3 MHz and 3 MHz. The ionospheric radio signals are propagated at radio frequencies within the HF frequency range, which is between 3 MHz and 30 MHz and refraction must be considered first for HF propagation. The HF frequencies are higher than the gyrofrequency, and therefore, this will reduce the effect of absorption on both the ordinary and extraordinary wave (Davies, 1965).

2.3.2.2. Deviative Absorption

Deviative absorption is absorption that occurs in a region where the deviation of the wave takes place, i.e. where ray bending occurs. Deviative absorption occurs in regions where the refractive index is dominated by the plasma ratio, as a result, the magnetic field and the collision frequency can be neglected. Deviation absorption can be calculated using the complex refractive index (Piggott, 1957), as shown in Equation 2.51 where μ' is the group refractive index. Equation 2.51 can be expressed in terms of the ionospheric parameters since the real component of the refractive index μ is approximately the reciprocal of the group refractive index μ'(Piggott, 1957), and μ is approximately the square root of $1 - X$. This yields Equation 2.52.

$$\kappa \approx \frac{{\omega_N}^2 \nu}{2\mu\omega^2 c} = \frac{\nu}{2c}\left(\frac{1}{\mu} - \mu\right) \approx \frac{\nu}{2c}(\mu' - \mu) \approx \frac{\nu}{2c}\mu' X \qquad \text{Equation 2.51}$$

$$\kappa = \frac{\nu}{2c}\frac{X}{(1-X)^2} \qquad \text{Equation 2.52}$$

The most common effect of deviative absorption is the reflection of the radio wave, since the operational frequency of the signal is lower than the plasma frequency of the ionospheric region. However, the effect of deviative absorption is small, since the signal is deviated and reflected towards the Earth's surface. Deviative absorption takes place in higher altitudes of the ionosphere, such as in the E region and F region, and therefore, most of the absorption takes place when the signal passes through the D region (Davies, 1965; McNamara, 1991).

2.3.3. High Frequency (HF) propagation

HF radio signals have a frequency range between 3 MHz and 30 MHz. They are used for long distance communication as the signals can be reflected/refracted off the ionosphere to achieve greater distances between transmitters and receivers than would be possible from direct line-of-sight propagation. Since HF communications are reliant on the ionosphere, the region's properties play a vital role in the propagation distance and the path of a given HF signal.

HF frequencies that are below the critical frequency transmitted vertically reflect back to the ground. This is the principle of operation of the instrument called the ionosonde. If a signal propagates at an angle, then the resulting propagation will travel along the horizontal distance before returning to the ground. This reflection process is known as a single hop (McNamara, 1991). As a result, the signal which is reflected from the ionosphere once is called a 1-hop propagation. However, this reflection can be

repeated by the ionosphere and the Earth's surface multiple times (McNamara, 1991). This means that long-distance propagation can be propagated in multiple hops known as multiple-hop propagation (McNamara, 1991). Nevertheless, the signal is required to propagate at an HF frequency higher than the critical frequency, and therefore, it is essential to determine the maximum frequency for long-distance propagation.

As mentioned before, HF signals used for communication must be transmitted with a finite incident angle, such that the ionosphere's refractive properties can be used to enable the signal to reach the receiver. The maximum frequency of the signal propagating at a given angle is known as the Maximum Usable Frequency (MUF), which is the function of the critical frequency and determined by the plasma frequency of the ionosphere. The MUF for a single hop propagation can be determined from the critical frequency and the incident angle into the ionosphere θ, as shown in Equation 2.53. If θ is 90 degrees, then the MUF will be equivalent to the critical frequency.

$$\mathrm{MUF} \approx \mathrm{f_c}/\cos\theta \qquad \text{Equation 2.53}$$

MUF is useful for radio communications in HF propagation because the angle of incidence is inversely proportional to MUF. The advantage of using MUF is that it encourages radio users to propagate signals at a lower elevation angle from the antenna to achieve propagation at longer distances. The radio users can determine the elevation angle φ to transmit the signal, as shown in Equation 2.54 and Equation 2.55.

$$\varphi = 90 - \theta \qquad \text{Equation 2.54}$$

$$\mathrm{MUF} = \mathrm{f_c}/\sin\varphi \qquad \text{Equation 2.55}$$

The other advantage of using MUF is that it reduces the effects of absorption on the signal strength, as mentioned in Section 2.3.1.2. This is because the MUF is significantly greater than the critical frequency of the ionospheric layer, as shown in Equation 2.53 and Equation 2.55. In addition, MUF is also significantly greater than the gyrofrequency of the electrons since MUF is within the HF range. This can reduce attenuation (Davies, 1965; McNamara, 1991).

2.4. High Frequency Propagation Paths

2.4.1. Introduction

In order to study radio propagation links from the WSPR dataset, as is the subject of this thesis, it is important to consider the known HF propagation paths through the ionosphere. Previous publications have used observations of HF data to investigate the effect of ionisation on radio propagation, such as (Carrara, De Giorgio and Pellegrini, 1970; McNamara *et al.*, 2008; Malik *et al.*, 2015). The most common HF propagation paths are daytime propagation, night-time propagation, greyline propagation, trans-equatorial propagation, great circle path, non-great circle path and round-the-world propagation.

Section 2.4.2. reviews the night-time and daytime propagation, while Section 2.4.3. gives a review on greyline propagation. The greyline is a terminator band that separates the part of the Earth lit up by the Sun from the night region. Greyline propagation is the radio propagation between two locations that are close to the terminator. Note that the term greyline propagation used in this chapter does not imply knowledge of the entire propagation path along the greyline terminator. It is simply defined as 'greyline' if the transmitter and receiver were located on or close to the greyline terminator. Section 2.4.4. reviews the great-circle path propagation followed by a review of the non-great circle path propagation in Section 2.4.5. The section will be concluded with a discussion on round-the-world propagation in section 2.4.6.

2.4.2. Daytime and night-time propagation

As discussed in Section 2.2, the structure of the ionosphere is strongly influenced by solar radiation. This means that the ionosphere in the daytime differs from that at night, such as the variations in the D, E, and F layers (Davies, 1965; McNamara, 1991; Hargreaves, 1992). It also affects the regions' ion production processes, giving rise to diurnal variations in the plasma and electron density, which consequently results in distinct daytime and night-time propagations. Since the plasma density is not homogenous across geographical regions, this also means that the diurnal propagation variations are differentiated by geographical position. (Davies, 1965; McNamara, 1991; Hargreaves, 1992).

There are two main characteristics of daytime propagation. First, HF communication during the daytime requires higher radio frequencies. This is because the daytime ionosphere has a higher plasma density than that at night due to the presence of solar radiation. This increases the critical frequency of the ionosphere, which in turn necessitates a higher transmission frequency to enable the signal to propagate into the ionosphere. Second, daytime propagation is often limited to short distances. This is because, as mentioned in Section 2.2. the daytime ionosphere has a lower ionospheric

height than in night-time, and as a result, the signals are reflected at lower ionospheric heights (Davies, 1965; McNamara, 1991; Hargreaves, 1992).

In contrast to the daytime, since the night-time ionosphere has a lower plasma density, the critical frequency decreases (Hargreaves, 1992), and HF communication can be achieved with lower frequencies. In addition, the night-time ionosphere has a higher ionospheric peak height than in the daytime. As a result, the signals can often propagate over longer distances than during daytime (Hargreaves, 1992). Signals propagating during the night also suffer less absorption, as ion production is at its minimum and the layer D-layer is absent during this time. For these reasons, night-time propagation enhances long-distance radio communication and enables the use of a wider range of frequencies for HF communication (Hargreaves, 1992).

2.4.3. Greyline propagation

Greyline propagation has been noted in various different forms for almost a century. For example an early reference from the Amateur Wireless magazine (1924) notes the propagation on wavelengths of 80 m and 95 m between the UK and New Zealand to be "*best between 6.30 am and 7 am*", and note this is thought to be "*because of the overlap of dawn and dusk*."(*Amateur Wireless and Electrics, Vol V. No. 126*, 1924).

It was more recently identified clearly by Hoppe (1975). Nichols, (2005) and a recent publication from Callaway (2016) has further strengthened these findings, confirming that ionisation along the terminators enhances the HF propagation. This is known as greyline propagation (Callaway, 2016), and is defined as radio propagation between two locations that lie along the terminator. This means that the dawn on one location will be the dusk on the other location. For example, radio propagation between the UK and New Zealand is classified as greyline propagation because the UK and New Zealand lay on the terminator. This is shown in Figure 2.6.

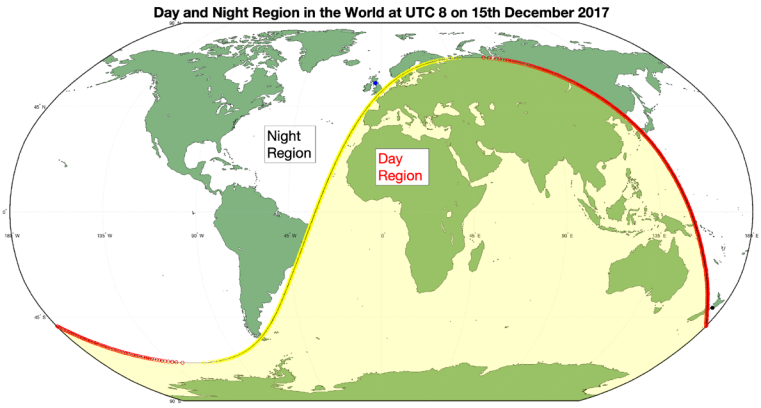

Figure 2.6 – Day and night region across the world at 8 UTC on 15th December 2017, with the sunrise terminator in yellow and the sunset terminator in red. The shaded region is the day region. The blue dot indicates the chosen location in the United Kingdom, and the black dot indicates the chosen location in New Zealand.

It must be noted that there are various propagation paths, which can be classified as greyline propagation. This is because greyline propagation simply defines radio propagation between two radio stations that are located along the same terminator, in other words, the 'greyline' radio stations. Nevertheless, it is possible that the links can be propagated in multiple paths, such as the true greyline propagation path. The true greyline propagation path means that the signal is propagating along the terminator (Nichols, 2005). This is possible for the 'greyline' stations where the local sunrise or the local sunset hours are located along the same terminator. The true greyline propagation is shown in Figure 2.7.

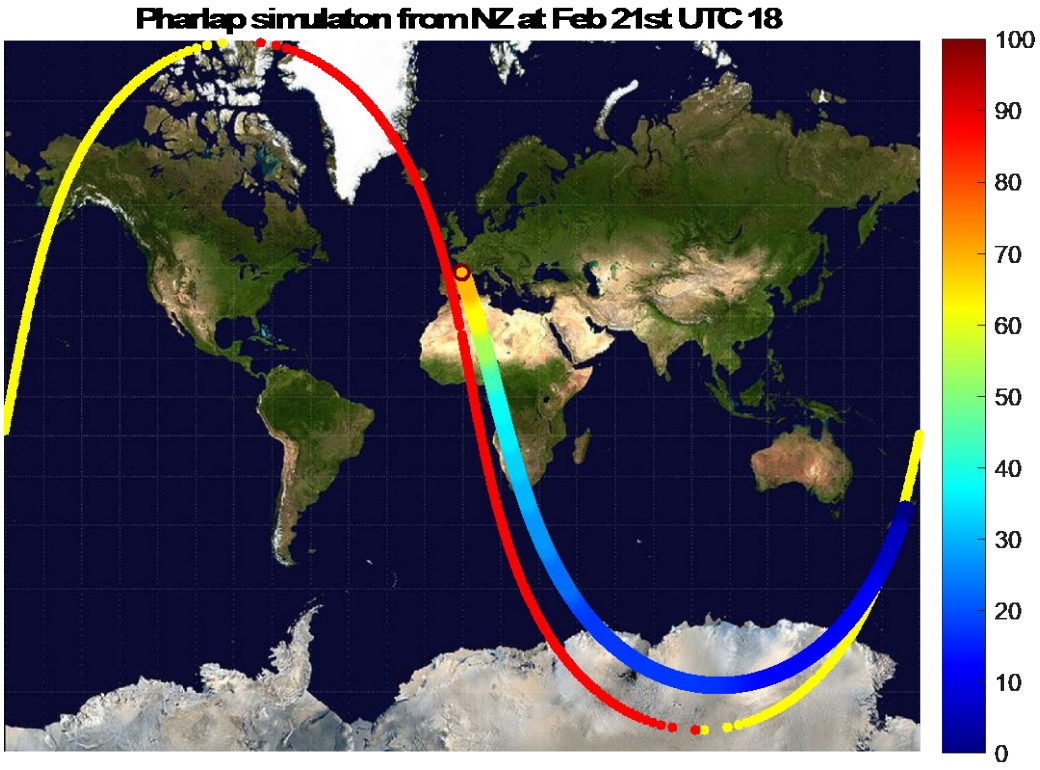

Figure 2.7 – A simulation of the true greyline propagation from New Zealand to the UK in the ray-tracing software PHaRLAP described in Chapter 3. The yellow solid line is the sunrise hours, the red solid line is the sunset hours, and the colorbar is the signal absorption along the path in dB.

The other likely greyline propagation path is through the night ionosphere, as the plasma density on the night side is significantly lower than that on the day side. This is shown in Figure 2.8.

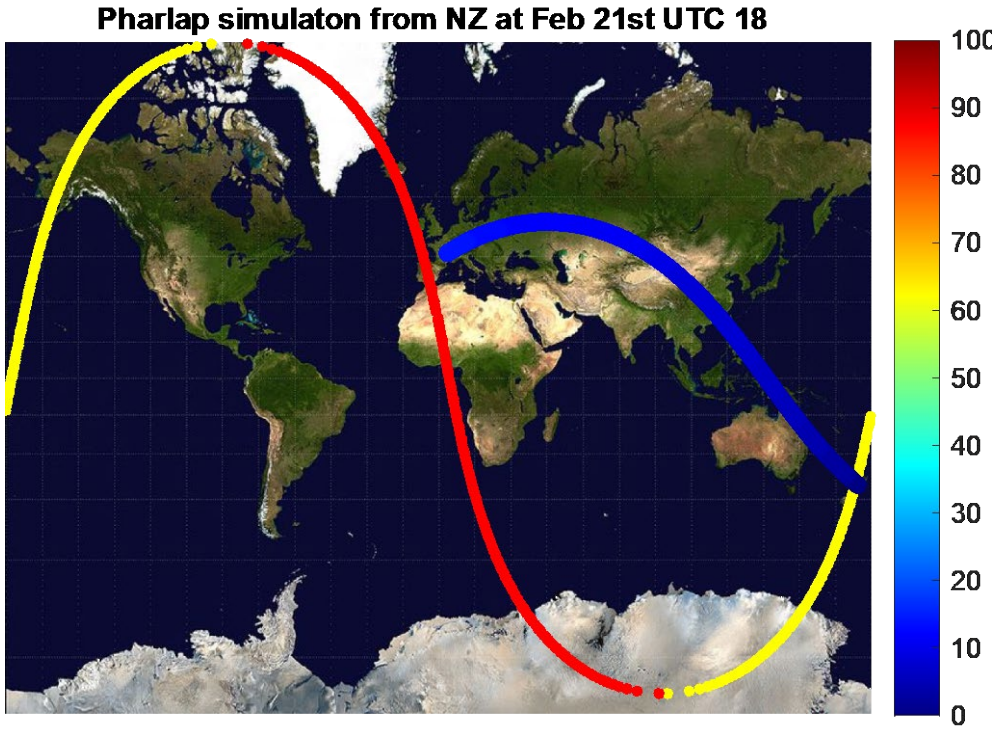

Figure 2.8 – A simulation of the greyline propagation from New Zealand to the UK through the night ionosphere in the ray-tracing software PHaRLAP described in Chapter 3. The yellow solid line is the sunrise hours, the red solid line is the sunset hours, and the colorbar is the signal absorption along the path in dB.

Figure 2.6 shows the geographical positions of the UK and New Zealand. They both lie on the terminator, and therefore it is possible for HF signals to travel along this terminator via greyline propagation. Since the UK and New Zealand are on opposite sides of the geographic and geomagnetic equator, this means a signal travelling via greyline propagation crosses both these equators. Propagation across the geomagnetic equator is known as Trans-Equatorial Propagation (TEP) and is discussed in the following sub-section.

2.4.4. Trans-Equatorial Propagation (TEP)

TEP was first addressed by radio amateurs (Tilton, 1947, 1957) when the signals were made from stations across the equator using frequencies in the Very High-Frequency (VHF) band. It was then observed with HF signals by Kelleher and Röttger (1973). The properties of TEP are dependent on the characteristics of the ionosphere in the equatorial region (McNamara, 1991). This is because HF propagation in the equatorial region is influenced by the equatorial anomaly and the variations in the plasma density, causing strong refraction and diffraction of radio signals. The effect is mostly developed in the afternoon and in the evening (post-sunset) and around the geomagnetic equator. These afternoon TEP (aTEP) and evening TEP (eTEP) are well-known propagation mechanisms, that have been observed to have different effects on HF propagation. The main differences between aTEP and eTEP are the path lengths and their effects on the signal's strength. A signal in the mode known as aTEP propagates through the equatorial anomalies on either side of the geomagnetic

equator (Harrison, 1972a, 1972b; McNamara, 1991; Harrison, 2007a). The propagation mode is known as a 'chordal hop', as the signal is reflected in the F-layer twice without a ground reflection. For this reason, aTEP is also known as 'super-mode' propagation, and it supports propagation in a skip distance of more than 6000 km while causing low signal loss (Harrison, 1972a, 1972b, 2007a).

In contrast, a signal in the mode known as eTEP propagates through 'guided' propagation along the magnetic field lines, as it propagates through the ionospheric phenomenon called field-aligned 'bubbles' (McNamara, 1991; Harrison, 2007b). These are areas of depleted ionisation developed across the equator (McNamara, 1991; Harrison, 2007b) eTEP supports propagation over distances between 3000 km and 6000 km with large signal losses (McNamara, 1991; Harrison, 2007b) as the 'guided' propagation path is shifted along the magnetic field lines causing Doppler shift. For example, if the 'guided' propagation path is shifted upwards due to the magnetic field, then eTEP will be propagated in shorter distances as the skip distance between the transmitter and the receiver is decreased (McNamara, 1991; Harrison, 2007b). In addition, the Doppler shift results in a strong signal fading, resulting in large signal losses (McNamara, 1991; Harrison, 2007b).

Both aTEP and eTEP are unpredictable because the equatorial anomaly is variable day to day. It is, therefore, important to understand the characteristics of TEP to improve HF communications propagating across the equatorial region by better utilising the ionospheric link that enhances HF propagation, such as greyline propagation.

2.4.5. Great Circle Path

As mentioned before, greyline propagation is propagation between radio stations that are located along the terminator. If the radio stations are located in the mid-latitude regions in both the north and south hemispheres, then the signal propagates across the equator, considered a TEP. However, it is also possible that radio signals propagating along the mid-latitude region, and across the equator will propagate through the shortest path called the Great Circle Path (GCP). This is because the propagating distance can reduce the effect of absorption along the path when the links are propagated at the appropriate time of day, such as propagating in the night-time ionosphere, or propagating along the terminator. For example, the UK and New Zealand are closely located to their antipodal points, as shown in Figure 2.9. The example of propagation between the UK and New Zealand indicates that the terminator path is through an auroral region.

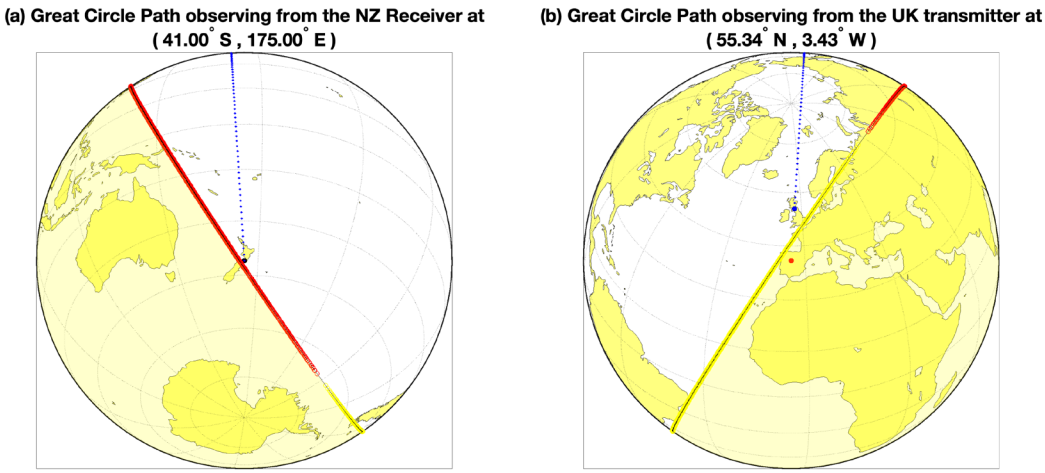

Figure 2.9 – The antipodal map observing between (a) New Zealand and (b) the UK. The yellow shade indicates the day region, and the white shade indicates the night region. The yellow line indicates the sunrise hours, and the red line indicates the sunset hours. The dotted blue line is the great circle path between New Zealand and the UK.

Figure 2.9 shows that the terminator path propagating between the UK and New Zealand is across the geographic polar region. However, since the UK and New Zealand are close to their respective antipodal points, there are many 'close to great circle' paths of similar distance that can connect them. Therefore, it is not straightforward to say that a great circle path between these locations is necessarily passing through the auroral or the polar ionosphere. There are many paths with similar distances that will pass through different ionospheric regions.

2.4.6. Non-Great Circle Path

Different ionospheric dynamics/disturbances can cause a signal to deviate from the great circle path, resulting in a propagation known as a non-great circle path (McNamara, 1991). Possible causes of a non-great circle path include scattering, signal reflection, deviations due to horizontal magnetic fields (McNamara, 1991), the ionospheric anomalies, such as geomagnetic variations and equatorial anomaly, which are mentioned in Section 2.2.4. (Jones and Reynolds, 1975). The deviation of the propagation path from the GCP can increase the path length between the locations. This needs to be considered when transmitting an HF radio signal, as the ionospheric phenomena along the path can degrade the signal.

2.4.7. Round-the-World Propagation

Round-The-World (RTW) propagation is where the signal travels around the world and reappears at an azimuth angle opposite to the transmitted azimuth (i.e. 180° from the original azimuth angle (McNamara, 1991)). Greyline propagation is not always

considered as RTW propagation, since ‘greyline’ simply means that the signals are propagated between locations close to the terminator line, and the great circle path between them is not always considered as RTW propagation. Nevertheless, it is possible that RTW propagation is considered as greyline propagation because the signals can be propagated from a ‘greyline’ transmitter to a ‘greyline’ receiver through RTW propagation. (McNamara, 1991) RTW propagation has been investigated by numerous researchers, such as Quaeck (1927), Fenwick (1963), Rumi (1975), and Gurevich and Tsedilina (1985).

2.5. Summary

The ionosphere acts as a dispersive medium for radio signals that propagate the region. For HF, this causes the signals to be refracted by the ionosphere (Davies, 1965; Hargreaves, 1992) as the refractive index impacts the propagating signal according to its operational frequency (Hargreaves, 1992).

Section 2.2 of this chapter gave an overview of the ionosphere, where the structure of the stratified layers and chemical processes of forming the plasma in the ionosphere were discussed. The ionosphere is not a static medium, and any variations and dynamics can affect radio signals, particularly those that are propagating over long distances. As long-distance propagation can span thousands of kilometres, the signals can encounter different ionospheric irregularities/anomalies that can disrupt the signals. As the chapter discussed, the main variations that are of concern to the work of this thesis are Sporadic-E, F region anomaly, geomagnetic variations and equatorial anomaly.

Section 2.3 introduced the Appleton-Hartree equation, which describes the refractive index for electromagnetic signals in a cold magnetised plasma. The equation showed that an electromagnetic signal will refract and attenuate as it travels through the ionosphere, depending on the plasma frequency (derived from the plasma density), signal frequency, the geomagnetic field (both strength and orientation) and the collision frequency. Signal attenuation through absorption can be non-deviative and deviative, based on the refractive indices of the ionospheric layers. Both types of absorption are a function of the signal frequency, with higher frequencies experiencing less attenuation.

HF signals propagating through the ionosphere can take many different paths to their destination, based on the conditions of the ionosphere. A particularly important path for HF communication is thought to be greyline propagation, which is the path that propagates along the terminator for the case of true greyline propagation.

The next chapter will introduce the main HF dataset studied in this thesis – the Weak Signal Propagation Report (WSPR) data – and the ray-tracing software used to analyse HF propagation – PHaRLAP.

3. WSPR Data and Simulation in PHaRLAP

3.1 Introduction

There are various methods to study the properties of the ionosphere using instruments and simulations. In this thesis, both experimental (from instruments) and simulation data are used together to study HF propagation in the ionosphere.

The Weak Signal Propagation Reporter (WSPR) network is used as the main data source, while simulation analysis is carried out using a ray-tracing software called PHaRLaP. WSPR, developed by Prof Joe Taylor (Taylor, 2019) and in operation since 2008, is a radio propagation protocol used to create an HF communication network between radio amateurs. PHaRLaP was developed by Dr Manuel Cervera in 2014 (Cervera and Harris, 2014) and is used to predict and study HF propagation. The International Reference Ionosphere (IRI) empirical model from 2016 is used to describe the ionosphere in the software. This chapter provides an overview of both these investigation methods.

The contents of this chapter are structured as follows: Section 3.1 discusses the WSPR network in detail, where it describes the WSPR system, the method to extract the WSPR data to study propagation, and the impact of the stations' activity on the WSPR data. In addition, the opportunities and challenges of using the WSPR network will also be addressed. Section 3.2 discusses the PHaRLaP software and its application to study HF propagation. Finally, the theory of analysing the simulations through PHaRLAP will be addressed, and it will be used to analyse the WSPR results.

3.2. WSPR

3.2.1. Introduction

The HF signals can be encoded in various modulation methods, such as WSPR, Phase Shift Keying (PSK) Reporter and Dial method. The purpose of modulation is to encode the information on the HF signals, such as the transmitters and receivers' callsigns, locations, signal strength, and operational frequency. When a receiver intercepts the HF signal, the receiver will demodulate and decode the signals to extract the information from the carrier wave. The information can then be used to study HF propagation.

The Weak Signal Propagation Reporter (WSPR) system is a radio communications protocol made by Professor Joe Taylor (radio callsign K1JT) (Taylor, 2019). It enables low-power radio communication links between amateur radio stations in many frequency bands, ranged between 1.83 MHz and 144 MHz (Taylor, 2019). Since WSPR can be used by radio amateurs globally, it has resulted in a network of WSPR users and an extensive database containing all radio propagation records between any two radio stations in the WSPR network. In addition, radio stations users who have internet access can report their decoded WSPR data into the WSPR database, which can be accessed on the WSPR website (WSPRnet).

One main advantage of WSPR is that it was developed for use by radio amateurs. It requires a simple setup and cheap antenna technology for achieving successful radio propagations. Licenses for amateur radio communication can also be obtained relatively easily in many countries, enabling radio amateurs to contribute to the WSPR database globally. Although it has some limitations and challenges (discussed in Section 3.2.8.), it is still regarded as a valuable recent dataset for ionospheric research purposes. Since the WSPR network is formed of amateur radio users, it is based on protocols used in amateur radio communications.

3.2.2. Amateur Radio Communication

Amateur radio communicators are identified using a radio callsign, which is a radio license number provided by the telecommunication authorities. The radio callsign contains a prefix, a separating number and a suffix (Radio Society of Great Britain, 2014). The prefix of a radio callsign is assigned by the International Telecommunication Union (ITU) to identify the region or the country's radio society. The separating number of the callsign is used to separate the callsign's prefix and the callsign's suffix, which represents the user. The radio callsign 'ZL1EE' shall be used as an example to identify the location and the user of the radio station. The prefix 'ZL' represents that the radio station is from New Zealand. The number '1' is used to separate the prefix and the suffix of the callsign. Finally, the suffix 'EE' represents the user.

Radio callsigns will be used to identify the data relevant to this study. The WSPR database is made up of radio stations that are represented by their radio callsigns. For example, the radio callsigns prefixes in the United Kingdom and New Zealand are shown in Table 3.1.

Table 3.1 - The radio callsign prefixes in the regions of interest

Location	Callsign Prefix
United Kingdom	2E, G, M
Wales	2W, GW, MW
Scotland	2M, GM, MM
Guernsey	2U, GU, MU
Jersey	2J, GJ, MJ
Isle of Man	2D, GD, MD
Northern Ireland	2I, GI, MI
New Zealand	ZL
Australia	VK
United States	A, K, N, W
Europe	CT1, DL, I, EA, ES, F, HA, HB, LA, LY, LZ, OE, OH, OK, OM, ON, OZ, PA, SM, SP, SV, TA, UA, UR, YO, YU

Table 3.1 also lists the callsign prefixes assigned to Australia, Europe, and the USA. These callsigns will be used for the WSPR data analysis in Chapter 4.

3.2.3. The WSPR System

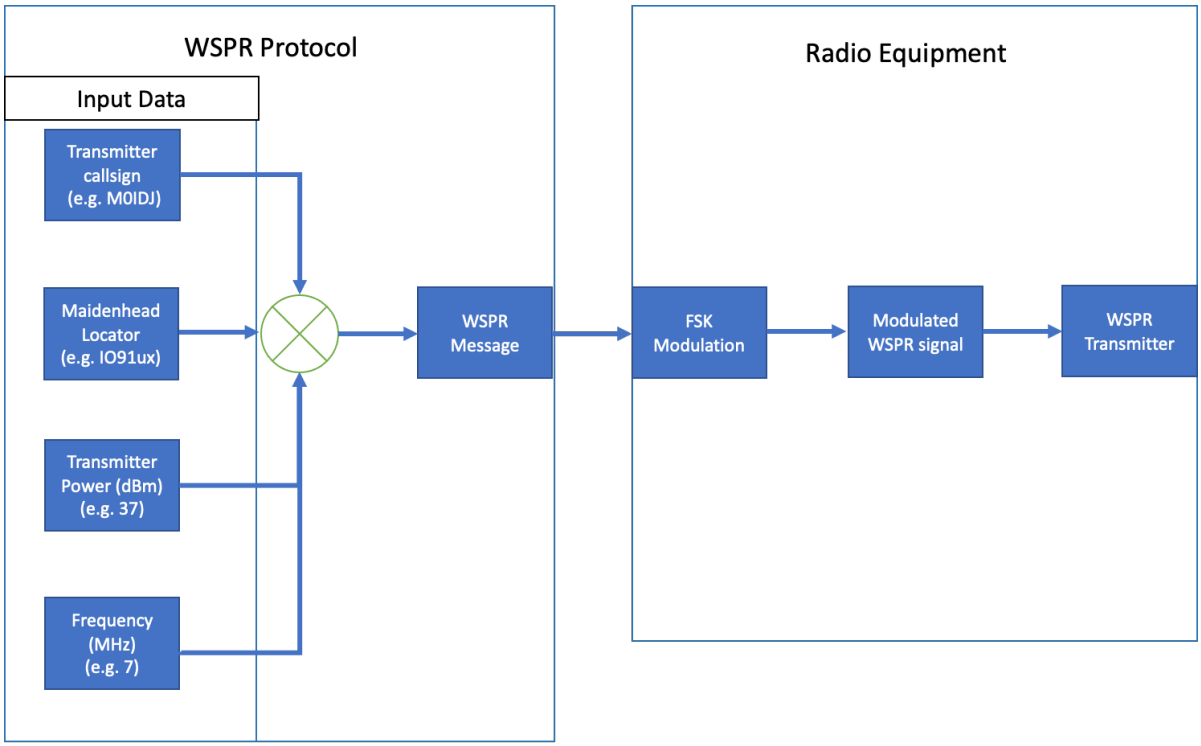

Figure 3.1 – WSPR System Block Diagram. In this project, the propagation of interest is through the ionosphere. However, Other modes of propagation may also be supported by WSPR.

Figure 3.1 shows the system block diagram for HF communication with WSPR. First, the WSPR Protocol encodes the information – the transmitter callsign, Maidenhead locator (location), frequency (MHz) and the transmitter power (dBm) – into a carrier signal using Frequency Shift Keying (FSK). After that, the carrier signal is input to the WSPR transmitter. The WSPR transmitter then sends the HF signal into the transmitter antenna, which transmits the signal.

The HF signal may then propagate through the ionosphere to a receiver via ionospheric propagation. A receiver antenna intercepts the HF signal. It will then be sent into the WSPR receiver to demodulate the HF signal and extract the WSPR message. This information can then be shared and stored in the WSPR database through an Internet connection. Table 3.2 shows an example of radio link information that can be obtained from the database.

Table 3.2 – Example of a WSPR link in the WSPR database

Spot ID	Timestamp	Reporter	Reporter's Grid	SNR	Frequency (MHz)
736696460	1488778440	'G3ZIL'	'IO90hw'	-25	7.040102

…

Call Sign	Grid	Power	Drift	Distance	Azimuth
'ZL3PX'	'RE66hm'	47	-1	19071	334

…

Band	Version	Code
7	'1.7.0-rc1'	0

3.2.3.1. Radio stations' locations in WSPR

The WSPR protocol requires radio stations to transmit their locations using the Maidenhead grid locator projected onto the Mercator projection map. The Maidenhead grid locator is a cartesian coordinate system that identifies a radio station's location anywhere in the world using six characters. It first divides the world into an 18-by-18 grid of fields, with each field spanning 20° in longitude and 10° in latitude. Next, the fields are represented in an alphabetical order 'A' to 'R', first from the west to the east (longitude) and then from the south to the north (latitude), as shown in Table 3.3 (Bruce Paige, 2000). Thus, for example, the first two characters, 'IO', cover the latitudes and longitudes, covering most of the UK. Likewise, the first two characters, 'RF' in Table 3.3, cover the latitudes and longitudes covering the North Island of New Zealand (Bruce Paige, 2000).

Table 3.3 – 1st and 2nd character of the Global Maidenhead locator Grid

AR	BR	CR	DR	ER	FR	GR	HR	IR	JR	KR	LR	MR	NR	OR	PR	QR	RR
AQ	BQ	CQ	DQ	EQ	FQ	GQ	HQ	IQ	JQ	KQ	LQ	MQ	NQ	OQ	PQ	QQ	RQ
AP	BP	CP	DP	EP	FP	GP	HP	IP	JP	KP	LP	MP	NP	OP	PP	QP	RP
AO	BO	CO	DO	EO	FO	GO	HO	IO	JO	KO	LO	MO	NO	OO	PO	QO	RO
AN	BN	CN	DN	EN	FN	GN	HN	IN	JN	KN	LN	MN	NN	ON	PN	QN	RN
AM	BM	CM	DM	EM	FM	GM	HM	IM	JM	KM	LM	MM	NM	OM	PM	QM	RM
AL	BL	CL	DL	EL	FL	GL	HL	IL	JL	KL	LL	ML	NL	OL	PL	QL	RL
AK	BK	CK	DK	EK	FK	GK	HK	IK	JK	KK	LK	MK	NK	OK	PK	QK	RK
AJ	BJ	CJ	DJ	EJ	FJ	GJ	HJ	IJ	JJ	KJ	LJ	MJ	NJ	OJ	PJ	QJ	RJ
AI	BI	CI	DI	EI	FI	GI	HI	II	JI	KI	LI	MI	NI	OI	PI	QI	RI
AH	BH	CH	DH	EH	FH	GH	HH	IH	JH	KH	LH	MH	NH	OH	PH	QH	RH
AG	BG	CG	DG	EG	FG	GG	HG	IG	JG	KG	LG	MG	NG	OG	PG	QG	RG
AF	BF	CF	DF	EF	FF	GF	HF	IF	JF	KF	LF	MF	NF	OF	PF	QF	RF
AE	BE	CE	DE	EE	FE	GE	HE	IE	JE	KE	LE	ME	NE	OE	PE	QE	RE
AD	BD	CD	DD	ED	FD	GD	HD	ID	JD	KD	LD	MD	ND	OD	PD	QD	RD
AC	BC	CC	DC	EC	FC	GC	HC	IC	JC	KC	LC	MC	NC	OC	PC	QC	RC
AB	BB	CB	DB	EB	FB	GB	HB	IB	JB	KB	LB	MB	NB	OB	PB	QB	RB
AA	BA	CA	DA	EA	FA	GA	HA	IA	JA	KA	LA	MA	NA	OA	PA	QA	RA

Each field is divided into a grid of 100 cells with an area of 2°-by-1° in longitude and latitude, respectively. The squares are represented by the third and fourth characters of the six-character locator, spanning from 0 - 99. The cell's grid for a given field is shown in Table 3.4.

Table 3.4 – Grid Locator System in the Maidenhead Locator System for the 3rd and the 4th character(Bruce Paige, 2000; Folke Rosvall, 2019; Karhu Koti LLC, 2019)

09	19	29	39	49	59	69	79	89	99
08	18	28	38	48	58	68	78	88	98
07	17	27	37	47	57	67	77	87	97
06	16	26	36	46	56	66	76	86	96
05	15	25	35	45	55	65	75	85	95
04	14	24	34	44	54	64	74	84	94
03	13	23	33	43	53	63	73	83	93
02	12	22	32	42	52	62	72	82	92
01	11	21	31	41	51	61	71	81	91
00	10	20	30	40	50	60	70	80	90

The last two characters of the locators represent a sub-cell within a cell listed in Table 3.4. Each sub-cell represents a region of 5′-by-2.5′ (minutes) in longitude and latitude. They are encoded in alphabetical order and in a base of 24; in other words, they are encoded from 'a' to 'x'. The characters are formatted in the same order as in Table 3.4. The locator grids for the last two characters are listed in Table 3.5 ('aa' to 'xl') and Table 3.6 ('am' to 'xx'). An example of the locator is represented in Table 3.2. For example, the locator 'RE66hm' confirms that the location is in New Zealand (Bruce Paige, 2000). The first two characters, 'RE', represent the longitudes ('R') and the latitudes ('E') of the grid, covering the North Island of New Zealand. The following two numbers, '66', represent the cell within the field 'RE'. The last two characters of the locator are 'hm', representing the sub-square within the 66th cell of the field 'RE'.

Table 3.5 – Maidenhead Grid Locator for the last two characters (‘am’ to ‘xx’)

ax	bx	cx	dx	ex	fx	gx	hx	ix	jx	kx	lx	mx	nx	ox	px	qx	rx	sx	tx	ux	vx	wx	xx
aw	bw	cw	dw	ew	fw	gw	hw	iw	jw	kw	lw	mw	nw	ow	pw	qw	rw	sw	tw	uw	vw	ww	xw
av	bv	cv	dv	ev	fv	gv	hv	iv	jv	kv	lv	mv	nv	ov	pv	qv	rv	sv	tv	uv	vv	wv	xv
au	bu	cu	du	eu	fu	gu	hu	iu	ju	ku	lu	mu	nu	ou	pu	qu	ru	su	tu	uu	vu	wu	xu
at	bt	ct	dt	et	ft	gt	ht	it	jt	kt	lt	mt	nt	ot	pt	qt	rt	st	tt	ut	vt	wt	xt
as	bs	cs	ds	es	fs	gs	hs	is	js	ks	ls	ms	ns	os	ps	qs	rs	ss	ts	us	vs	ws	xs
ar	br	cr	dr	er	fr	gr	hr	ir	jr	kr	lr	mr	nr	or	pr	qr	rr	sr	tr	ur	vr	wr	xr
aq	bq	cq	dq	eq	fq	gq	hq	iq	jq	kq	lq	mq	nq	oq	pq	qq	rq	sq	tq	uq	vq	wq	xq
ap	bp	cp	dp	ep	fp	gp	hp	ip	jp	kp	lp	mp	np	op	pp	qp	rp	sp	tp	up	vp	wp	xp
ao	bo	co	do	eo	fo	go	ho	io	jo	ko	lo	mo	no	oo	po	qo	ro	so	to	uo	vo	wo	xo
an	bn	cn	dn	en	fn	gn	hn	in	jn	kn	ln	mn	nn	on	pn	qn	rn	sn	tn	un	vn	wn	xn
am	bm	cm	dm	em	fm	gm	hm	im	jm	km	lm	mm	nm	om	pm	qm	rm	sm	tm	um	vm	wm	xm

Table 3.6 – Maidenhead Grid Locator for the last two characters (‘aa’ to ‘xl’)

al	bl	cl	dl	el	fl	gl	hl	il	jl	kl	ll	ml	nl	ol	pl	ql	rl	sl	tl	ul	vl	wl	xl
ak	bk	ck	dk	ek	fk	gk	hk	ik	jk	kk	lk	mk	nk	ok	pk	qk	rk	sk	tk	uk	vk	wk	xk
aj	bj	cj	dj	ej	fj	gj	hj	ij	jj	kj	lj	mj	nj	oj	pj	qj	rj	sj	tj	uj	vj	wj	xj
ai	bi	ci	di	ei	fi	gi	hi	ii	ji	ki	li	mi	ni	oi	pi	qi	ri	si	ti	ui	vi	wi	xi
ah	bh	ch	dh	eh	fh	gh	hh	ih	jh	kh	lh	mh	nh	oh	ph	qh	rh	sh	th	uh	vh	wh	xh
ag	bg	cg	dg	eg	fg	gg	hg	ig	jg	kg	lg	mg	ng	og	pg	qg	rg	sg	tg	ug	vg	wg	xg
af	bf	cf	df	ef	ff	gf	hf	if	jf	kf	lf	mf	nf	of	pf	qf	rf	sf	tf	uf	vf	wf	xf
ae	be	ce	de	ee	fe	ge	he	ie	je	ke	le	me	ne	oe	pe	qe	re	se	te	ue	ve	we	xe
ad	bd	cd	dd	ed	fd	gd	hd	id	jd	kd	ld	md	nd	od	pd	qd	rd	sd	td	ud	vd	wd	xd
ac	bc	cc	dc	ec	fc	gc	hc	ic	jc	kc	lc	mc	nc	oc	pc	qc	rc	sc	tc	uc	vc	wc	xc
ab	bb	cb	db	eb	fb	gb	hb	ib	jb	kb	lb	mb	nb	ob	pb	qb	rb	sb	tb	ub	vb	wb	xb
aa	ba	ca	da	ea	fa	ga	ha	ia	ja	ka	la	ma	na	oa	pa	qa	ra	sa	ta	ua	va	wa	xa

In order to select the relevant data for this thesis, records of interest were identified in the WSPR files first by filtering the transmitter and the receiver columns' information to select appropriate call prefixes. This identification is made to extract the data for the area of interests, such as the UK, the USA, New Zealand, Europe, and Australia. Then, the filtered data is stored in a CSV file and searched to find successful transmission links between the desired locations. For example, the Maidenhead locator prefixes show that the starting characters for the UK locations are 'IO' and 'JO', as shown in Table 3.7.

Table 3.7 - Maidenhead Locators Starting Prefixes of the Locations

Locations	**Maidenhead Locator Starting Prefixes**
The UK	IO, JO
The USA	CN, DN, EN, FN, CM, DM, EM, FN
New Zealand	RE, RF
Europe	IN, JN, KN, IM, JM, KM, IO, JO, KO, IP, JP, KP
Australia	OH, PH, QH, OG, PG, QG, OF, PF, QF QE

3.2.3.2. Frequency Bands

The WSPR protocol is used across a range of frequencies, in particular, Low Frequency (LF), High Frequency (HF) and Very High Frequency (VHF) ranges. There are distinct bands within each range of frequency with an allocated dial frequency for use by the WSPR protocol. These dial frequencies are dedicated to the 'ham' amateur radio users who have the WSPR software. Table 3.8 shows the frequency band plans for the radio amateur users who have the UK radio license, including the HF frequency bands. The HF bands in WSPR range between 3.5 MHz and 28 MHz. The work in this thesis will investigate the propagation effects on 7 MHz signals.

Table 3.8 – Frequency band plans in the United Kingdom radio license

Frequency Category	UK Frequency Band Plan (MHz)	Frequency Band (MHz)	WSPR Dial Frequency (MHz)
LF	1.843 – 2	1.8	1.8366
HF	3.59 – 3.62	3.5	3.5926
	5.288 – 5.292	5	5.2872
	7 – 7.04	7	7.0386
	10.13 – 10.15	10	10.1387
	14.089 – 14.099	14	14.0956
	18.1095 – 18.109	18	18.1046
	21.09 – 21.11	21	21.0946
	24.915 – 24.929	24	24.9246
	28.12 – 28.15	28	28.1246
VHF	50.2 – 50.3	50	50.293
	144.4 – 144.49	144	144.4885

3.2.4. WSPR Signal Transmission

Andy Talbot (callsign G4JNT), an amateur radio hobbyist, developed information to help explain how the WSPR symbols were generated (Talbot, 2009). The WSPR signal is formed of a message carrying the callsign, locator, frequency and transmitter power input by the user, which is encoded using the WSPR protocol. The encoded signal is a 162-bit WSPR message, which is then modulated onto the HF (or other) carrier signal using Frequency Shift Keying (FSK) modulation. The FSK modulation is toned at 1.46 baud, which is 1.46 Hz from the centre frequency, to modulate and encode the message to the carrier signal. The length of the encoded signal is 162 bits taking the FSK modulation process 120 seconds to complete a WSPR message. This length ensures that there is time for error correction before the WSPR message is modulated into the carrier signal. Therefore, the message will be sent every 2 minutes, recorded in UTC time. The relevant block diagram that describes the signal transmission is shown in Figure 3.2.

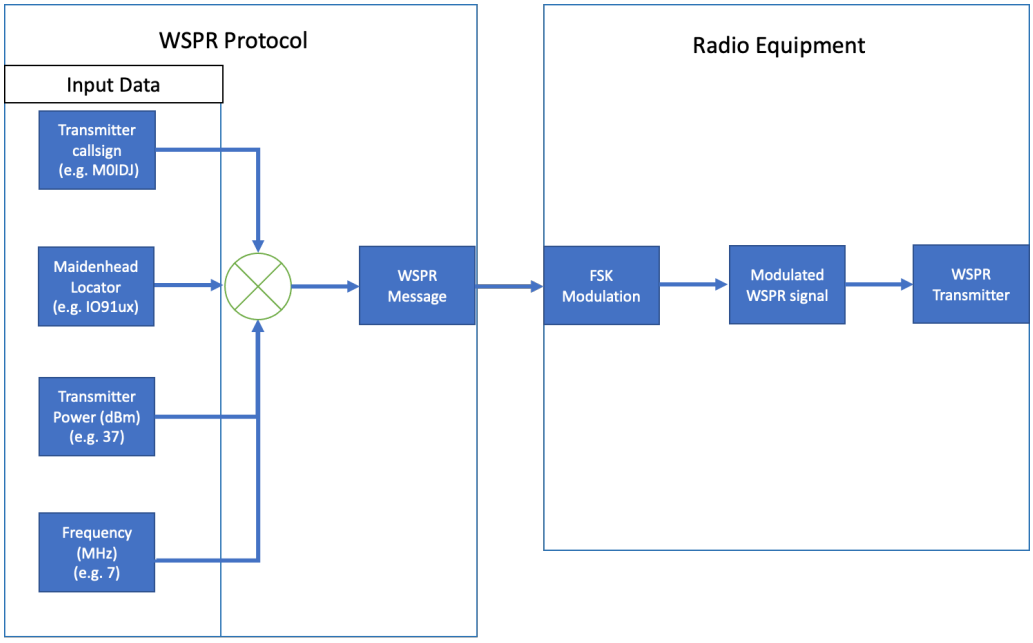

Figure 3.2 – WSPR Transmitter block diagram

3.2.5. WSPR Signal Reception

The WSPR Receiver System has an antenna, a radio receiver, and the WSPR protocol software in a computer, as shown in Figure 3.3.

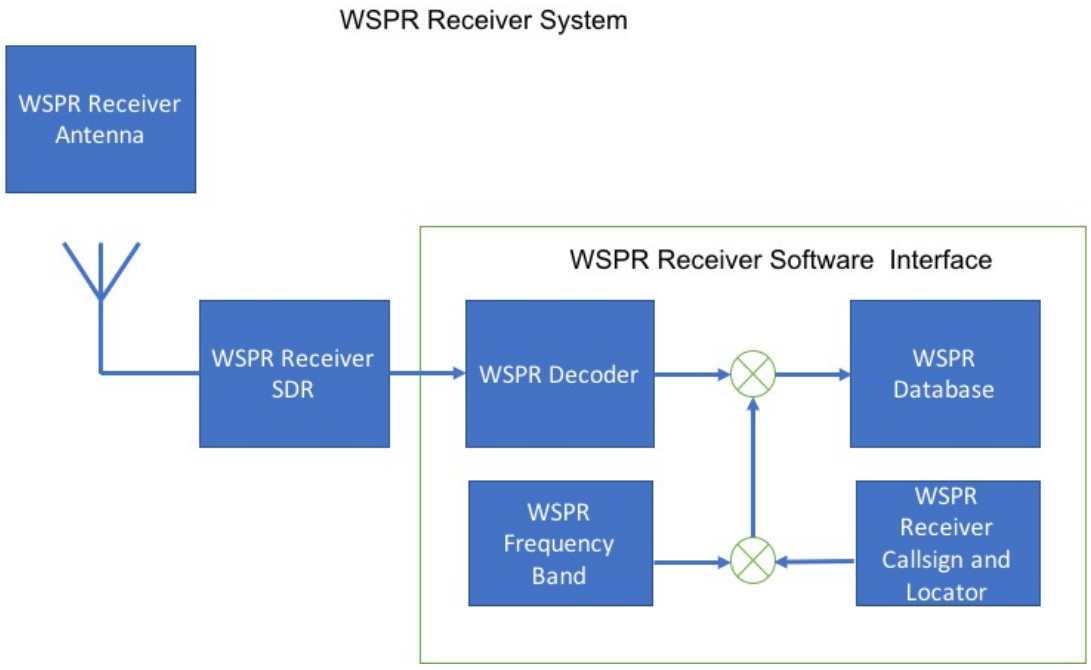

Figure 3.3 – WSPR receiver block diagram

3.2.5.1. The receiver antenna

The receiver antenna intercepts the HF (or another amateur) radio waves propagating in the atmosphere. Different antennas can be used for amateur radio communications, such as half-wave dipole antennas, quad antennas and Yagi-Uda antennas. Table 3.8 shows the frequency bands and the dial frequency of the WSPR signals. For example, the WSPR frequency bands have a dial frequency of 7.0386 MHz allocated to the 7 MHz HF frequency band. Therefore, the setup designed for receiving the data at 7 MHz must have an antenna capable of receiving signals around 7 MHz.

For example, a half-wave dipole antenna can be tuned to a frequency of 7 MHz for HF signal reception. The length of each leg of the dipole antenna can be calculated by taking a quarter of the signal's wavelength to be received. For 7 MHz (40m band) signal reception, this would result in the total length of the dipole is about 20 m (approximately 0.5 x speed of light divided by the radio frequency). The antenna can be made by using several thin copper conductors twisted together. The final antenna is determined according to Equation 3.1, where L is the length of the antenna leg in metres, c is the speed of light, and f is the operational frequency.

$$\mathrm{L\ (m)} = \frac{0.96 \times \mathrm{c}}{4\mathrm{f}} \qquad \text{Equation 3.1}$$

As the dipole requires the antenna wire legs to be straight, a nylon cord can be used to hold the antenna ends onto a supportive railing. An isolator is required to connect the wire end and the nylon cord, as it can increase the distance between this dipole antenna and other antennas, avoiding signal interference. It must be noted that although each conductor (leg) of the dipole needs to be a quarter-wavelength long, the actual antenna length would be shorter, as the total length includes the isolators at the wire ends.

While the dipole antenna has a structure symmetrical to the Earth, the coaxial cable does not. As a result, it contributes to an impedance mismatch, causing the receiver not to receive maximum receiver power. Therefore, the antenna requires a balance-to-unbalance transformer known as a balun at the dipole's feed point at the antenna's centre. A lightning arrester is also used in this dipole antenna to protect it by diverting sudden lightning charges to the ground. It must be connected to the balun and the receiver with the coaxial cables. The structure of the dipole antenna is illustrated in Figure 3.4

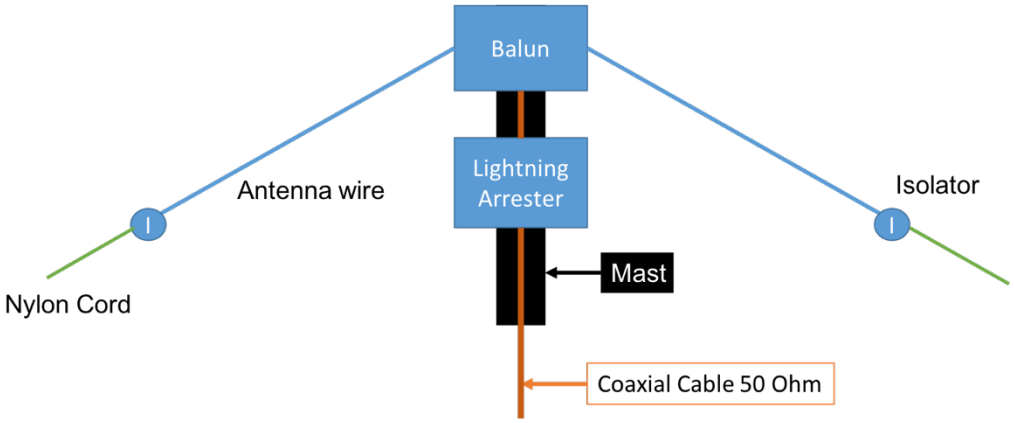

Figure 3.4 – Half-wave dipole antenna block diagram

3.2.5.2. WSPR Software-Defined-Radio (SDR) receiver

The receiver demodulates the signal to an audio signal encoded in FSK modulation. This encoded FSK signal is decoded in the WSPR receiver software, known as WSPR 2.0 or the WSJT-X software, to recover the data message sent from the transmitters. The data is then uploaded to the WSPRnet website via an Internet connection. The Internet connection is vital for the receiver module to report its signals from other transmitters. If the receiver's status is offline, then the receiver will not be able to report the signal into the WSPR database even if it is active. Therefore, the WSPR database will not be able to record the successful transmission.

The WSPR system requires a time accuracy of 2 seconds between the transmitter and the receiver, requiring time synchronisation of the WSPR receiver with a UTC clock. It is done through the Internet but can also be set more accurately using GPS timing. It is crucial to ensure that the Internet connection is secured and the time synchronisation in the computer is regularly updated.

The WSPR data recorded into the WSPR database is saved as a CSV file monthly. It gives the users an archive to download the CSV files to study desired propagation. In addition, all the WSPR data recorded in the database can be downloaded as a compressed ZIP file. The CSV file records the WSPR data in 15 columns, and each column represents the data that the WSPR protocol has decoded, as listed in Table 3.9.

Table 3.9 – WSPR data columns and the type of the recorded data

Column Number	Type of recorded data	Source
1	SpotID	Receiver
2	Timestamp	Receiver
3	Receiver's Callsign (Reporter)	Receiver
4	Receiver Location (Reporter Grid)	Receiver
5	SNR (dB) from the receiver	Receiver: Receiver power and Receiver noise
6	Frequency (MHz)	Transmitter
7	Transmitter Callsign (Call)	Transmitter
8	Transmitter Location (Transmitter Grid)	Transmitter
9	Power (dBm)	Transmitter
10	Drift	Receiver
11	Distance (km)	Receiver
12	Azimuth	Transmitter
13	Band	Transmitter
14	Version	Receiver
15	Code	Receiver

The WSPR observations can be shown in a live map to display the radio signals propagating between the transmitters and receivers in different frequency bands. For example, the 7 MHz WSPR propagation is shown in Figure 3.5 (a). Figure 3.5 (b) shows the WSPR radio signals received by a receiver with the callsign 'M0IDJ' over a specific region. Finally, Figure 3.5 (c) shows an example of the reception of signals in 'M0IDJ' in a two-week time window.

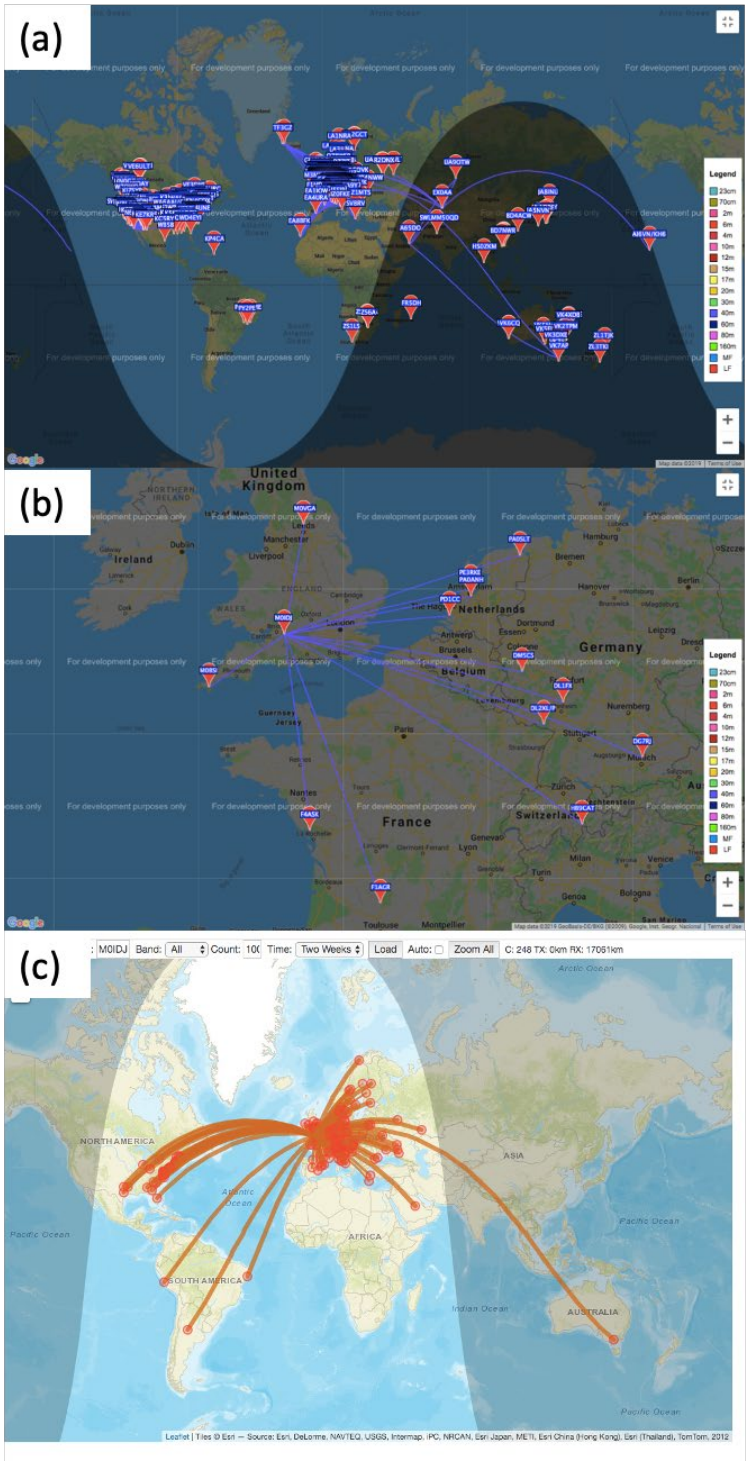

Figure 3.5 – (a) Example of the World Map with WSPR Radio Propagation at 7 MHz (40m band) (b) Examples of the WSPR Radio signals received the radio station with the callsign M0IDJ at 7 MHz (40m band) (c) Example of the WSPR signals received by the receiver with a callsign 'M0IDJ' from other radio transmitters. Note that this is a 2-week window with the signals received at the 7 MHz band.

The recorded azimuth angle represents the estimation of the direction of the propagating path from the WSPR transmitters. However, it does not represent the transmitter's actual propagating path to the receiver as the ionospheric conditions will affect the direction. The Signal-To-Noise Ratio (SNR) represents the SNR relative to

the receiver equipment; in other words, the SNR recorded by the receiver. The locator grids report the transmitters and receivers' locations in the Maidenhead Locator Grid format.

The reception of radio stations from different radio transmitters is dependent on the time of day/month/year and the transmitters' locations, as radio propagation is dependent on the effects of ionisation on the propagating path. Furthermore, as individual amateur radio users maintain the radio stations in the WSPR network, the setup configurations of the radio transmitters differ from each other. These configurations mean that the signal properties at transmission, such as the radiating direction from the transmitters and the transmitter power, will differ between stations. The setup configurations can be found in the QRZ (QRZ) database, accessed by the amateur radio users who registered for the 'ham' radio callsign. The QRZ will save the information that the amateur radio users have entered, such as the information of their radio equipment and antennas. For example, the receiver station set by the radio amateur with callsign M0IDJ has a half-wave dipole antenna and a software-defined radio (SDR). However, it must be noted that this database is not fully consistent, as entering this information is not mandatory and not every radio amateur has presented their data.

3.2.6. SNR Measurements in WSPR

For a communication link between two stations, the WSPR database records the transmitter power in dBm and the received Signal-to-Noise Ratio (SNR) in dB. However, while the transmitter power is a known value entered by the user, the SNR is measured and confirmed by the receiver equipment. For this reason, it is essential to understand how the SNR results are measured in WSPR. This section discusses the method WSPR uses to derive the SNR of the received signal.

SNR uses the link budget equation (Davies, 1965; Barclay & Bacon, 2013), as shown in Equation 3.2 where $\mathrm{P_t}$ is the transmitter power in dBm, $\mathrm{L_t}$ is the transmission loss, including the propagation loss and noise, in dB, and $\mathrm{P_n}$ is the noise power in the receiver measured in WSPR in dBm. Therefore, this calculation requires WSPR to measure the receiver signal and the receiver noise power to measure the SNR.

$$\mathrm{SNR\ (dB)} = \mathrm{P_t} - \mathrm{L_t} - \mathrm{P_n} \qquad \text{Equation 3.2}$$

The WSPR system measures the SNR by calculating the receiver power and the noise power within a 200 Hz bandwidth, searched by the WSPR decoder (Taylor, 2019). However, the WSPR protocol does not separately decode both the measured receiver power and the measured noise power in the WSPR database. Nevertheless, the signal monitoring software, such as the PowerSDR, can observe the signal strength through observing the spectrogram, as shown in Figure 3.6 and Figure 3.7. Furthermore, it enables WSPR to decode the signals that are above its SNR threshold at the receiver, which is around -30 dB. WSPR can then decode signals into messages.

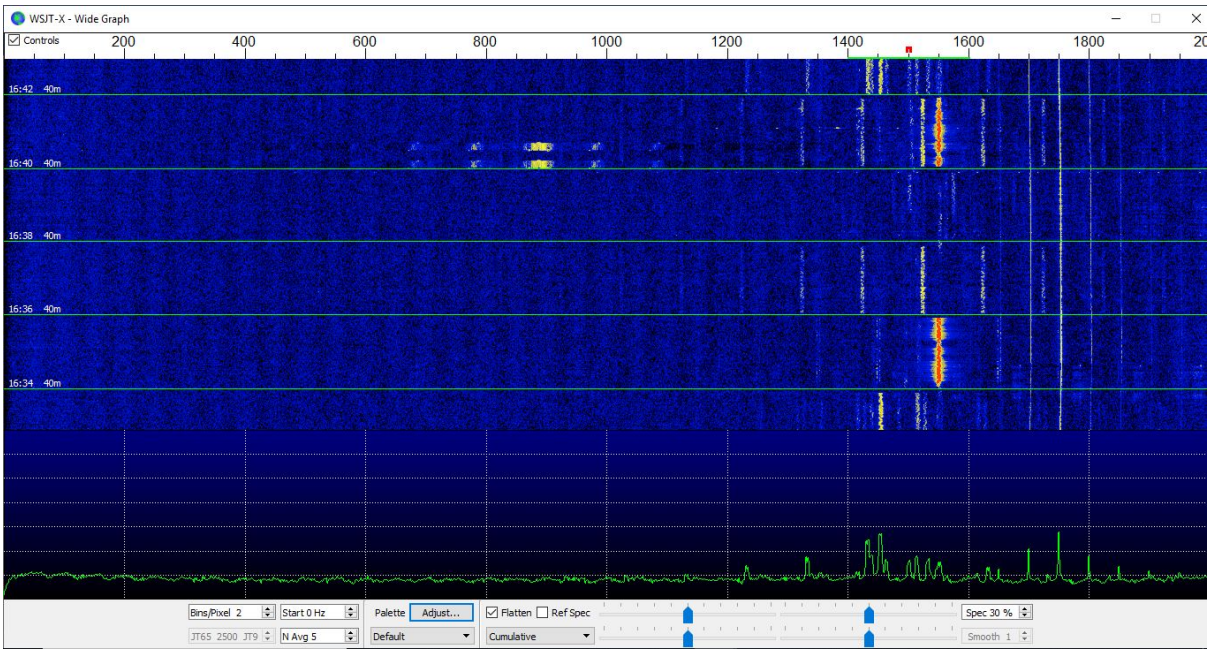

Figure 3.6– Example of the WSPR spectrogram recorded in the WSJT-X software, which measures signals within the 7 MHz band. Note that the frequency range for recording the WSPR data in this software is between 1400 Hz and 1600 Hz. Thus, the bandwidth for recording the WSPR signals is 200 Hz.

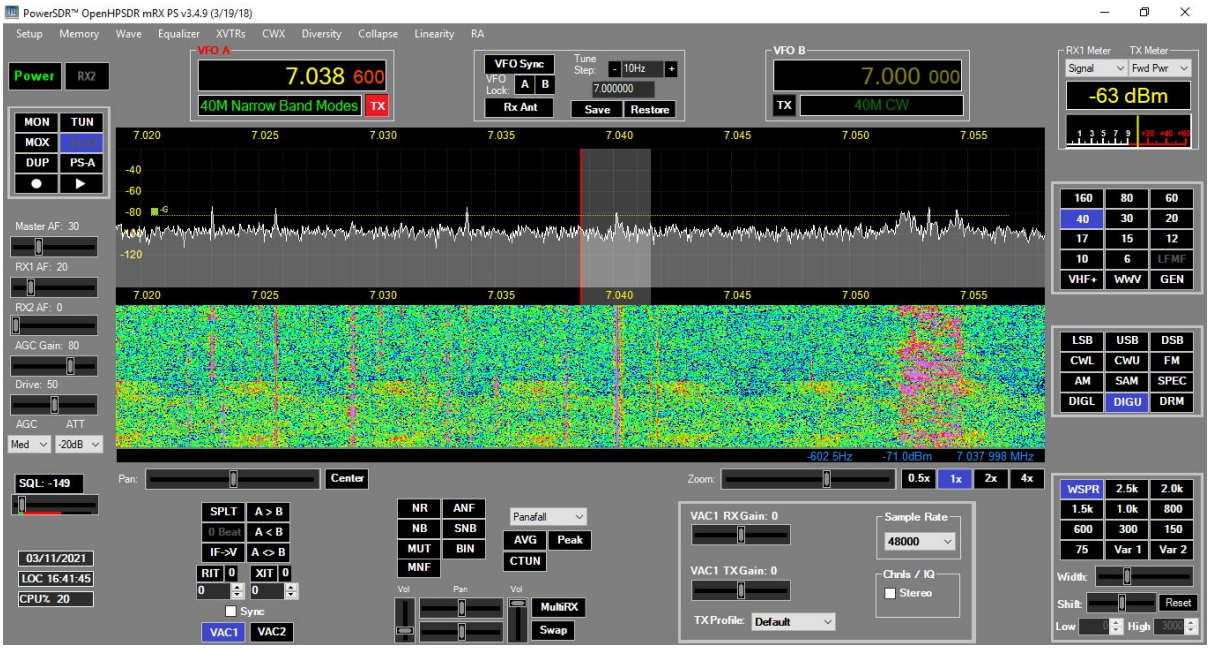

Figure 3.7 – Software interface of the radio receiver using the PowerSDR to intercept the radio signal. The reception is at 7.0386 MHz (40 m WSPR band) with a noise level at approximately – 100 dBm and a reception signal power at – 63 dBm.

3.2.7. Retrieving propagation data between the UK and New Zealand

One key analysis that is conducted in this thesis is on propagation between the UK and New Zealand. Therefore, the WSPR links between the UK and New Zealand are observed to identify any evidence of greyline propagation from the links' time propagation patterns. The method of retrieving the relevant links and analysing the time propagation pattern is described in this section.

The WSPR dataset containing the recorded links between the UK and New Zealand is retrieved and identified using radio callsign prefixes that designate the relevant transmitting and receiving stations (or persons) and the Maidenhead locators. In order to identify the time during which links are made, a solar position algorithm is used to predict the average solar sunrise, solar sunset and solar noon hours at the stations' locations (François Beauducel, 2019). The algorithm requires inputs from a given location's latitude, longitude, altitude, time zone, and dates. It calculates the declination angles, the hour angle, and the solar position in the UTC timescale, which results in the solar hours for sunrise, sunset, and solar noon.

The location for sunrise and sunset hours is predicted in this work by taking the median location of stations recorded in the WSPR database over a defined geographical area. The median coordinates are considered approximately the centre of the station locations, from which the average sunrise and sunset are identified. For example, the median locations of the UK and New Zealand stations will be used to determine the sunrise, sunset and solar noon hours in the UK and New Zealand. Figure 3.8 a) and b) show these locations for the UK and New Zealand, respectively. The blue dots indicate the locations of UK/New Zealand stations obtained from the WSPR database, while the magenta dots indicate the median location. The average sunrise, sunset and solar noon times for the corresponding median locations are given in Figure 3.8 c) and d).

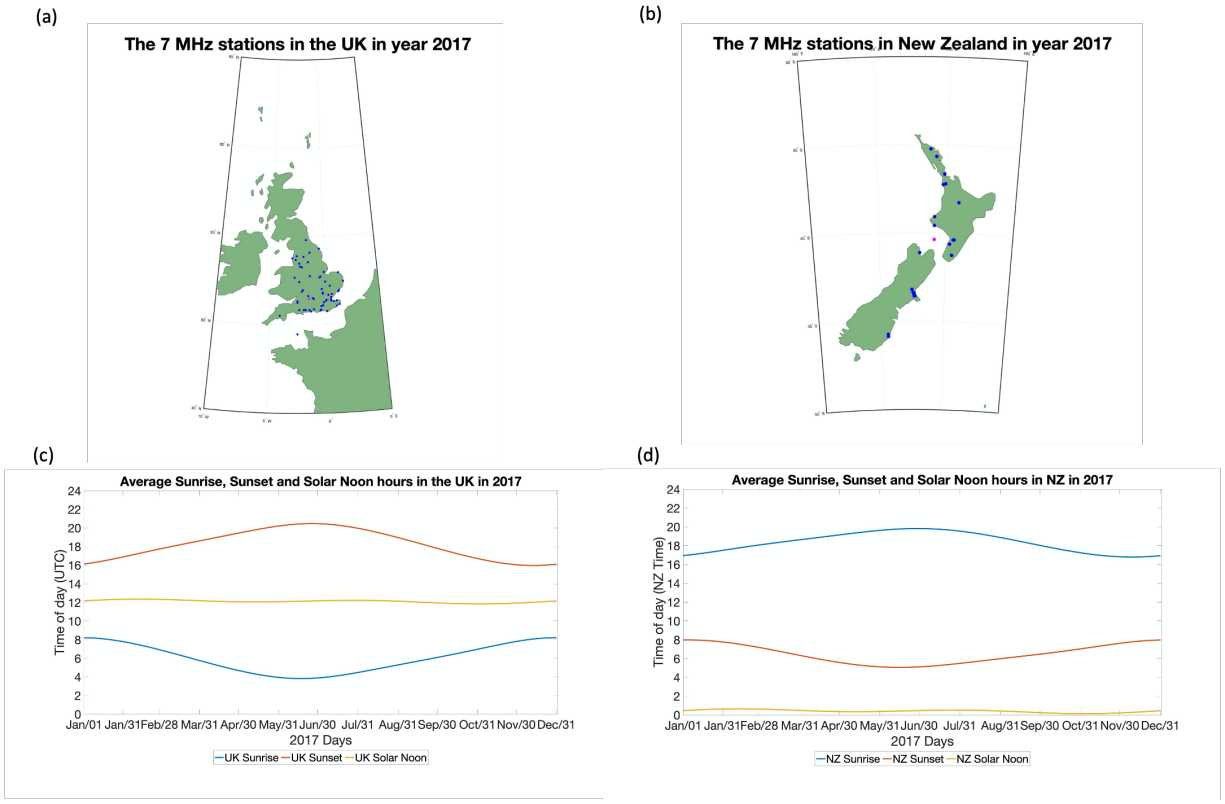

Figure 3.8 – (a) Locations of the 7 MHz transmitters in the UK in 2017. The blue dots are the WSPR transmitters recorded in the WSPR database, and the magenta dot is the median point of the transmitters. (b) Locations of the 7 MHz transmitters in New Zealand in 2017. The blue dots are the locations of the New Zealand transmitters, and the magenta dot is the median location of the transmitters (c) Average sunrise, sunset and solar noon hours in the UK in 2017 (d) Average sunrise, sunset and solar noon hours in New Zealand in 2017

Since the UK and New Zealand has a local time difference of 12 hours, both countries' sunrise and sunset hours will be close to the terminator. Thus, it can be graphically shown when combining the UK and New Zealand solar time plots, as given in Figure 3.9 (a). This overlap of sunrise/sunset hours indicates that greyline propagation could be more probable during those times, as shown in Figure 3.9 (b).

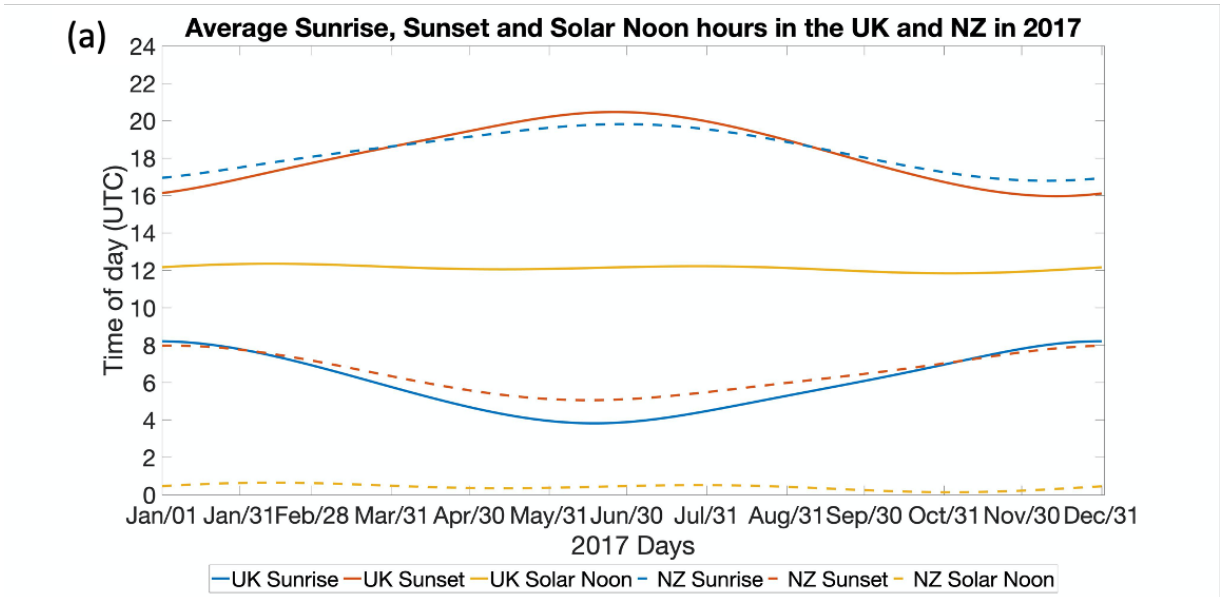

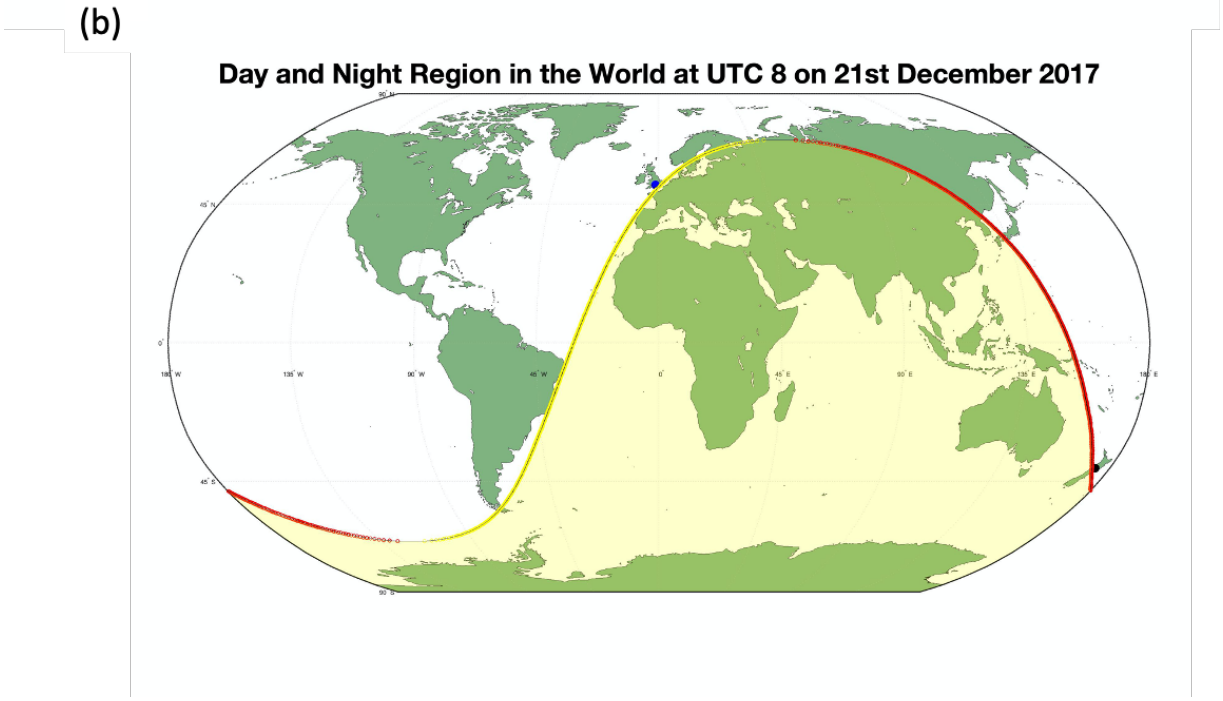

Figure 3.9 – (a) The United Kingdom and New Zealand Solar Time in UTC Time Zone. The UK sunrise, sunset and solar noon hours are shown in solid lines. The New Zealand sunrise, sunset and solar noon hours are shown in dash lines. (b) Day and Night Region in the Flat World Map at UTC 8 on 21st December 2017 with the sunrise terminator shown by the yellow line and the sunset terminator by the red line. The shaded region is the day region. The blue dot indicates the chosen location in the United Kingdom, and the black dot indicates the chosen location in New Zealand.

3.2.8. Opportunities and Challenges of using the WSPR data

The WSPR system has its advantages and disadvantages when it is used to carry out research. The advantages of using WSPR are threefold: firstly, the license can be easily obtained. Secondly, it has a global network of radio amateur users who use WSPR for recreational and communication purposes, giving a rich dataset. Third, the format laid in the WSPR system can be easily read. However, the WSPR data also has its limitations, including producing inconsistent data as the quality of records is dependent on the radio amateurs' input. Some of the key advantages and disadvantages of using WSPR for ionospheric and radio science research are discussed here.

3.2.8.1. Opportunities with WSPR

WSPR is a protocol created for communications between radio amateurs for recreational purposes and non-profitable research. Therefore, it requires an amateur radio license to transmit on WSPR, which can be easily obtained as WSPR is operated within amateur radio bands. The license conditions for the amateur radio license are regulated and authorised by the radio licensing authorities, which sets examinations and procedures to obtain a radio transmission license in a given country.

A further advantage of WSPR is based on the way the WSPR data is centrally collated and clearly and systematically formatted. It is formatted in a table that clearly states the time, the location and the callsigns which have made connections between station (i.e. links). It contains a timestamp that can be easily converted to the time and date of the link. WSPR uses the Maidenhead locator units, which is popular with the hobbyist to identify an area where the radio station exists. It can identify the location where the user operates the radio station. The information on the communication link can also easily be extracted from the database, as shown in Table 3.2.

The greatest advantage given by WSPR is it offers global coverage from a large number of sites and long-term data collection.

3.2.8.2 Challenges with the WSPR data for scientific research

While WSPR offers a global network for the radio user community to upload their records into the database, the WSPR data can be inconsistent due to human error. Although it is possible that a communication link cannot be made due to signal reception at the receiver being below the SNR threshold for WSPR, which is around –30 dB, the inconsistencies in the information may also be due to user activity. This

means a communication link cannot be made between two stations if the transmitter or receiver is inactive. Since WSPR radio stations are operated largely by hobbyists, the WSPR data links are dependent on the number of active radio users at a given time. For example, the activity from the radio transmitter with a callsign ZL3TKI is observed in Figure 3.10 and Figure 3.11.

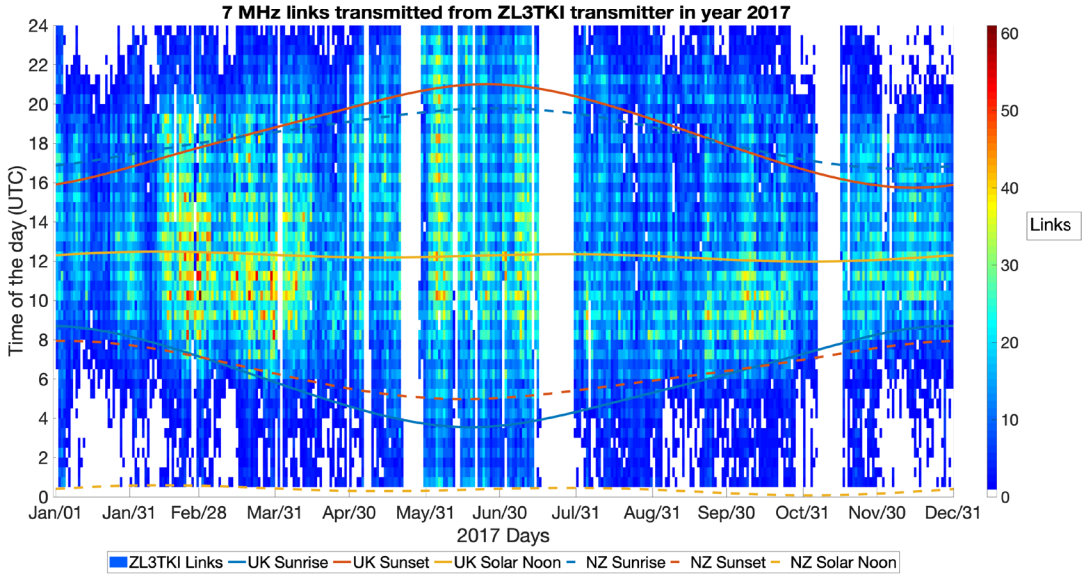

Figure 3.10 – Number of links from the New Zealand transmitter ZL3TKI in 2017. Only receivers with a proven capability to cover the distance from the station ZL3TKI to any radio stations are shown. The colours indicate the number of links available in each half-hour interval.

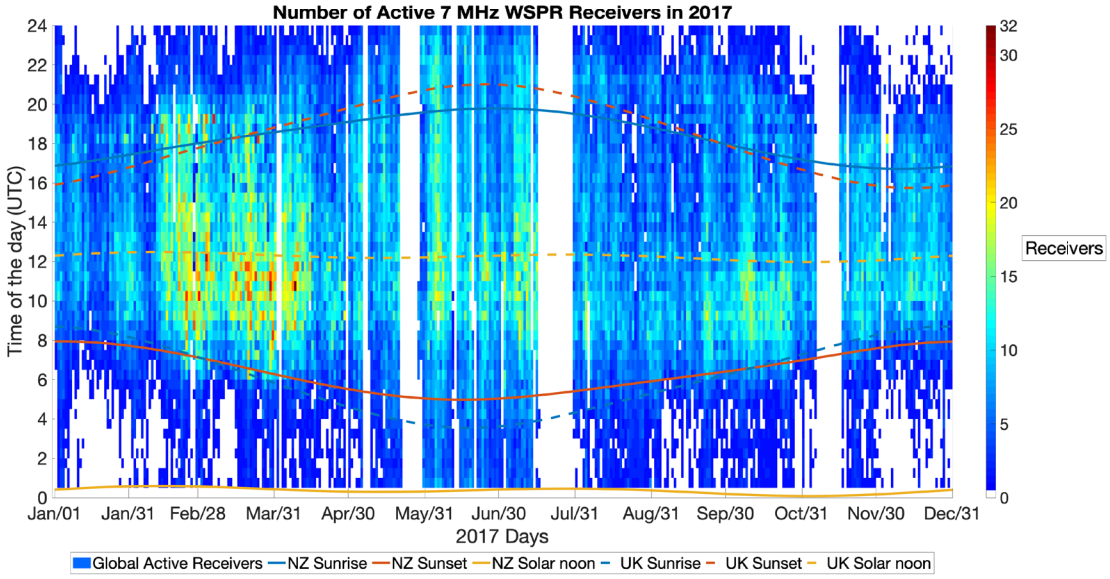

Figure 3.11 – Number of global active receivers operating at 7 MHz in 2017. Only receivers with a proven capability to cover the distance from the station ZL3TKI to any radio stations are shown. The colours indicate the number of active receivers received in each half-hour interval.

Figure 3.10 shows the links transmitted from the radio station ZL3TKI and Figure 3.11 shows the number of active receivers globally that made a link with ZL3TKI. It shows that although the station may be active most of the time in 2017, the established links are also dependent on the active receivers elsewhere in the global network.

Another disadvantage is that the trajectory path is only an estimation derived from the great circle path. The azimuth angle listed in the WSPR database is the direction in which the signal was transmitted. However, it is only an estimation. The specific path a link would take when propagating through the ionosphere is unknown as it only gives the time of transmission and an initial azimuth angle as an estimation.

Despite the noted challenges with the WSPR database, the data can be used for radio propagation analysis since it is recent, updated regularly and already has existing data from a global radio station network. The data can be easily analysed to locate and observe the time propagation patterns of the recorded links. Although the data is inconsistent due to the varying operational hours from the radio amateurs and similarly, the azimuth angle is just an estimation, the data gives sufficient information for scientists to locate the radio stations and time of transmissions. Coupling with simulation and other research tools and experimental data, this information can enable vital research on ionospheric signal propagation to help both the ionospheric science community and HF communication users.

3.2.9. Summary

The WSPR network was discussed in Section 3.2. It showed that WSPR could be used as a protocol for HF communications between radio amateurs. The WSPR network setup was discussed in Section 3.2.3. and the data analysed in Section 3.2.4. Section 3.2.5. described the method to retrieve the solar time for the area of interest, particularly the UK and New Zealand. Section 3.2.6. described the method to retrieve the results for radio propagation between the UK and New Zealand. Section 3.2.7. described the transmitters and receivers' activity in the UK and New Zealand and observed the impact of the stations' activity on radio propagation. Section 3.2.8. identified some of the WSPR system challenges, such as inconsistent user activity and arbitrary estimation on the propagating direction. Nevertheless, the WSPR system is a network that is globally used, and the users' locations are straightforward to locate.

3.3. PHaRLAP

3.3.1. Introduction

There are various methods to computationally predict and analyse the propagation of radio signals in the ionosphere. One such method is ray-tracing, which is used to simulate various parameters in HF propagation, such as absorption, phase velocity, group velocity and signal paths. Ray-tracing can also be used to analyse the effect of plasma density and the Earth's magnetic field on radio propagation, such as the time propagation patterns, absorption, and propagation paths. This understanding allows radio users to improve HF communications by better analysing the predicted paths and ionospheric absorption, which can significantly affect HF communications.

This chapter focuses on the theory and simulations of ray-tracing as done in PHaRLAP - the software toolkit used to analyse the WSPR results presented in this thesis. PHaRLAP is developed by Dr Manuel Cervera and in operation since 2014.

The contents of this chapter are structured as follows: Section 3.2.2. describes the theory of HF ray-tracing techniques. Section 3.2.3. describes an overview and the theory of PHaRLAP simulations using the ionospheric model IRI 2016, described in Section 3.2.4. Finally, the chapter is concluded with a summary in Section 3.2.5.

3.3.2. Theory of HF ray-tracing techniques

Ray-tracing can help identify how signal propagation is affected by the ionosphere. It can be a very useful tool to understand HF propagation in a region by providing some information about the current ionospheric conditions through models and ionospheric

data. The algorithms in ray-tracing techniques compute numerous properties related to propagation. The most common properties related to propagation are the propagation paths, absorption, locations where the ray returns to the Earth, and propagating distance. Other properties, such as the propagation path's initial and final elevation angles, the initial and final azimuth angles of the propagation path, doppler shift, and phase change, are also computed in the algorithm. HF ray-tracing techniques are based on the Appleton-Hartree Equation that describes the refractive index of magnetised plasma.

As discussed in Chapter 2, Section 2.3, the complex refractive index of the ionosphere can be explained through the Appleton-Hartree equation, where parameters X, Y and Z describe the influence of the plasma density, geomagnetic field and collision frequency, respectively (Equations 2.26 – 2.30). The ordinary (O) and extraordinary (X) rays of the propagating signal are also defined in this equation through the +/- sign in the denominator. As a result, the paths of the O and X rays could be obtained from the ray-tracing analysis. The Appleton-Hartree equation given in Chapter 2 is re-iterated here in Equation 3.3 for clarity. The $\pm$ sign in Equation 3.3 gives the refractive index for $(+)$ ordinary (O) and $(-)$ extraordinary (X) rays.

$$n^2 = 1 - \frac{X}{1 - jZ - \left[{Y_T}^2/2(1 - X - jZ)\right] \pm \left\{\left[{Y_T}^4/4(1 - X - jZ)^2\right] + {Y_L}^2\right\}^{1/2}} \quad \text{Equation 3.3}$$

The equations for the HF propagation ray paths were set up by Haselgrove (1955). Many publications have used Haselgrove's equations over the years to study HF propagation (Cervera and Harris, 2014; Pederick and Cervera, 2016; Heitmann et al., 2018). Similarly, many researchers such as Croft (1968) and Coleman (1997) developed simplified formulations of Numerical Ray-Tracing (NRT) for their studies, such as the Analytical Ray-Tracing (ART) and 2D ray-trace modelling. However, ART and 2D ray-tracing modelling ignore the effect of the Earth's magnetic field because of the high computational overheads (Coleman, 1997; Cervera and Harris, 2014). Nevertheless, they are used in ray-tracing software for HF propagation studies, as the simplified models are sufficient for several applications, such as backscatter studies. The work in this thesis uses the ray-tracing toolkit called PHaRLAP to analyse WSPR data, which will be presented in this section.

PHaRLAP provides a range of ray-tracing algorithms for 2D and 3D simulation and analysis. This section focuses on the 3D ray-tracing technique implemented by Haselgrove (1963) in PHaRLAP, used for the simulation analysis in this thesis.

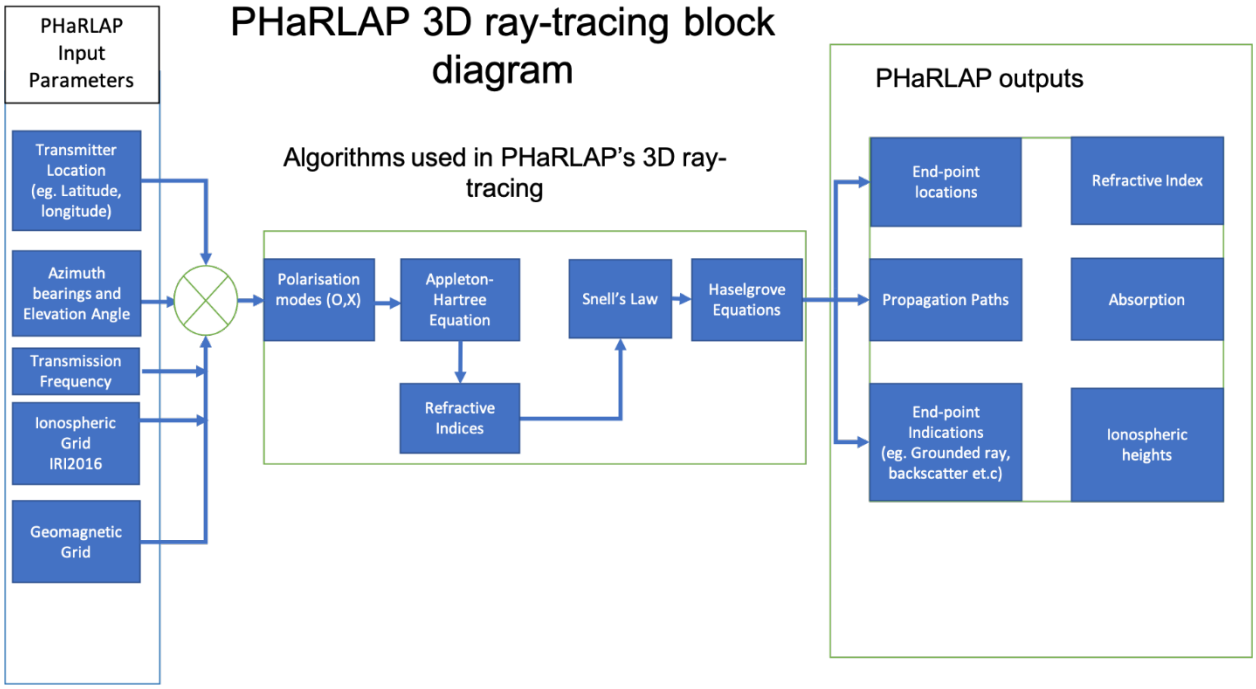

Figure 3.12 – PHaRLAP 3D ray-tracing block diagram

3.3.2.1. PHaRLAP inputs

The fundamental requirement to predict the propagation paths is to set the transmitter's location in latitude and longitude (degrees) as a starting point of all propagation paths. In reality, the radio waves emitted from the transmitter will propagate in a direction largely determined by the directionality of the transmission antenna. Therefore, the azimuth bearings are required to set the propagation paths for the simulation at the initial stage. In addition, the radio wave propagates from the antenna at multiple elevation angles and enters the ionosphere at multiple incident angles, which influence the refractivity of the signals. For this reason, the elevation angles are also set in PHaRLAP as an input. The transmission frequency is also an important input to the simulations as it will influence the refractive indices calculated by the Appleton-Hartree equation, and consequently, the signal's propagation paths. It is also necessary to indicate whether either or both O and X paths should be traced.

An ionospheric grid and a geomagnetic grid are required to generate a simulated ionosphere and compute the refractive indices of the ionospheric layers, which are then used to predict the propagation paths. In this simulation, PHaRLAP requires the geodetic coordinates, such as latitude, longitude and height, and the number of increments for each geodetic coordinate to generate both the ionospheric grid and the geomagnetic grid parameters, which is listed in Table 3.10.

Table 3.10 – Required inputs for the ionospheric grid (light grey shade) and geomagnetic grid (grey shade), and the outputs generated by PHaRLAP simulations

<table>
<tr><th>Grid</th><th>Inputs</th><th>Outputs</th></tr>
<tr><td rowspan="3">Ionospheric grid</td><td rowspan="3">Initial geodetic latitude (degrees)
Initial geodetic longitude (degrees)
Latitude increment (degrees)
Longitude increment (degrees)
Number of latitudes
Number of longitudes
Initial geodetic height (km)
Height increments (km)
Number of heights
UTC Time
R12 sunspot number
Doppler flag
Ionospheric Reference Model (IRI)
International Geomagnetic Reference Field (IGRF)</td><td>Ionospheric plasma density grid</td></tr>
<tr><td>Ionospheric plasma frequency grid</td></tr>
<tr><td>Collision frequency</td></tr>
<tr><td>Geomagnetic grid</td><td>Geomagnetic grid
X component (Bx)
Y component (By)
Z component (Bz)</td></tr>
</table>

Table 3.10 shows the ionospheric and geomagnetic parameters required to run the ray-tracer and generate parameters such as plasma density, plasma frequency and collision frequency. In this thesis, PHaRLAP uses IRI2016 (Pederick and Cervera, 2016) as a reference model to generate the ionospheric grid and compute the ionospheric properties, such as plasma density, plasma frequency and collision frequency. These properties (listed as “Outputs” in Table 3.10) are used to determine the ionospheric parameters in the Appleton-Hartree Equation, which subsequently generate the refractive indices of the ionospheric layers. Similarly, PHaRLAP uses the International Geomagnetic Reference Frame (IGRF) to generate the geomagnetic grid with the inputs (Pederick and Cervera, 2016) used to generate the ionospheric grid. Finally, it computes the geomagnetic parameters, such as the X component (Bx), Y component (By), and Z component (Bz). The geomagnetic grid properties (listed as “Outputs” in Table 3.10) gives the intensity of the geomagnetic field in different directions, with Bx representing the north component of the horizontal intensity, By representing the east component of the horizontal intensity and Bz representing the vertical intensity of the geomagnetic field.

3.3.2.2. Ray tracing algorithm

As mentioned before, the ray-tracing algorithm in PHaRLAP predicts the propagation paths of the HF radio waves and their end-point locations. It includes the Appleton-Hartree Equation, Snell’s Law, and Haselgrove Equations. Firstly, PHaRLAP uses the Appleton-Hartree Equation to generate the refractive indices of the ionospheric layers, which considers various properties, such as the plasma density, operational frequency, collision frequency, and magnetic field. As mentioned in Chapter 2.3, the magnetic field causes the ionosphere to be birefringent. For this reason, the ray-tracing algorithm used in PHaRLAP includes the refractive indices of the ordinary (O) ray, the extraordinary (X) ray. It also considers the propagation of the ray in the

absence of a magnetic field and collision frequency. In addition, the Appleton-Hartree Equation predicts the absorption of the rays, as mentioned in Chapter 2.3.

Snell's Law is the next step in the PHaRLAP software, used to compute the refraction angle of the ray entering the ionosphere, and the subsequent ionospheric layers, by using the elevation angles and the refractive indices calculated through the Appleton-Hartree Equation prior, giving the reflection and refraction points of the rays, which are measured as ionospheric heights. The locations of where these reflections and refractions take place are then computed by the Haselgrove Equations (Haselgrove, 1955), followed by the generation of the ray paths and the end-point locations.

3.3.2.3. PHaRLAP outputs

The objectives of generating the PHaRLAP outputs are to identify the properties of the signal along the path and at the end-point location and to observe the ionospheric effects from the IRI2016 model on the propagation paths. This will help analyse the WSPR data. The outputs of PHaRLAP indicate the height of the ray paths (in km), absorption calculated along the path (in dB), and end-point labels, such as grounded rays and scattered rays. Furthermore, the absorption along the signal path can give an insight into the ray properties and highlight the potential patterns of radio propagation between specific countries, which will be discussed in Chapter 6.

3.3.3. Signal propagation in PHaRLAP

The refractive index for the rays in the absence of the magnetic field and collision frequency can be computed in PHaRLAP as shown in Equation 3.4. The electron mass m, the electron charge e, and the permittivity ϵ_0 are constants, and the signal is propagated at a fixed frequency ω. Thus, the refractive index for a ray is dependent on the electron concentration N in the ionospheric layer.

$$\mathrm{n}^2 = 1 - \mathrm{X} = 1 - \frac{{\omega_\mathrm{N}}^2}{\omega^2} = 1 - \mathrm{Ne}^2/\epsilon_0 \mathrm{m}\omega^2 \qquad \text{Equation 3.4}$$

However, to simulate HF propagation more accurately, the effect of the Earth's magnetic field on the refractive index must also be accounted for. It is because the magnetic field contributes to the Faraday rotation of the wave, which produces the polarised O- and X-modes of the propagation signal, as mentioned in Chapter 2. The effect of the Earth's magnetic field on signal propagation is presented in Figure 3.13. The inputs which are required to generate Figure 3.13 are listed in Table 3.10. Figure 3.13 shows the ray paths for O-mode, X-mode and 'No-field' mode for a propagating signal with a given frequency and transmission angle.

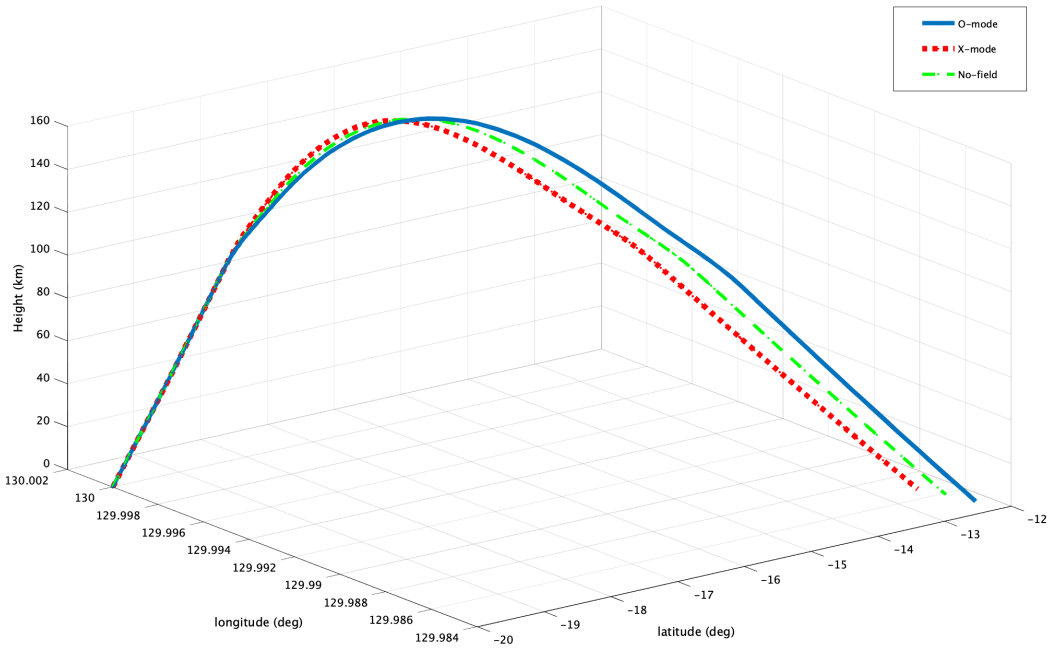

Figure 3.13 – The single-hop propagation paths for three rays, which are reflecting from the ionosphere for ordinary (O - blue) propagation, extraordinary (X- red) propagation, and the no magnetic field case (green). All rays are propagating into the ionosphere at the same frequency and launch angles. (Example from PHaRLAP).

If the magnetic field is considered during propagation, then the rays will be split into an O-mode or into an X-mode, resulting in polarised waves. This alters the refractive indices and the paths of the signals as shown by the blue and red paths (the O and X-mode, respectively) in Figure 3.13. This is because the refraction angle varies when it is affected by the Earth's magnetic field, which results in the propagation distance of X-mode being shorter than the non-magnetic ray and the O ray.

If the magnetic field is neglected during propagation – for example, where a simpler understanding of the propagation is needed or where the effect of the lower atmosphere is considered – then only Snell's Law can be used. The incident angle of the signal that enters the boundaries between the ionospheric layers and between the neutral atmosphere and the ionosphere influences the refraction angle of the signal, which can be determined through Snell's Law. Snell's Law applies to HF propagation, as the incident angle of the signal can be used to calculate the elevation angle from the transmitter. The refraction angle of the signal in a given ionospheric layer is therefore influenced by the refractive indices of both ionospheric layers and its incident angle, as shown in Equation 3.5.

$$n_1 \sin\theta_1 = n_2 \sin\theta_2 \qquad \text{Equation 3.5}$$

Equation 3.5 shows that the refractive angle (θ_2) is influenced by the incident angle (θ_1) and the refractive indices n_1 and n_2, where n_1 and n_2 are the refractive indices of the two layers. When the ray reaches the edge of a given layer, it will refract into another layer. However, it must be noted that the ratio between the refractive indices

of the layers must be lesser or equal to 1 to achieve refraction. This is known as the critical angle, as shown in Equation 3.6.

$$\sin\theta_c = \sin^{-1}\frac{n_2}{n_1} \qquad \text{Equation 3.6}$$

The critical angle θ_c is essential for HF propagation since it determines the elevation angle of the radio signal sent from the transmitter. It is used to ensure that the radio signal will be refracted and reflected into the Earth's surface, where the radio receivers will receive it. Thus, the critical angle θ_c and the plasma frequency can be used to determine the radio frequency of the signals. It is also used to determine the transmission's elevation angle for long-distance HF propagation through total internal reflection (TIR). TIR occurs when the incident angle of the ray is greater than the critical angle. This means that if the radio frequency is higher than the plasma frequency, then the refractive index will be a real number.

For this reason, the incident angle of the ray is required to be greater than the critical angle to reflect the ray towards the Earth's surface. An example of using Snell's Law in PHaRLAP simulation is shown in Figure 3.14. Figure 3.14 shows the simulation of the links which propagate at a frequency higher than the maximum plasma frequency.

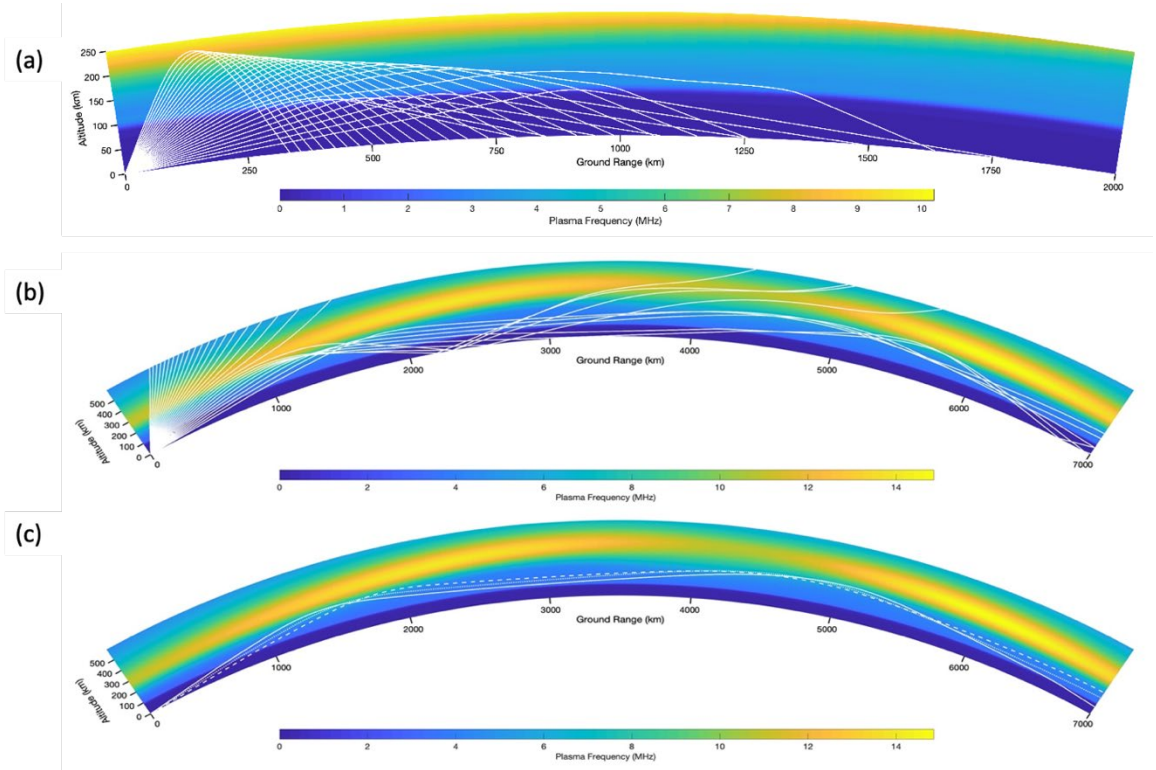

Figure 3.14 - Example images showing the ionospheric plasma frequency (colour) with the propagation of a radio signal and a fixed frequency equivalent to or above the peak plasma frequency. Note that the higher elevation rays pass through the ionosphere, but the lower elevation rays are refracted back to Earth. The distance from the transmitter to the closest return of the signal to the ground is called the skip zone.

When the ray is transmitted into the ionosphere at a high elevation angle, the ray propagates through the ionosphere. This is because propagation at a high elevation angle gives low incident angles. On the contrary, when the ray is transmitted into the ionosphere at a low elevation angle, the ray will be reflected back to the Earth's

surface. It is because the incident angle of the ray entering the boundary between the stratified layers is high. Therefore, from Equation 3.5, if the sine of the incident angle $\sin\theta_1$ is greater than the ratio $\frac{n_2}{n_1}$, the ray will be reflected towards the Earth's ground surface at the same angle as the incident angle due to TIR.

The applications of using 3D ray-tracing techniques are to analyse the effects of plasma density on the ray paths and analyse the absorption along the propagation paths. An ionospheric model is used to give a reference plasma density for predicting the propagation paths. The IRI2016 model, which computes the plasma density from various instruments, has been widely accepted as a standard in the ionospheric research community. The next section will describe this model.

3.3.4. IRI 2016

The ray-tracing program PHaRLAP can use IRI2016 as a reference ionospheric grid to analyse the effects of ionospheric conditions on HF propagation through HF ray-tracing techniques. The IRI2016 model is an empirical statistical ionospheric model (Bilitza *et al.*, 2017), which is sponsored by the radio science communities, such as the Committee on Space Research (COSPAR) and the International Union of Radio Science (URSI). The ionospheric data used to make the IRI2016 model were sourced from the historical measurements made from the ground-based and space-based instruments, such as ionosondes, incoherent scatter radars, satellites and rockets. It is widely used for studying HF propagation through ray-tracing techniques (Bilitza, 2001; Bilitza et al., 2014, 2017).

The advantage of using IRI2016 is the model is based on experimental evidence from all available ground-based and space-based instruments to study the ionosphere rather than computing from theoretical understandings of the ionosphere. This model gives a realistic model to study the ionosphere and its effects on radio propagation. As a result, the IRI2016 gives a standard of reliable ionospheric data for studying HF propagation through HF ray-tracing techniques (Bilitza, 2001; Bilitza et al., 2014, 2017).

The IRI2016 model will be used to generate the refractive medium for the ray-tracing simulations in the research. The most important measurement for ray-tracing simulations is the electron density, as it influences the refractive index described by the Appleton-Hartree Equation. IRI2016 can model various ionospheric variations, including diurnal variation, seasonal variation, and geographical variation, which can be shown through the measure of the integrated electron density known as the ionospheric Total Electron Content (TEC). An example of TEC, derived from IRI2016, is shown in Figure 3.15, presenting the effect of diurnal variation.

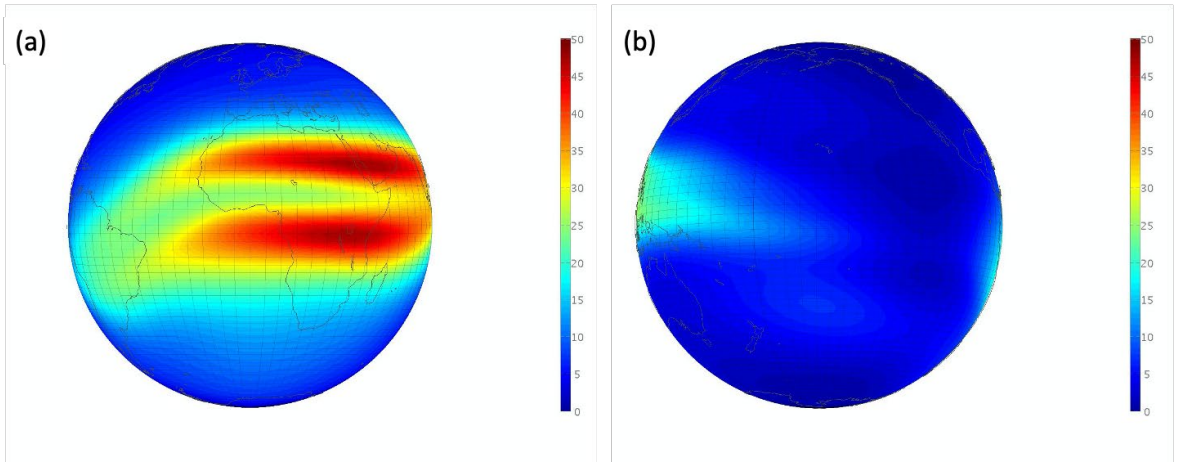

Figure 3.15 - (a). IRI2016 for the day ionosphere on March 21st at 12 UTC 2017(b) IRI2016 for the night ionosphere on March 21st at 12 UTC 2017

Figure 3.15 illustrates the effect of the diurnal variation on the TEC in the ionosphere produced by IRI2016. From Figure 3.15, it can be seen the difference between the day and night ionosphere (Figure 3.15 (a) and Figure 3.15 (b)), as well as the extent of the sunspot number can have on the ionisation during the night (Figure 3.15 (b)). The variation of the TEC with the geographical location can also be seen in all two subgraphs. A clear belt of higher density can be seen in the equatorial regions in comparison to the mid-latitudes. The fact that IRI2016 can simulate a whole world picture of the ionospheric conditions is very beneficial, especially for the research conducted in this thesis.

3.3.5. PHaRLAP Absorption

The objective of using PHaRLAP is to observe the effects of ionospheric conditions on HF propagation, including absorption. As mentioned in Chapter 2, the signal will suffer attenuation because of the plasma density in the ionosphere. Therefore, the simulation of absorption will be useful for analysing the effects of ionospheric conditions on the ray paths. Furthermore, it is because absorption affects the signal strength in HF propagation. As a result, it will also affect the ability of the signal to travel to certain regions of the world. There are two types of absorption – non-deviative and deviative absorption – as mentioned in Chapter 2.

The 3D ray-tracing simulation in PHaRLAP generates the total absorption and deviative absorption of each endpoint. The details of how PHaRLAP calculates absorption are given in Pederick and Cervera (2014). The total absorption of each endpoint indicates the sum of non-deviative and deviative absorption at the endpoints from the simulations. In contrast, deviative absorption is simply the deviative absorption calculated at the endpoints. Both absorption data will be useful for the analysis of the WSPR data. First, however, the total absorption will be used to observe its effects on the ray path in Chapter 6, as it includes both types of absorption (Cervera and Harris, 2014; Pederick and Cervera, 2014).

3.3.6. Summary

This chapter described the methods that are used in this thesis to investigate the ionosphere and HF propagation. The first method is using the WSPR data, described in Section 3.2. The WSPR system is a protocol which generates which enables weak signal communication in amateur radio bands. It is the primary observation data used in this thesis, and it is mainly used for HF communications. Sections 3.2.2. to 3.2.6. described the process of generating WSPR data and prediction methods in the WSPR protocol. In addition, the method of retrieving the relevant data to study HF propagation is described in Section 3.2.7. The details of the system and the strengths and weaknesses of using WSPR have been outlined. Finally, it highlighted that WSPR is useful to this research as it gives sufficient data to study HF propagation.

The simulation work in this thesis uses the ray-tracing software called PHaRLAP, which is described along with the ionospheric model IRI2016. PHaRLAP can be used to analyse the effect of ionospheric conditions on radio signals, such as the time propagation patterns, absorption, and propagation paths. The method of using PHaRLAP is described in Sections 3.3.2, 3.3.3, 3.3.4, and 3.3.5. PHaRLAP allows radio users to improve HF communications by better analysing the predicted paths and ionospheric absorption, which can significantly affect HF communications.

The next chapter will look at some initial results from WSPR.

4. Radio Propagation using WSPR at 7 MHz

4.1. Introduction

In this chapter, HF radio observations using the WSPR database described previously in Chapter 3 are analysed to provide an initial overview of the WSPR data. The aim is to see if patterns in the propagation times of day and year are evident.

Initial observation of the database described in Chapter 3 showed that many of the links in WSPR are propagated between these countries: 1. the UK; 2. New Zealand; 3. Italy and the adjacent regions (ITADR) ; 4. the USA and 5. Australia. This is partly because of the activity of radio amateurs in these countries.

Figures 4.1 to 4.4 will show a heatmap of the established links with New Zealand (Figure 4.1 and Figure 4.2) and the UK (Figure 4.3 and Figure 4.4), where the colour represents the number of links in the log 10 scale. The graphs are also grouped by whether the country is receiving or transmitting the radio signals. Figure 4.1 and Figure 4.3 are the transmission from New Zealand and the UK, respectively, and Figure 4.2 and Figure 4.4 the reception by New Zealand and the UK, respectively.

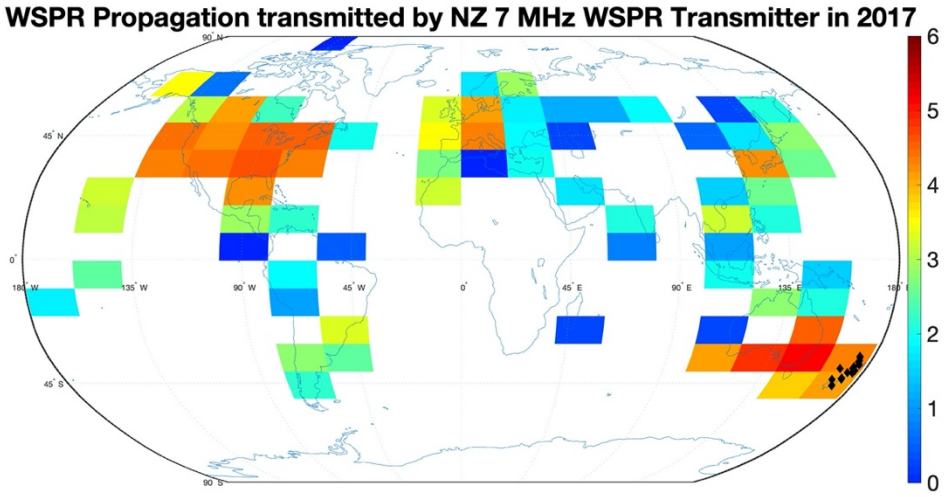

Figure 4.1 – Links transmitted from the New Zealand Transmitters in 2017. Only specific selected transmitters with a proven capability to repeatedly link to the United Kingdom have been used to produce this figure. The colours indicate the number of links received in each region on a logarithmic scale to base 10.

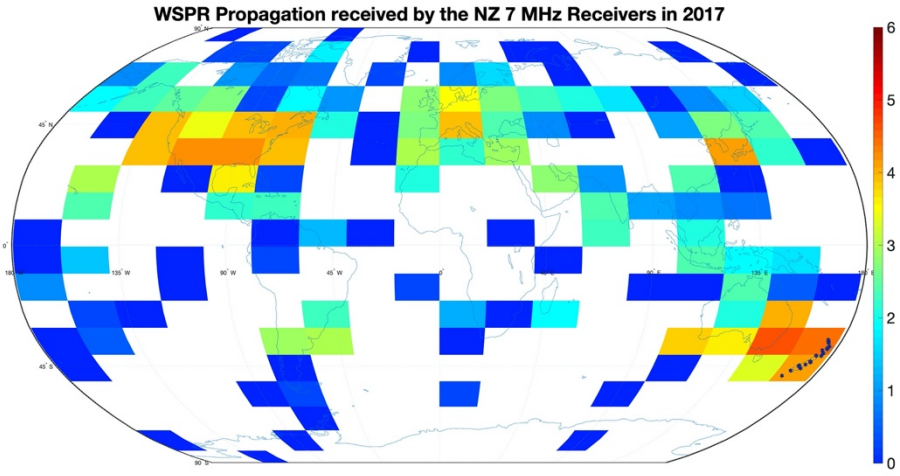

Figure 4.2 – Links received by the New Zealand Receivers in 2017. Only specific selected receivers with a proven capability to repeatedly link from the United Kingdom have been used to produce this figure. The colours indicate the number of links received in each region on a logarithmic scale to base 10.

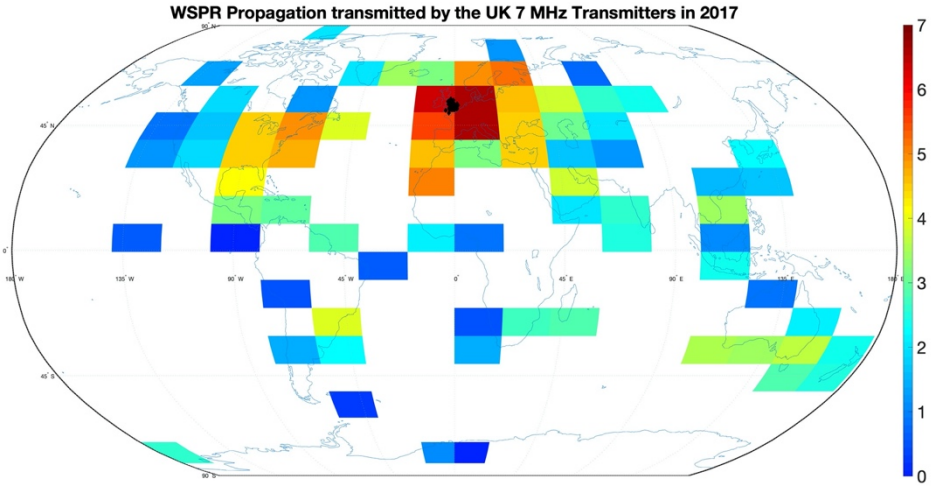

Figure 4.3 – Links transmitted from the UK Transmitters in 2017. Only specific selected transmitters with a proven capability to repeatedly link to New Zealand have been used to produce this figure. The colours indicate the number of links received in each region on a logarithmic scale to base 10.

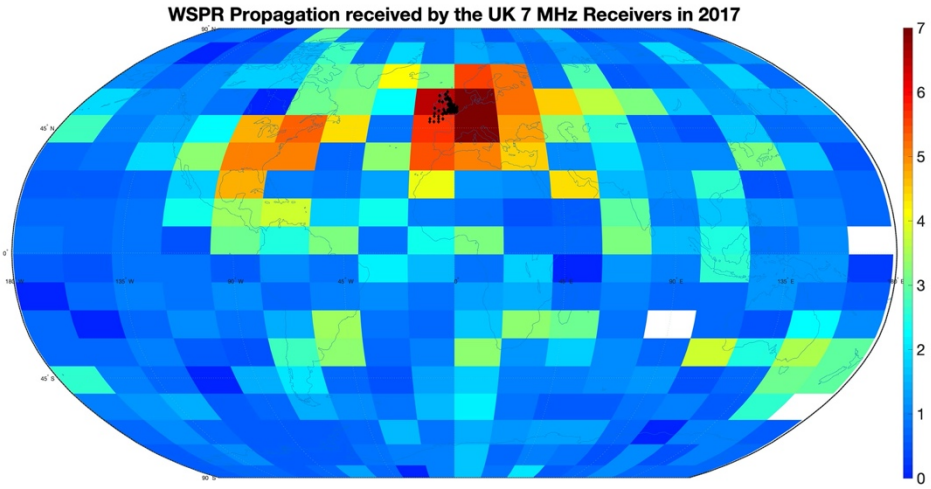

Figure 4.4 – Links received by the UK receivers in 2017. Only specific selected receivers with a proven capability to repeatedly link from New Zealand have been used to produce this figure. The colours indicate the number of links received in each region on a logarithmic scale to base 10.

The results from Figure 4.1 to Figure 4.4 provide an overview of the numbers of links made by receivers and transmitters in the UK and New Zealand. The research focus is on radio links at 7 MHz, a popular frequency choice among many radio amateurs, specifically the records from the year 2017. In addition, the data retrieved from WSPR is used in this chapter to investigate whether there are preferential times of day and year when the links are generally made.

The propagation is expected to be subjected to considerable variability as it is dependent on the electron density in the ionosphere. Furthermore, it is well established that the ionospheric conditions change with daily, monthly, and yearly cycles, which will affect the available propagation paths on a daily, monthly, and yearly basis. For this reason, the links obtained from the WSPR database over a long period of time and between multiple transmitters and receivers may be useful to illustrate any preferential propagation patterns.

Section 4.2. in this chapter analyses the WSPR links propagating between the UK and New Zealand. Section 4.3. describes the WSPR links propagating from the USA with Section 4.4, the WSPR links propagating from Italy and the adjacent regions (ITADR). In addition, Section 4.5. describes the WSPR links propagating from Australia, and finally, the summary will be described in Section 4.6.

4.2. WSPR Links between the UK and New Zealand

The WSPR links shown in this section are the links between the UK and New Zealand. These locations are chosen because they are on opposite sides of the Earth and lie along the terminator simultaneously. The propagation pattern found from WSPR between New Zealand and the UK is illustrated in Figure 4.5 and Figure 4.6. The x-axis of Figure 4.5 and Figure 4.6 is the day of the year 2017, whereas the y-axis of Figure 4.5 and Figure 4.6 is the time of the day in UTC hours. The red shaded area is the UK daytime hours. The yellow shaded area is the common daytime hours, and the white shaded area is the common night hours. The solid lines are the UK's sunrise (blue), sunset (red) and solar noon (yellow) hours. The dash lines are the NZ's sunrise (blue), sunset (red) and solar noon (yellow) hours. These are defined by the locations on the ground for a particular receiver location defined from the median of the actual receiver location. The colours indicate the number of links available in each half-hour interval.

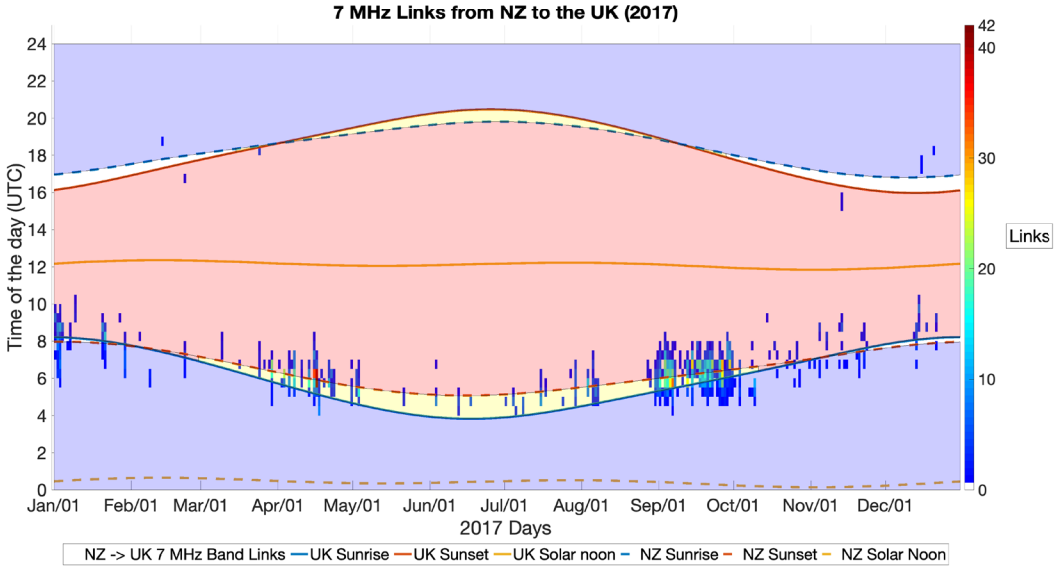

Figure 4.5 – 7 MHz Radio Links made from New Zealand to the UK in 2017. The blue shaded area is the New Zealand daytime hours. The red area is the UK daytime hours. The yellow shaded area is the common daytime hours, and the white shaded area is the common night hours. The colours indicate the number of links available in each half-hour interval.

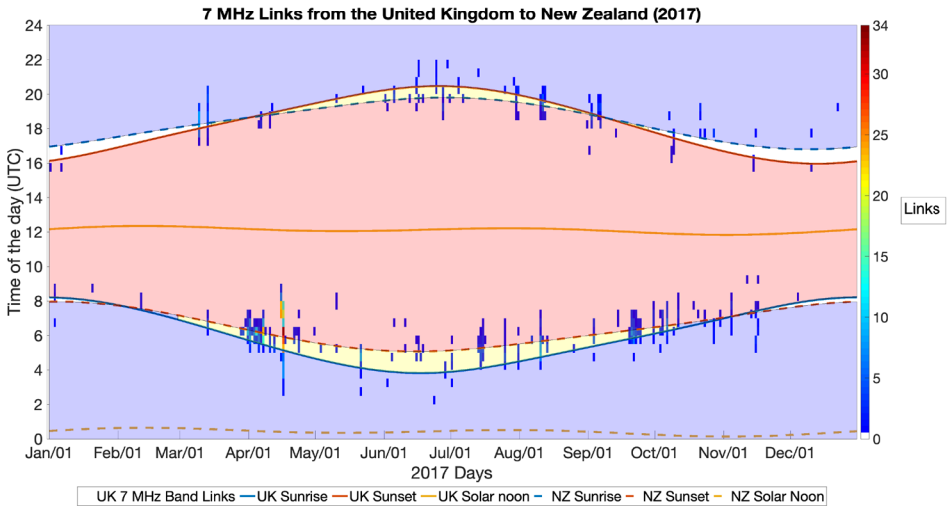

Figure 4.6 – 7 MHz Radio Links made from the UK to New Zealand in 2017. The blue shaded area is the New Zealand daytime hours. The red area is the UK daytime hours. The yellow shaded area is the common daytime hours, and the white shaded area is the common night hours. The colours indicate the number of links available in each half-hour interval.

From the graphical results shown in Figure 4.5 (New Zealand to the UK), it can be observed that the links appear to cluster around the common daytime hours, which is approximately the UK sunrise/New Zealand sunset hours. Thus, there is evidence of the so-called greyline propagation. It can also be seen that there are very few links made from New Zealand to the UK around the UK sunset/New Zealand sunrise hours, and there are none in the UK summer.

The pattern of activity for the WSPR stations throughout the year for the locations in this chapter is shown in Appendix A.

Figure 4.6 (the UK to New Zealand) also shows that there is evidence of greyline propagation. However, in this case, the dawn/dusk asymmetry seen in Figure 4.5 is not shown, i.e., there are links in both the UK dawn and the UK dusk.

It was expected that the times that the links are made would be clustered around the terminators, as this has been previously reported by the radio amateurs (Nichols, 2002). However, the exact modes and paths of propagation are not known. However, it is interesting to confirm the terminator clustering with the WSPR dataset and demonstrate it with actual observations over a full year.

The asymmetry in the UK sunrise/sunset links from New Zealand to the UK has not been reported before. This particular observation is therefore surprising, and the reason for this is not immediately obvious. From this, a second question arises: why is this sunrise/sunset asymmetry in the pattern not seen in the UK to New Zealand direction?

In the rest of this chapter, the radio propagation links between New Zealand and other countries, and similarly, between the UK and other countries, will be investigated to see if the patterns observed in Figure 4.5 and Figure 4.6 can be corroborated and understood.

4.3. United States

Section 4.2. indicates an asymmetry between the UK sunrise and sunset links from New Zealand to the UK, with this pattern not seen in the reciprocal direction. Therefore, it is interesting to see if similar patterns emerge when radio links are propagated from New Zealand to other countries and between the UK and other countries. For this reason, a wider study of links between countries/regions is undertaken here. From Figure 4.1 to Figure 4.4, they show that most of the links are received by or transmitted from the stations in the USA. Therefore, in this section, the radio links propagating between the USA and New Zealand and between the USA and the UK will be observed. The objective is to discover if the time propagation pattern from these radio links experiences the same type of asymmetry.

4.3.1. Radio Links propagating between New Zealand and the USA

The radio links propagating between New Zealand and the USA will be observed in this section. Firstly, the propagation between NZ and Eastern USA is presented in Figure 4.7 and Figure 4.8.

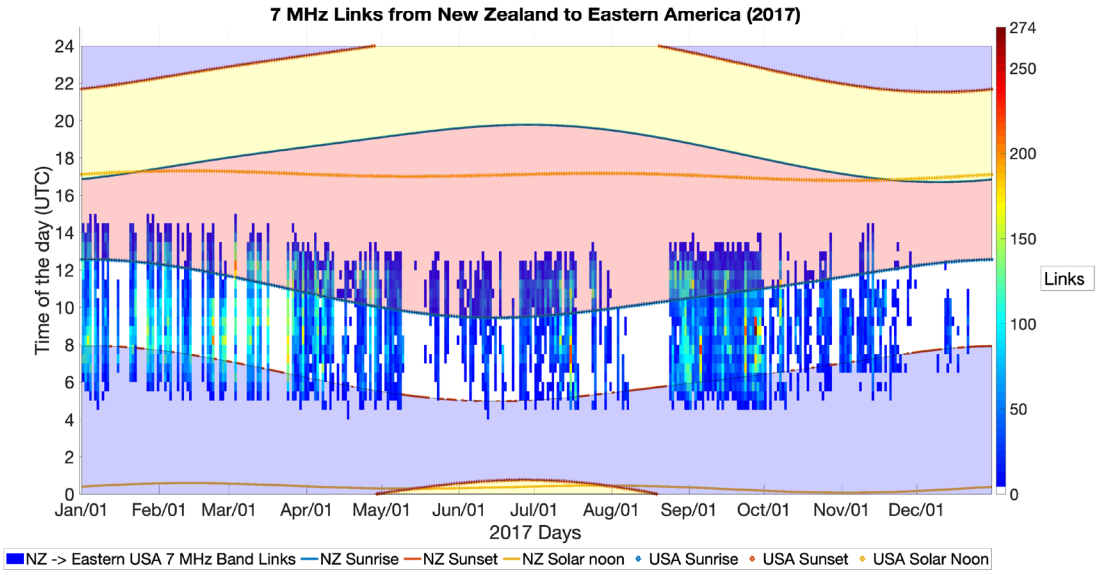

Figure 4.7 – 7 MHz Radio Links made from New Zealand to Eastern America in 2017. The blue shaded area is the New Zealand daytime hours. The red area is the Eastern USA daytime hours. The yellow shaded area is the common daytime hours, and the white shaded area is the common night hours. The colours indicate the number of links available in each half-hour interval.

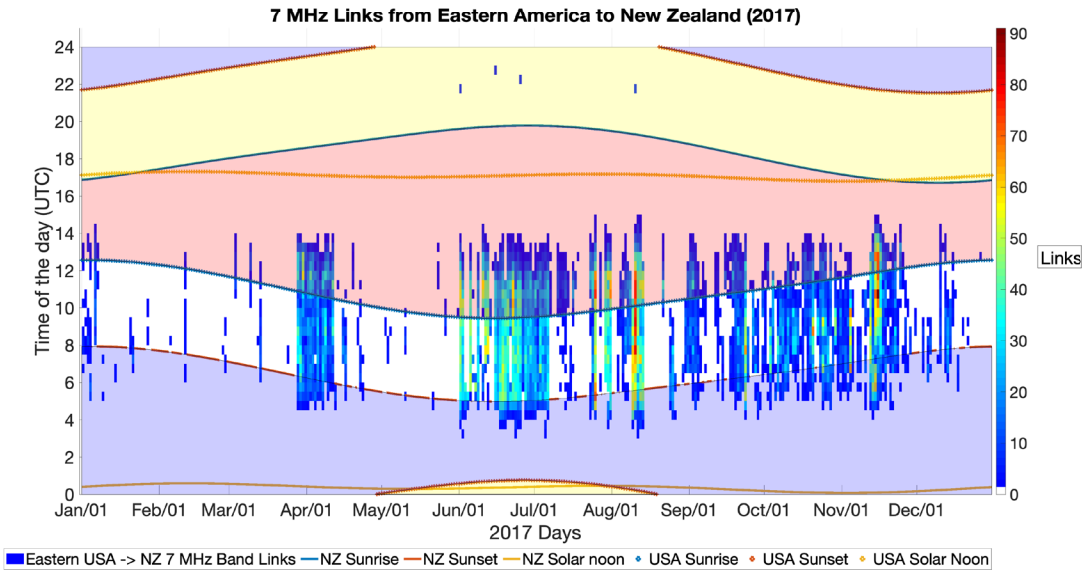

Figure 4.8 – 7 MHz Radio Links made from Eastern America to New Zealand in 2017. The blue shaded area is the New Zealand daytime hours. The red area is the Eastern USA daytime hours. The yellow shaded area is the common daytime hours, and the white shaded area is the common night hours. The colours indicate the number of links available in each half-hour interval.

The radio links propagating between Eastern USA and New Zealand in Figure 4.7 and Figure 4.8 show common night propagation. This is expected since the propagation across the common night will allow for less low-altitude absorption of the radio signals.

Next, the propagation between Western America and New Zealand will be observed to see if the propagation pattern in both directions is similar. This is shown in Figure 4.9 and Figure 4.10.

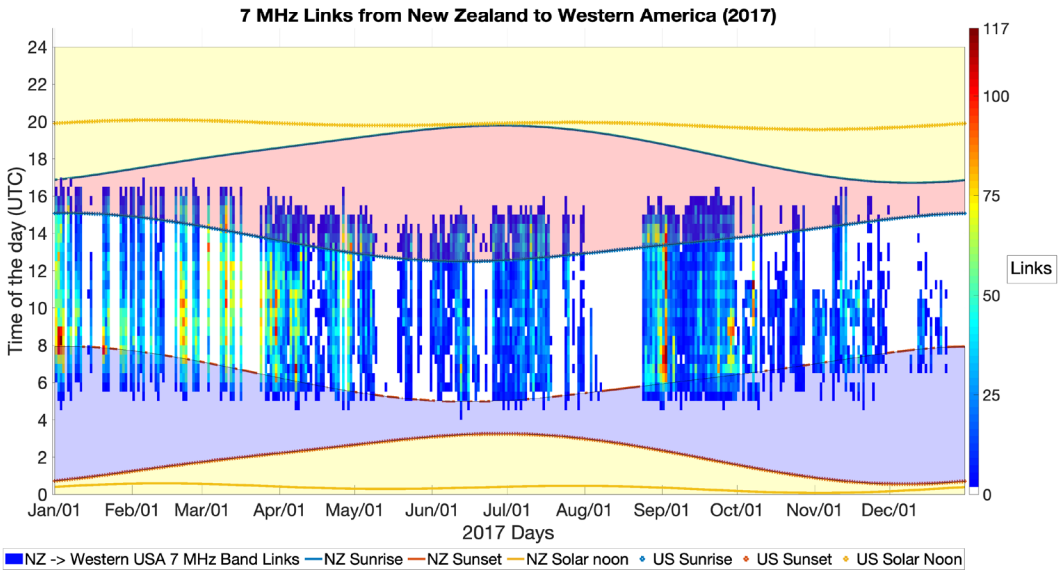

Figure 4.9 – 7 MHz Radio Links made from New Zealand to Western America in 2017. The blue shaded area is the New Zealand daytime hours. The red area is the Western USA daytime hours. The yellow shaded area is the common daytime hours, and the white shaded area is the common night hours. The colours indicate the number of links available in each half-hour interval.

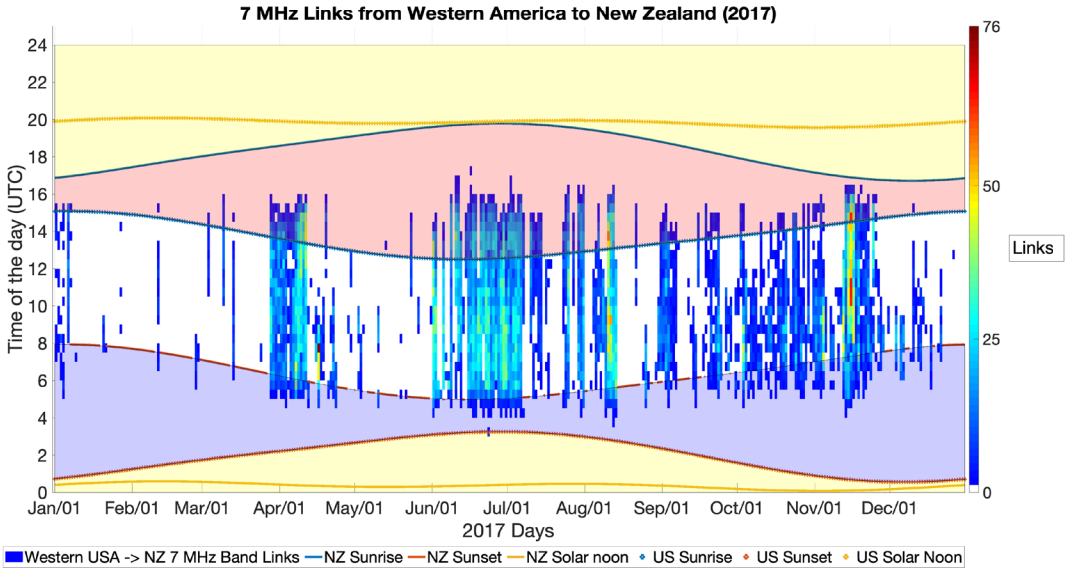

Figure 4.10 – 7 MHz Radio Links made from Western America to New Zealand in 2017. The blue shaded area is the New Zealand daytime hours. The red area is the Western USA daytime hours. The yellow shaded area is the common daytime hours, and the white shaded area is the common night hours. The colours indicate the number of links available in each half-hour interval.

From Figure 4.10, it can be seen that the radio propagation between New Zealand and Western USA is also similar to the pattern observed between New Zealand and Eastern USA in Figure 4.9. As a result, it shows that radio propagation between New Zealand

and the USA in both occurs mainly during the common night and little during the New Zealand dusk and the USA dawn hours. There is more consistent propagation from New Zealand to the USA throughout the year and significant gaps in the USA to New Zealand in the first half of the year. The long gaps in the propagation pattern are partly due to the New Zealand receiver inactivity, as mentioned in Chapter 3. Nevertheless, this indicates that the propagation links between New Zealand and the USA show mostly night-time propagation as expected because of the lower absorption at night.

Next, the radio links propagating between the USA and another country will be observed in Section 4.3.2.

4.3.2. Radio Links propagating between Australia and the USA

The Eastern region of Australia has only a 2-hour time zone difference from New Zealand. Therefore, an observation of the radio links propagating between Eastern Australia and the USA will be investigated to see if similar patterns have been seen between New Zealand and the USA. In addition, the radio links propagating between 1) Eastern Australia and Eastern America and 2) Eastern Australia and Western America will be observed to compare the time propagating pattern between Australia and the two American regions. This is to confirm that if the time propagation patterns between Eastern Australia and the USA are similar to those between New Zealand and the USA. The radio links propagating between Eastern Australia and the Eastern USA are shown in Figure 4.11 and Figure 4.12.

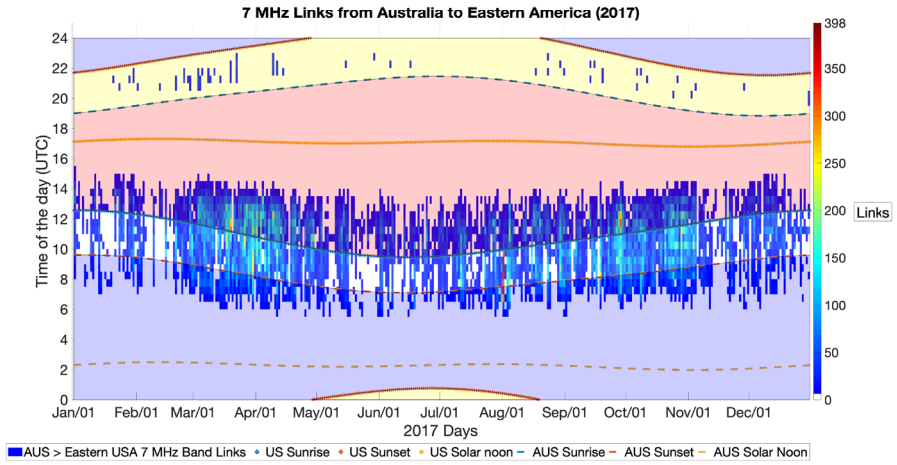

Figure 4.11 – 7 MHz Radio Links made from Australia to Eastern America in 2017. The blue shaded area is Australia daytime hours. The red area is the Eastern USA daytime hours. The yellow shaded area is the common daytime hours, and the white shaded area is the common night hours. The colours indicate the number of links available in each half-hour interval.

Figure 4.11 shows the links between Australia to the Eastern USA in 2017. The radio links propagating from Australia to the Eastern USA show common night propagation and partly across into the Australia dusk and the USA dawn. This is the same as was seen for New Zealand. However, this time, when we look at Australia, there is also common daytime propagation. The times when the links were observed during the

common daytime are confined strictly to the common daytime hours. Figure 4.11 also shows that more links are made at the common night hours than during the common daytime hours.

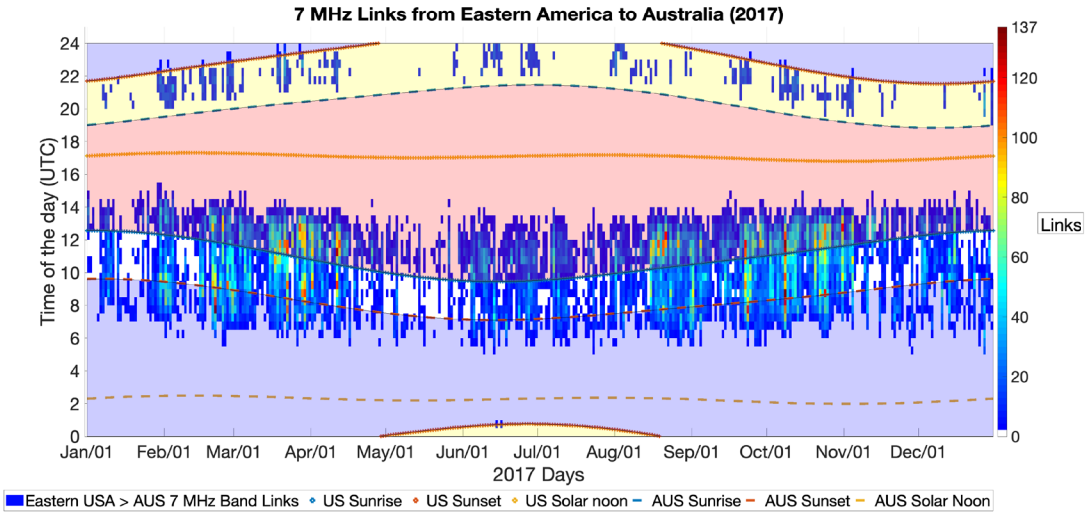

Figure 4.12 – 7 MHz Radio Links made from Eastern America to Australia in 2017. The blue shaded area is Australia daytime hours. The red area is the Eastern USA daytime hours. The yellow shaded area is the common daytime hours, and the white shaded area is the common night hours. The colours indicate the number of links available in each half-hour interval.

The radio links propagating from the Eastern USA to Australia in Figure 4.12 also show common night propagation and common-day propagation. However, the common daytime propagation is confined strictly to daytime hours. These results show that Australia's links to the Eastern USA and the reciprocal direction (the USA to Australia) look primarily symmetric, i.e., the signals are propagating in both directions at similar times.

The propagation between Western America and Australia will now be observed to see if the propagation matches the pattern observed from Eastern America to Australia. The propagation pattern between Western America and Australia is shown in Figure 4.13 and Figure 4.14.

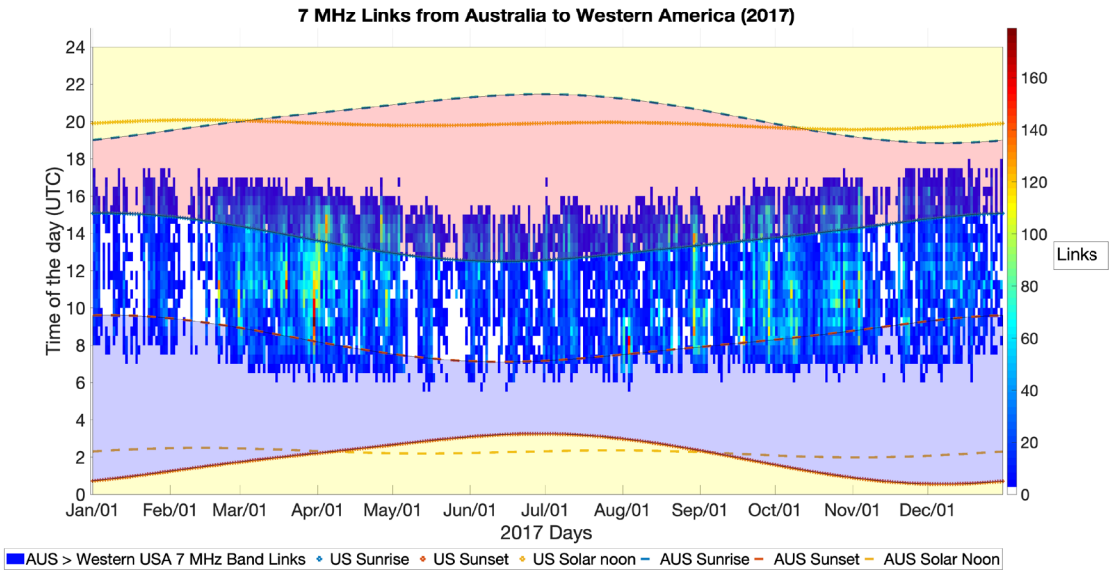

Figure 4.13 – 7 MHz Radio Links made from Australia to Western America in 2017. The blue shaded area is Australia daytime hours. The red area is the Western USA daytime hours. The yellow shaded area is the common daytime hours, and the white shaded area is the common night hours. The colours indicate the number of links available in each half-hour interval.

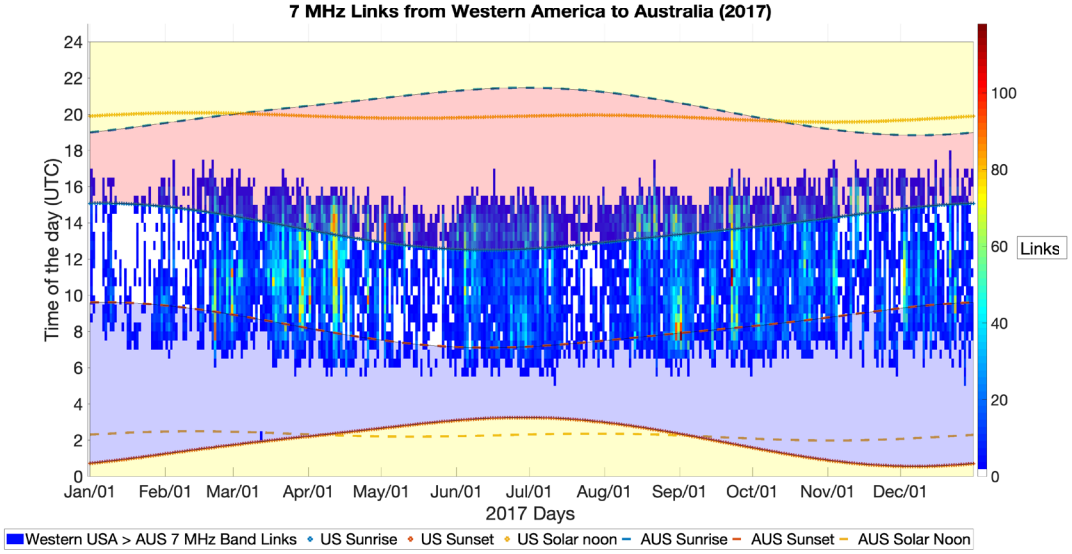

Figure 4.14 – 7 MHz Radio Links made from Western America to Australia in 2017. The blue shaded area is Australia daytime hours. The red area is the Western USA daytime hours. The yellow shaded area is the common daytime hours, and the white shaded area is the common night hours. The colours indicate the number of links available in each half-hour interval.

Figure 4.13 and Figure 4.14 show that many links are propagating between Australia and the Western USA. The radio links propagating between Western USA and Australia also show common night propagation, but no common daytime links are made. Therefore, the diurnal propagation pattern between the Western USA and Australia looks mostly symmetrical, i.e., propagating in both directions at similar times.

The radio links propagating between Australia and the USA were shown from Figure 4.11 to Figure 4.14. Figure 4.11 to Figure 4.14 shows that the radio links favour propagating during the transmitter and receiver, both in night-time hours. Figure 4.11 to Figure 4.12 also showed that there is common day propagation in the radio links between Australia and the Eastern USA. However, they are heavily confined into the common daytime hours.

The time propagation patterns between Eastern Australia and the USA show that they appear to be symmetrical in both directions at similar times. This confirms that these time propagation patterns are similar to those propagating between New Zealand and the USA, indicating that the radio links propagating between Australia/New Zealand (Australia and New Zealand) and the USA are symmetrical in both directions at similar times. For this reason, the time propagation patterns of the radio links propagating between the UK and the USA will be observed in Section 4.3.3. to see if the time propagation patterns between the UK and the USA are symmetrical in both directions at similar times.

4.3.3. Radio Links propagating between the UK and the USA

The patterns from the radio links between New Zealand and Eastern USA and those between Australia and Eastern USA have been shown. However, they did not show any evidence of asymmetry in the propagation direction. Therefore, it was decided to investigate if the New Zealand/UK asymmetry appears in the radio propagation links between Eastern USA and other countries across the Atlantic Ocean, such as the UK and Italy and the adjacent regions (ITADR).

In addition, Figure 4.3 and Figure 4.4 indicated that numerous radio links were made between Eastern USA and the UK. Therefore, in this section, the radio propagation links between the UK and Eastern USA are analysed. Figure 4.15 shows the propagation from Eastern USA to the UK. The links are made during the common night-time and absent from common day time, with the propagation from the UK to the Eastern US matching the same pattern, as shown in Figure 4.16.

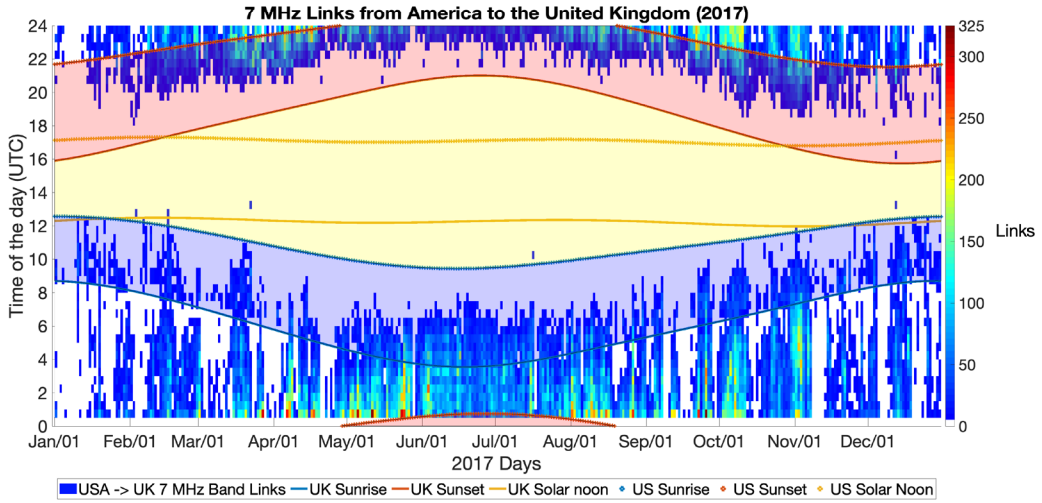

Figure 4.15 – 7 MHz Radio Links made from Eastern America to the United Kingdom in 2017. The blue shaded area is the United Kingdom daytime hours. The red area is the Eastern USA daytime hours. The yellow shaded area is the common daytime hours, and the white shaded area is the common night hours. The colours indicate the number of links available in each half-hour interval.

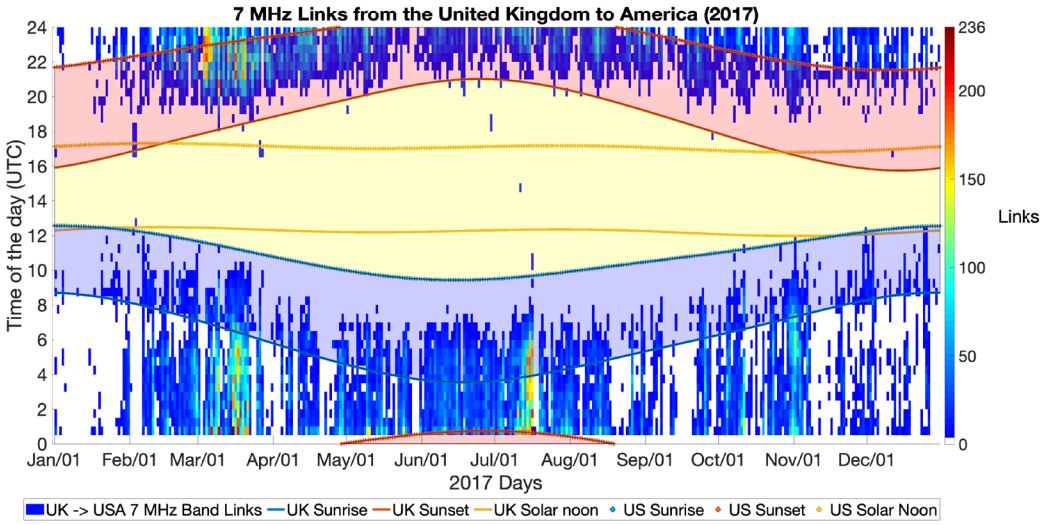

Figure 4.16 – 7 MHz Radio Links made from the United Kingdom to Eastern America in 2017. The blue shaded area is the United Kingdom daytime hours. The red area is the Eastern USA daytime hours. The yellow shaded area is the common daytime hours, and the white shaded area is the common night hours. The colours indicate the number of links available in each half-hour interval.

The propagation extends from the common night into the UK dawn and the US dusk. There are also very few links in the common daytime. This propagation illustrates that the propagation between Eastern USA and the UK is symmetrical as the radio links show a similar time propagation pattern in both directions at similar times. For this reason, it was decided to investigate the radio links between the USA and a country that is close to the UK to compare with the UK results and see if there is a similar time propagation pattern in both directions at similar times.

4.3.4. Radio Links propagating between Italy and the adjacent regions (ITADR) and the USA

Italy is a country that is within a 2-hour time zone difference further east from the UK and has significant radio amateur activity on the WSPR network. Hence, Italy and the adjacent regions (ITADR) were chosen for the analysis. The radio links propagating between Italy and the adjacent regions (ITADR) and the Eastern USA are shown in Figure 4.17 and Figure 4.18.

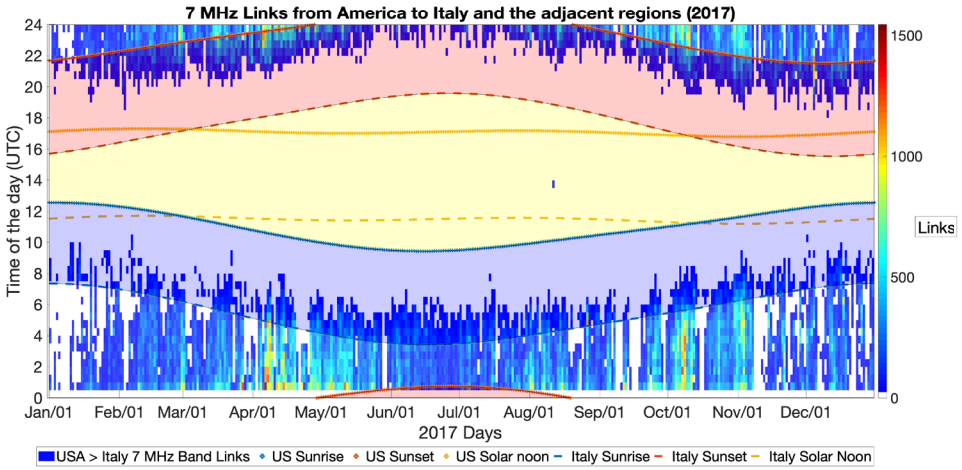

Figure 4.17 – 7 MHz Radio Links made from Eastern America to Italy and the adjacent regions in 2017. The blue shaded area is Italy and the adjacent regions daytime hours. The red area is the Eastern USA daytime hours. The yellow shaded area is the common daytime hours, and the white shaded area is the common night hours. The colours indicate the number of links available in each half-hour interval.

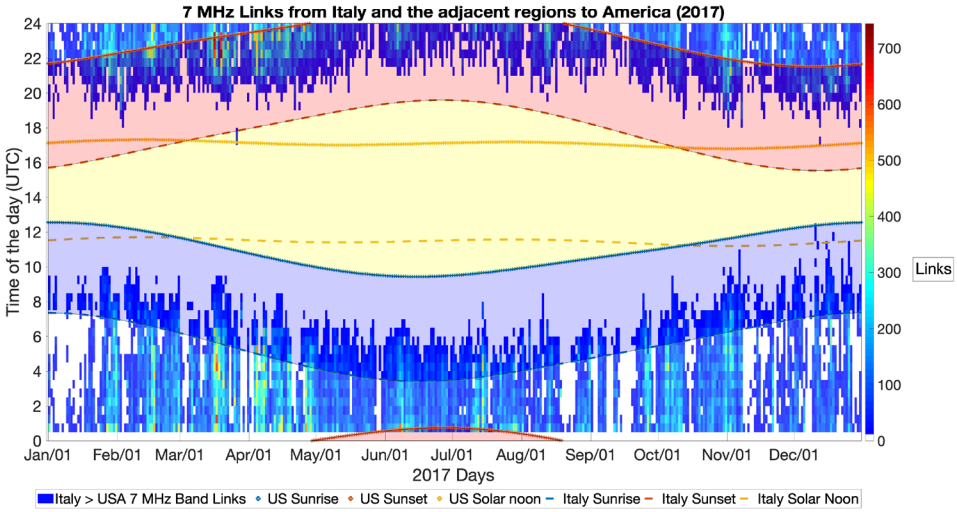

Figure 4.18 – 7 MHz Radio Links made from Italy and the adjacent regions to Eastern America in 2017. The blue shaded area is Italy and the adjacent regions daytime hours. The red area is the Eastern USA daytime hours. The yellow shaded area is the common daytime hours, and the white shaded area is the common night hours. The colours indicate the number of links available in each half-hour interval.

The radio propagation links from Eastern USA to Italy and the adjacent regions in Figure 4.17 exhibit the same propagation pattern observed between Eastern USA and UK. Similarly, the propagation pattern is the same in the reciprocal direction (Figure 4.18). These findings show that the UK and Eastern USA radio propagation links and those between Italy and the adjacent regions (ITADR) and the Eastern USA look similar. Thus, they exhibit the expected preference for night-time when the ionospheric absorption at low altitudes is lowest.

The results indicate that the asymmetrical time propagation patterns between the evening and in the daytime seen between New Zealand and the UK (Figure 4.5 and Figure 4.6) do not occur from the radio propagation links propagating to and from the USA. As a result, the asymmetrical time propagation patterns may be found from the radio links propagating between New Zealand and Italy and the adjacent regions. Therefore, an observation of the radio links between New Zealand and Italy and the adjacent regions will be observed in Section 4.4.

4.4. Radio Propagation Links between New Zealand and Italy and the adjacent regions (ITADR)

The radio links propagating between New Zealand and the UK, as shown in Section 4.2. indicate that there is an apparent dawn/dusk asymmetry in the propagation links. However, the radio links propagating between the USA and other countries, as shown in Section 4.3. suggest that the directional pattern is symmetric. Figure 4.19 presents the propagations links from New Zealand to Italy and the adjacent regions, and Figure 4.20 - from Italy and the adjacent regions to New Zealand.

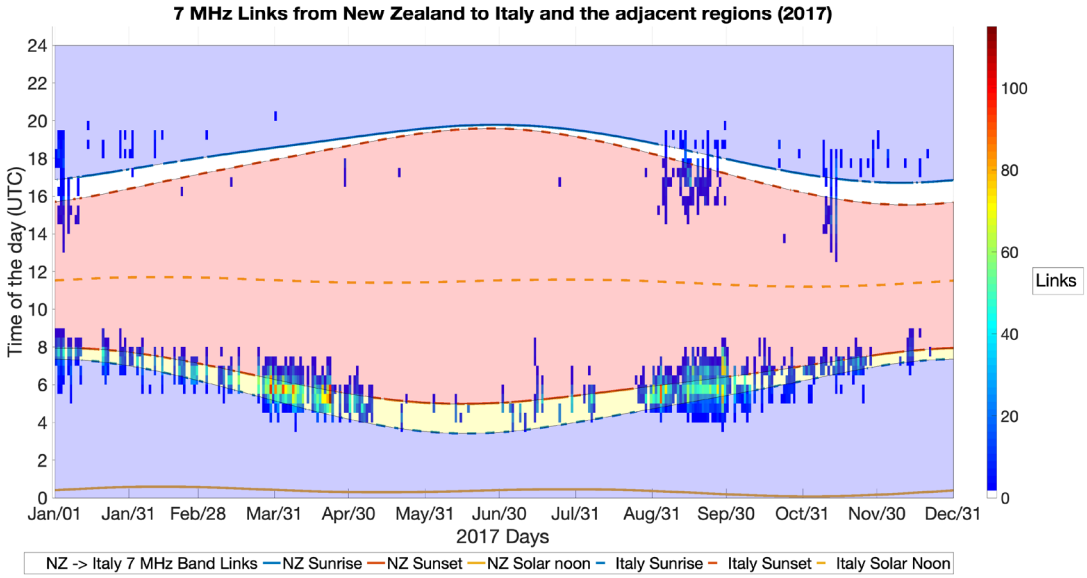

Figure 4.19 – 7 MHz radio links made from New Zealand to Italy and the adjacent regions in 2017. The blue shaded area is the New Zealand daytime hours. The red area is Italy and the adjacent regions daytime hours. The yellow shaded area is the common daytime hours, and the white shaded area is the common night hours. The colours indicate the number of links available in each half-hour interval.

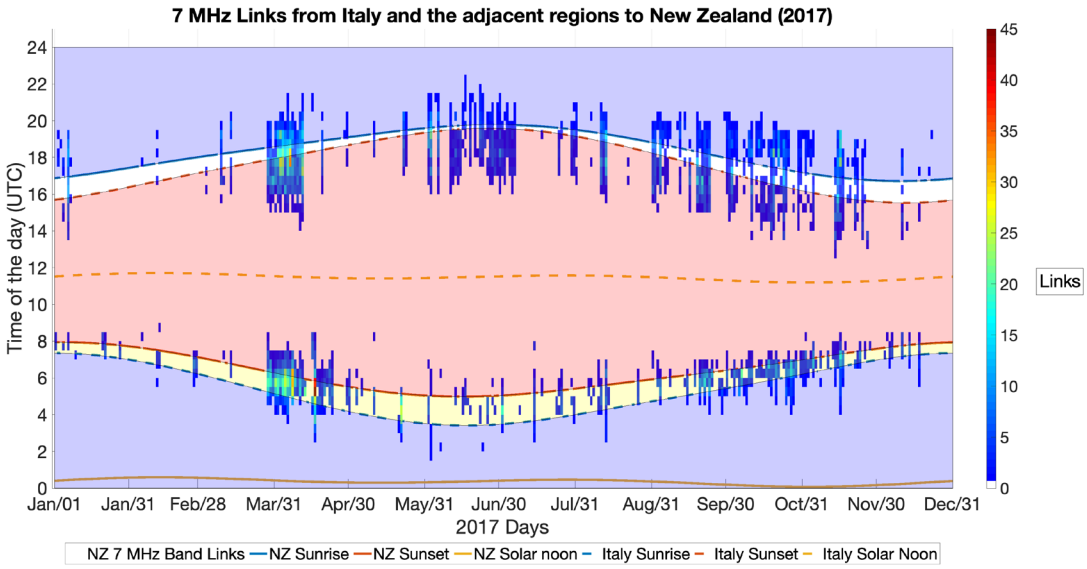

Figure 4.20 – 7 MHz radio links made from Italy and the adjacent regions to New Zealand in 2017. The blue shaded area is the New Zealand daytime hours. The red area is Italy and the adjacent regions daytime hours. The yellow shaded area is the common daytime hours, and the white shaded area is the common night hours. The colours indicate the number of links available in each half-hour interval.

Figure 4.19 and Figure 4.20 both illustrate that there is an asymmetry pattern between the UTC evening and morning hours. They show that there are similar numbers of links made in both directions in the UTC morning, but there are fewer links made in New Zealand to Italy and the adjacent regions direction in the UTC evening.

The patterns seem to be similar to the radio links between NZ and the UK, described in Section 4.2. However, further checks can be made by comparing Australia to the UK and Australia to Italy and the adjacent regions in Section 4.5. Australia is chosen as it is close to New Zealand and has significant radio amateur activity through WSPR.

4.5. Radio Propagation Links between Australia and Europe

The radio propagation links between Australia and Europe are observed to compare their time pattern to the one already seen between NZ and UK. Specifically, the radio links between Australia and the UK and radio links between Australia and Italy and the adjacent regions (ITADR) will be analysed. Firstly, the radio propagation between Australia and the UK are presented in Figure 4.21 and Figure 4.22. The radio links transmitted from Australia to the UK show a sparsity of connections in the UK summer evening (Figure 4.21) which is not seen in the UK to Australia direction (Figure 4.22). It indicates that there is an asymmetry in the time propagation patterns between the UTC evening and morning hours in both directions at similar times.

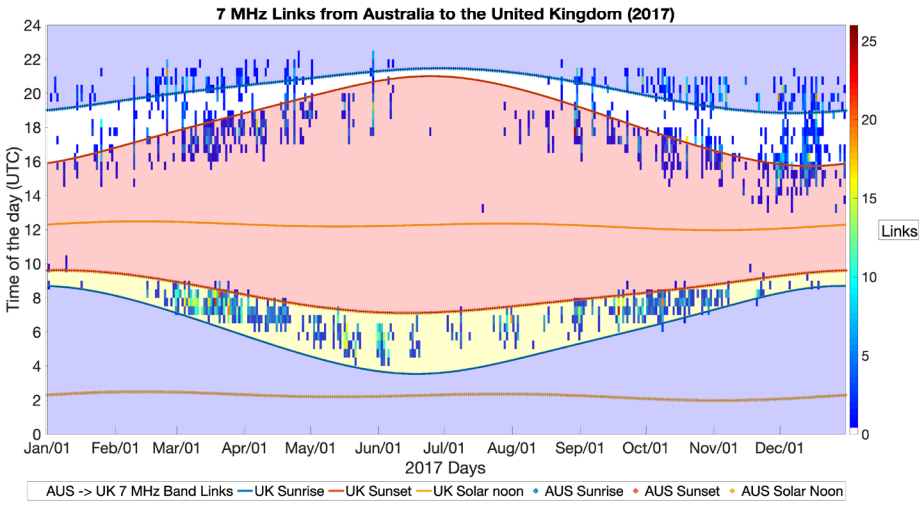

Figure 4.21 – 7 MHz Radio Links made from Australia to the United Kingdom in 2017. The blue shaded area is Australia daytime hours. The red area is the UK daytime hours. The yellow shaded area is the common daytime hours, and the white shaded area is the common night hours. The colours indicate the number of links available in each half-hour interval.

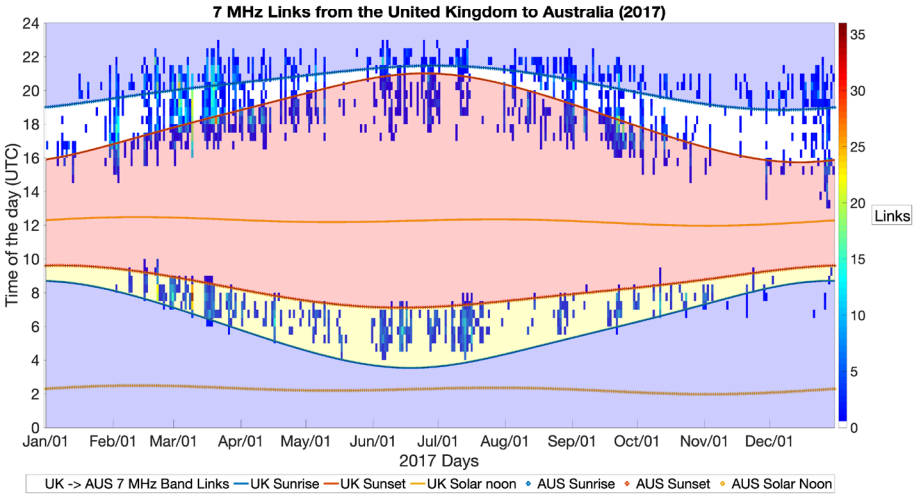

Figure 4.22 – 7 MHz Radio Links made from the United Kingdom to Australia in 2017. The blue shaded area is Australia daytime hours. The red area is the UK daytime hours. The yellow shaded area is the common daytime hours, and the white shaded area is the common night hours. The colours indicate the number of links available in each half-hour interval.

The radio links propagating between Italy and the adjacent regions and Australia are shown in Figure 4.23, and Figure 4.24 are also observed to see if the pattern is similar.

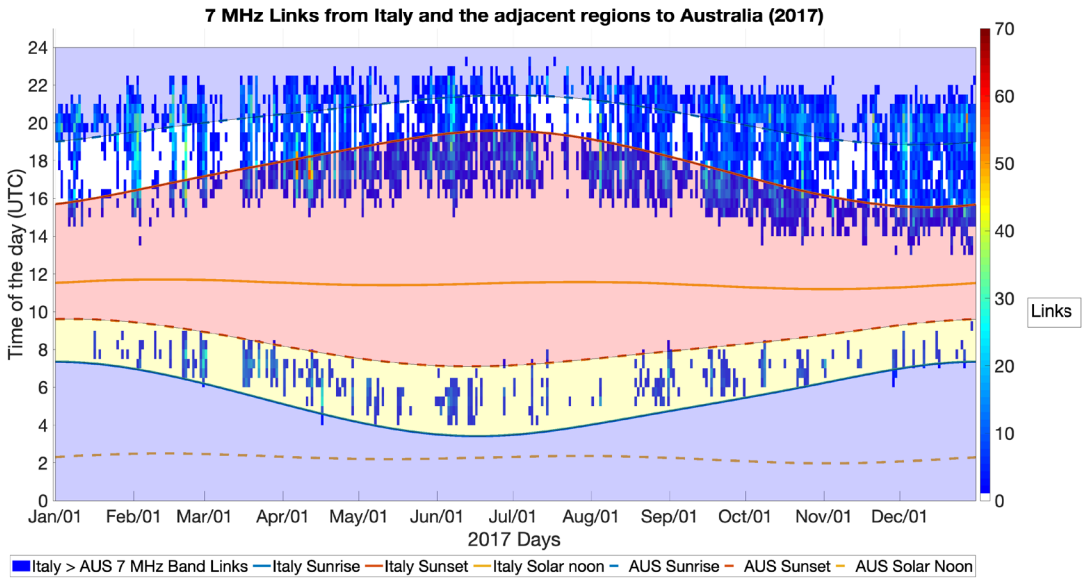

Figure 4.23 – 7 MHz Radio Links made from Italy and the adjacent regions to Australia in 2017. The blue shaded area is Australia daytime hours. The red area is Italy and the adjacent regions daytime hours. The yellow shaded area is the common daytime hours, and the white shaded area is the common night hours. The colours indicate the number of links available in each half-hour interval.

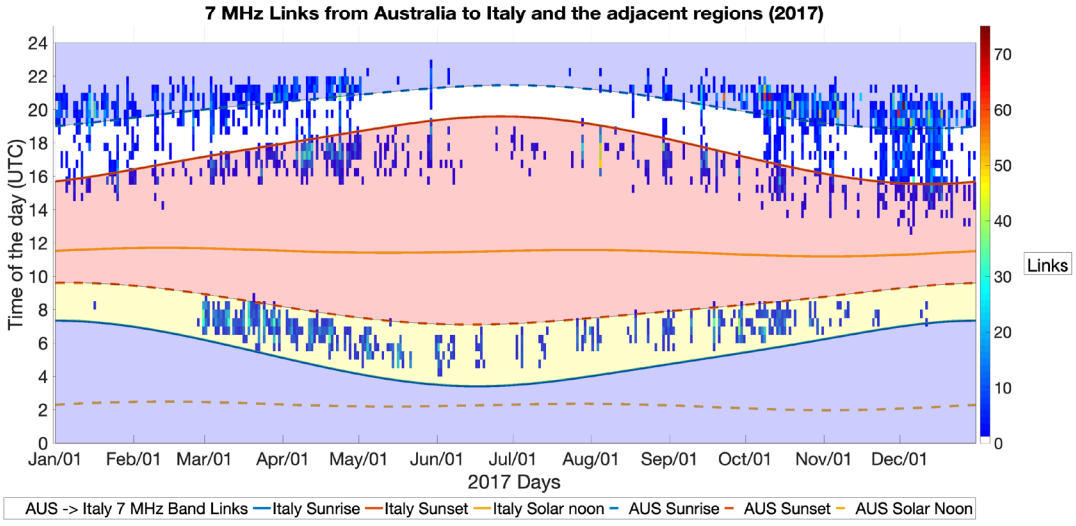

Figure 4.24 – 7 MHz Radio Links made from Australia to Italy and the adjacent regions in 2017. The blue shaded area is Australia daytime hours. The red area is Italy and the adjacent regions daytime hours. The yellow shaded area is the common daytime hours, and the white shaded area is the common night hours. The colours indicate the number of links available in each half-hour interval.

Figure 4.23 and Figure 4.24 show that radio links transmitted from Australia to Italy and the adjacent regions (ITADR) have a sparsity of connections in the Italian summer evening (Figure 4.24), which is not seen in the reciprocal direction (Figure 4.23). The propagation pattern from Italy and the adjacent regions to Australia shows that the links

were made in both night and daytime hours with a significant spread in the night-time and a significant concentration in daytime hours.

Therefore, the propagation data from Australia to the UK and Australia to Italy and the adjacent regions (ITADR) support the surprising result from the start of this chapter. There is a lack of links in one of the propagation directions and not the other (Australia to Europe/UK) during the European/UK summertime post-sunset. Alternatively, the same statement can be written in another way: there is a lack of links (Australia to Europe/UK) in the Australia/New Zealand wintertime pre-sunrise.

There are also missing links during the European/UK wintertime at sunrise.

4.6. Summary

The results showed that many of the links in WSPR propagated between these countries at 7 MHz frequency band in the year 2017: 1. the UK; 2. New Zealand; 3. Italy and the adjacent regions; 4. the USA and 5. Australia, as illustrated from Figure 4.1 to Figure 4.4. The existence of the links was partly because of the activity of radio amateurs in these countries, meaning that the radio amateurs in these countries are the most active. The pattern of activity for the WSPR stations in these countries throughout the year is shown in Appendix A.

The observations of the links were analysed in Section 4.2. (New Zealand and the UK), Section 4.3. (The USA to Europe and Australia/New Zealand), Section 4.4. (New Zealand and Italy and the adjacent regions) and Section 4.5. (Australia and Europe). The analysis was used to determine if there was a preferential time pattern for propagation between the two countries, which in turn showed that an asymmetry between the evening and morning propagation times existed. It also shows that there is a directional asymmetry with propagation from the UK/Europe region to Australia/New Zealand during the UK/Europe sunset hours in the summer but not in the opposite direction.

Section 4.3. showed that propagation between Europe and the USA, and similarly, between Australia/New Zealand and the USA, favoured common night-time propagation but was not closely confined to the night-time. For example, radio propagation between the USA and Europe, presented in Figure 4.15 - Figure 4.18, revealed that radio propagation between the regions favoured common night-time propagation. This diurnal propagation pattern was similar between Australia/New Zealand and the USA, as presented in Figure 4.11 - Figure 4.14.

Section 4.3. also signified that there was propagation during times when both the transmitter and the receiver were in daytime hours (in sunlight on the ground). This could be seen from radio links between Australia/New Zealand and the USA. However, the common daytime propagation appeared between the USA and Australia but apparently not between the USA and New Zealand.

The results from Australia to the UK and Australia to Italy and the adjacent regions supported the surprising result from the start of this chapter that indicated that there was a dawn/dusk asymmetry in the propagation. Furthermore, the results indicated that it is more difficult to make a link from Australia/New Zealand to Europe in the UT evening hours from May to September, which is in the middle of the year than it is to make a link from Europe to Australia/New Zealand at the same time.

The next chapter, Chapter 5, will investigate the local noise effects on the UK and New Zealand results. The aim is to observe whether the local noise influences the patterns of reception observed in this chapter.

5. Investigation into the influence of signal-to-noise

5.1. Introduction

Chapter 4 provided an overview of the 7 MHz WSPR links throughout 2017 between selected countries. The purpose was to look for patterns in the times when those links were made. This chapter will further investigate the results from the WSPR data analysed from Chapter 4, focusing on those links made between Australia, New Zealand, and the UK. The main focus is to examine the relationship between the received signal-to-noise ratio (SNR) and the transmission power of the recorded transmissions.

One of the most interesting results in Chapter 4 is the clustering of links around dawn and dusk, confirming the evidence previously reported from the so-called 'grey-line propagation' radio amateur community. However, the results from WSPR also showed another new interesting result - a sparsity of links from Australia/New Zealand to the UK/Europe in the European summer dusk. On the other hand, the propagation in the opposite direction did not show a sparsity of links in the European summer dusk. It is not immediately obvious why this asymmetry would happen, but one possibility could be differences in the local noise effects at the reception. These are investigated in this chapter.

The approach here needs to consider that WSPR provides SNR but not signal strength or noise separately. However, it does provide information on the transmission power. For this reason, it is required to work with the transmission power and the SNR values from multiple locations and to try to work out if there is anything notable in the patterns that are seen that could be used to explain the observations in Chapter 4.

This chapter is structured as follows: Section 5.2 reports on some initial investigations on the worldwide WSPR signals coming into the UK and into the Australia/New Zealand region; Section 5.3. will investigate the WSPR results from the UK to Australia and New Zealand to observe if the SNR can provide any further information to help explain the patterns that have been observed. This will be investigated by observing the received SNR and the transmission power recorded in the WSPR dataset and Section 5.4. will investigate the WSPR results from Australia and New Zealand to the UK with the same structure as Section 5.3. Section 5.5. will summarise the results.

5.2. Initial investigations

Considering the effect of noise, if there was a large amount of noise in the evening in Europe, but not in the morning in Australia/New Zealand, then that could prevent some of the weaker WSPR signals from being received in Europe. However, that could be an effect that would also prevent some of the other signals from elsewhere from being received, so it should manifest in other observations.

The x-axis of Figure 5.1 represents the day of the year 2017, whereas the y-axis represents the time of day. The colours indicate the number of links, the SNR (dB) or the transmitter power (dBm) in each half-hour intervals. The number of links and the higher minimum SNRs detected by the UK receivers will be observed first.

The UK receivers were able to detect signals from outside of Europe in the Europe summer dusk, as illustrated in Figure 5.1, and received some of the signals with higher minimum SNRs, as shown in Figure 5.2. It is noteworthy from Figure 5.1 that there are significantly more links received in the dawn/morning and that the links received in the summer dusk/evening often had a higher minimum SNR indicating that there is either less noise or stronger signal strength, or both.

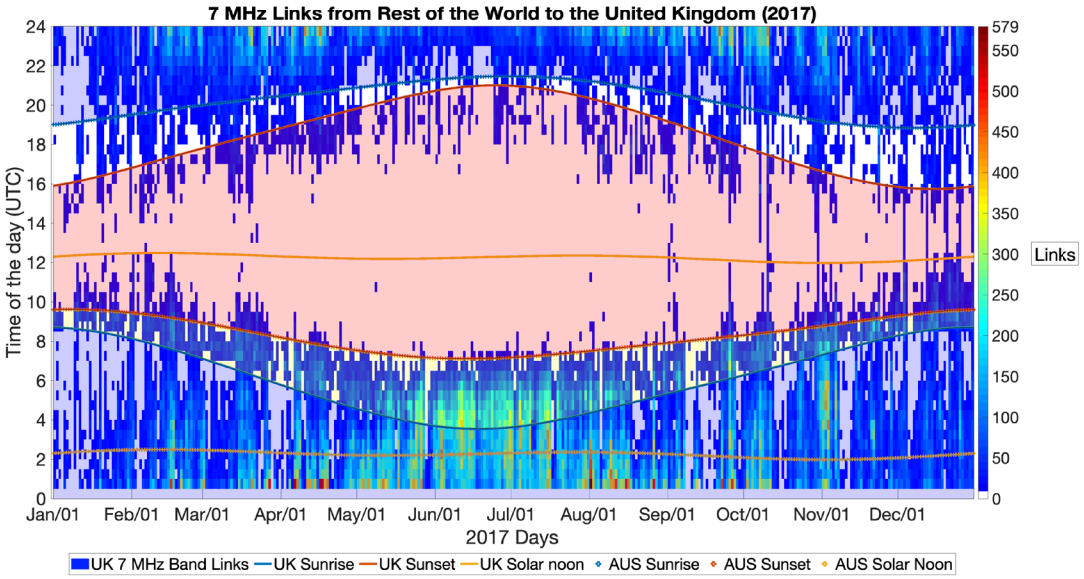

Figure 5.1 – 7 MHz links propagated from the Rest of the World (outside of Europe) to the UK. The colours in the colorbar indicate the number of observations in each half-hour intervals.

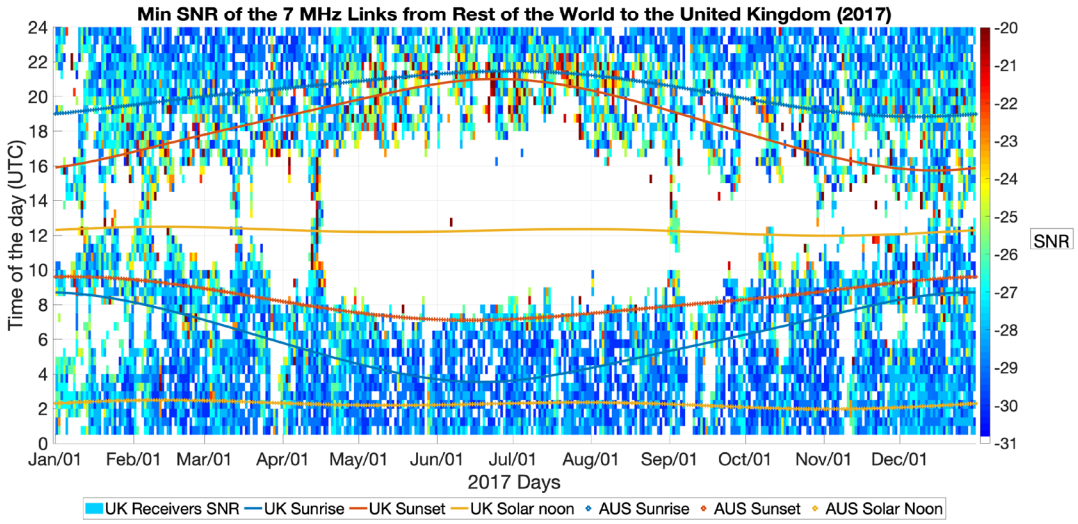

Figure 5.2 – Minimum SNR received by the UK receivers from 7 MHz WSPR links transmitted from outside of Europe. The colours in the colorbar indicate the number of observations in each half-hour intervals.

There is no direct evidence from Figure 5.1 and Figure 5.2 that the signal reception in the European summer evenings was affected by higher local noise. However, the SNR during the summer evenings in Figure 5.2 is elevated compared to the corresponding values in the morning.

The links transmitted from Australia and New Zealand are analysed, as shown in Figure 5.3 and Figure 5.4. Figure 5.3 and Figure 5.4 show that there are fewer links during the summer UTC dusk time (Australian and New Zealand winter dawn) in evidence for links transmitted from Australia (Figure 5.3), and the same pattern is seen in New Zealand (Figure 5.4). This indicates that the lack of data may be related to the propagation from Australia and New Zealand.

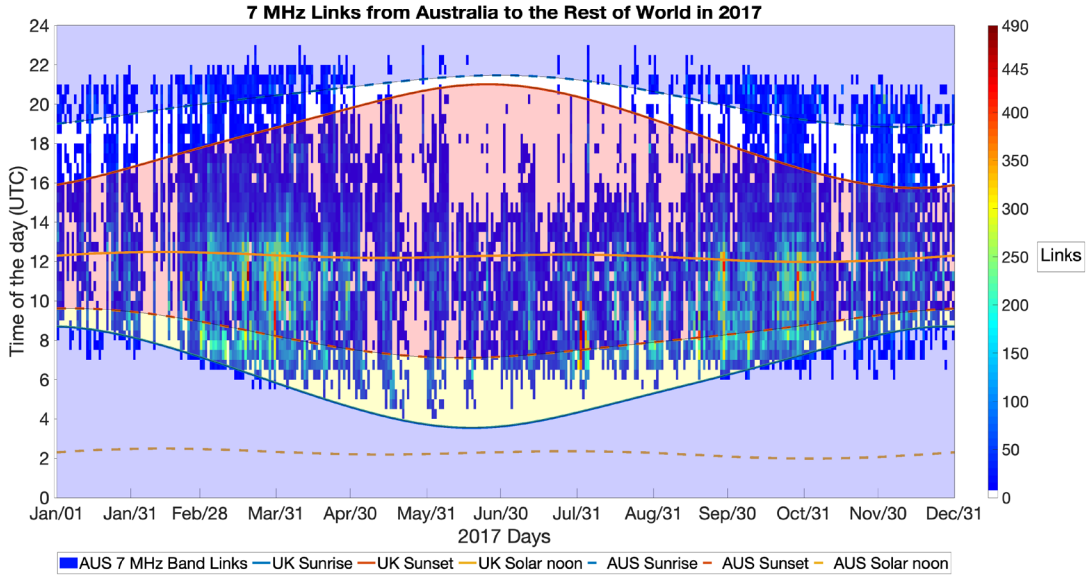

Figure 5.3 – 7 MHz links from Australia to the Rest of the World. The colours in the colorbar indicate the number of observations in each half-hour intervals.

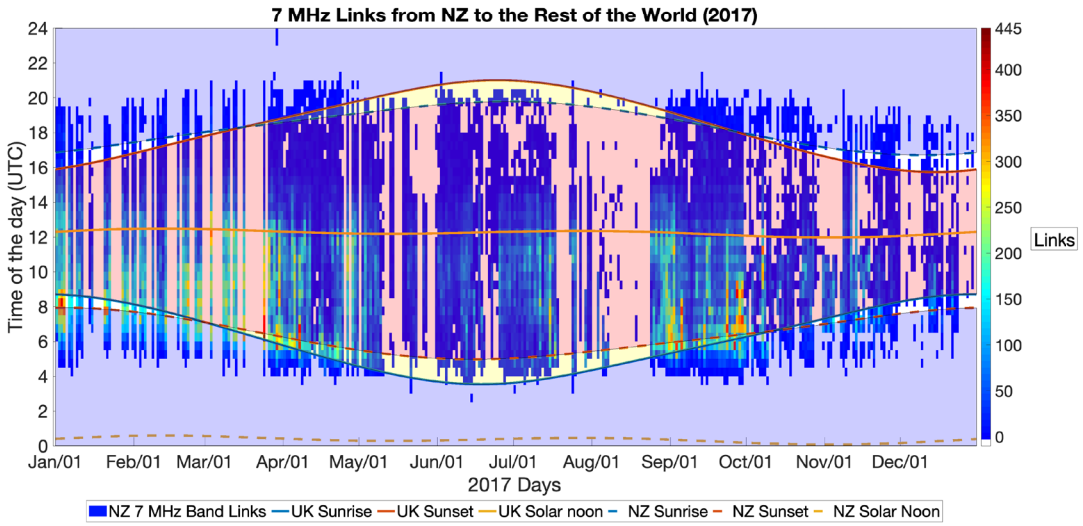

Figure 5.4 – 7 MHz links from New Zealand to the Rest of the World. The colours in the colorbar indicate the number of observations in each half-hour intervals.

Figure 5.3 and Figure 5.4 show that there were only a few signals propagating in the Australian winter mornings compared with those in other seasons. It is not expected that local noise in Australia/New Zealand had affected the signal nor that this would be causing the receivers outside Australia/New Zealand to be unable to detect signals from Australia/New Zealand. However, it is possible that increased ionospheric absorption of the signal has occurred.

Nevertheless, it could be that the local noise in the receivers' regions had influenced the signal reception. Therefore, the SNR received by these distant (Rest of the World) receivers will be observed, which are illustrated in Figure 5.5 and Figure 5.6.

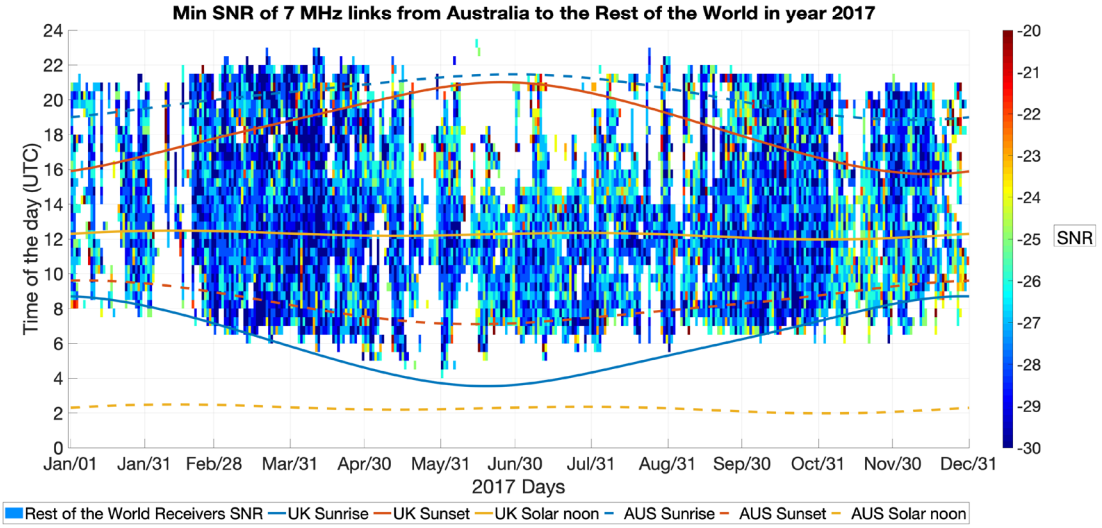

Figure 5.5 – Min SNR of the 7 MHz links from Australia to the Rest of the World. The colours in the colorbar indicate the minimum SNR in dB in each half-hour intervals.

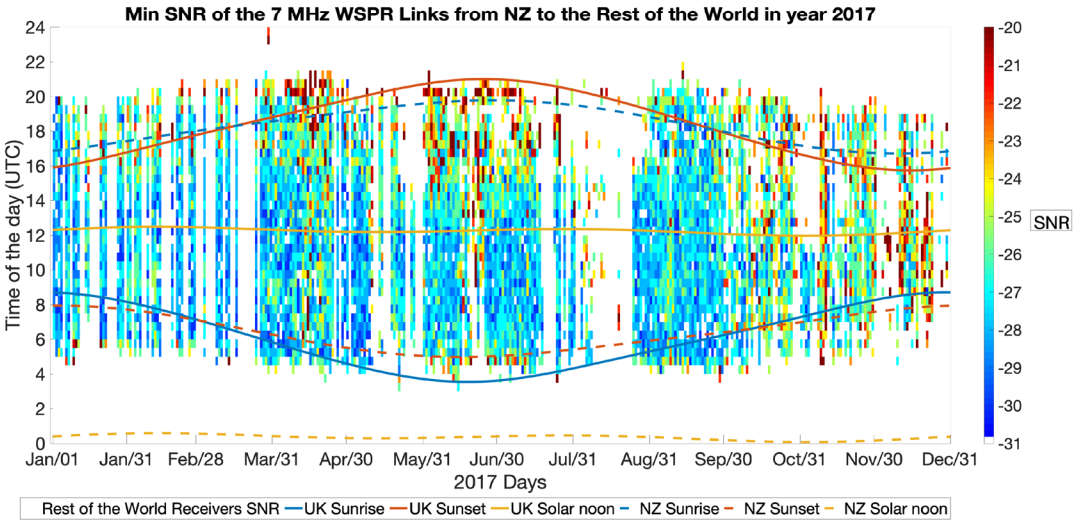

Figure 5.6 – Min SNR of the 7 MHz links from New Zealand to the Rest of the World. The colours in the colorbar indicate the minimum SNR in dB in each half-hour intervals.

Figure 5.5 and Figure 5.6 illustrate the signals' SNR patterns at the distant (Rest of the World) receivers that received signals from Australia/New Zealand. It shows that the SNR from the stations outside of Australia/New Zealand is apparently between – 25 and – 27 dB, with some of the signals been detected with higher SNR during the Australia/New Zealand morning hours.

Figure 5.7 and Figure 5.8 present the minimum transmitter power of the 7 MHz links from Australia to the distant (Rest of the World) stations and from New Zealand to the distant (Rest of the World) stations, respectively. Figure 5.7 shows that the minimum transmitter power is between 25 and 40 dBm for most of the year, whereas Figure 5.8 shows that the minimum power is between 25 dBm and 35 dBm for most of the year. However, Figure 5.8 shows that the transmitter power is very high during September, which is around 50 dBm. Nevertheless, the SNR recorded from the distant (Rest of the World) stations, as illustrated in Figure 5.6, shows that the SNR during September is the same as those in the rest of the year, which is between – 25 dB and – 27dB.

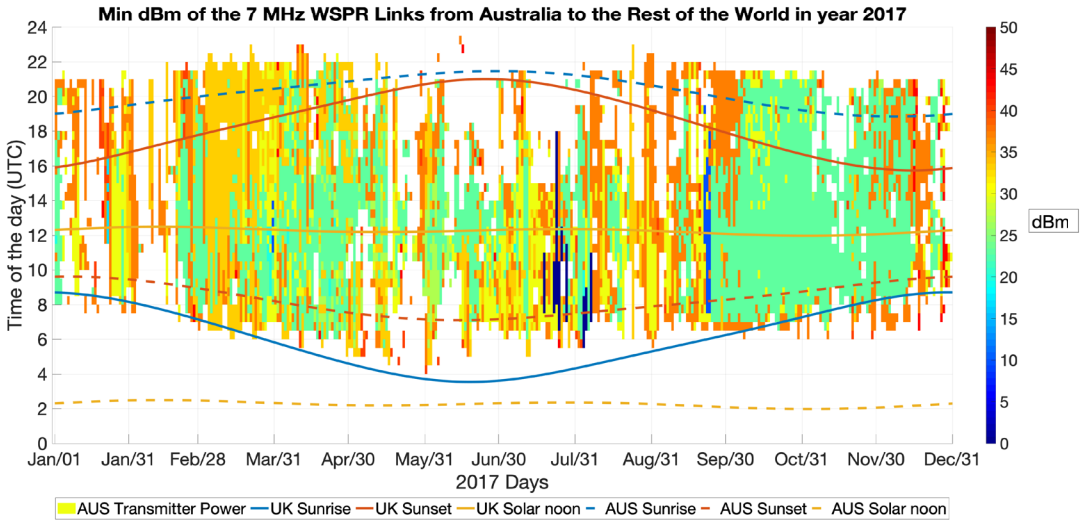

Figure 5.7 – Min transmitter power of the 7 MHz links from Australia to the Rest of the World. The colours in the colorbar indicate the minimum transmitter power in dBm in each half-hour intervals.

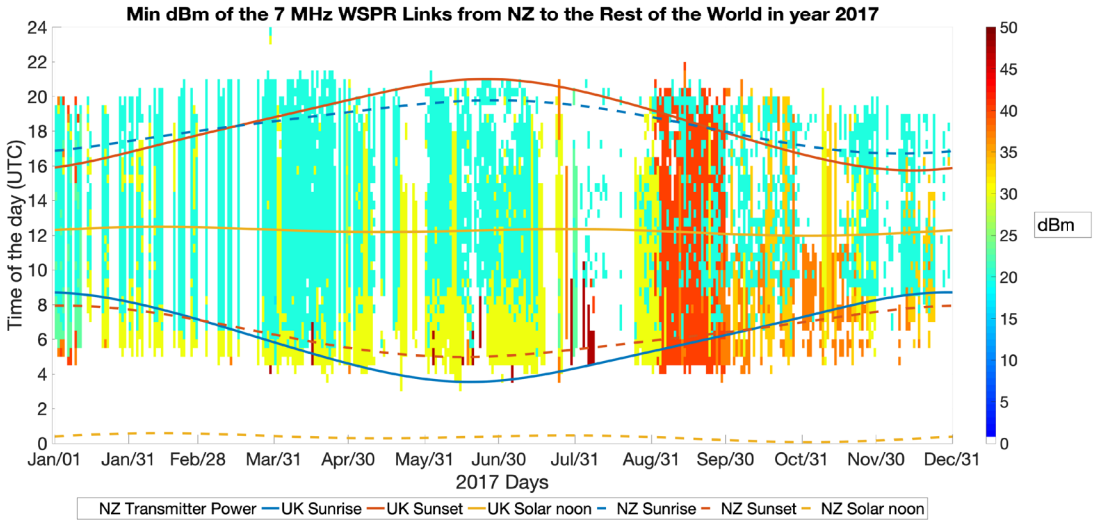

Figure 5.8 – Min transmitter power of the 7 MHz links from New Zealand to the Rest of the World. The colours in the colorbar indicate the minimum transmitter power in dBm in each half-hour intervals.

Figure 5.9 and Figure 5.10 present the maximum transmitter power of the 7 MHz links from Australia to the distant (Rest of the World) stations and from New Zealand to the distant (Rest of the World) stations, respectively. Figure 5.9 and Figure 5.10 show that the maximum transmitter power is approximately 40 dBm for most of the year, whereas Figure 5.7 and Figure 5.8 show that the minimum power is between 30 dBm and 40 dBm for most of the year.

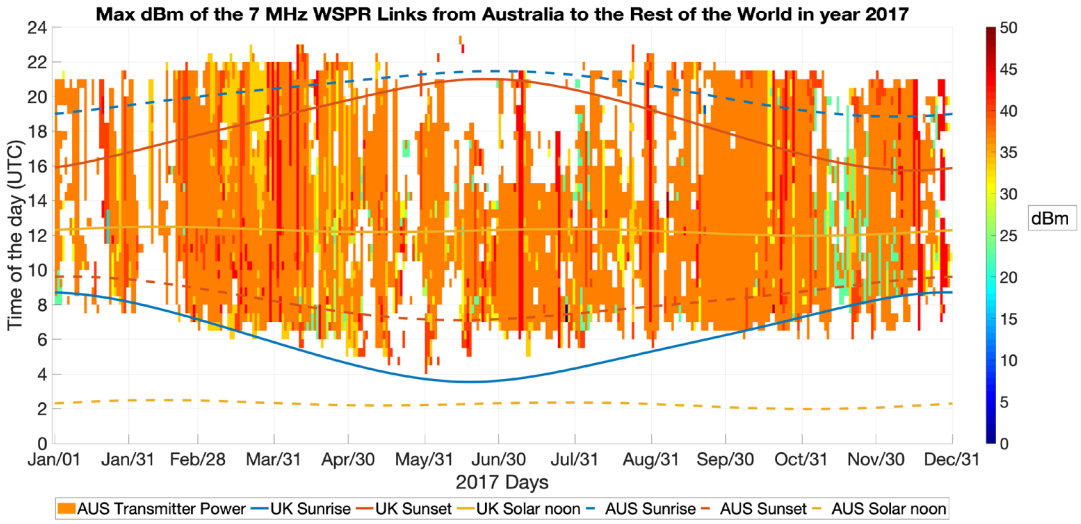

Figure 5.9 – Max transmitter power of the 7 MHz links from Australia to the Rest of the World. The colours in the colorbar indicate the maximum transmitter power in dBm in each half-hour intervals.

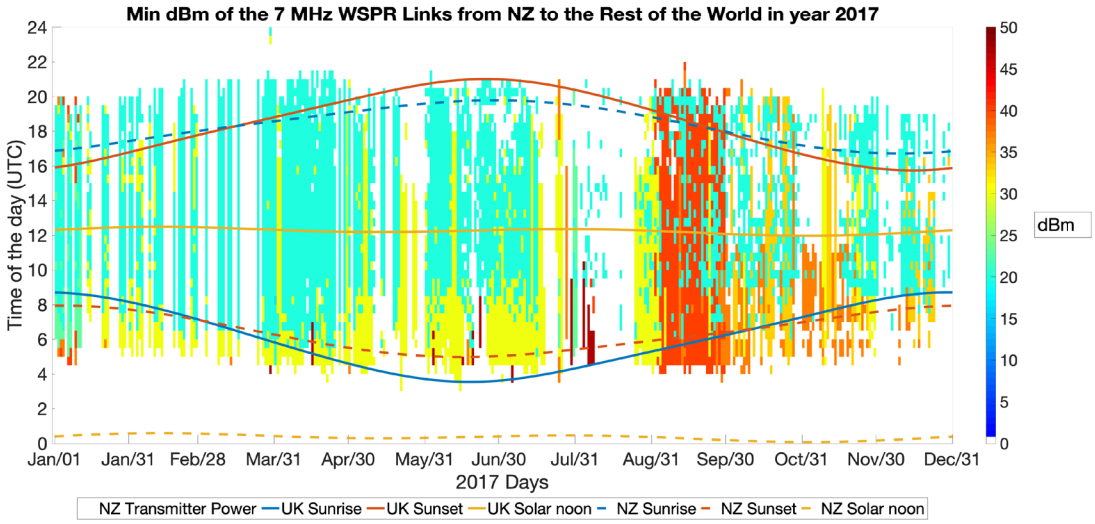

Figure 5.10 – Max transmitter power of the 7 MHz links from New Zealand to the Rest of the World. The colours in the colorbar indicate the maximum transmitter power in dBm in each half-hour intervals.

The other interesting result is the distant (Rest of the World) receivers did not receive signals from Australia/New Zealand during the European summer evenings (Australia winter morning), but they received signals from Australia/New Zealand during the same times in other seasons. As a result, it is possible that the results are being influenced by a seasonal variation in the propagation from the Australia/New Zealand region, which has inhibited the signals propagating from Australia/New Zealand to regions outside of Australia/New Zealand. It is also possible that there is elevated local noise at multiple reception sites for these signals, and the weak signals coming from Australia/New Zealand into these sites are not being received.

5.3. WSPR Results from the UK to New Zealand and Australia

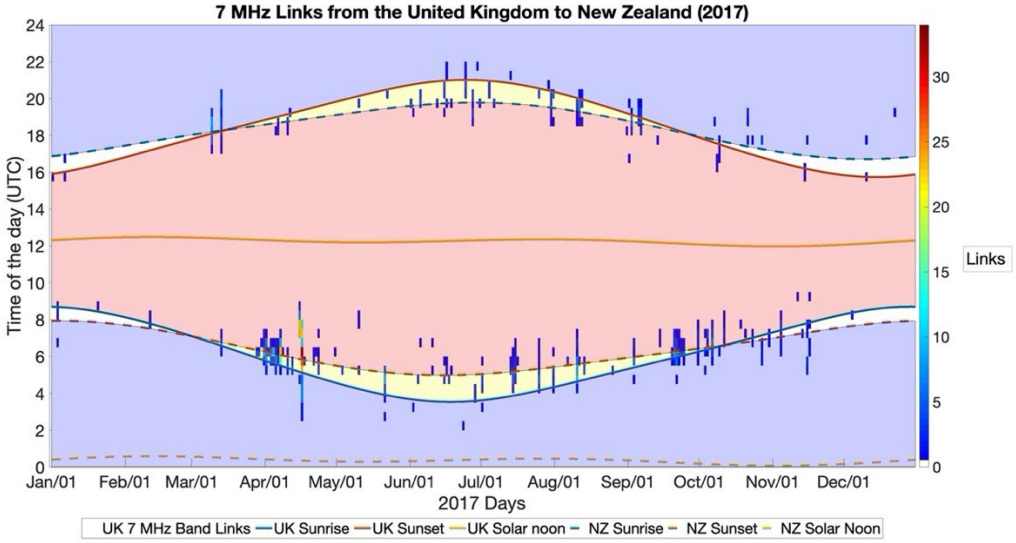

Figure 5.11 – 7 MHz Links that propagated from the UK to New Zealand. The colours in the colorbar indicate the number of observations in each half-hour intervals. The red shade indicates the UK daylight hours. The blue shade indicates the New Zealand daylight hours. The yellow shade indicates the daylight hours in both countries, and the white shade indicates the night-time hours in both countries.

Figure 5.11 is an important figure from first presented in Chapter 4, showing the number of links made from the UK to New Zealand in the 7 MHz frequency band during 2017 from the WSPR database. The x-axis is the dates throughout the year, and the y axis the time of day. The colours indicate the number of observations in each half-hour interval. The light red shading indicates the UK daylight hours, and the blue shading indicates New Zealand's daylight hours. The yellow shading indicates the daylight hours in both countries, and the white shading indicates the night-time hours in both countries.

It is interesting to observe that the links seem to be sparsely populated around the UK sunrise/New Zealand sunset hours and the UK sunset/New Zealand sunrise hours. There is symmetry between the links being received in the UK sunrise hours and the UK sunset hours.

It is important to note that there are not many receivers operating in New Zealand. Table 5.1 shows the number of links recorded in New Zealand coming from the UK each month, and they are very sparse. However, the number of links recorded in Australia in Table 5.2 is significantly more than those in Table 5.1, as Australia has more operational equipment than those in New Zealand. For this reason, the results from Australia are also considered in parallel. These will provide additional evidence for the investigations. Table 5.2 shows the same information but for links made to Australia from the UK.

Table 5.1 – Number of 7 MHz UK WSPR links recorded in New Zealand from the 18th to the 24th of each month in the year 2017.

Month	Number of the UK WSPR links recorded in New Zealand
January	2
February	0
March	0
April	13
May	17
June	8
July	0
August	0
September	51
October	11
November	0
December	5

Table 5.2 - Number of the 7 MHz UK WSPR links recorded in Australia from the 18th to the 24th of each month in the year 2017

Month	Number of 7 MHz UK WSPR links recorded in Australia
January	22
February	92
March	267
April	128
May	61
June	14
July	7
August	20
September	142
October	132
November	65
December	566

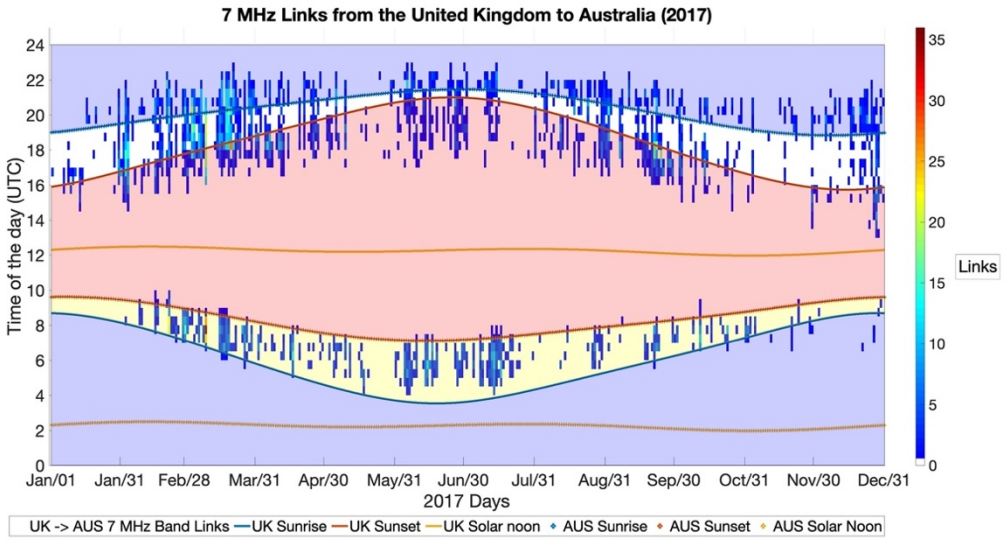

Figure 5.12 – 7 MHz Radio Links made from the United Kingdom to Australia in 2017. The blue shaded area is the Australia daytime hours. The red area is the UK daytime hours. The yellow shaded area is the common daytime hours, and the white shaded area is the common night hours. The colours indicate the number of links available in each half-hour intervals.

Figure 5.12 shows the UK to Australia links. Here, they support the pattern observed from the UK to New Zealand observations in Figure 5.11 - that is, the links are predominantly made around the terminator hours. Interestingly, at Australia dusk, there is confinement to common UK/Australia daytime, whereas, in the Australian dawn, the times of reception are spread across the pre-dawn and post-dawn Australian hours. Compared to Figure 5.11, the UK-New Zealand results showed evidence of terminator clustering but were not confined to the common daylight hours. A note of caution is that the idea of a 'common daytime' is perhaps not a very meaningful concept in this case where the terminator crosses both regions at close to the same time.

5.4. Local noise effects

The local noise can affect the SNR at the receiver, and if this is causing the receiver to not record a weak signal coming in, it would therefore logically require a higher transmitter power to achieve a link. The SNR in dB and the transmitter power in dBm are provided in the WSPR database. For example, see the information and format of the WSPR data presented in Table 5.3. (Noted that there are ellipses in Table 5.3 because the table columns have been moved to a new line due to no space. This would be an extension of the table row.)

Table 5.3 – Example of a WSPR link in the WSPR database. The Reporter ‘VK1AAH’ is an Australian receiver, and the Call Sign ‘G3KEV’ is a UK transmitter.

Spot ID	Timestamp	Reporter	Reporter's Grid	SNR	Frequency (MHz)
680343359	1483287480	'VK1AAH'	'QF44mp'	-24	7.040083

…

Call Sign	Grid	Power	Drift	Distance	Azimuth
'G3KEV'	'IO94sh'	37	0	16861	61

…

Band	Version	Code
7	'1.6.0'	0

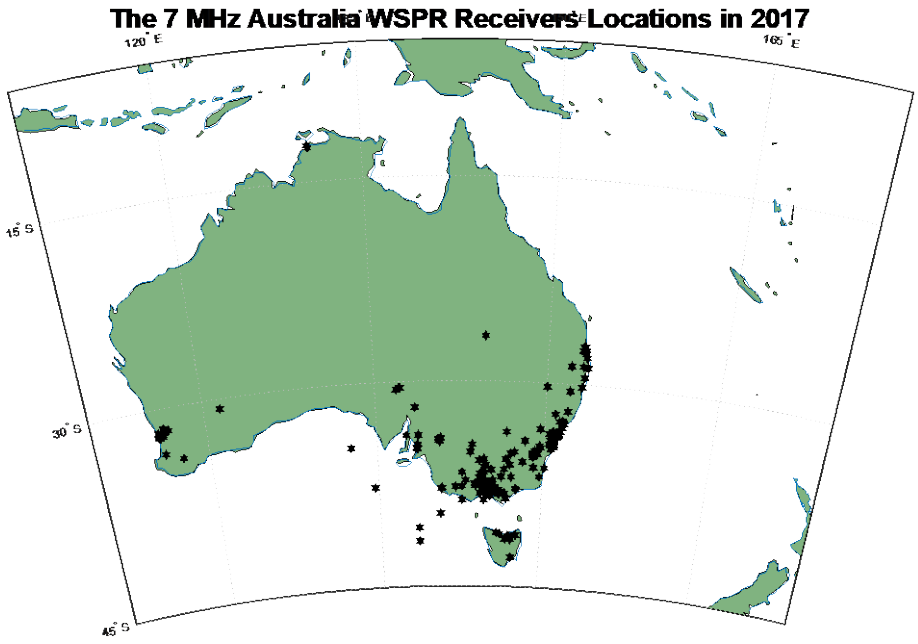

Figure 5.13 – Geographical locations of the 7 MHz WSPR Receivers from Australia. The * in black indicates their relevant locations from the Maidenhead Grid.

Figure 5.13 illustrates the Australian stations’ locations, which were operational for the relevant times considered in Figure 5.12.

The objective here is to identify whether the reception of weak signals from distant (Rest of the World) stations is, at any time of day and year, dropping in SNR because

of a temporary increase in local noise or because of a decrease in signal strength. Unfortunately, the transmitter power and SNR are the only information available in the WSPR database. Thus, the question can be phrased in this way: is there any indication that the signals with the lowest transmitter power are received in a pattern, indicative of variation in the local noise around the receiver at certain times of day/year or perhaps in a variation of the ionospheric absorption throughout the signals' path?

Now Figure 5.14, which is the transmitter power of the signals propagating from Australia and New Zealand to the Australian stations, will be observed first. Generally, the lowest transmitter powers seem to be around the 10 dB to 20 dB range. There seem to be certain days with significantly reduced minimum SNR receptions, for example, in September – October. Figure 5.15 shows the same type of display for the signals transmitted from outside of Australia/New Zealand, which is the 'great distance' case. Figure 5.14 and Figure 5.15 show that there is generally a much lower minimum signal transmission power needed from 'close' stations than from 'great distance' stations. This result is logical and is expected - the further the travel distance, the greater the loss of the power from absorption and spreading. So, therefore stronger transmission power is needed from more distant (Rest of the World) signals.

Figure 5.14 shows the lowest signal strength from Australia and New Zealand to the Australian stations. There are certain times of year that the lowest transmitter signal strength drops down, but does not seem to vary systematically by the time of day. In contrast, Figure 5.15 shows the lowest signal strength from the rest of the world to the Australian stations. Again, there are certain times of year and day where higher signal strength seems to be needed, particularly after March until the rest of the year.

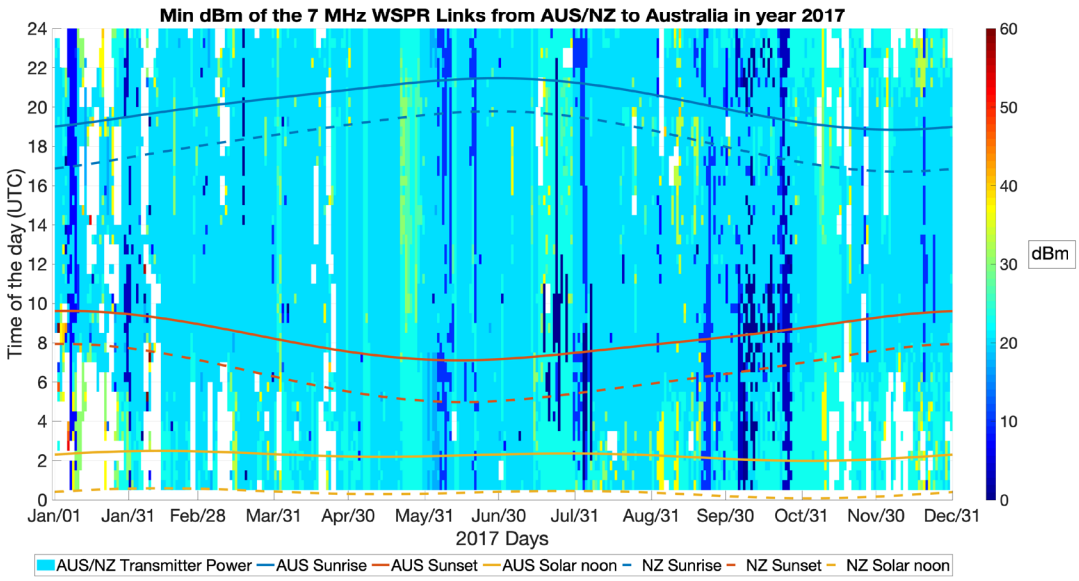

Figure 5.14 – Minimum transmitter power of WSPR links from Australia and New Zealand to the Australian stations in dBm. The colours indicate the transmission power in dBm. The colours indicate the power in every half-hour interval.

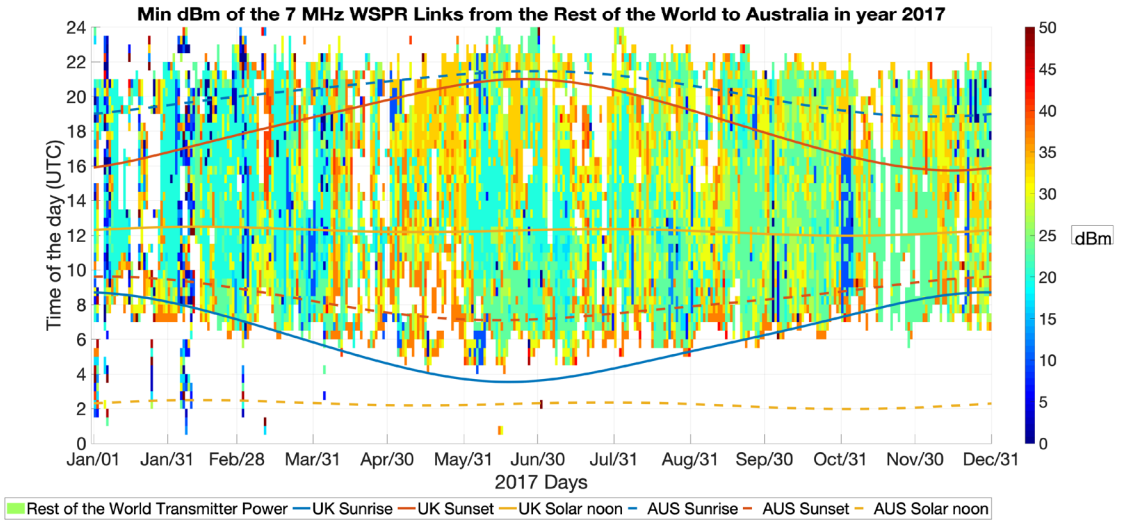

Figure 5.15 – Minimum transmitter power of WSPR links from the Rest of the World to the Australian stations in dBm. The colorbar indicates the transmission power in dBm. The colours indicate the power in every half-hour interval.

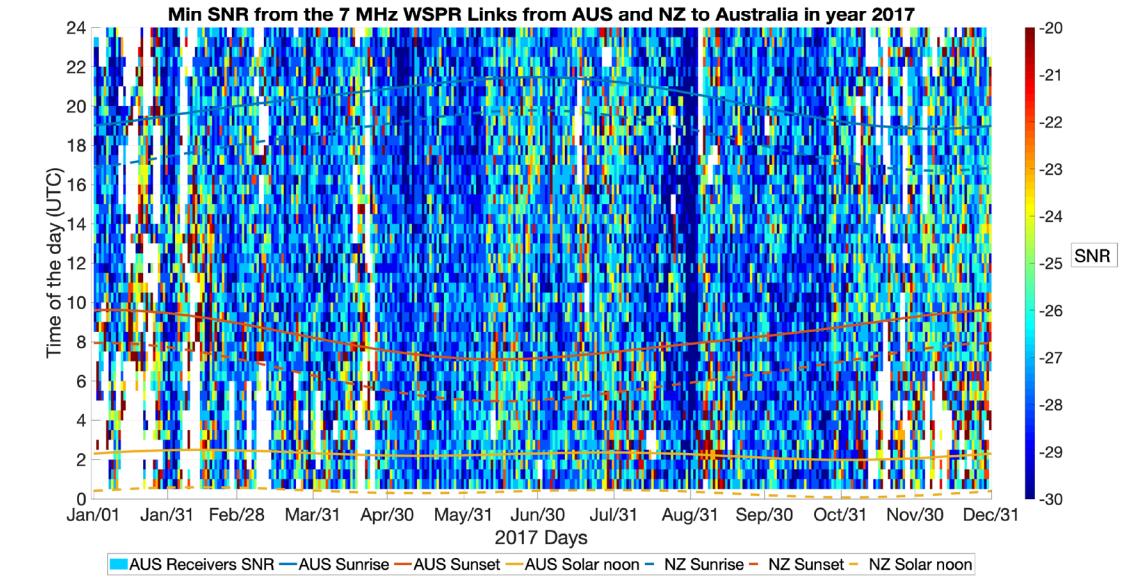

Figure 5.16 – Minimum SNR received by the Australian receiver stations from the Australian and New Zealand WSPR links in dB. The colorbar indicates the SNR in dB. The colours indicate the SNR in every half-hour interval.

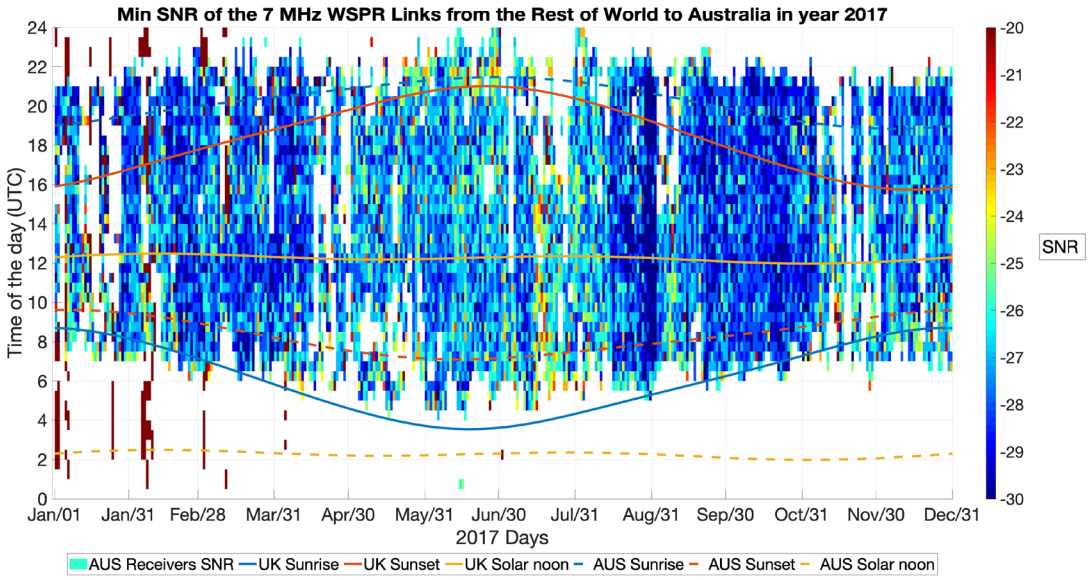

Figure 5.17 – Minimum SNR received by the Australian receiver stations from the Rest of World WSPR links in dB. The colorbar indicates the SNR in dB. The colours indicate the SNR in every half-hour interval.

Figure 5.16 and Figure 5.17 show the minimum SNRs from the Australian receivers. They show that the minimum SNR from the 'rest of the world' signals is, apparently, not significantly different from the local signals. However, there is evidence of a generally higher minimum SNR at distant reception sites during the Australian winter, which is noted in Figure 5.17.

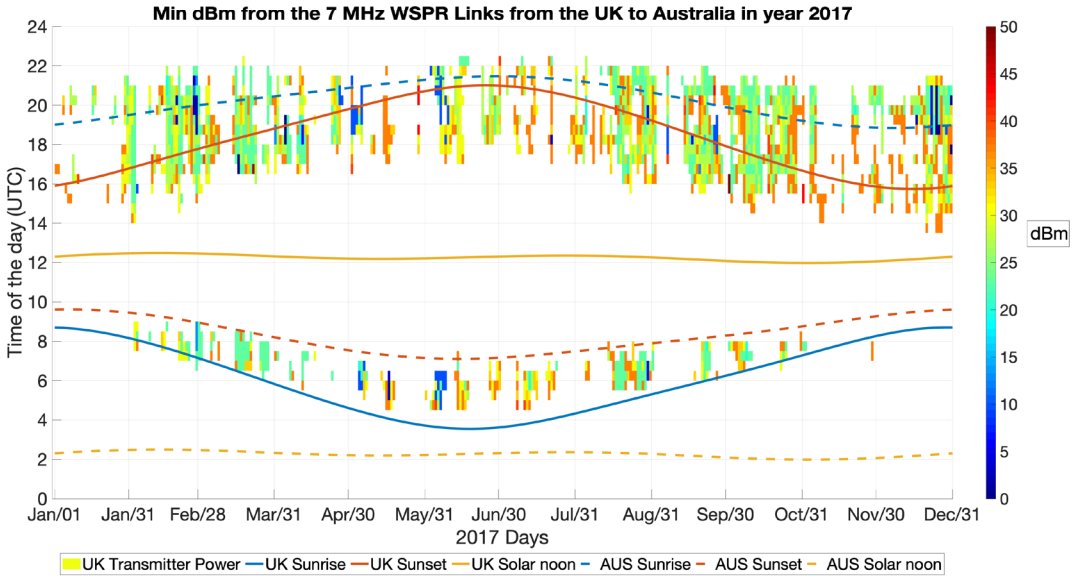

Figure 5.18 – Minimum transmitter power received by the Australian receiver stations from the UK WSPR links in dBm. The colorbar indicates the transmitter power in dBm. The colours indicate the dBm in every half-hour interval.

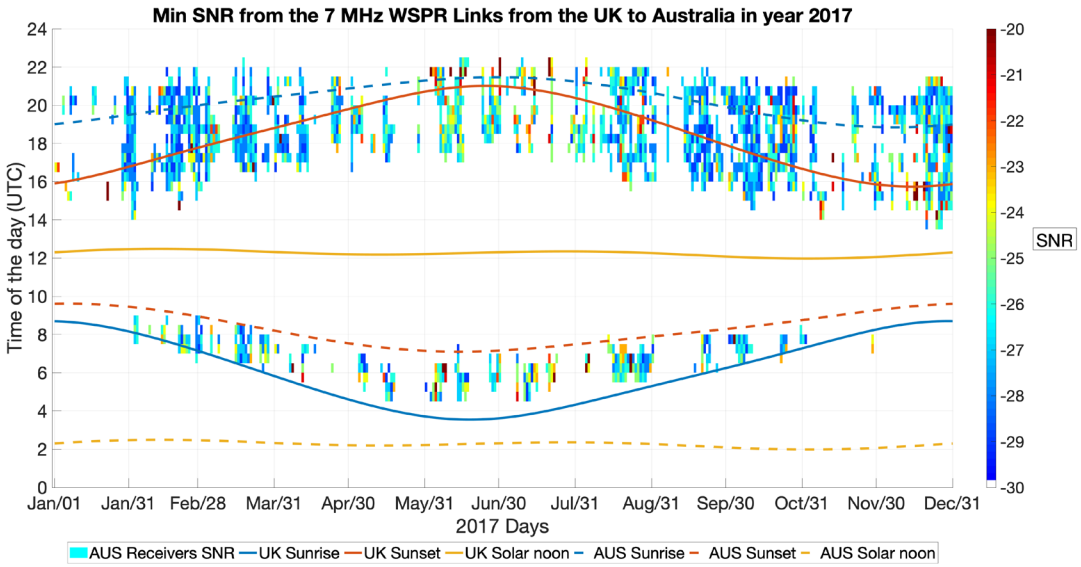

Figure 5.19 – Minimum SNR received by the Australian receiver stations from the UK WSPR links in dB. The colorbar indicates the SNR in dB. The colours indicate the SNR in every half-hour interval.

Figure 5.18 and Figure 5.19 illustrate the minimum transmitter power and the minimum SNR at the Australian receivers receiving links from the UK. Figure 5.18 shows that the minimum transmitter power received in the morning is apparently similar to that in the evening. On the other hand, Figure 5.19 shows there are generally higher minimum SNRs in the Australian winter. So the question is: Is this because there is lower local noise, or are the incoming signals stronger (for example, they are less absorbed) during the Australian winter? It would be interesting to investigate this pattern further, and the question is, what does it look like in the other direction? Now, the propagation from Australia to the UK will be investigated.

5.5. WSPR Results from Australia/New Zealand to UK

Figure 5.20 shows the number of links made from New Zealand to the UK in the 7 MHz frequency band during the year 2017 from the WSPR database. Figure 5.21 shows the reception of Australia 7 MHz WSPR transmitters in the UK. The SNR and the transmitter power for radio links propagating from Australia and New Zealand to the UK will now be examined.

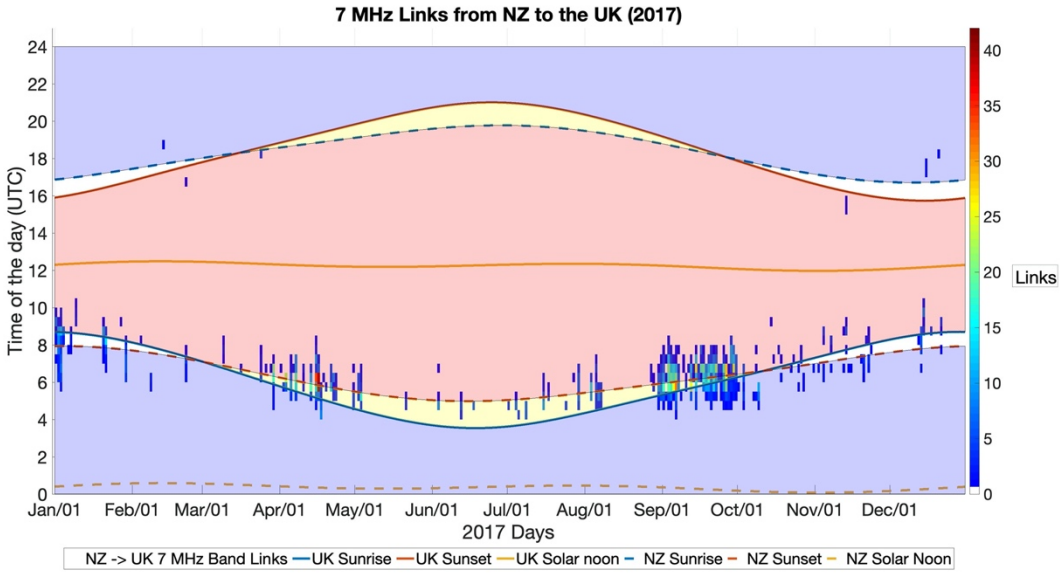

Figure 5.20 – Reception of New Zealand 7 MHz WSPR transmitters in the United Kingdom. The colours in the colour bar indicate the number of observations in each half-hour intervals. The red shading indicates the UK daylight hours. The blue shading indicates the New Zealand daylight hours. The yellow shading indicates the daylight hours in both countries, and the white shading indicates the night-time hours in both countries.

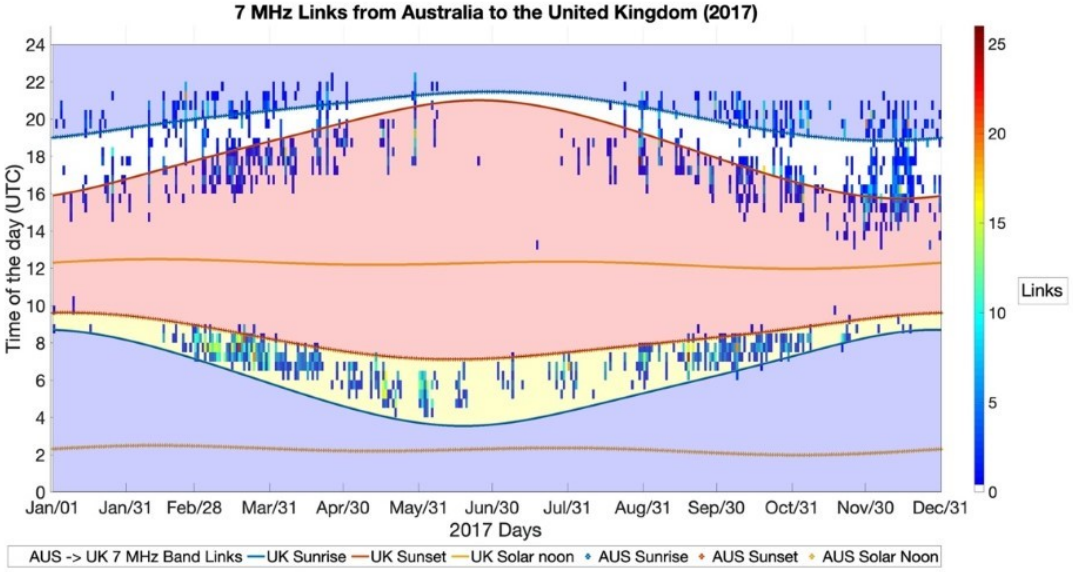

Figure 5.21 – Reception of Australia 7 MHz WSPR transmitters in the United Kingdom. The colours in the colour bar indicate the number of observations in each half-hour intervals. The red shading indicates the UK daylight hours. The blue shading indicates the New Zealand daylight hours. The yellow shading indicates the daylight hours in both countries, and the white shading indicates the night-time hours in both countries.

The SNR and the transmitter power for Australia and New Zealand to the UK will be examined in Figure 5.22 and Figure 5.23.

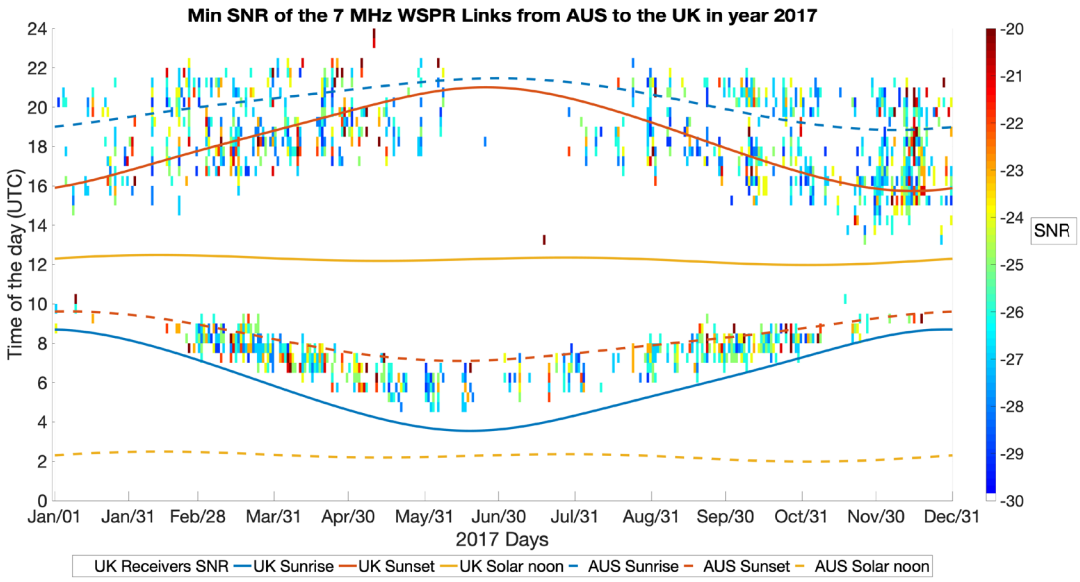

Figure 5.22 – Minimum SNR received by the UK receivers from the Australian WSPR links in dB. The colours indicate the SNR in dB. The colours indicate the SNR in every half-hour interval.

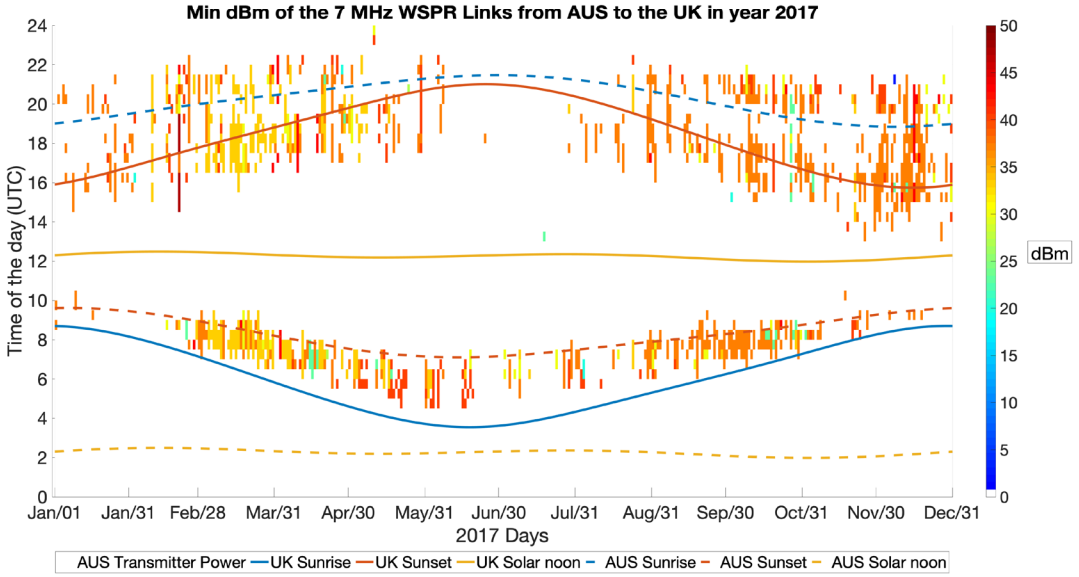

Figure 5.23 – Minimum transmitter power received by the UK receivers from the Australian WSPR links in dBm. The colours indicate the transmitter power in dBm. The colours indicate the dBm in every half-hour interval.

Figure 5.22 and Figure 5.23 illustrates that the SNR and transmitted power seen from the Australian links during the morning hours is similar to those received during the evening hours at the times of year that signals are received. On the other hand, Figure 5.24 and Figure 5.25, from New Zealand, mostly only show signals received in the UK morning hours and do not display any notable patterns in the SNR.

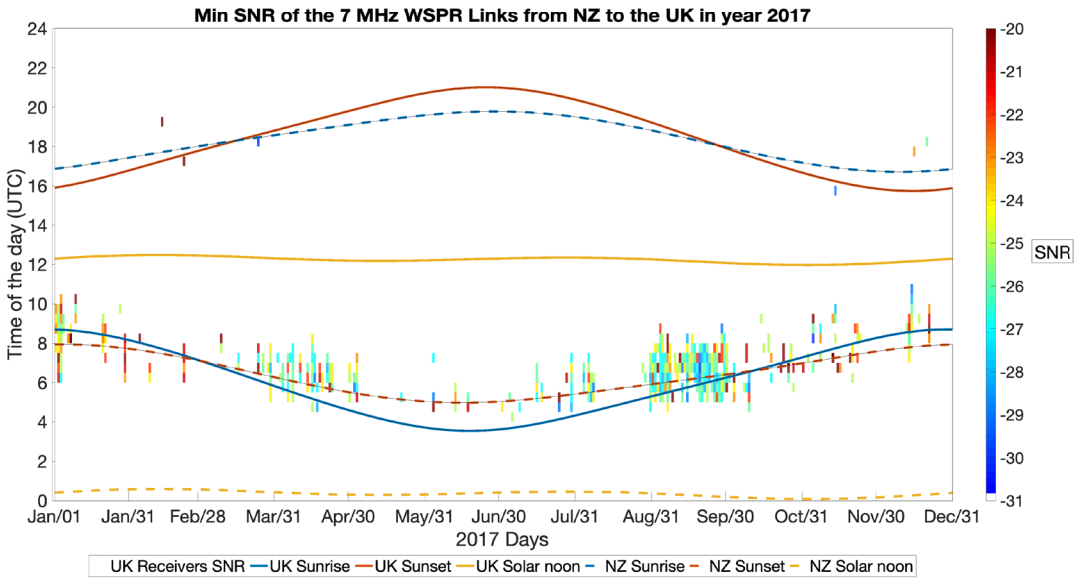

Figure 5.24 – Minimum SNR received by the UK receivers from the New Zealand WSPR links in dB. The colorbar indicates the SNR in dB. The colours indicate the SNR in every half-hour interval.

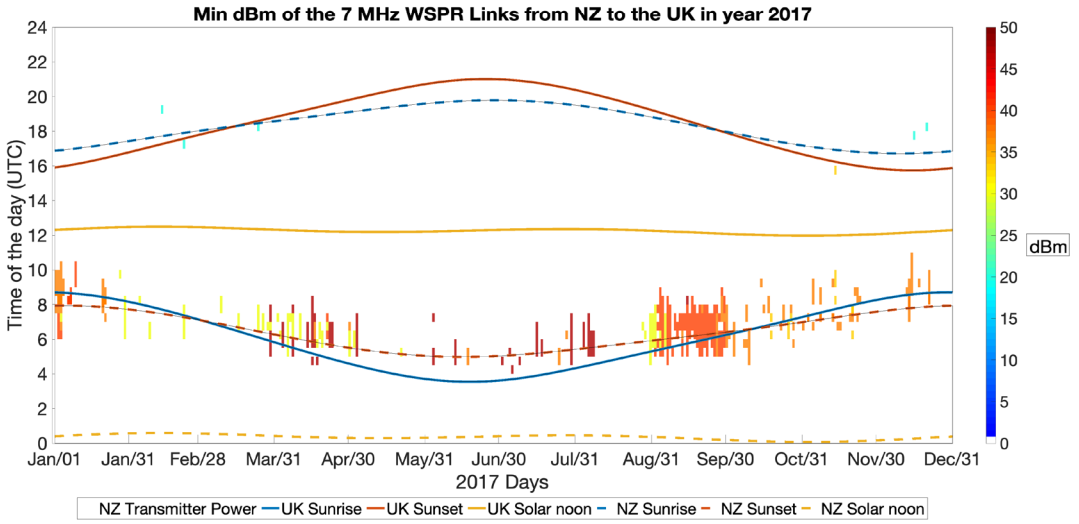

Figure 5.25 – Minimum transmitter power received by the UK receivers from the New Zealand WSPR links in dBm. The colorbar indicates the transmitter power in dBm. The colours indicate the dBm in every half-hour interval.

So, Australia to the UK has a reduced number of links in the UK summer evening, whereas New Zealand to the UK lacks links in the UK evening all through the year. There is no unusual pattern apparent in the SNRs received in the UK. However, the minimum transmitter power is lower in the spring, higher in the summer and lower again in the autumn. This suggests that a higher transmitter power may have been required in the summer in order to establish a transmission link.

5.6. Summary

This chapter further investigated the results from Chapter 4, focusing on those links made between Australia, New Zealand, and the UK. The relationship between the received SNR and the transmission power was examined. The results in Chapter 4 revealed that propagation was sparse from Australia/New Zealand to the UK/Europe in the European summer dusk but not in the reciprocal direction at the same time. It was not immediately obvious why this asymmetry would happen. However, one possibility could be differences in the local noise effects at reception, which were investigated in this chapter with limited information from the WSPR SNR and transmitter power.

The initial observation looked at the worldwide propagation of the WSPR signals. It was noted that (i) more links are received from Australia/New Zealand in the UK during the UK summer morning hours than the rest of the time, and (ii) generally higher minimum SNRs is required on the Australia/New Zealand reception in the Australian morning and winter. There is generally a reduction of links transmitted from Australia/New Zealand to distant locations in the Australian winter morning hours. The lowest SNRs of the links at reception from Australia to the rest of the world are generally lower than those from New Zealand throughout the year. It may be related to differences between the transmission power from each country.

The investigations in this chapter have revealed some interesting patterns in the transmitter power and the SNR. However, they do not explain the asymmetry in the links made between Europe and Australia/New Zealand seen in Chapter 4.

The next chapter (Chapter 6) will investigate the WSPR time propagation patterns using a ray-tracing technique to see if the patterns are explainable by analysing the propagation paths through ray-tracing.

6. Simulation results and interpretation using PHaRLAP

6.1. Introduction

This chapter investigates whether ray-tracing through a standard ionosphere model will produce links over the long distances considered in this thesis and whether any unusual pattern in these links is found. The main objective is to compare these patterns to the recordings in the WSPR database from Chapter 4 to observe if any similarities can be detected. This can then lead to some insights into the presence of the directional asymmetry, discovered in Chapter 4.

The simulation will be conducted using ray-tracing software, called PHaRLAP, alongside an ionospheric representation derived from the International Reference Ionosphere (IRI2016). PHaRLAP is a research-grade ray-tracer capable of computationally describing the propagation of radio signals through a given medium. The advantages of using PHaRLAP over other tools is that it offers a considerable amount of information about the signals, such as propagation delay, Doppler and even propagation noise and absorption levels. A full description of PHaRLAP can be found in Section 3.2 in this thesis. IRI2016 was chosen to simulate the ionospheric conditions because it is a universally accepted standard model in the ionospheric community. For more information, please refer to Section 3.2.

Section 6.2 will describe the method for simulating PHaRLAP ray-tracing links to observe potential time propagation pattern from the links made in various countries. The links, which will be observed, will be the same as those observed in Chapter 4. The observations of the PHaRLAP and WSPR results will be observed in Section 6.3, and a summary will be concluded in Section 6.4.

6.2. Method

As previously mentioned, PHaRLAP is a ray-tracing software tool that can computationally simulate the propagation path and characteristics of radio signals, given a description of the ionospheric medium. Thus, it can quickly be deployed in a MATLAB simulation and produce estimates of the propagation channels, given a set of initial parameters, such as starting point and transmission direction. In this study, the predicted endpoint geographical location and absorption, as mentioned in Chapter 3, will be obtained from PHaRLAP.

The method to create these simulated parameters and the links is: (i) to calculate a centre location from a group of WSPR transmitters under consideration that will act as

the starting point of the ray-traced signals. This will be done by taking the median transmitter points of their geographical coordinates (latitude and longitude); (ii) to define the boundaries of receivers' geographical area in which the ray-traced signals will land; (iii) to ray-trace propagating radio signals and their path every half hour for 24 hours. In order to account for different propagation modes and propagation paths that a signal can reach the reception area, each half-hour, the simulation will propagate signals from the transmitter location directed at different azimuths and elevation. Thus, the simulation will sweep through 360 degrees in azimuth in steps of 2 degrees (starting at true North) and 50 degrees of elevation in steps of 1 degree (starting at an elevation of 1 degree off the ground).

The results will be presented in a figure, divided into four graphs. The graphs will be identified as a) the recorded WSPR links between the transmission and reception region, b) the simulated PHaRLAP links between the median transmission location and the reception area, c) mean absorption levels from the simulated signals for each half-hour window, and d) minimum absorption levels from the simulated signals for each half-hour window. With these figures, it will be possible to compare the WSPR observations with the PHaRLAP simulations to observe if PHaRLAP was successful in replicating the time propagation patterns seen in the WSPR data. The figures will be presented in Section 6.3. Further information is given in Appendix B.

6.2.1. Locations of the 7 MHz transmitters

In Chapter 4, five separate transmission regions were investigated using the data from the WSPR database – UK, Italy and the adjacent regions, the USA, New Zealand, and Australia. In this chapter, the PHaRLAP simulations were also divided into five transmission regions in order to match the analysis in Chapter 4 for comparison. As it was mentioned before, the transmitter locations for the PHaRLAP simulation are calculated by taking the median of the geographical locations (both latitude and longitude) of all the operational WSPR transmitters in the given region. The median was chosen because the mean could have been influenced by an outlier location. For example, the median point of the Australian transmitters is 36.4793° S by 147.375° E. The calculated transmitter locations are illustrated in Figure 6.1 to Figure 6.5, and a full list of the simulation transmission points is presented in Table 6.1. The relevant coordinates of the transmitters' locations from the WSPR database are noted by the magenta points in the above maps, while the transmission point for the PHaRLAP simulations – by the magenta dot. The average sunrise/ sunset hours are also calculated for the graphical interpretation of the results. These are calculated at ground level.

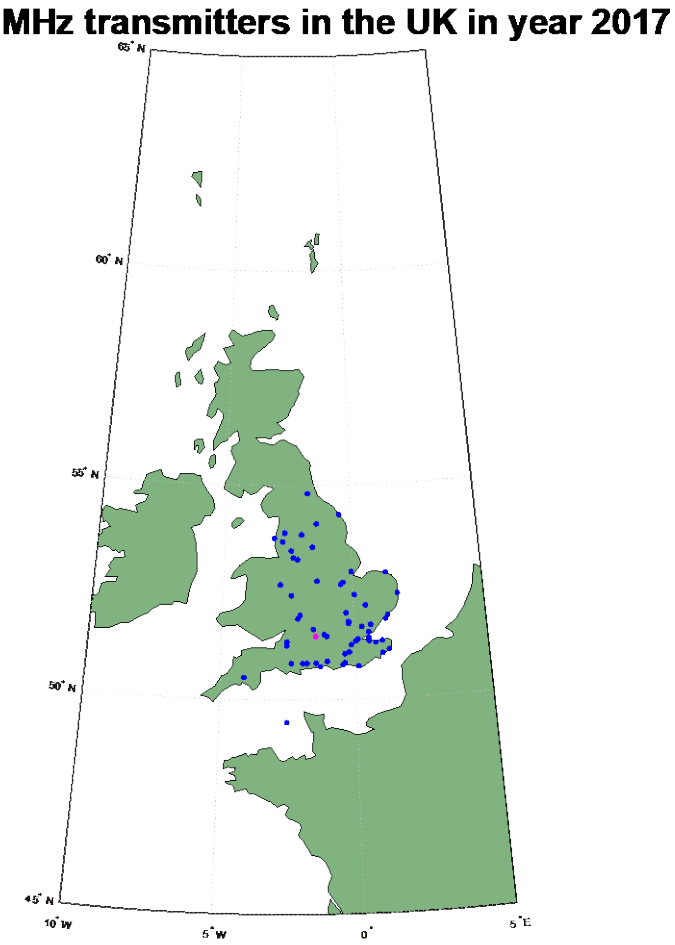

Figure 6.1 – Locations of the 7 MHz transmitters in the UK in the year 2017. The colour spots in blue are the transmitters in the UK recorded in the WSPR database. The colour spot in magenta is the transmitter point used for PHaRLAP simulations.

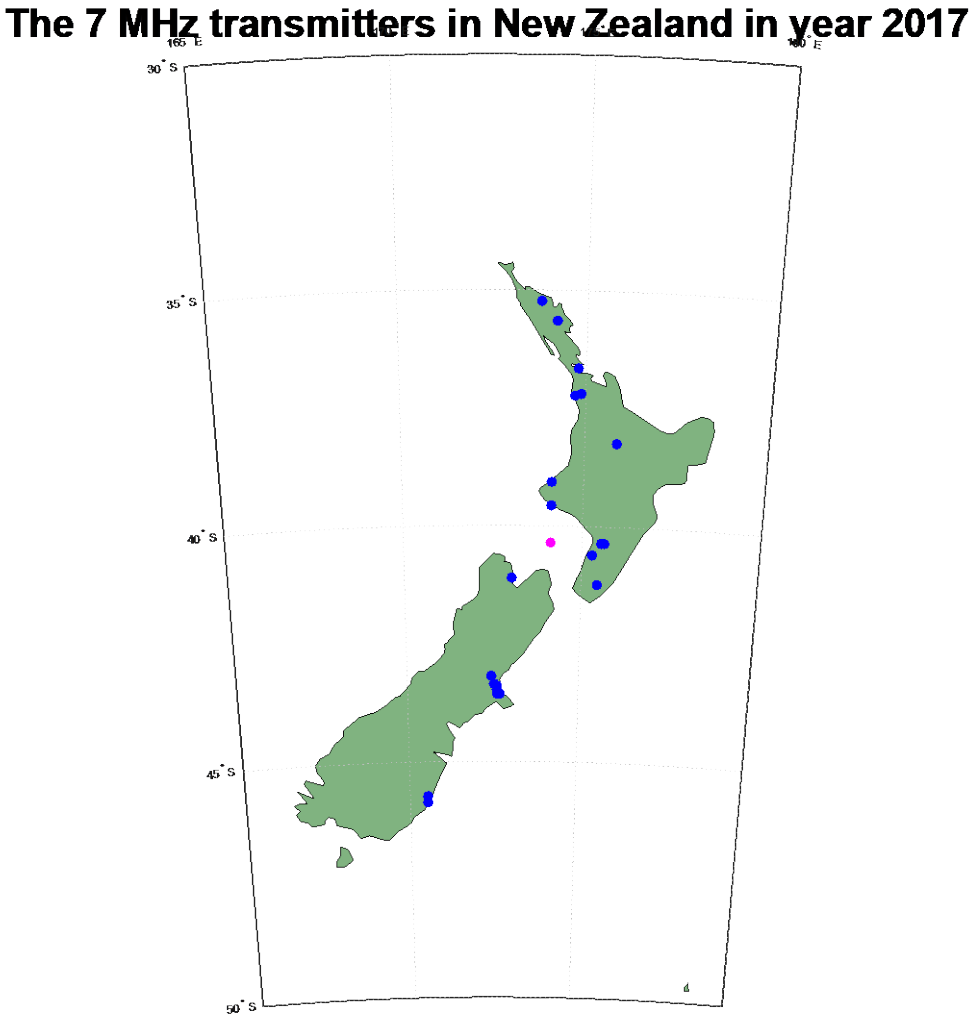

Figure 6.2 – Locations of the 7 MHz transmitters in New Zealand in the year 2017. The colour spots in blue are the transmitters in New Zealand recorded in the WSPR database. The colour spot in magenta is the transmitter point used for PHaRLAP simulations.

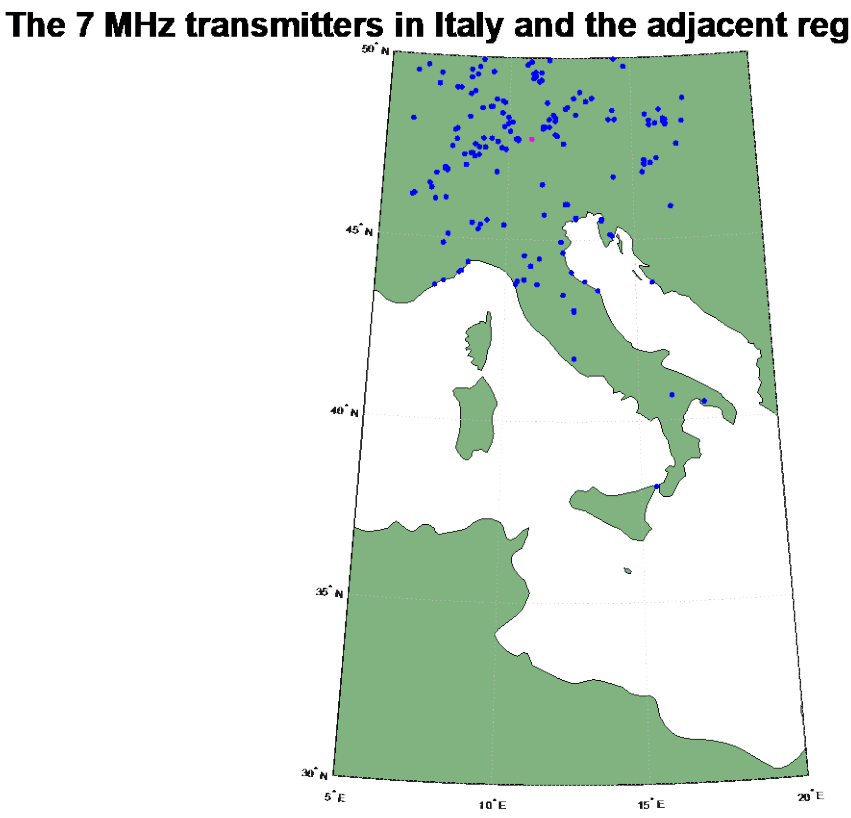

Figure 6.3 – Locations of the 7 MHz transmitters in Italy and the adjacent regions in the year 2017. The colour spots in blue are the transmitters in Italy and the adjacent regions recorded in the WSPR database. The colour spot in magenta is the transmitter point used for PHaRLAP simulations.

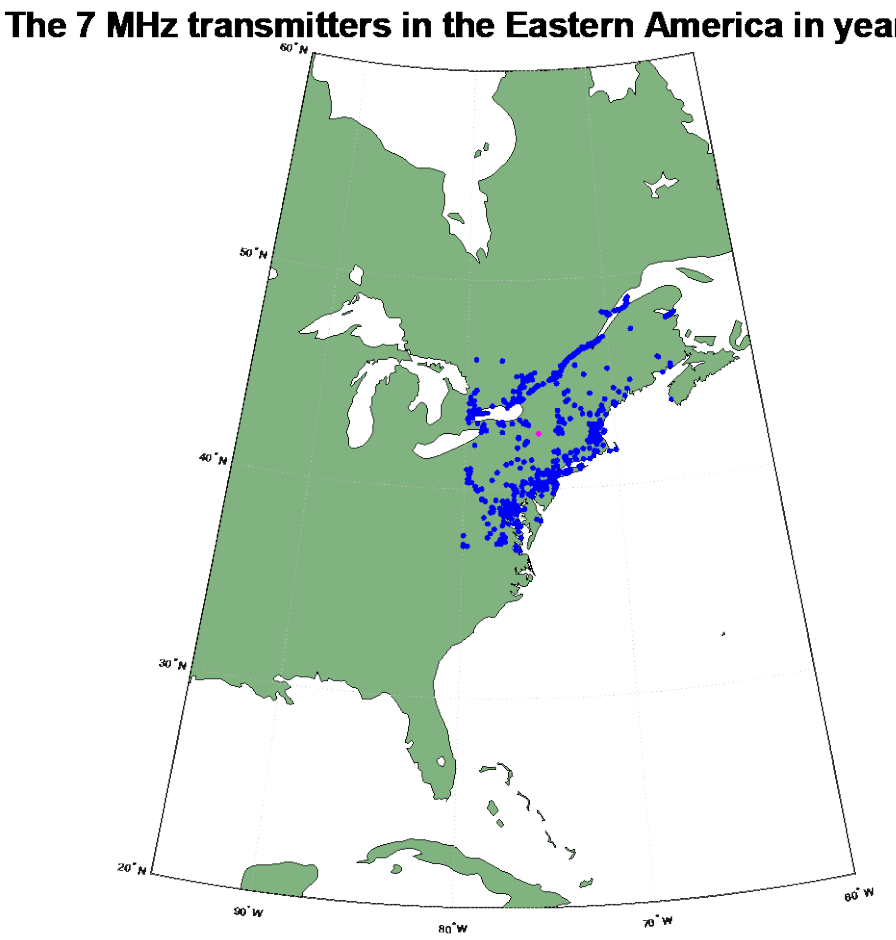

Figure 6.4 – Locations of the 7 MHz transmitters in Eastern USA in the year 2017. The colour spots in blue are the transmitters in Eastern USA recorded in the WSPR database. The colour spot in magenta is the transmitter point used for PHaRLAP simulation.

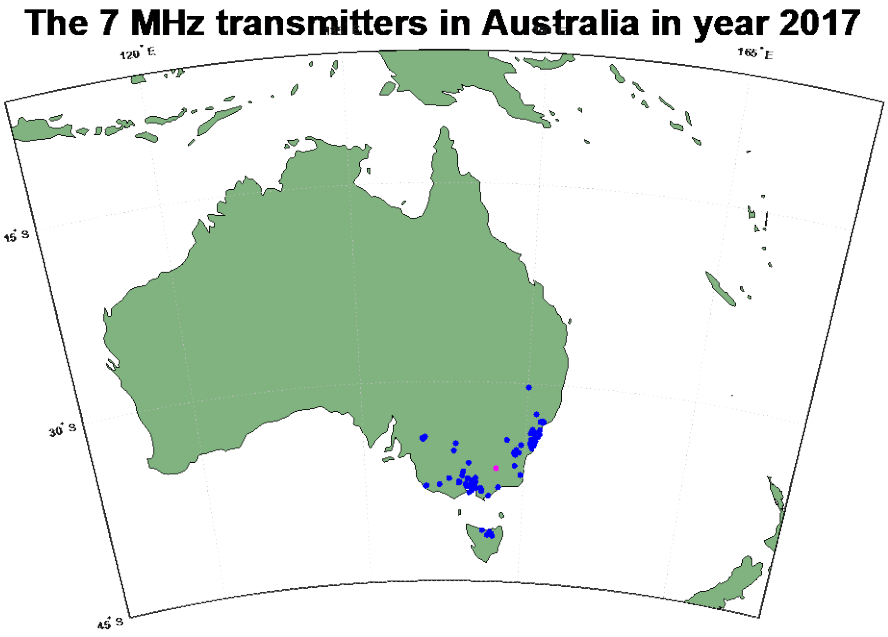

Figure 6.5 – Locations of the 7 MHz transmitters in Australia in the year 2017. The colour spots in blue are the transmitters in Australia recorded in the WSPR database. The colour spot in magenta is the transmitter point used for PHaRLAP simulations.

Table 6.1 – Transmitters' Locations for PHaRLAP simulations

Transmitters' Locations for PHaRLAP simulations		
Country	**Latitude (°)**	**Longitude (°)**
Australia	-36.4793	147.375
New Zealand	-40.3542	174.125
United Kingdom	51.4792	-1.4583
Italy and the adjacent regions	47.9128	10.7083
United States	42.6458	-75.125

6.2.2. Receivers' Locations

The objective of setting a nominal region of interest for receivers is to observe the number of links and their absorption levels according to the reception regions investigated in Chapter 4. The locations where the links are mostly received in WSPR are Australia/New Zealand, the UK, the USA and Italy and the adjacent regions (ITADR). Therefore, the boundaries of the receiver regions are required to cover these regions: the UK, the USA, Italy and the adjacent regions, Australia and New Zealand. These boundaries mean that the receivers' locations will include one of the regions: Australia/New Zealand, Europe or the USA. The boundaries of the locations of the receivers are equal in area. The aim is to see 1) if the PHaRLAP simulation predicts the same time propagation pattern in the links observed from WSPR and 2) if it gives any evidence and hence insight into the asymmetry in the links by investigating the propagation paths. The geographical coordinates for the receivers' locations are listed

in Table 6.2, and the receivers' locations are illustrated in Figure 6.6, Figure 6.7, and Figure 6.8.

Table 6.2 – Receiver's regional boundaries for PHaRLAP simulations

Receivers' Locations for PHaRLAP simulations				
Regions	**Latitude (°)**		**Longitude (°)**	
	Min	**Max**	**Min**	**Max**
Australia/New Zealand	- 48	- 13	114	179
Europe	35	70	- 45	47
USA	25	60	- 130	- 54

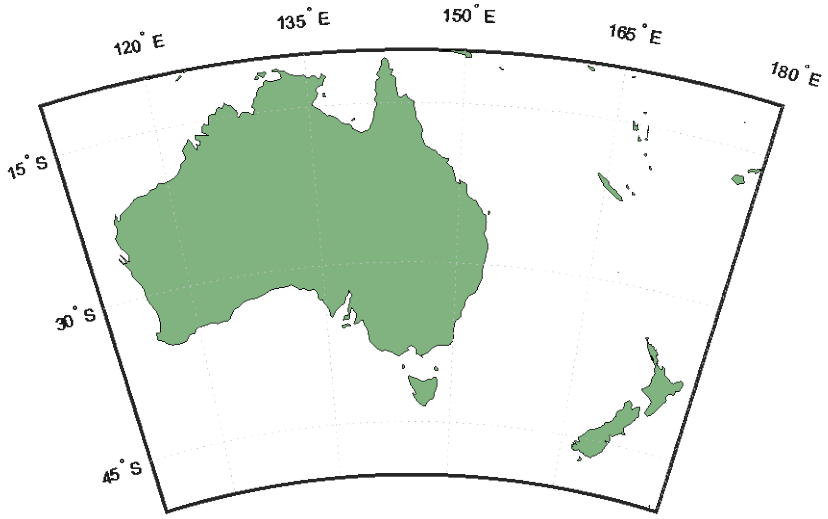

Figure 6.6 – Receivers' area in Australia/New Zealand in year 2017.

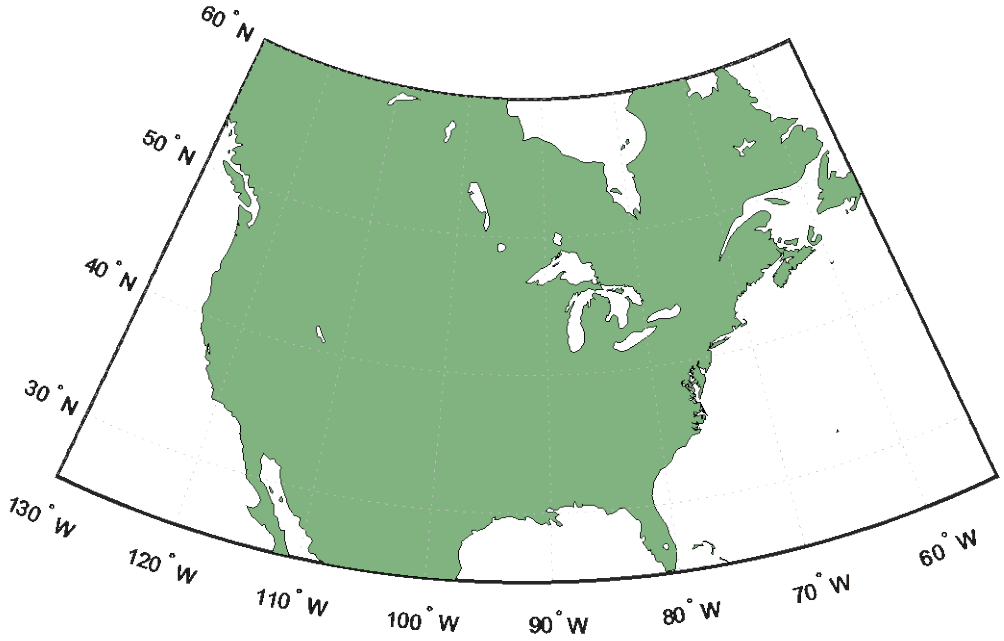

Figure 6.7 – Receivers' area in the USA in year 2017.

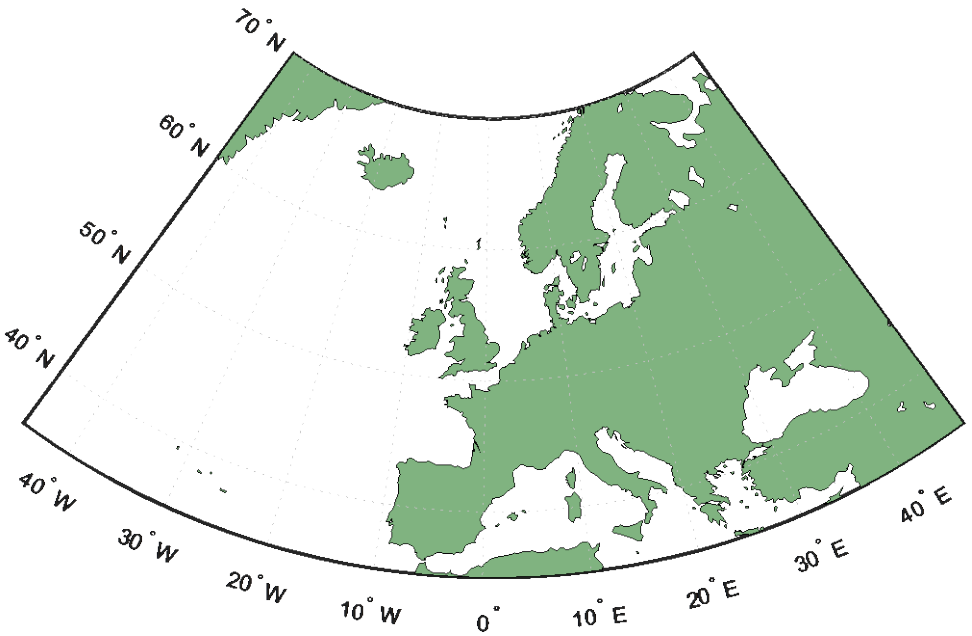

Figure 6.8 – Receivers' area in Europe in year 2017.

For this study, the PHaRLAP ray-tracing software has been set up to interface with the global ionosphere using IRI2016 on an ionospheric grid. And similarly, set up to interface with the global geomagnetic field using the International Geomagnetic Reference Field (IGRF) on a geomagnetic grid. Importantly, this will also include the possibility to model absorption in lower altitudes in the D and E layer. The absorption of the links will be affected by the full path along with the propagation, but mostly at lower altitudes.

Sections 6.3. will present the time propagation pattern between 1) New Zealand and the UK, 2) New Zealand the USA, 3) Australia and the USA, 4) the UK and the USA, 5) Italy and the adjacent regions (ITADR) and the USA, 6) New Zealand and Italy and the adjacent regions (ITADR), 7) Australia and the UK, and 8) Italy and the adjacent regions (ITADR) and Australia.

6.3. Results from PHaRLAP simulations

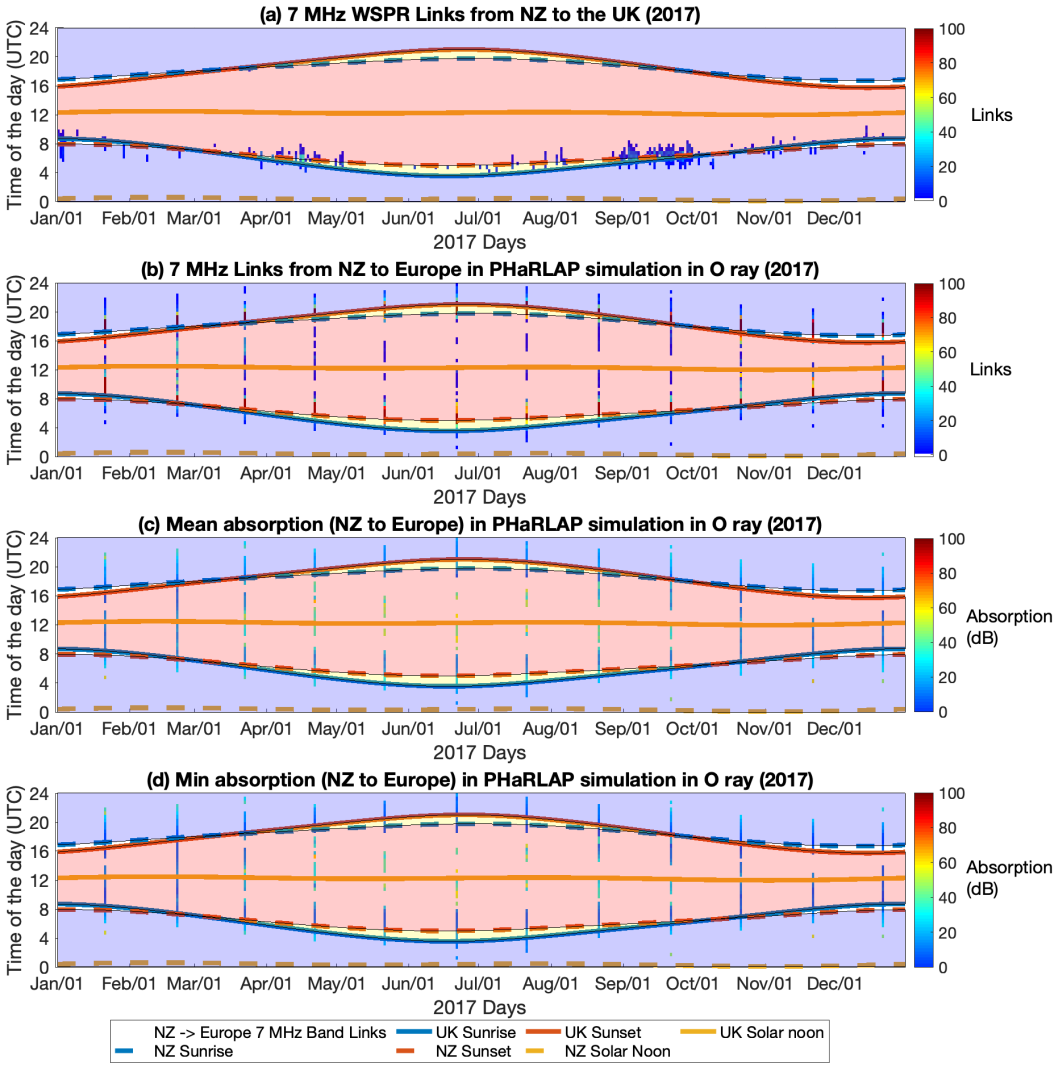

Figure 6.9 – (a) 7 MHz WSPR Links from New Zealand to the UK (b) 7 MHz Links from New Zealand to Europe in PHaRLAP simulation in O ray (c) Mean absorption (New Zealand to Europe) in PHaRLAP simulation in O ray (d) Min absorption (New Zealand to Europe) in PHaRLAP simulation in O ray.

Figure 6.9 shows (a) the WSPR links from New Zealand to the UK, (b) the simulation of the links by the number of links, (c) mean absorption and (d) minimum absorption along the path of the received simulated signals. The minimum absorption is of interest to see if any links would get through without too much loss of the signal through absorption.

In Figure 6.9, it can be seen that there are a number of links that do get through with a relatively low amount of absorption. It is known that WSPR is able to pick up signals down to an SNR of -30 dB. It is noteworthy that in December, the only links predicted

by PHaRLAP are close to the common terminator times and into the UK day. However, for the majority of the year, the links are predicted throughout the day and only really stop during the UK night.

There are two important factors to consider here. The first is whether the simulated ionosphere from IRI2016 is sufficiently ionised to provide a possible link through for these simulated one-hop paths. That is showing that links could be supported for most of the UK daytime period. The second point is whether there is too much absorption of the signal that would stop a particular link from being strong enough to be picked up by the receiver. It can be seen that the daytime links are predicted to be absorbed more, and hence some of the differences in the daytime could be because they are not strong enough to be recorded on WSPR.

A question raised from Figure 6.9. is why the links show higher UK daytime absorption (lower UK night-time absorption) using this IRI/PHaRLAP approach in July but are opposite in December? This difference is interesting to compare with the results of Chapter 5, which will be discussed in Chapter 7.

Figure 6.10 shows the comparison results from the UK to New Zealand direction. Figure 6.10 (a) presents the recorded WSPR links from the UK to New Zealand, (b) the number of simulated links received in the Australia/New Zealand region, (c) mean absorption and (d) minimum absorption. Again, it can be seen that there are a number of links that do get through with a low amount of predicted absorption. It is noteworthy that in December, for example, the only links are close to the common terminator times. However, for the majority of the year, the links are predicted throughout the day and only really stop during the UK night. If a cut-off level was taken from the absorption, then there would be predictions of more links made in the evening than in the morning. However, in reality, the links are very sparse, and the simulation seems to overpredict them into the UK night-time.

Figure 6.11 shows (a) the WSPR links from New Zealand to the USA, (b) the number of simulated links received in the American region, (c) mean absorption and (d) minimum absorption. It shows that a large number of links are made over the common night-time, but these are not predicted by the simulation. The simulations predict that a majority of the links are made in either the day hours in New Zealand or in the USA. The simulations also show that there are several links that do get through relatively low absorption. However, the common night-time is supposed to be the hours where there is lower absorption compared to any other time of the day, yet there are only a few links in common night-time compared to those in the day hours.

Figure 6.12 shows (a) the links from the USA to New Zealand, (b) the number of simulated links received in the Australia/New Zealand region, (c) mean absorption and (d) minimum absorption. Again, the WSPR data shows that a large number of links are made over the common night-time, but these are not predicted by the simulation in Figure 6.12 b). The simulations predict that a majority of the links are made in either the day hours in Australia/New Zealand or in the USA, as well as in their common daytime. The simulations also show that there are several links that do get through with a low amount of absorption, as shown in Figure 6.12 c) and d). Similarly to Figure 6.11, the common night-time is supposed to be the hours where there are lower absorption

levels than any other time of the day, yet there are only a few links in common night-time compared to those in the day hours. Nevertheless, the common daytime propagation is very sparse.

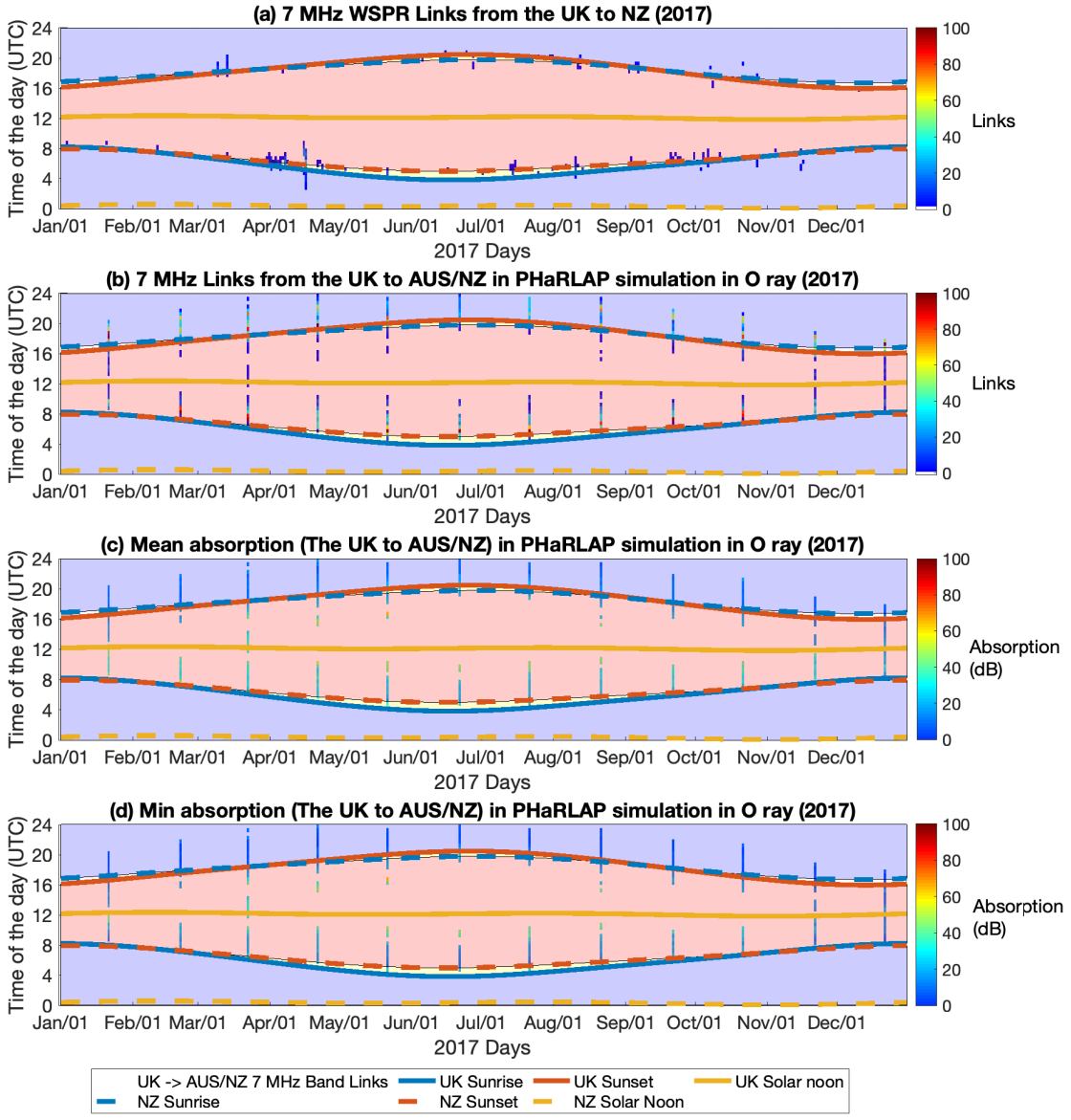

Figure 6.10 – (a) 7 MHz WSPR Links from the UK to New Zealand (b) 7 MHz Links from the UK to Australia/New Zealand in PHaRLAP simulation in O ray (c) Mean absorption (the UK to Australia/New Zealand) in PHaRLAP simulation in O ray (d) Min absorption (the UK to Australia/New Zealand) in PHaRLAP simulation in O ray.

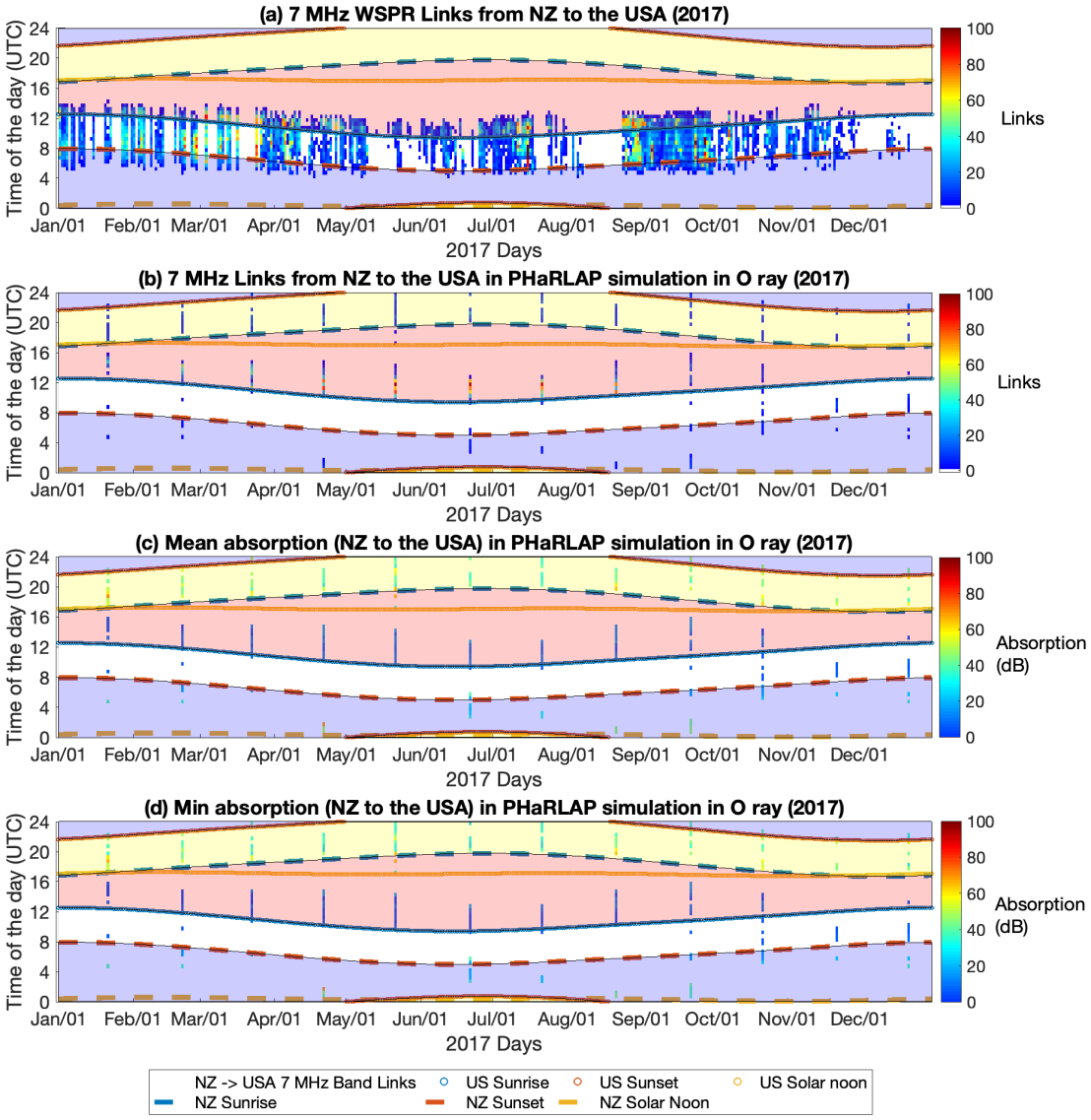

Figure 6.11 – (a) 7 MHz WSPR Links from New Zealand to the USA (b) 7 MHz Links from New Zealand to the USA in PHaRLAP simulation in O ray (c) Mean absorption (New Zealand to the USA) in PHaRLAP simulation in O ray (d) Min absorption (New Zealand to the USA) in PHaRLAP simulation in O ray.

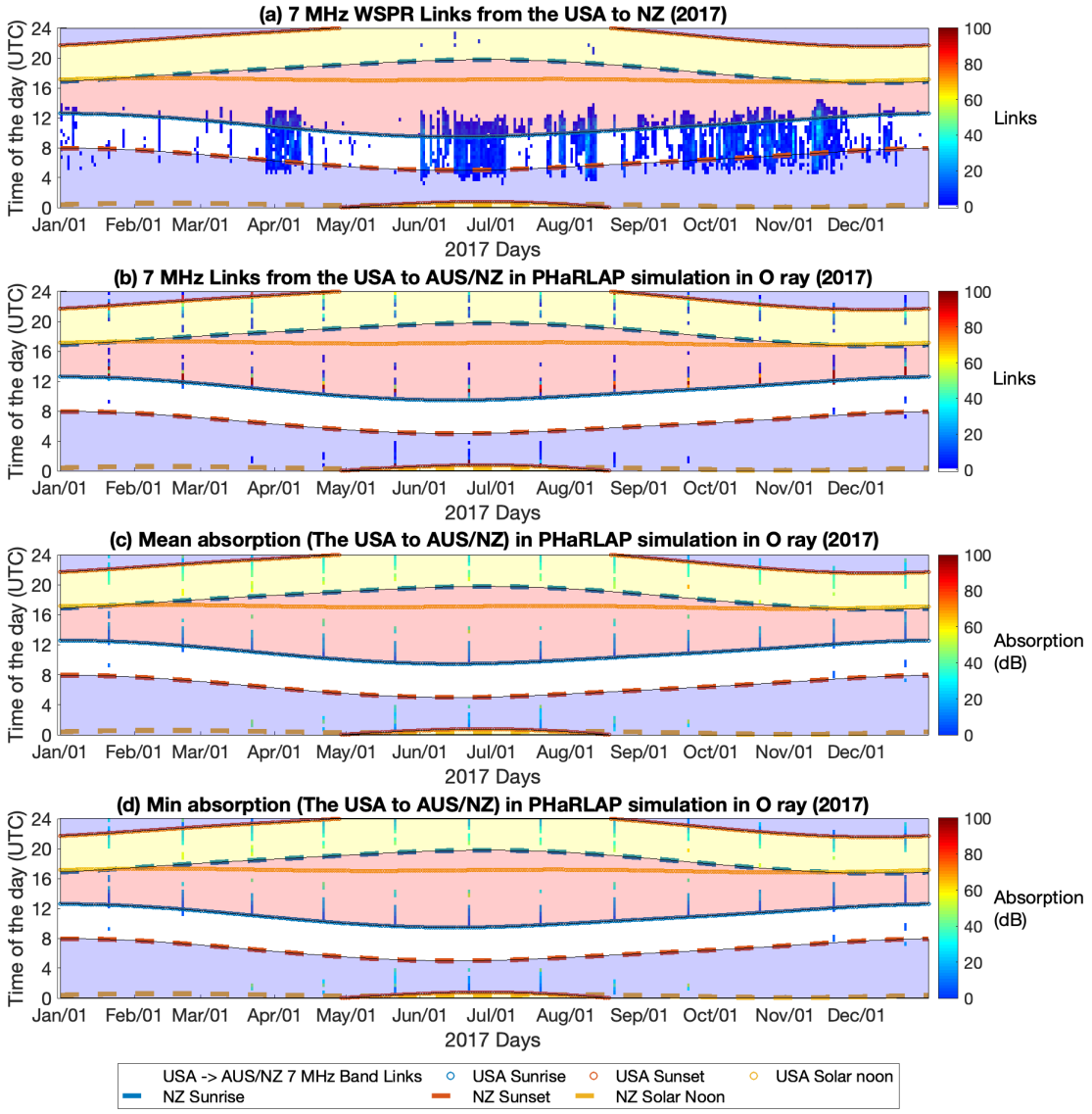

Figure 6.12 – (a) 7 MHz WSPR Links from the USA to New Zealand (b) 7 MHz Links from the USA to Australia/New Zealand in PHaRLAP simulation in O ray (c) Mean absorption (the USA to Australia/New Zealand) in PHaRLAP simulation in O ray (d) Min absorption (the USA to Australia/New Zealand) in PHaRLAP simulation in O ray.

Figure 6.13 and Figure 6.14 show the results from Australia to the USA and from the USA to Australia. The results for the Australia/USA are similar to those between New Zealand and the USA, as both shows links across the common night-time and inside the common daytime in the WSPR dataset (Figure 6.13 (a) and Figure 6.14 (a)) that are not predicted by the simulation. However, at the end of the year in Figure 6.13, the predictions look quite good, with common night-time links predicted with low absorption and common daytime links predicted with higher absorption. In Figure 6.14 (b, c and d), the predictions differ from those in Figure 6.13 (b, c and d).

Figure 6.15 and Figure 6.16 show the results for the UK to the USA. Figure 6.15 (a) and Figure 6.16 (a) both show that the links are represented quite well by the simulation during the UTC morning hours and less so at the end of the UTC day.

Figure 6.17 and Figure 6.18 show the results for Italy and the adjacent regions to the USA, showing again that the links are represented quite well by the simulation during the UTC morning hours and less so at the end of the UTC day.

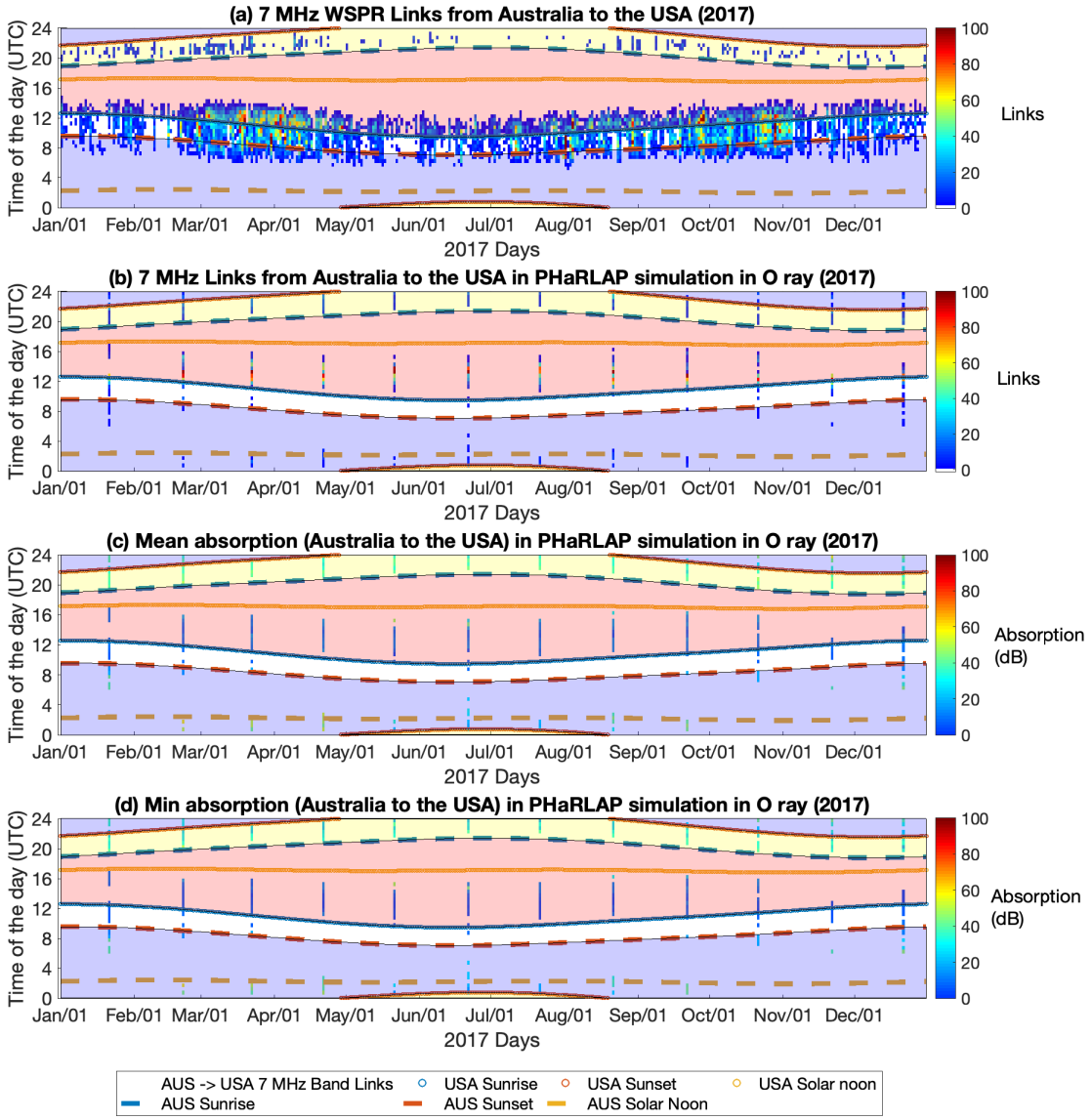

Figure 6.13 – (a) 7 MHz WSPR Links from Australia to the USA (b) 7 MHz Links from Australia to the USA in PHaRLAP simulation in O ray (c) Mean absorption (Australia to the USA) in PHaRLAP simulation in O ray (d) Min absorption (Australia to the USA) in PHaRLAP simulation in O ray.

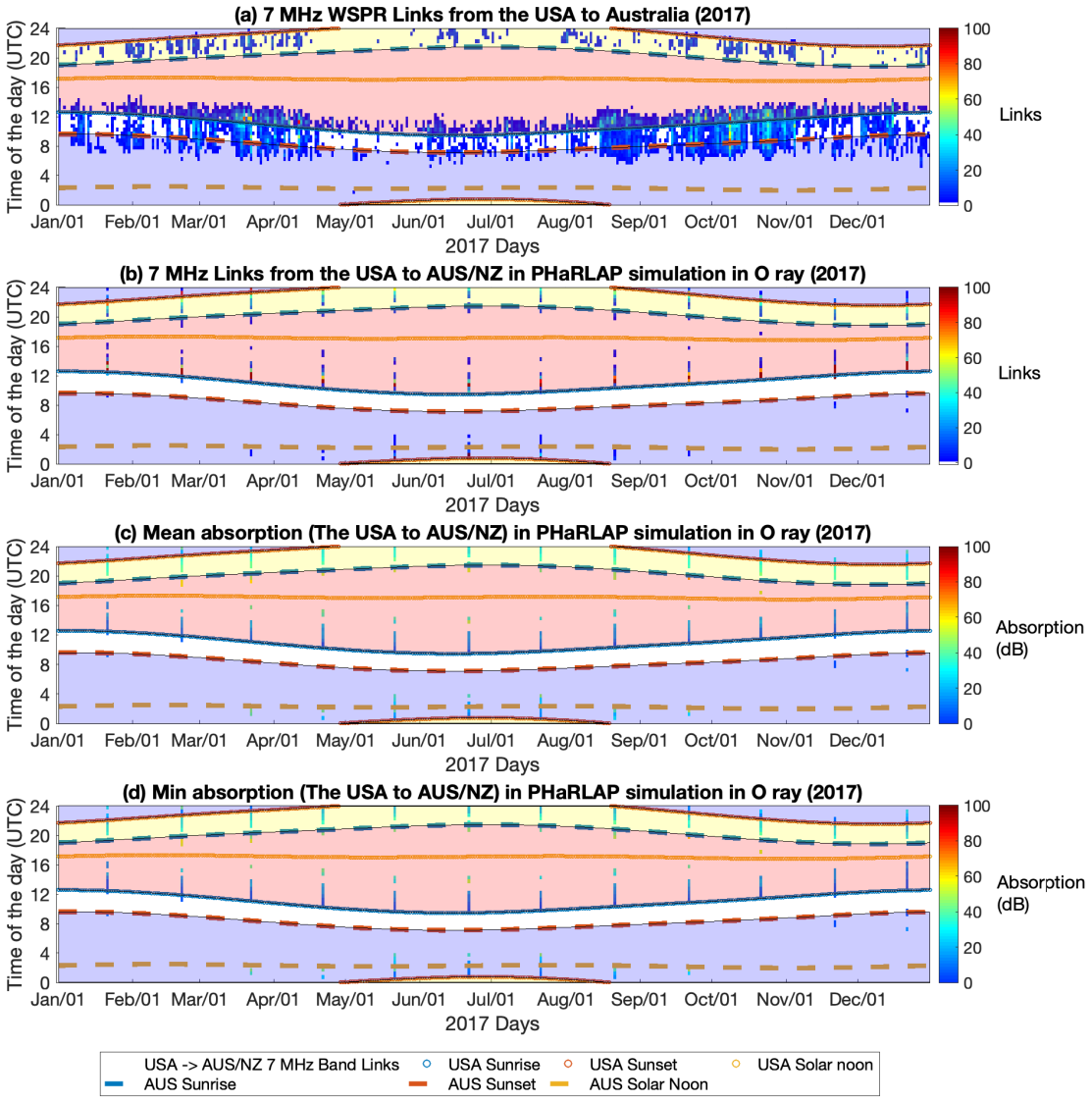

Figure 6.14 – (a) 7 MHz WSPR Links from the USA to Australia (b) 7 MHz Links from the USA to Australia/New Zealand in PHaRLAP simulation in O ray (c) Mean absorption (the USA to Australia/New Zealand) in PHaRLAP simulation in O ray (d) Min absorption (the USA to Australia/New Zealand) in PHaRLAP simulation in O ray.

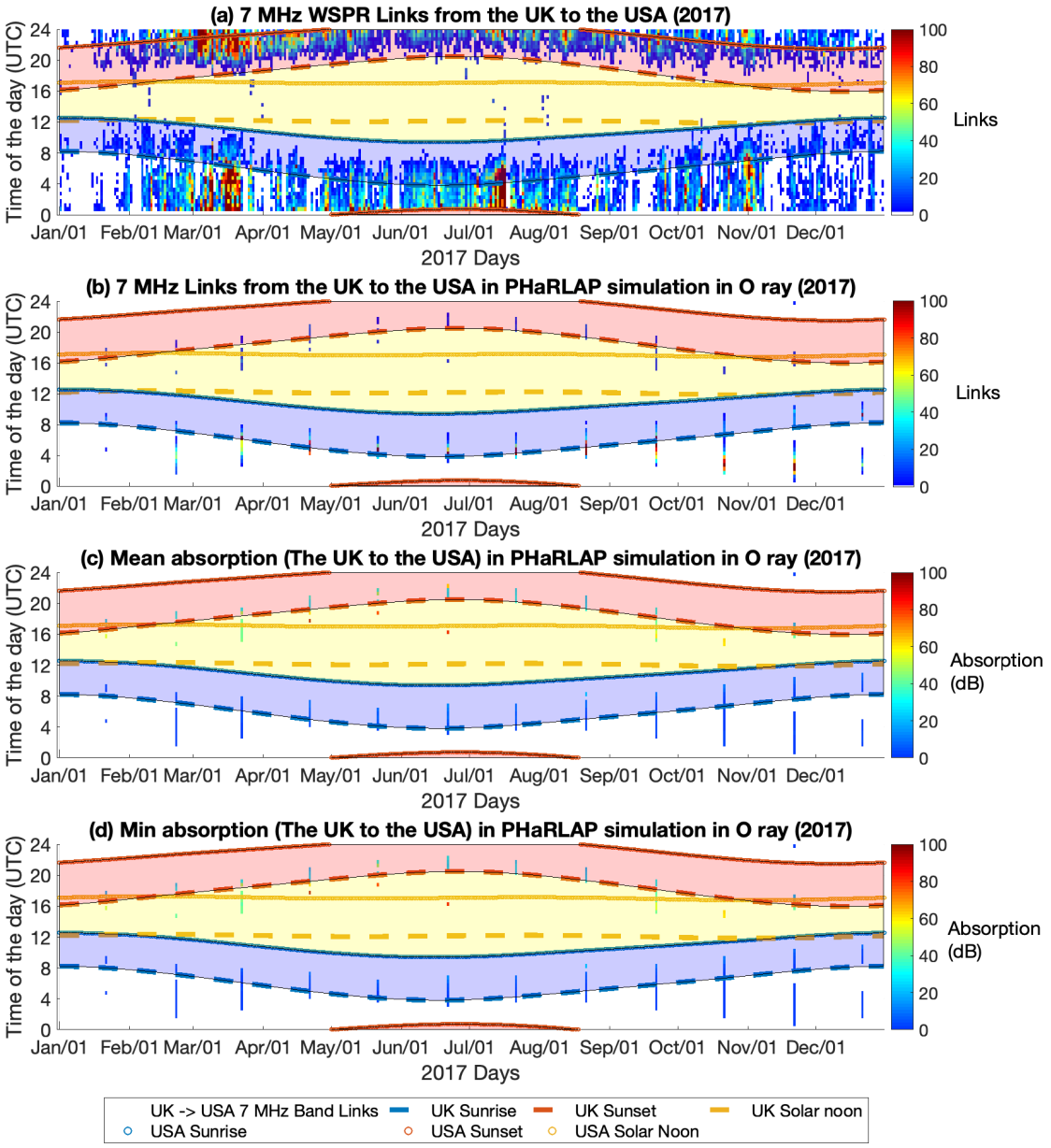

Figure 6.15 – (a) 7 MHz WSPR Links from the UK to the USA (b) 7 MHz Links from the UK to the USA in PHaRLAP simulation in O ray (c) Mean absorption (the UK to the USA) in PHaRLAP simulation in O ray (d) Min absorption (the UK to the USA) in PHaRLAP simulation in O ray.

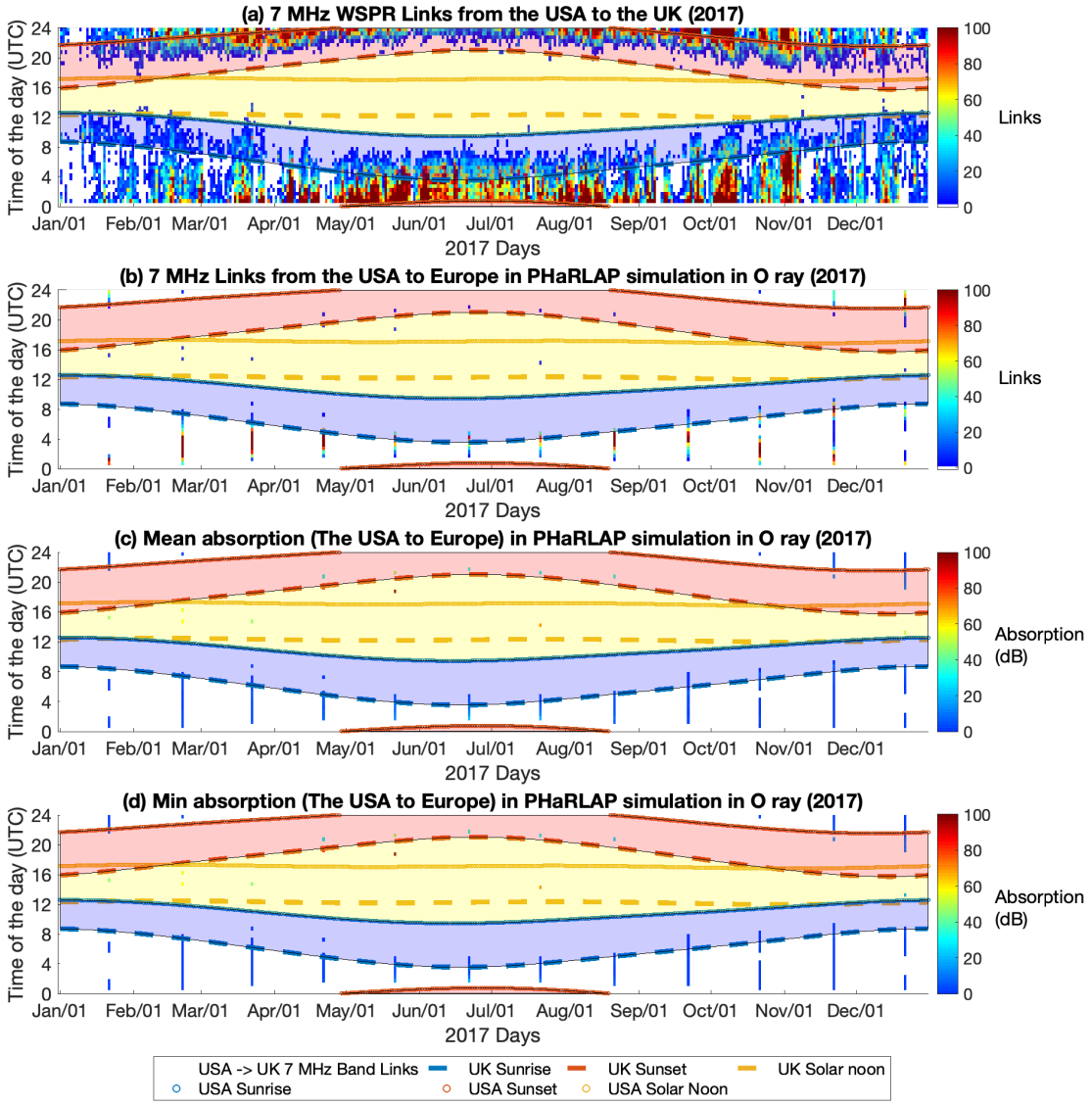

Figure 6.16 – (a) 7 MHz WSPR Links from the USA to the UK (b) 7 MHz Links from the USA to Europe in PHaRLAP simulation in O ray (c) Mean absorption (the USA to Europe) in PHaRLAP simulation in O ray (d) Min absorption (the USA to Europe) in PHaRLAP simulation in O ray.

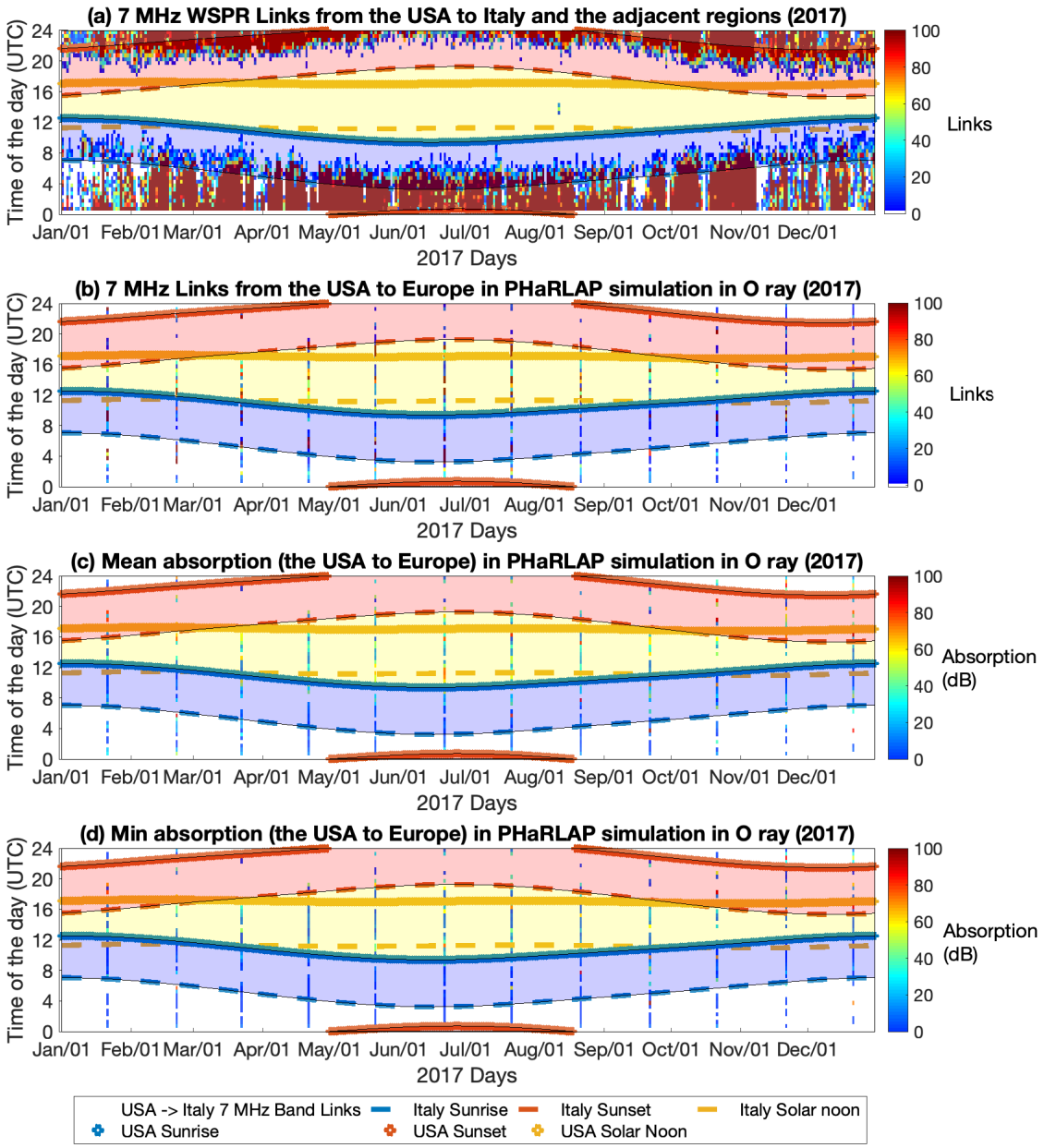

Figure 6.17 – (a) 7 MHz WSPR Links from the USA to Italy and the adjacent regions (b) 7 MHz Links from the USA to Italy and the adjacent regions in PHaRLAP simulation in O ray (c) Mean absorption (the USA to Italy and the adjacent regions) in PHaRLAP simulation in O ray (d) Min absorption (the USA to Italy and the adjacent regions) in PHaRLAP simulation in O ray.

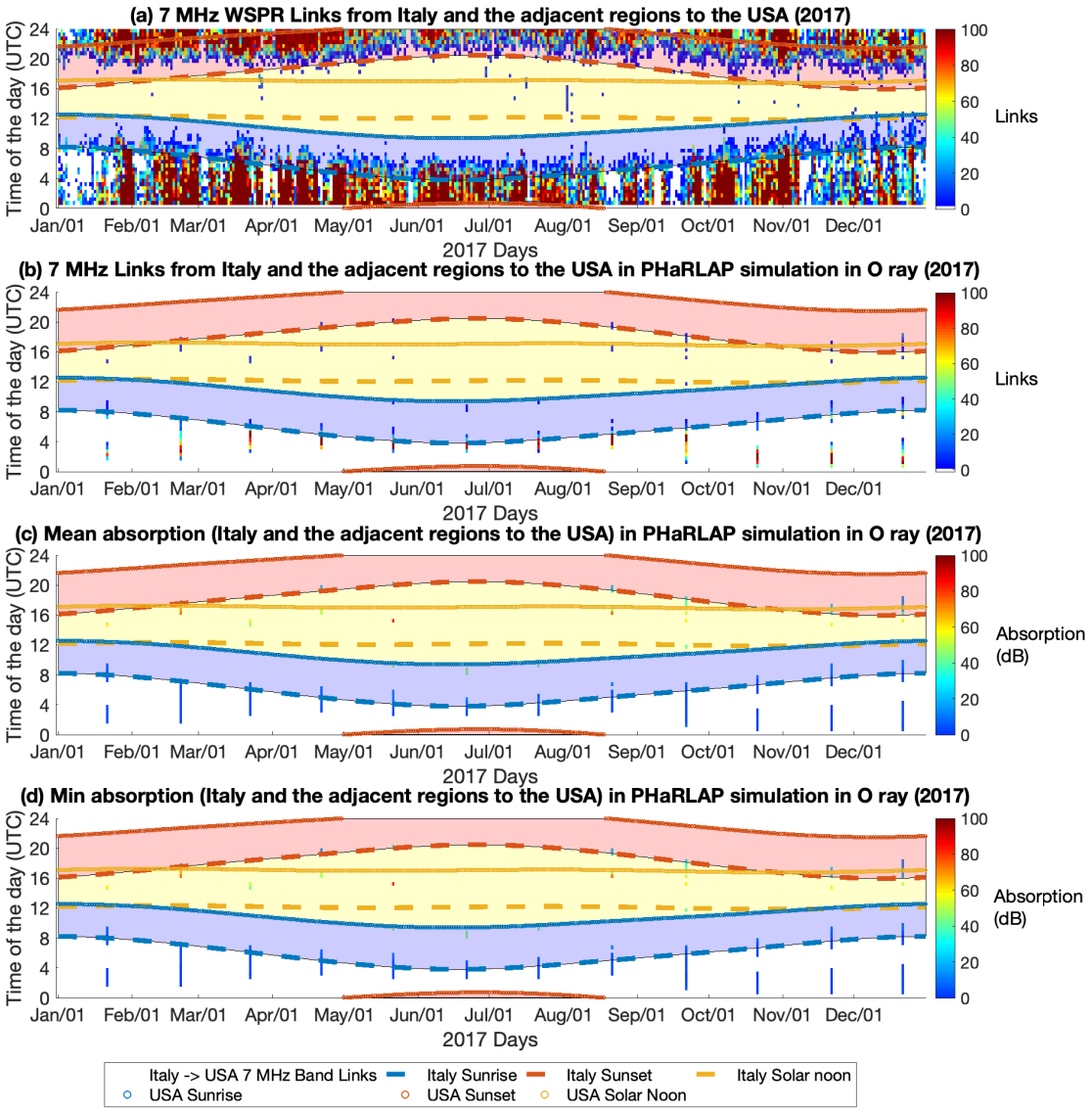

Figure 6.18 – (a) 7 MHz WSPR Links from Italy and the adjacent regions to the USA (b) 7 MHz Links from Italy and the adjacent regions to the USA in PHaRLAP simulation in O ray (c) Mean absorption (Italy and the adjacent regions to the USA) in PHaRLAP simulation in O ray (d) Min absorption (Italy and the adjacent regions to the USA) in PHaRLAP simulation in O ray.

Figure 6.19 and Figure 6.20 present the comparison results for the Italy and the adjacent regions and New Zealand links. The WSPR links from New Zealand to Italy and the adjacent regions (Figure 6.19 (a)) show that a majority of the links are made in the morning UTC hours rather than in the evening hours, whereas Figure 6.20 (a) shows that the links from Italy and the adjacent regions to New Zealand are made in both morning and evening UTC hours. The simulations in Figure 6.19 (b, c, d) show that the links are predicted throughout the day, and several links are propagated through with a low amount of absorption around the terminator hours. If anything, there is better propagation (lower absorption) indicated in the evening than the morning UTC hours for the links propagating from Italy and the adjacent regions to New Zealand.

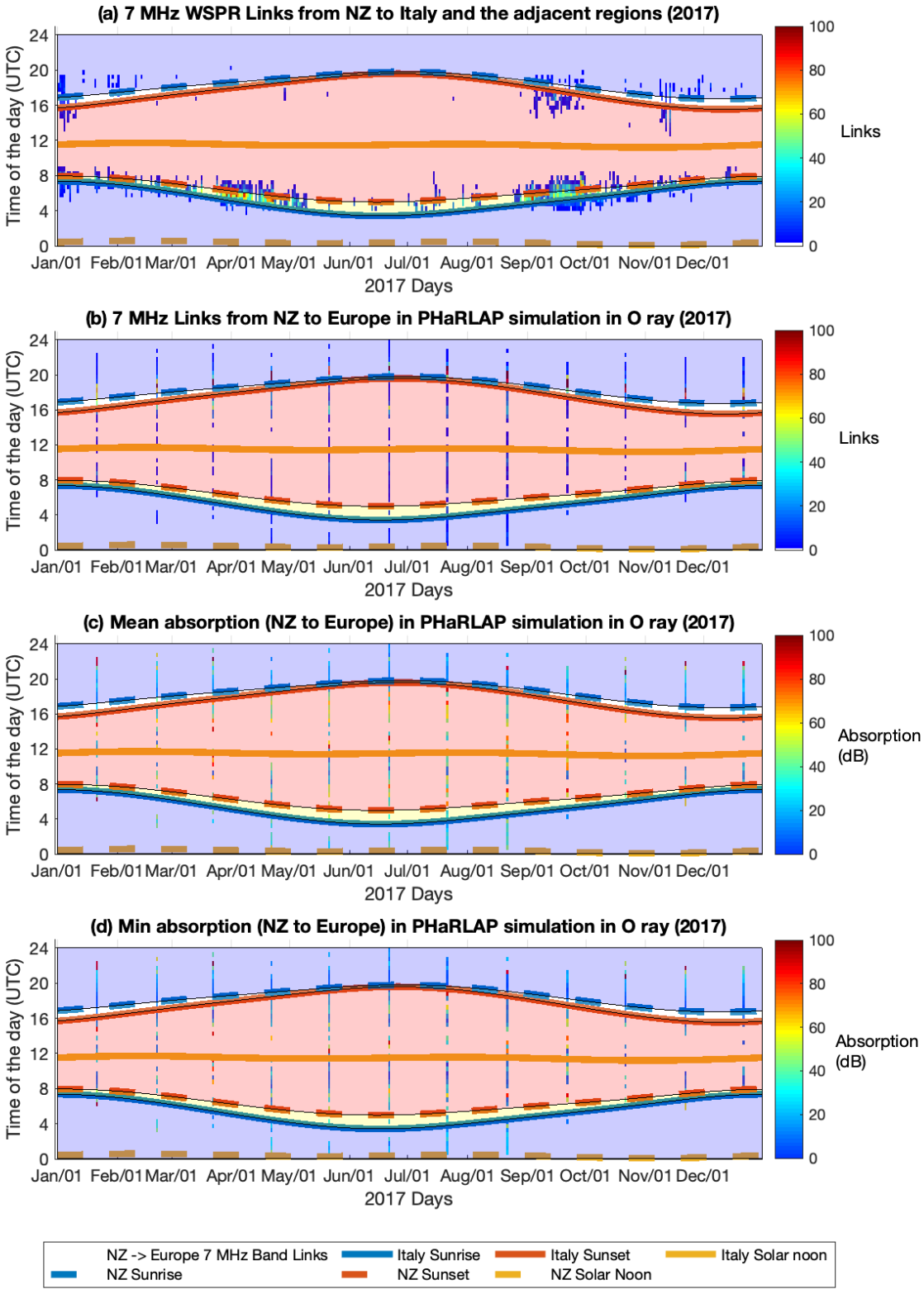

Figure 6.19 – (a) 7 MHz WSPR Links from New Zealand to Italy and the adjacent regions (b) 7 MHz Links from New Zealand to Europe in PHaRLAP simulation in O ray (c) Mean absorption (New Zealand to Europe) in PHaRLAP simulation in O ray (d) Min absorption (New Zealand to Europe) in PHaRLAP simulation in O ray.

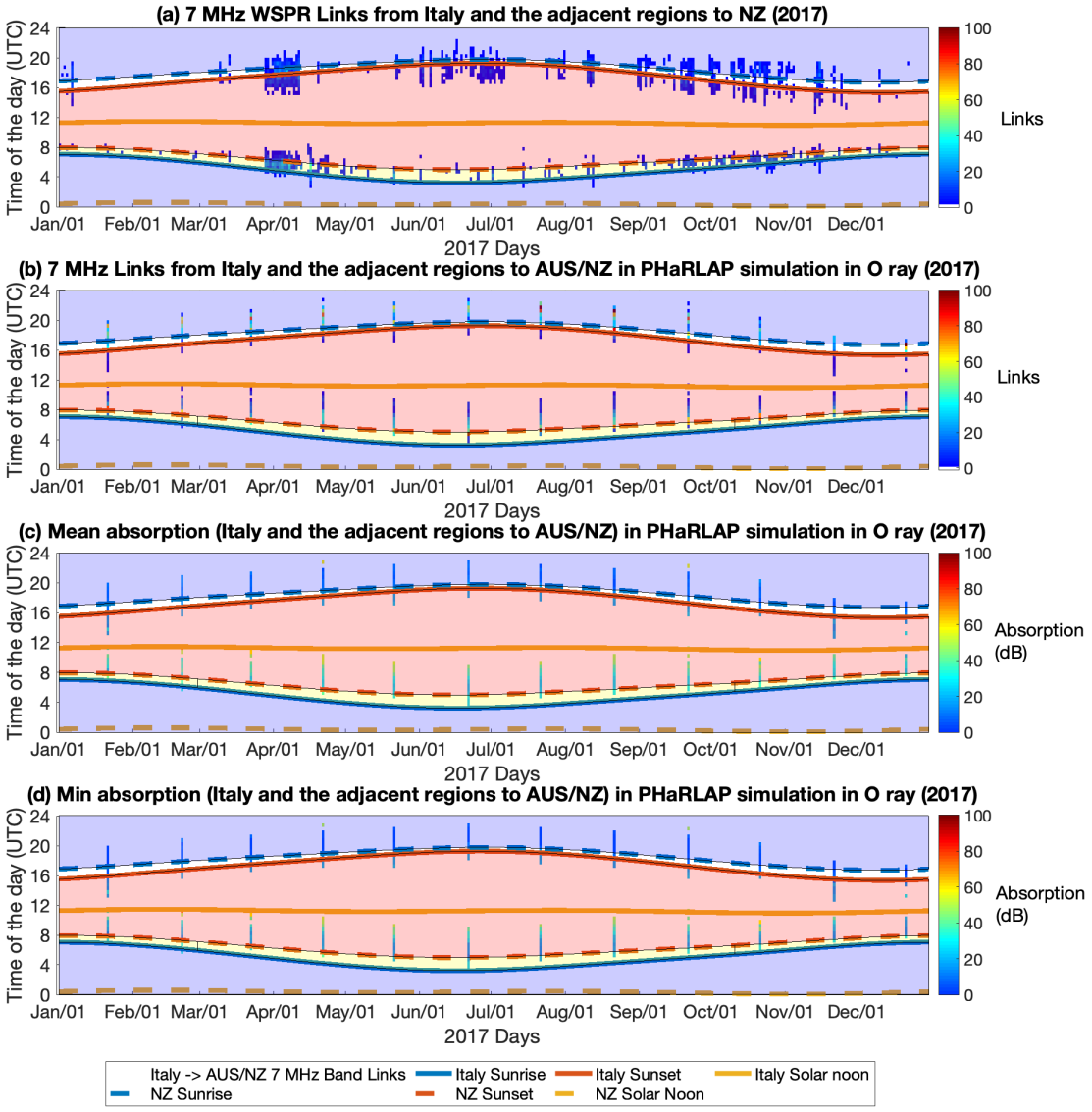

Figure 6.20 – (a) 7 MHz WSPR Links from Italy and the adjacent regions to New Zealand (b) 7 MHz Links from Italy and the adjacent regions to Australia/New Zealand in PHaRLAP simulation in O ray (c) Mean absorption (Italy and the adjacent regions to Australia/New Zealand) in PHaRLAP simulation in O ray (d) Min absorption (Italy and the adjacent regions to Australia/New Zealand) in PHaRLAP simulation in O ray.

Figure 6.21 and Figure 6.22 show the links from Australia to the UK with a simulation reception region set to Europe. The results indicate that there is a general trend to follow the terminator with more absorption in the common daytime, as expected. The corresponding results for Italy and the adjacent regions are shown in Figure 6.23 and Figure 6.24.

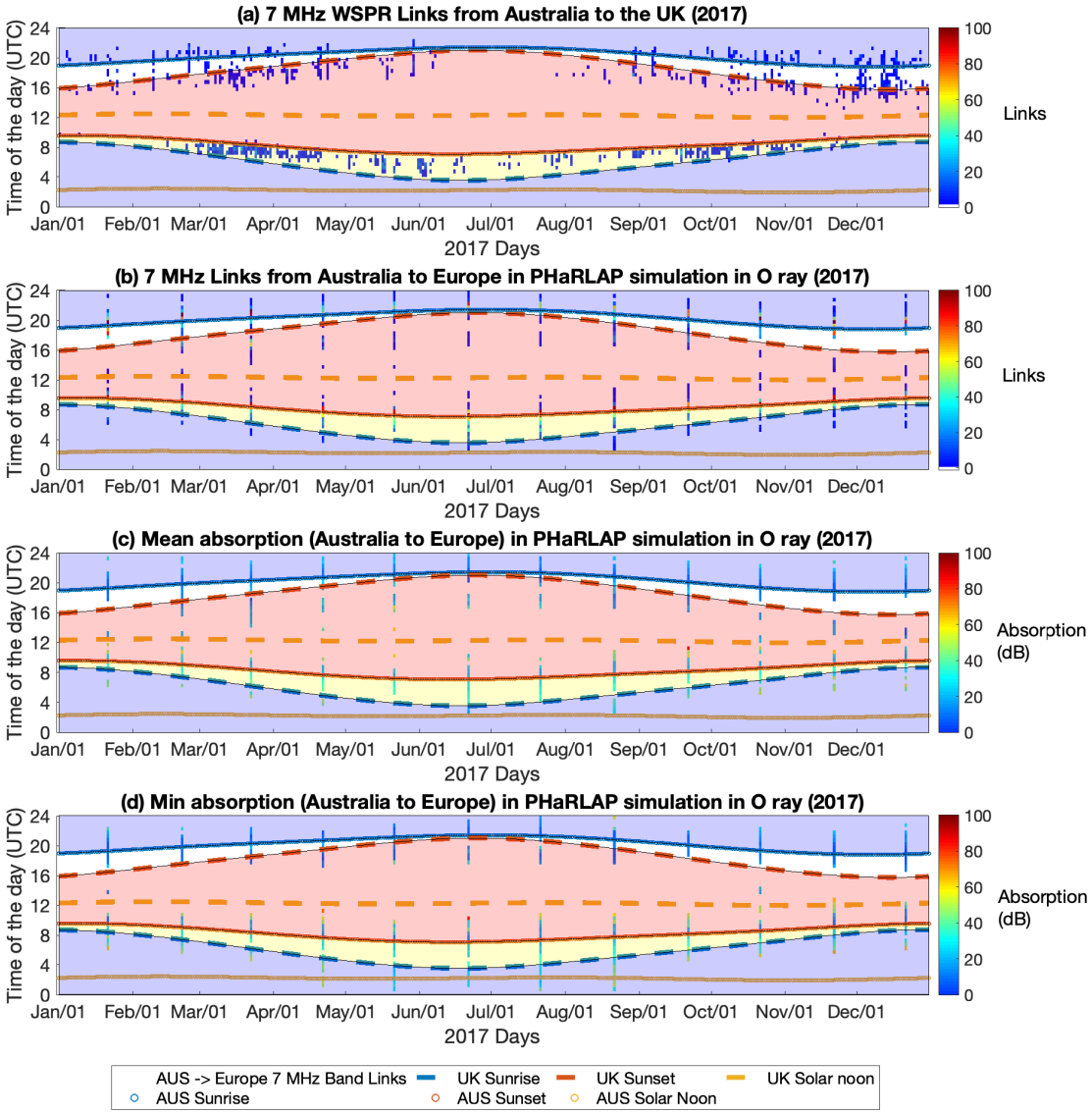

Figure 6.21 – (a) 7 MHz WSPR Links from Australia to the UK (b) 7 MHz Links from Australia/New Zealand to the UK in PHaRLAP simulation in O ray (c) Mean absorption (Australia/New Zealand to the UK) in PHaRLAP simulation in O ray (d) Min absorption (Australia/New Zealand to the UK) in PHaRLAP simulation in O ray.

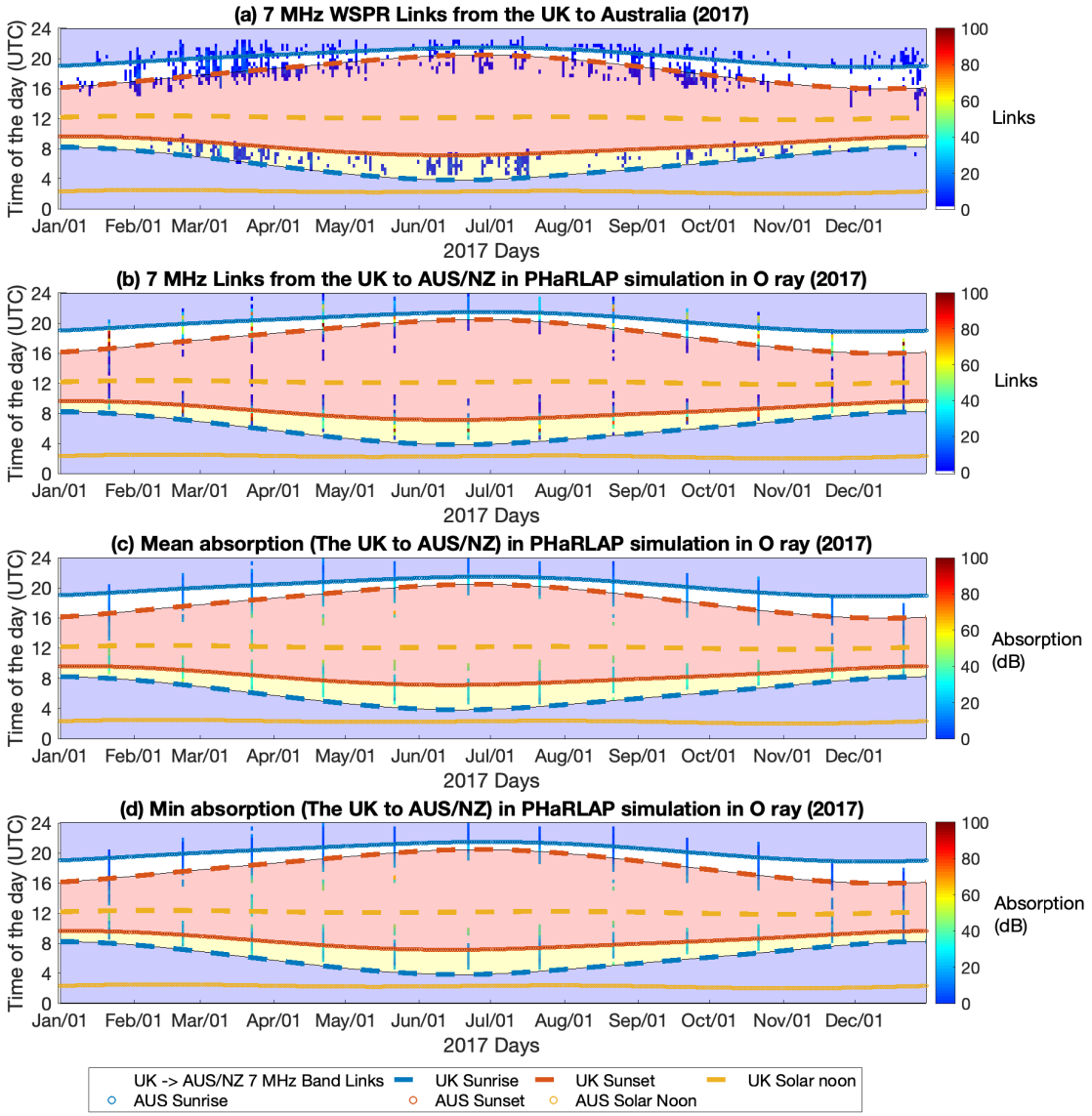

Figure 6.22 – (a) 7 MHz WSPR Links from the UK to Australia (b) 7 MHz Links from the UK to Australia/New Zealand in PHaRLAP simulation in O ray (c) Mean absorption (the UK to Australia/New Zealand) in PHaRLAP simulation in O ray (d) Min absorption (the UK to Australia/New Zealand) in PHaRLAP simulation in O ray.

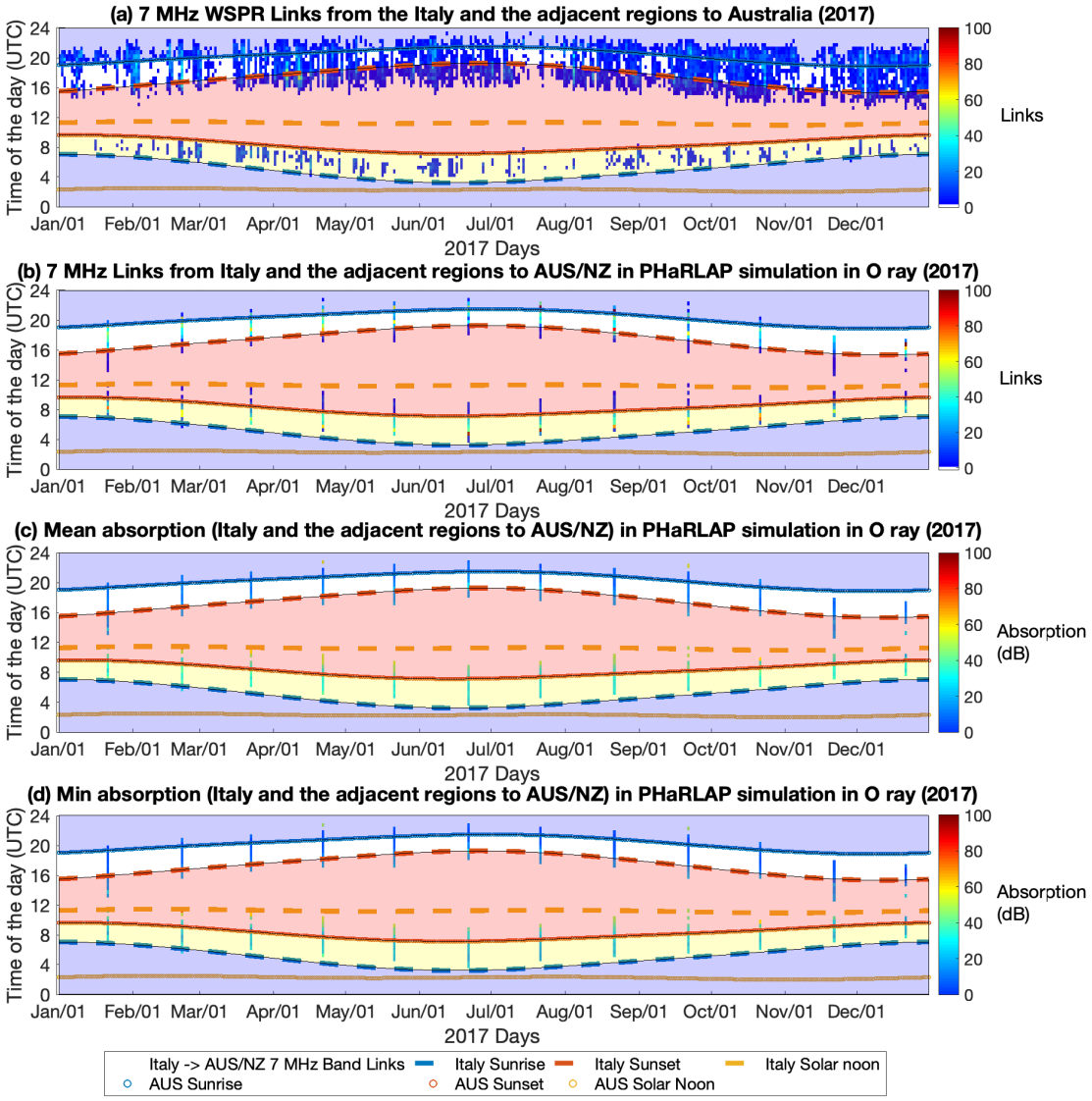

Figure 6.23 – (a) 7 MHz WSPR Links from Italy and the adjacent regions to Australia (b) 7 MHz Links from Italy and the adjacent regions to Australia/New Zealand in PHaRLAP simulation in O ray (c) Mean absorption (Italy and the adjacent regions to Australia/New Zealand) in PHaRLAP simulation in O ray (d) Min absorption (Italy and the adjacent regions to Australia/New Zealand) in PHaRLAP simulation in O ray.

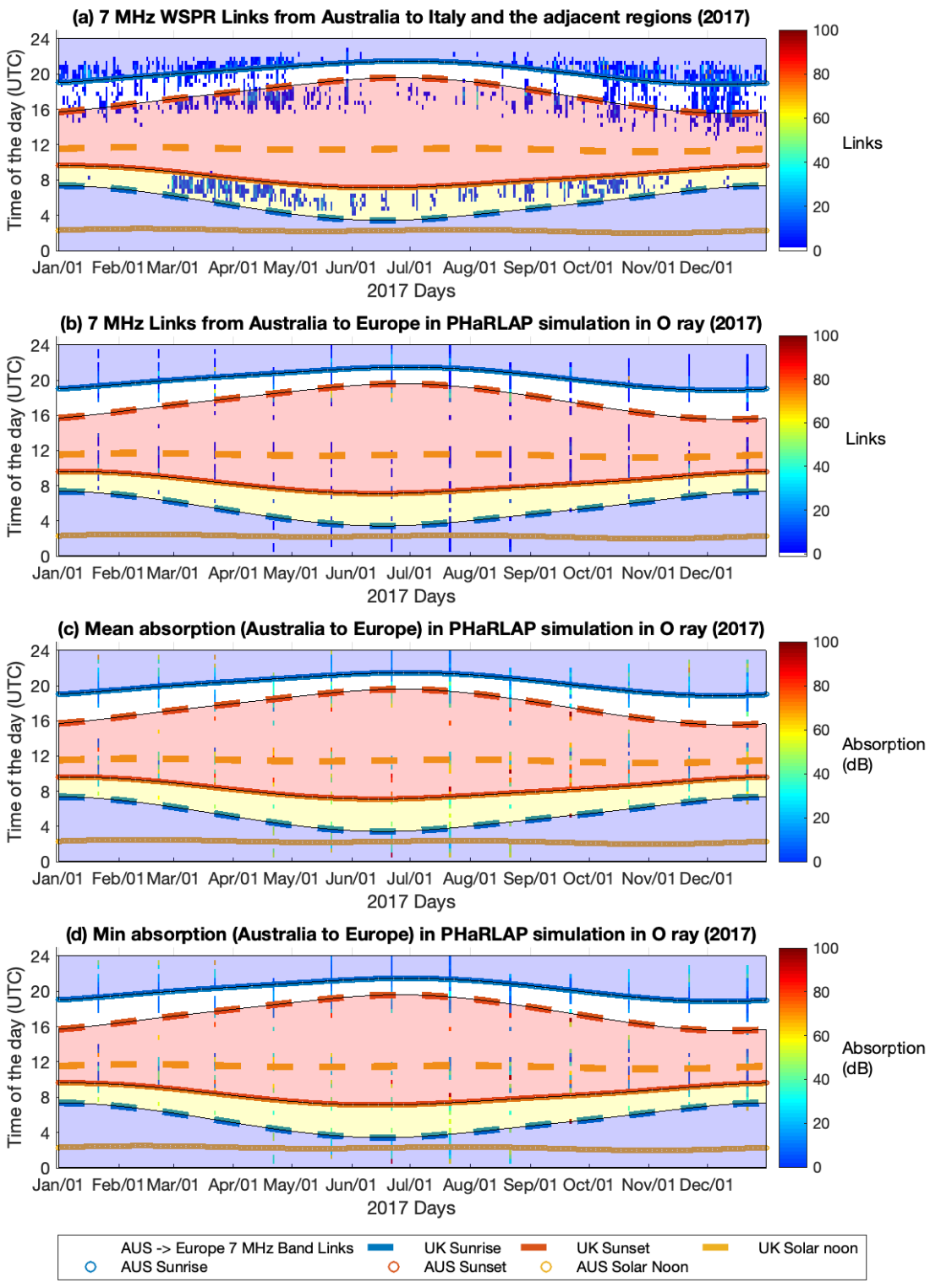

Figure 6.24 – (a) 7 MHz WSPR Links from Australia to Italy and the adjacent regions (b) 7 MHz Links from Australia to Europe in PHaRLAP simulation in O ray (c) Mean absorption (Australia to Europe) in PHaRLAP simulation in O ray (d) Min absorption (Australia to Europe) in PHaRLAP simulation in O ray.

6.4. Summary

The WSPR results in Chapter 4 showed evidence of clear propagation patterns of successful links throughout the day and year. However, the analysis of the SNR and transmission powers in Chapter 5 could not explain the cause of the asymmetrical elements in these time propagation patterns. These elements included the links being from Europe to Australia/New Zealand in the European summer evening but are not being made in the other direction.

In order to give some insights into the patterns observed in the WSPR data, this chapter conducted a single-hop signal propagation simulation using a ray-tracing software PHaRLAP and the ionospheric model IRI2016. The chapter presented a comparison between the WSPR data and the simulated links by simulating the number of links received in the reception region and the mean and minimum absorption levels along the propagation paths. This predicted some of the patterns, in particular the interesting terminator related pattern between Australia/New Zealand and Europe. However, this did not explain the apparent directional asymmetry in the European summer evening.

PHaRLAP, as a ray-tracing software, is heavily dependent on the ionospheric conditions used in the simulations. As IRI2016 is an empirical ionospheric model, it is not capable of representing variable ionospheric events. IRI2016 with the PHaRLAP ray-tracer may not show very accurate absorption on a day-to-day basis, but it does show variation throughout the day, indicating variation of absorption at different times of the day.

Chapter 7 will discuss the possible explanations of the time propagation pattern and the asymmetry of the ionosphere seen in the WSPR links.

7. Discussion

7.1. Introduction

This chapter aims to propose possible explanations and suggest future studies to investigate the patterns seen in the WSPR links. The structure of this chapter is as follows: Section 7.2 discusses absorption while Section 7.3. discusses the noise effects. Section 7.4. discusses the use of ionospheric models such as IRI2016 and propagation models such as PHaRLAP and Section 7.5. discusses the future work.

7.2. Absorption

The solar radiation varies the plasma density in the ionosphere, which in turn affects the properties of a radio signal, propagating through the ionospheric layers. One of the important properties affected by the ionospheric conditions is signal strength. This is because the plasma density variations in the ionosphere can cause the signal to be affected by absorption, as discussed in Chapter 2.

The WSPR results from the UK to the USA in Chapter 4 show that the links are established during the common night hours. This is because absorption in the night ionosphere is lower than that in the day ionosphere. Therefore, provided that there is sufficient ionisation to support a link, there needs to be not too much ionisation at lower altitudes, absorbing the signal.

There are limitations to the simulations using the IRI2016 empirical model in Chapter 6. As a result of the limitation in both neutral and ionisation representation, the absorption estimates in the simulations are unable to identify the effects of absorption at a particular instant. The effects of absorption are dependent on the ionospheric conditions and the operational frequency of the radio signal (Davies, 1965). Ionospheric absorption occurs in D, E and F layers. However, most of the absorption occurs in the D layer because it is situated at lower altitudes, between 60 km and 90 km from the Earth's surface (Davies, 1965). As the radio signal will first pass through the D layer of the ionosphere, the signal strength is reduced by the collision between the electrons and neutral atoms. As a result, the D layer is the main contributor to the signal's absorption.

Chapter 2 mentioned that the attenuation (A) of the signal is inversely proportional to the square of the radio frequency (f) in the absence of a geomagnetic field. However, the attenuation in the presence of a geomagnetic field is also influenced by the gyrofrequency (f_L), as shown in Equation 7.1.

$$A \propto 1/(f \pm f_L)^2 \qquad \text{Equation 7.1}$$

This shows that radio signals propagating in extraordinary (X) mode suffer more attenuation than those propagating in an ordinary (O) mode. In addition to that, radio signals which propagate at lower HF frequencies, such as 7 MHz, will be heavily attenuated when the signals pass through the D region. As a result, the signal strength will be significantly reduced in the day ionosphere. However, the night-time ionosphere has less absorption due to the absence of the D layer. Therefore, long-distance radio signals are capable of propagating at the night ionosphere.

7.2.1. Possible Explanations of Absorption on the WSPR Results

The WSPR results in Chapter 4 showed that long-distance radio links are mostly established in the common night hours, such as the links between the USA and Australasia, the USA and Europe, and Australasia and Europe. This is likely to be because the signals are absorbed in the day region due to the D layer. However, the plasma density in the D layer is relatively low during the sunrise and the sunset hours because of the less solar radiation. As a result, the signal could enter the ionosphere at these times when the low altitude ionisation is still relatively low. However, the ionosphere has sufficient ionisation in the F layer heights to allow for propagation.

This section will investigate and discuss whether absorption can explain the observed propagation patterns and asymmetry seen in WSPR data in Chapter 4. For example, there is a lack of daytime-to-daytime propagation from Eastern Australia to Western America. However, there is some daytime-to-daytime propagation from Eastern Australia to Eastern America. This asymmetry could be explained by absorption. If the transmitter and receiver locations are away from the terminator, such as Western America and Eastern Australia, the distance to travel from the terminator to the receiver via the nightside will be longer. For Eastern America, which is closer to the terminator, then the propagation could still travel via the nightside. Other propagation results which may be explained by absorption are listed in Table 7.1.

Figure 7.1 shows an example from PHaRLAP of a predicted propagation path, mostly on the nightside from Eastern Australia to Western America.

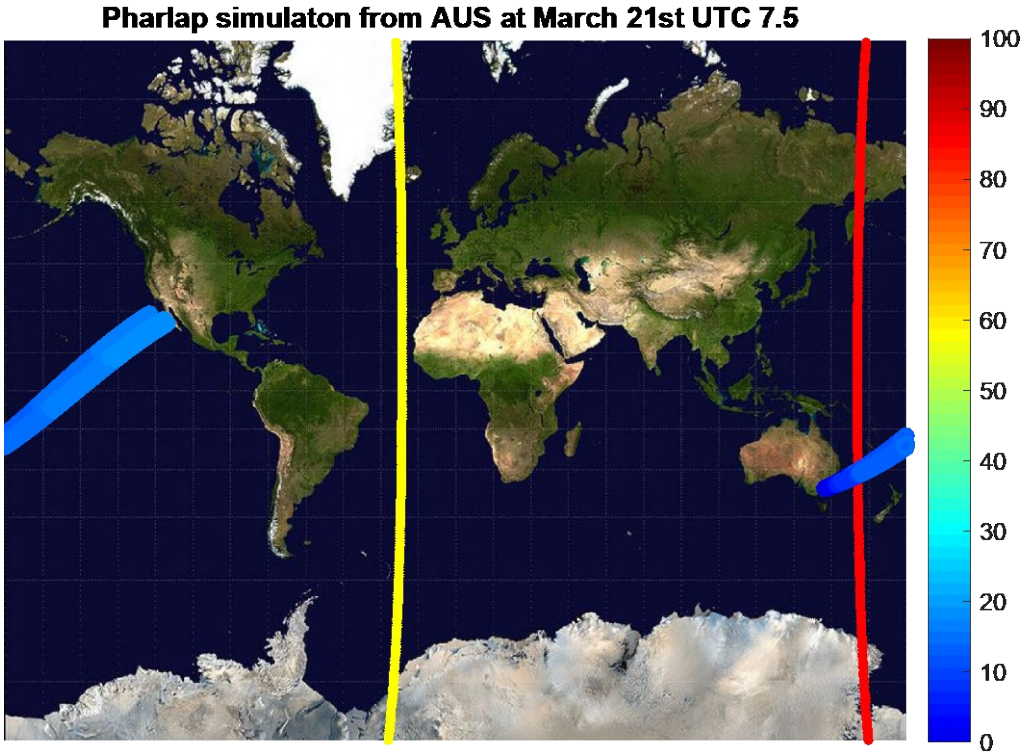

Figure 7.1 – Propagation paths from Eastern Australia to Western America at UTC 7.5 on March 21st. The path propagates mostly at the nightside of the ionosphere. The colorbar indicates the absorption in dB.

Table 7.1 – The transmitters and receivers' locations with the relevant propagation types and possible explanations of absorption on the radio propagation links

Transmitters Location (Tx)	**Receivers Location (Rx)**	**Propagation Type**	**Absorption**
New Zealand	**The UK**	Greyline	Absorption does not explain this pattern.
Eastern Australia	**Eastern USA**	Common night propagation Common day propagation	Only a few links propagated in common day propagation. The links mostly propagate via the nightside.
Eastern USA	**Eastern Australia**	Common night propagation Common day propagation	Only a few links propagated in common day propagation. The links mostly propagate via the nightside.
Western USA	**Eastern Australia**	Common night propagation	Lack of daytime-to-daytime propagation.
Eastern Australia	**Western USA**	Common night propagation	Lack of daytime-to-daytime propagation.
New Zealand	**Italy and the adjacent regions**	Greyline	Absorption does not explain this propagation pattern.
Eastern Australia	**The UK**	Common night propagation Common day propagation	Absorption could partially explain this propagation pattern.
Eastern Australia	**Italy and the adjacent regions**	Common night propagation Common day propagation	Absorption could partially explain this propagation pattern.

7.2.2. New Zealand and the UK

Figure 7.2 and Figure 7.3 show examples of the full paths of the predicted links from New Zealand to Europe for the 6 and 18 UTC. It is interesting to see that there are many possible paths to the conjugate point on the Earth and that all travel on the nightside. The predicted UTC morning paths are through the American region and the UTC evening paths through the Asian region.

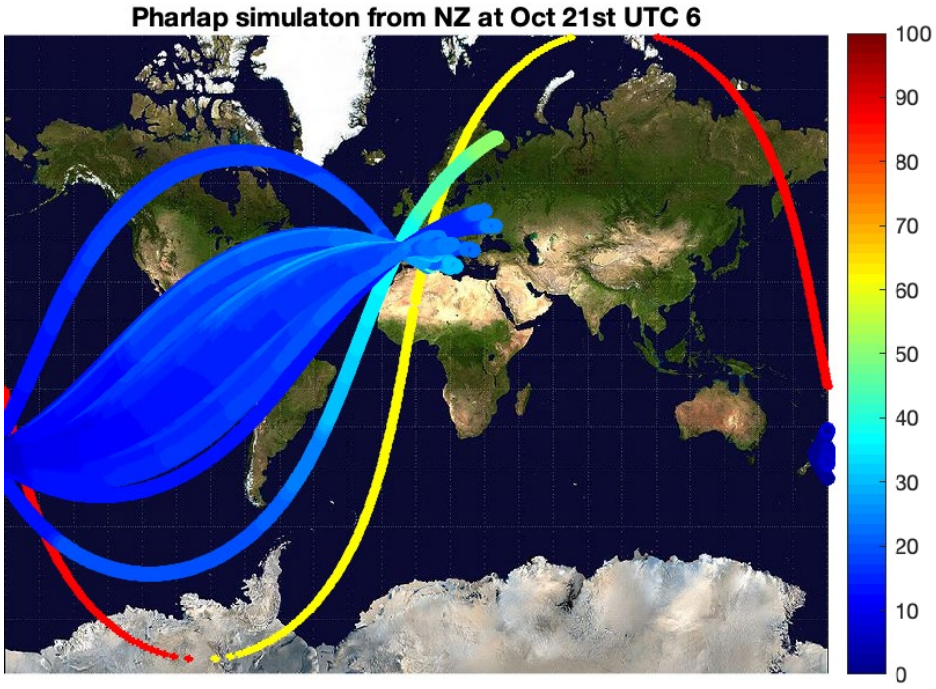

Figure 7.2 – Propagation Paths from New Zealand to Europe at UTC 6 on October 21st 2017. The propagation paths propagate through the American sector. The colorbar indicates the absorption in dB.

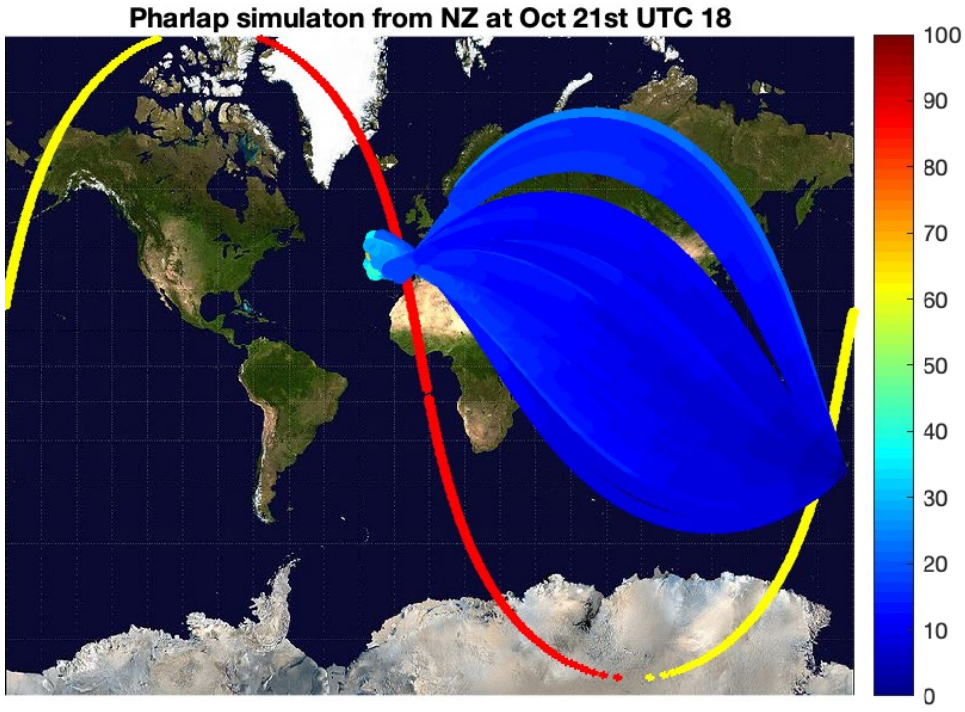

Figure 7.3 – Propagation Paths from New Zealand to Europe at UTC 18 on October 21st 2017. The propagation paths propagate through the Asian sector. The colorbar indicates the absorption in dB.

The links observed from WSPR showed that there was evidence of greyline propagation between New Zealand and the UK. However, the links are made at the New Zealand dusk/UK dawn hours, but not during the New Zealand dawn/UK dusk hours.

The links propagating in the reciprocal direction, from the UK to New Zealand, were also observed. However, the links propagating from the UK to New Zealand showed that the links propagated both during the UTC morning and UTC evening hours. This indicated that the time propagation patterns in the morning and in the evening, from the UK to New Zealand, were symmetrical to each other.

The links from New Zealand to the UK indicated that there was a directional asymmetry in the propagation pattern. It was difficult to see why there would be absorption for signals propagating in one direction and not the other. Potentially, one explanation for the asymmetry in the propagation could be from the differences in the propagation of the O and the X rays of the signal, which could be explored in future work.

It is also possible that absorption of an incoming signal could push the signal-to-noise ratio low enough that the signal would not be registered at the receiver. Thus, an equal amount of absorption in both directions of travel could be impacted by the differences in the local noise at either end of the links and prohibit some of the signals

from being registered. It is further intensified because the local absorption could influence the local noise – an absorbing ionosphere will also reduce the 'ionospherically propagated noise.'

7.2.3. Eastern America to Eastern Australia

The WSPR links between Eastern America to Eastern Australia show that there is day-night or night-day propagation and daytime to daytime propagation. However, more links are propagated in common night propagation than in common day propagation. Therefore, the possible explanation of the time propagation patterns is that the links propagating from Eastern America to Eastern Australia favour common night propagation. It indicates that the links are propagated along the night ionosphere through the American region, as shown in Figure 7.4.

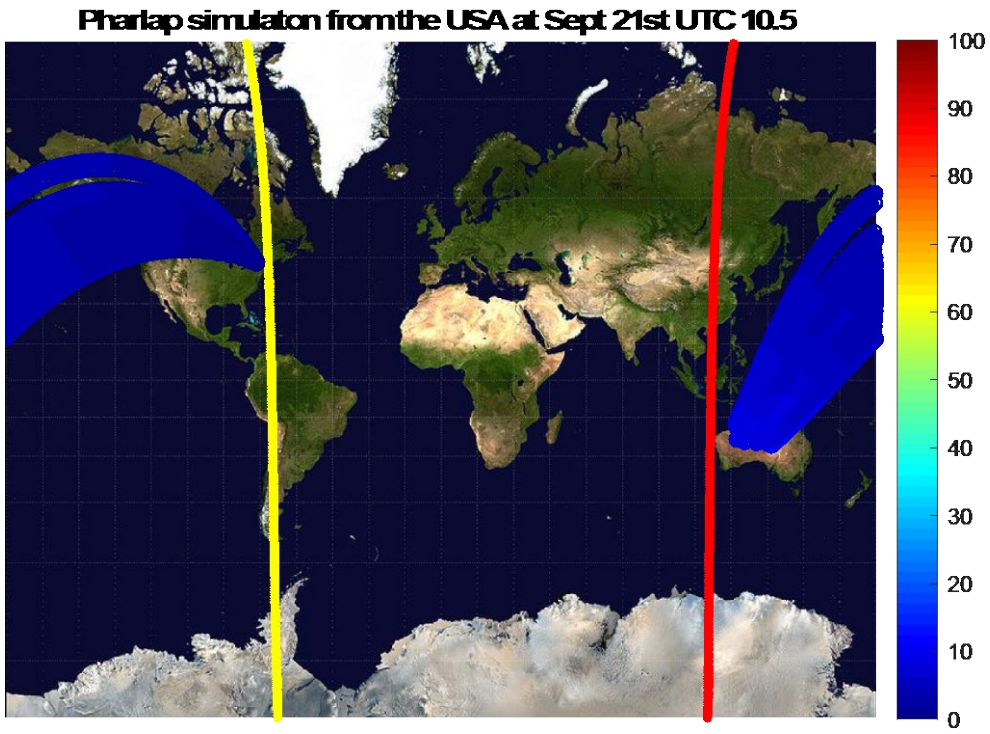

Figure 7.4 – Propagation paths from Eastern America to Australia at UTC 10.5 on September 21st 2017. The colorbar indicates the absorption in dB.

There may be absorption that inhibits the propagation during the common day hours. Nevertheless, some links achieve daytime to daytime propagation because the distance between Eastern America and Eastern Australia is far enough to propagate mainly through the night ionosphere (i.e. the long way around). The possible explanation for the daytime-to-daytime propagation is the links from Eastern America propagate towards the terminator, which enables propagation through the night ionosphere, as shown in Figure 7.5.

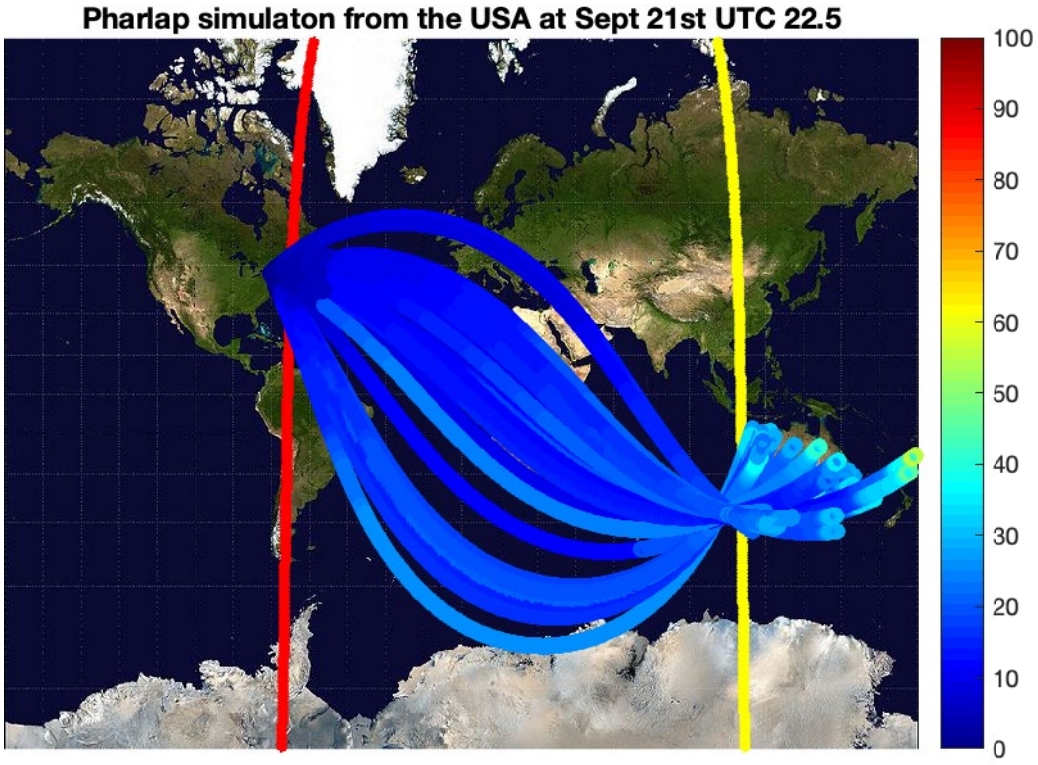

Figure 7.5 – Propagation paths from Eastern America to Australia at UTC 22.5 on September 21st 2017. The colorbar indicates the absorption in dB.

7.2.4. Eastern Australia to Eastern America

The WSPR links between Eastern Australia and Eastern America show common night propagation and daytime to daytime propagation. However, more of the links are propagated through the common night than in the common day. The possible explanation of the time propagation patterns is that the links propagating from Eastern Australia to Eastern America favour common night propagation through the American region, as shown in Figure 7.6.

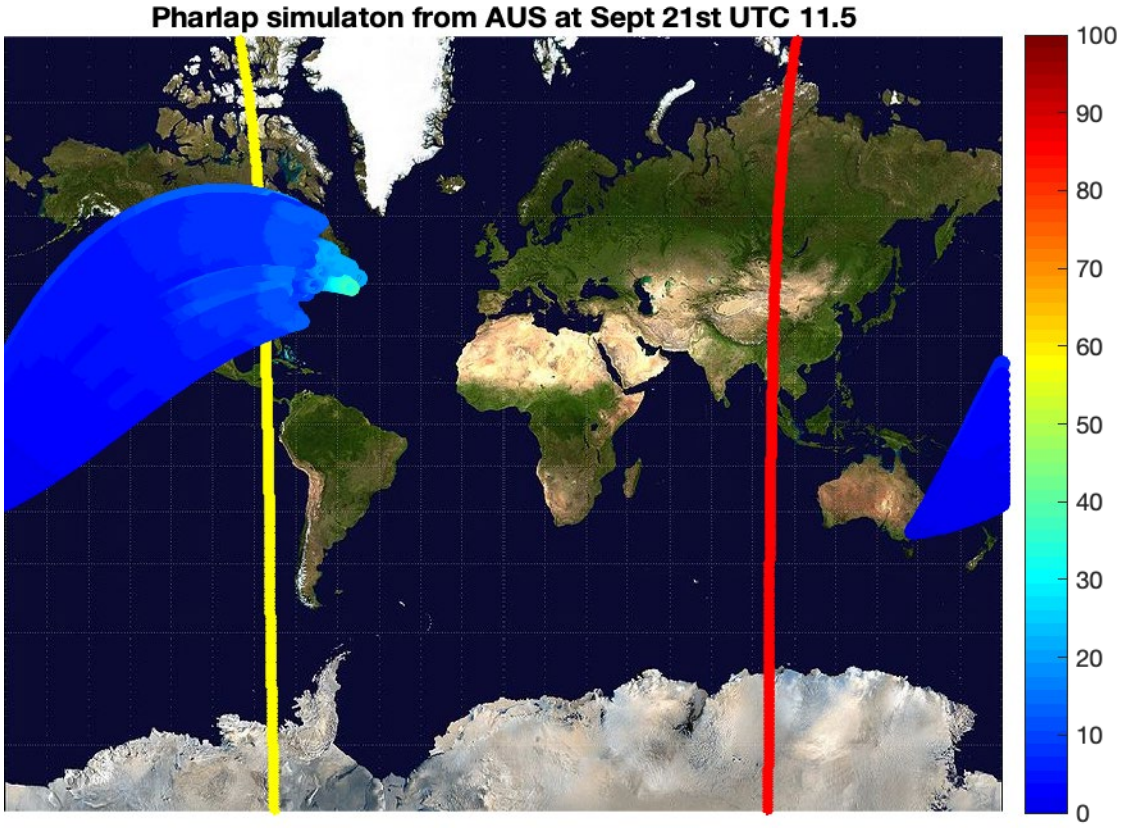

Figure 7.6 – Propagation paths from Eastern Australia to America at UTC 11.5 on September 21st 2017. The colorbar indicates the absorption in dB.

There may be absorption that inhibits the propagation during the common day hours. Nevertheless, some links achieve daytime to daytime propagation because the distance between Eastern Australia to Eastern America is far enough to propagate through the night ionosphere. The possible explanation for the daytime-to-daytime propagation is the links from Eastern Australia propagate towards the sunset terminator, which enables long-distance propagation through the night ionosphere.

The other set of results, observed in Chapter 6, is the propagation from Eastern Australia to Eastern America. It shows that there is common daytime propagation from Eastern Australia to Eastern America. Again, PHaRLAP is used to simulate the propagation paths, as shown in Figure 7.7. It shows that the links propagate towards the sunrise terminator, enabling long-distance propagation through the nightside of the ionosphere entering Eastern America.

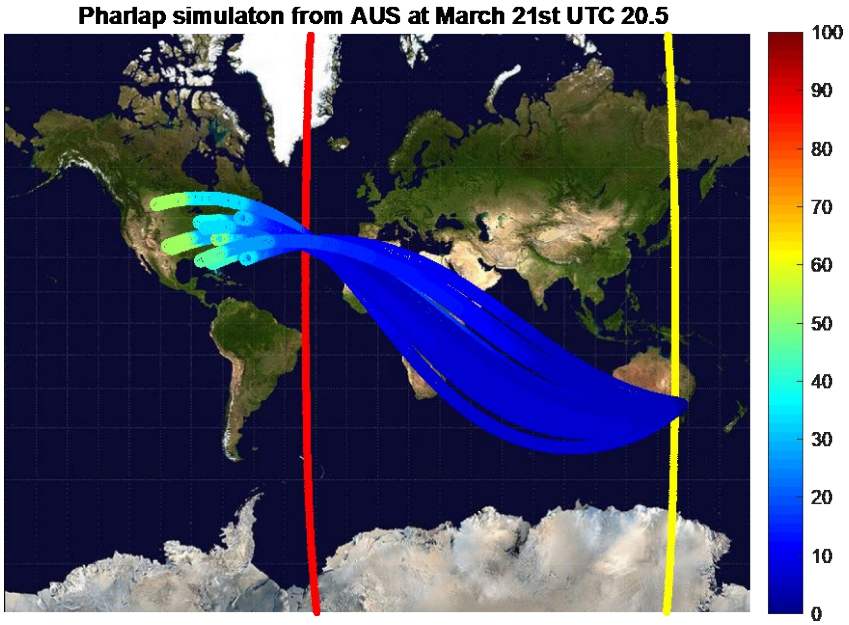

Figure 7.7 – Propagation paths from Eastern America to Australia at UTC 20.5 on September 21st 2017. The colorbar indicates the absorption in dB.

7.2.5. Western America to Eastern Australia

The links between Western America to Eastern Australia shows that there is common night propagation. However, there is a lack of daytime-to-daytime propagation compared to Eastern America's propagation to Eastern Australia. The possible explanation of these patterns is that the common night propagation is propagated across the Pacific region. Therefore, through the night ionosphere direction for common day links, the long path could be the path of Eastern America to Eastern Australia links. However, Western America is far away from the terminator when Eastern Australia is during the daytime. This means the links are heavily absorbed in the day ionosphere. As a result, the links propagated from Western America to Eastern Australia may indicate that absorption influences the time propagation patterns.

7.2.6. Eastern Australia to Western America

The links propagating from Eastern Australia to Western America also show that there is common night propagation. However, there is a lack of daytime-to-daytime propagation compared to those propagating from Eastern Australia to Eastern America. This shows that the time propagation patterns of the links propagating between Eastern Australia and Western USA are symmetrical. The possible explanation of these patterns is that the common night propagation is propagating through the Pacific region, which is most likely through the great circle path.

Therefore, the long path in which the links propagated through the night ionosphere for common day propagation occurs to the links propagated from Eastern Australia to Eastern America. However, Western America is far away from the terminator when Eastern Australia is during the daytime. This means that the links are heavily absorbed in the day ionosphere. As a result, the links propagated from Eastern Australia to Western America may indicate that absorption influences the time propagation patterns.

7.2.7. New Zealand to Italy and the adjacent regions

The time propagation patterns from New Zealand to Italy and the adjacent regions demonstrate that there is greyline propagation on the links propagating from New Zealand to Italy and the adjacent regions. It should be noted that the links start and stop close to the terminator. However, the full propagation path is not necessarily fully along the terminator, as shown by the PHaRLAP predicted links between New Zealand and Europe, shown in Figure 7.2 and Figure 7.3.

The WSPR results indicate that the links are propagating at the New Zealand dusk/Italy and the adjacent regions' dawn hours but not during the New Zealand dawn/Italy and the adjacent regions dusk hours. This is an asymmetry in the time propagation patterns between the morning and evening hours. However, the links propagating from Italy and the adjacent regions to New Zealand showed that the links were propagating during the UTC morning and UTC evening hours. This again indicates that there is an asymmetry in the propagation between New Zealand and Italy and the adjacent regions (ITADR), but the absorption does not explain it from the simulations.

7.2.8. Eastern Australia to the UK

The time propagation patterns of the link propagated from Eastern Australia to the UK illustrate that the links are propagating at Eastern Australian dusk/UK dawn hours and during the Eastern Australian dawn/UK dusk hours. The patterns show that the links propagate at common day and common night propagation. The common day propagation shows that the links are confined to daytime hours, whereas the common night propagation shows sparsity in the patterns. In addition, there are no links during the UTC summer from Eastern Australia to the UK. As a result, there is an asymmetry in the time propagation pattern. However, links propagating from the UK to Eastern Australia show links are propagated during the UTC morning and UTC evening hours. The patterns from the UK to Eastern Australia show symmetrical time propagation pattern in the morning and in the evening. Therefore, it also indicates that there is an asymmetry in the links, but the absorption does not explain it from the simulations.

7.2.9. Eastern Australia to Italy and the adjacent regions

The links propagated from Eastern Australia to Italy and the adjacent regions are propagated at the Eastern Australian dusk/Italy and the adjacent regions' (ITADR) dawn hours and during the Eastern Australian dawn/Italy and the adjacent regions dusk hours. The time propagation pattern at the Eastern Australian dusk/Italy and the adjacent regions dawn hours showed that the links are propagated in common day propagation, confined to daytime hours. Similarly, the time propagation pattern at the Eastern Australian dawn/Italy and the adjacent regions' (ITADR) dusk hours illustrated that the links are propagated in the common night. However, the links propagated at common night propagation show sparsity in the pattern. This means that most of the links are established along Eastern Australia's dawn hours and along Italy and the adjacent regions' dusk hours, and the links are sparsely populated during the common night hours. In addition, there are only a few links propagated during the UTC evening hours during the Italian summer. This indicates that there is an asymmetry in the time propagation patterns between the morning and evening hours. On the contrary, the links propagating from Italy and the adjacent regions to Eastern Australia show links are propagated during the UTC morning and UTC evening hours. It also shows symmetrical time propagation pattern in the morning and in the evening.

7.2.10. Absorption summary

The propagation patterns, which were presented in Table 7.1, could be partly explained by ionospheric absorption. The most common effect of absorption was the links favoured common night propagation as the absorption at the night ionosphere was significantly lower than that in the day ionosphere.

Table 7.1 also showed common day propagation from some patterns, such as the links propagating between Eastern Australia and the UK and between Eastern Australia and the USA. Nevertheless, these common day propagation links were most likely to be propagated through the night ionosphere because of low absorption. The possibility of these night-time paths was evidenced by the PHaRLAP/IRI2016 simulation.

In summary, many of the patterns in the propagation can be explained by the preference for night-time propagation where there is low absorption. Further, the daytime to daytime propagation can be explained by signals taking the long path through the nightside ionosphere.

7.3. Simulation limitations

As it was stated in Chapter 3, IRI2016 is an empirical model statistically computed from historical sets of ionospheric data (Bilitza *et al.*, 2017). IRI2016 is widely used as a background ionosphere for radio propagation studies, including HF ray-tracing (Bilitza *et al.*, 2017). The limitation of IRI2016 is that the output of the model is a monthly median representation of the ionosphere. However, other short term variations due to the driving of the ionosphere from the lower atmosphere, from sources, such as atmospheric tides and other atmospheric waves, also play a role in ionospheric variations. Further, important drivers from solar variabilities, such as solar flares, coronal mass ejections and other solar emissions, will change the short-term behaviour of the ionosphere. Therefore, IRI2016 is unable to predict the real-time ionospheric variations in the ionosphere. Nevertheless, it is still very useful for the studies here because it has allowed a statistical representation of the ionospheric conditions for the HF propagation study.

PHaRLAP was used to predict probable propagation paths and to discover whether its time propagation patterns will give possible explanations of the patterns seen in WSPR. However, the limitations of using PHaRLAP is that PHaRLAP establishes links and absorption whenever there is a link made in the simulation, which is inherently ‘tied’ to the accuracy of the ionospheric model. Furthermore, as PHaRLAP uses the IRI2016 model as a simulation environment to calculate the phase refractive indices and the propagation paths, the results will be influenced by the accuracy of the electron concentration, modelled in the IRI2016.

7.4. Local Noise

The patterns of links made between different countries found in Chapter 4 from the WSPR data have been partly understood through the simulations in Chapter 6. However, the propagation pattern between New Zealand/Australia and Italy and the adjacent regions/UK showed that the link pattern has directional asymmetry, which is not explained by the PHaRLAP/IRI2016 simulations.

A possible explanation for this directional asymmetry could be different local noise levels at either end of the links. Measurements of local noise in the HF bands were sought but were not found for the studies in this thesis. Instead, the WSPR measurements themselves provided SNR at reception.

Recent measurements of HF radio noise have started to be taken in Germany through a project run by radio amateurs (Eichel *et al.*, 2021). It is interesting to note that these measurements are already showing indication of diurnal noise changes during the month of June 2021. While there are not yet enough measurements to do a full year's study, these new measurements will provide evidence that can help explain whether local noise across the European region is higher during the European dusk than the European dawn. Suppose this is the case and show seasonal variation. In that case, this could explain the lack of reception of the long-distance WSPR signals arriving in Europe from Australia and New Zealand during the European sunset summertime.

7.5. Summary

This chapter discussed possible explanations for the results that were found in the thesis and linked them together with the observations and simulations.

Section 7.2. discussed the role of absorption in explaining the propagation patterns that were found in this research. Section 7.3. outlined several limitations of the investigation tools that were used (PHaRLAP and IRI2016). Section 7.4. highlighted the need for local noise measurements to be made and references a new project starting to take such HF measurements in Europe.

8. Conclusions and future work

The amateur radio network WSPR opens up a new opportunity to monitor and record radio communication links globally, including HF propagation. The research in this thesis was facilitated by the availability of this new HF data source from across the world using the amateur radio network. This extensive resource opens up new opportunities for investigating HF communication links across the world.

The WSPR data contains a range of discrete radio frequencies, but 7 MHz was chosen because it was a frequency that propagates well during the lower periods of the sunspot cycle and is also a popular choice for WSPR equipment. This was important because the research required large quantities of data, and the year 2017 was chosen, which was the most recent full year of data at the start of the research.

Chapter 1 introduced the thesis, and Chapter 2 reviewed the literature. Finally, chapter 3 describes the data source and research tools used in this thesis.

The Chapter 4 results showing the links between the UK and New Zealand revealed evidence of a strong preference for links to start and end close to the terminator times. It was important to note that this did not imply that the signals necessarily propagated along the terminator for the entire path – what was known is simply that the links started and ended close to the terminator. This is an important distinction when discussing the so-called greyline propagation. In general terms, greyline propagation is often reported from the existence of links being made where the transmitter and receiver are located close to the terminator. True greyline propagation involves the entire propagation path being along the terminator.

The interest in greyline propagation has lasted for over a century, but it has mainly been reported in recent years by the amateur radio community. These reports have been consistent over the years but are often not documented in formal scientific literature. Reports include long-distance communications between the UK and New Zealand often being made in the UK early morning close to sunrise. Such reports provided a background motivation for some of the research in this thesis, and the WSPR database allowed the investigation to look for statistical evidence to support these reports.

A more comprehensive study was done in Chapter 4 that investigated patterns emerging from the links between other countries/regions. The first question was: do links between other regions show evidence of terminator clustering of the links? The answer to this was yes, and several long-distance links show this evidence. This terminator pattern came out very clearly in the links between Australia or New Zealand with UK or Italy and the adjacent regions.

There was good evidence of links during common night-time between many of the regions investigated. These common night-time links were expected because there would be less absorption of the signal during the night-time.

A further interesting result that emerged from Chapter 4 was the asymmetry of the propagation pattern over the long-distance links between Australia/New Zealand and the UK/Italy and the adjacent regions. It was evident that there were fewer links from Australia or New Zealand to UK or Italy and the adjacent regions in the UTC evening in the European summer than in the other direction. It was also evident that there were fewer links from Australia or New Zealand to UK or Italy and the adjacent regions in the UTC morning in the European winter than in the other direction. Previous reports of this asymmetry were not found.

Chapter 5 investigated the evidence of noise effects on the time propagation pattern seen in Chapter 4. The information available was the signal-to-noise at the receiver and the transmitter power. The results from Chapter 5 indicated that for the signals propagating from the UK to Australia/New Zealand, the lowest transmitter power that got through did not vary systematically throughout the year, but the lowest received SNR was higher in the Australian winter.

Chapter 6 used PHaRLAP with IRI2016 to discover if a 3D propagation simulation could explain the reasons for the time propagation patterns seen in WSPR. The results showed that some of the patterns could be understood from the simulations. In particular, the interesting terminator related pattern between Australia/New Zealand and Europe is predicted by the simulations. However, the simulation did not explain the apparent asymmetry observed in Chapter 4.

It was noted that the simulation had limitations. PHaRLAP was used with an empirical model IRI2016 and was dependent on the ionospheric model and, of course, did not include any variable ionospheric events. IRI2016 with the PHaRLAP ray trace might not show very accurate absorption on a day-to-day variability basis, but it did show variation throughout the day as required here to make an estimation of the links. It was very useful to demonstrate the possible propagation paths that could exist.

Chapter 7 discussed possible explanations for the results that were found in the thesis and linked them together with the observations and simulations. The role of absorption was discussed in the context of explaining the propagation patterns that were found in this research. PHaRLAP and IRI2016 provided useful simulations that help to explain some of the propagation patterns. The availability of SNR in WSPR was a limitation as separate noise measurements were not available. This highlighted the need for more local noise measurements to be made. HF noise measurements are now being made routinely in Europe (Germany), and these will provide additional information to help explain patterns in HF communication links in the future. This leads to the first recommendation for future research equipment in this field – that the WSPR observations should routinely record the noise separately from the SNR.

The second recommendation for future research in this field is that the ionospheric model should include more real-time updated information that could be used on a global basis to replicate the instantaneous conditions. Examples of the information that could be useful would be updates on HF absorption, electron density from more instrumentation such as ionosondes and oblique HF signals, and using real-time reconstructed ionospheres instead of IRI, to check whether it could better reproduce what is found experimentally, when coupled with PHaRLAP.

The WSPR equipment is not designed to record separate ordinary and extraordinary rays through polarisation discrimination at reception and is not designed to record the direction of arrival of incoming signals. When trying to discover the directions of particular propagation paths, it would be advantageous to have at least some of the WSPR equipment (or other HF equipment running simultaneously) designed and upgraded to have this capability. Further, an accurate time delay record for investigating the propagation paths would potentially also be of use for distinguishing between alternative propagation paths.

Therefore, a third recommendation is to make these upgraded capabilities available to some of the WSPR equipment. The ability to take the globally distributed observations or WSPR and to combine them with a subset of sites that have the directional, polarisation and timing capability would be very useful for future scientific study.

This study only used a subset of WSPR data for one year at one frequency. The database contains WSPR data for other years at other frequencies. This could give a comparison of the time propagation patterns in this study with another subset of WSPR data for another year at the same frequency. In addition, comparing other subsets of WSPR data with other frequencies could give information about communication links through the ionosphere on a long-term basis.

There are other similar systems to WSPR, such as the Phase Shift Keying (PSK) reporter. The PSK Reporter collects observations like WSPR, which provides key parameters to study HF propagation, such as frequency, distance, signal strength, time etc.

Another useful system is the reverse beacon network. This is a receiver system for radio users to receive signals from radio transmitters such as beacons and report the received signals into the network giving the transmitters' callsigns, locations and signal reception. These other systems can be used in a similar way to the use of the WSPR described in this thesis.

Looking across the available HF radio link records that have arisen and are now available on a routine basis now it is clear that the advent of software radio has made a real change to the types and quantity of available observations. These types of instruments are often not set up for scientific grade study, and individual errors can occur and not be noticed, such as an incorrect location input to the database. Nevertheless, overall, they offer a huge amount of information about the ionosphere and about the propagation conditions. This research has shown that they can be used to provide new data that can be applied to answer questions about the statistical nature of propagation conditions. There is a huge amount of such data out there not yet analysed, and this work should provide encouragement for further amateur radio data to be used for scientific research.

References

Alsina-Pagès, R. *et al.* (2016) ‘Physical Layer Definition for a Long-Haul HF Antarctica to Spain Radio Link’, *Remote Sensing*. Multidisciplinary Digital Publishing Institute, 8(12), p. 380. doi: 10.3390/rs8050380.

Amateur Wireless and Electrics, Vol V. No. 126 (1924) ‘Bridging 12000 miles of space’.

Appleton, E. and Barnett, M. (1925) ‘Local Reflection of Wireless Waves from the Upper Atmosphere’. Available at: https://www.nature.com/articles/115333a0.pdf (Accessed: 31 August 2018).

Appleton, E. and Beynon, W. J. G. (1940) ‘The application of ionospheric data to radio-communications problems: part 1’, *Proceedings of the Physical Society*, 52(4). Available at: http://iopscience.iop.org/article/10.1088/0959-5309/52/4/311/pdf (Accessed: 31 August 2018).

Appleton, E. and Beynon W J G (1947) ‘The application of ionospheric data to radio communication problems: part II’, *Proceedings of the Physical Society*, 59(1). Available at: http://iopscience.iop.org/article/10.1088/0959-5309/59/1/311/pdf (Accessed: 31 August 2018).

Appleton, E. V. (1932) ‘Wireless studies of the ionosphere’, *Journal of the Institution of Electrical Engineers*, 71(430), pp. 642–650. doi: 10.1049/jiee-1.1932.0144.

Appleton, E. V (1925) ‘The Existence of more than one Ionised Layer in the Upper Atmosphere’. Available at: https://www.nature.com/articles/120330a0.pdf (Accessed: 31 August 2018).

Balan, Nanan, Liu, L. and Le, H. (2018) ‘A brief review of equatorial ionization anomaly and ionospheric irregularities’, *Earth and Planetary Physics*, 2, pp. 257–275. Available at: https://agupubs.onlinelibrary.wiley.com/doi/epdf/10.26464/epp2018025 (Accessed: 26 November 2020).

Balan, N., Liu, L. and Le, H. (2018) ‘A brief review of equatorial ionization anomaly and ionospheric irregularities’, *Earth and Planetary Physics*. Earth and Planetary Physics, 2(4), pp. 1–19. doi: 10.26464/epp2018025.

Barclay, L. and Bacon, D. (2013) ‘Radio Waves’, in Barclay, L. (ed.) *Propagation of Radiowaves*. 3rd edn. London: The Institution of Engineering and Technology, pp. 17–34.

Beynon, W. J. G. (1975) ‘Marconi, radio waves, and the ionosphere’, 10(7), pp. 657–664. Available at: http://users.df.uba.ar/dasso/curso_alta_atmosfera_cuat1_2012/beynon75_radio_science_sobre_marangoni_historia_descub_ionosfera.pdf (Accessed: 1 September 2018).

Bilitza, D. (2001) ‘International Reference Ionosphere 2000’, *Radio Science*, 36(2), pp. 261–275. Available at: http://irimodel.org/docs/iri_2000_rs.pdf (Accessed: 16 June 2021).

Bilitza, D. *et al.* (2014) ‘The International Reference Ionosphere 2012 – a model of international collaboration☆; The International Reference Ionosphere 2012 – a model of international collaboration☆’, *Space Weather Space Climate*, 4. doi: 10.1051/swsc/2014004.

Bilitza, D. *et al.* (2017) ‘International Reference Ionosphere 2016: From ionospheric climate to real-time weather predictions’, *Space Weather*, 15(2), pp. 418–429. doi: 10.1002/2016SW001593.

Bridgman, R. (2001) ‘Guglielmo Marconi: radio star’, *Phys. World*, 14(12), p. 29. Available at: http://iopscience.iop.org.ezproxy1.bath.ac.uk/article/10.1088/2058-7058/14/12/30/pdf (Accessed: 1 September 2018).

Bruce Paige, K. (2000) *Maidenhead Grid Squares*. AMSAT. Available at: http://www.amsat.org/amsat/articles/houston-net/grids.html (Accessed: 11 September 2019).

Bust, G. S., Liles, W. and Mitchell, C. (2021) ‘Space Weather Influences on HF, UHF, and VHF Radio Propagation’, in Coster et al., A. J. (ed.) *Space Physics and Aeronomy, V5, Space Weather Effects and Applications*. AGU Monograph, pp. 153–164.

Callaway, E. (2016) ‘Gray Line Propagation, or Florida to Cocos (Keeling) on 80 m’.

Carrara, N., De Giorgio, M. T. and Pellegrini, P. F. (1970) ‘Guided propagation of HF radio waves in the ionosphere’, *Space Science Reviews*, 11(4), pp. 555–592. doi: 10.1007/BF00183029.

Cervera, M. A. and Harris, T. J. (2014) ‘Modeling ionospheric disturbance features in quasi-vertically incident ionograms using 3-D magnetoionic ray tracing and atmospheric gravity waves’, *Journal of Geophysical Research: Space Physics*. John Wiley & Sons, Ltd, 119(1), pp. 431–440. doi: 10.1002/2013JA019247.

Chamberlain, J. W. (1978) *Theory of Planetary Atmospheres: An Introduction*. New York: Academic Press.

Chapman, S. (1931) ‘The absorption and dissociative or ionizing effect of monochromatic radiation in an atmosphere on a rotating earth part 11. Grazing incidence’, *Proceedings of the Physical Society*, 43(483–501). Available at: http://iopscience.iop.org/article/10.1088/0959-5309/43/5/302/pdf (Accessed: 31 August 2018).

Chulliat, Arnaud *et al.* (2015) ‘The US/UK World Magnetic Model for’. doi: 10.7289/V5TB14V7

Coleman, C. J. (1997) ‘On the simulation of backscatter ionograms’, *Journal of Atmospheric and Solar-Terrestrial Physics*. Pergamon, 59(16), pp. 2089–2099. doi: 10.1016/S1364-6826(97)00038-2.

Davies, K. (1965) *Ionospheric radio propagation*. US Department of Commerce, National Bureau of Standards. doi: 10.6028/NBS.MONO.80.

Davies, K. (2008) *Ionospheric Radio*. 2nd edn. Edited by P. Clarricoats, Y. Rahmat-Samii, and J. Wait. London: The Institution of Engineering and Technology.

Eccles, W. H. (1912) *On the Diurnal Variations of the Electric Waves Occurring in Nature, and the Propagation of Electric Waves Round the Bend of the Earth*. Available at: http://rspa.royalsocietypublishing.org/ (Accessed: 3 September 2018).

Eichel, K. *et al.* (2021) *ENAMS @ Deutscher Amateur-Radio-Club e.V.* Available at: http://enams.de/index.php (Accessed: 17 June 2021).

Fenwick, R. B. (1963) *Round-the-World High-Frequency Propagation, TR. 71, Radioscience Lab, Stanford University*.

Folke Rosvall, S. (2019) ‘The Locator System’, *jonit.com*. Available at: http://www.jonit.com/fieldlist/maidenhead.htm (Accessed: 11 September 2019).

François Beauducel (2019) *SUNRISE: sunrise and sunset times*, *MATLAB Central File Exchange*. Available at: https://uk.mathworks.com/matlabcentral/fileexchange/64692-sunrise-sunrise-and-sunset-times (Accessed: 21 May 2019).

Frissell, N. A. *et al.* (2014) ‘Ionospheric Sounding Using Real-Time Amateur Radio Reporting Networks’, *Space Weather*, 12, pp. 651–656. doi: 10.1002/2014SW001132.

Frissell, N. A. *et al.* (2019) ‘High Frequency Communications Response to Solar Activity in September 2017 as Observed by Amateur Radio Networks’, *Space Weather*. doi: 10.1029/2018SW002008.

Gilmor, C. (1976) ‘The history of the term “ionosphere”’, *Nature*, 262. Available at: http://www.nature.com.ezproxy1.bath.ac.uk/articles/262347a0.pdf (Accessed: 1 September 2018).

Gurevich, A. V. and Tsedilina, E. E. (1985) ‘Introduction - Long Distance Propagation of HF Radio Waves’, in Lanzerotti, L. J. and Hill, M. (eds) *Long Distance Propagation of HF Radio Waves*. Springer-Verlag, pp. 1–25.

HamSCI. Available at: https://hamsci.org/ (Accessed: 23 June 2021).

Hargreaves, J. (1979) ‘Basic Physical Principles’, in *The Upper Atmosphere and Solar-Terrestrial Relations*. New York: Van Nostrand Reinhold Co. Ltd, pp. 5–24.

Hargreaves, J. K. (1992) *The Solar Terrestrial Environment*, *Cambridge Atmospheric and Space Science Series*. Cambridge University Press.

Hargreaves, J. K. and Hunsucker, R. D. (2003) ‘Basic principles of the ionosphere’, in *The high-latitude ionosphere and its effects on radio propagation*, pp. 1–60. Available at: https://pdfs.semanticscholar.org/3b2b/62abd1abdd0972b7d5a9c98e7b39d9980f9c.pdf (Accessed: 11 September 2019).

Harrison, R. (2007a) *Afternoon Transequatorial VHF Propagation* . Available at: http://home.iprimus.com.au/toddemslie/aTEP-Harrison.htm (Accessed: 3 May 2021).

Harrison, R. (2007b) *Evening transequatorial V.H.F. propagation*. Available at: http://home.iprimus.com.au/toddemslie/eTEP-Harrison.htm (Accessed: 3 May 2021).

Harrison, R. L. (1972a) ‘V.H.F. Transequatorial Propagation’, *Amateur Radio (Aust.)*, 40(6), pp. 6–7. Available at: https://worldradiohistory.com/AUSTRALIA/Amateur-Radio/Amateur-Radio-AU-1972.pdf.

Harrison, R. L. (1972b) ‘V.H.F. Transequatorial Propagation’, *Amateur Radio (Aust.)*, 40(5), pp. 3–8. Available at: https://worldradiohistory.com/AUSTRALIA/Amateur-Radio/Amateur-Radio-AU-1972.pdf.

Haselgrove, J. (1955) ‘The physics of the ionosphere’, *The Physical Society*, p. 355.

Heaviside, O. (1902) ‘Telegraphy’, *Encyclopaedia Britannica IX*, 33, p. 215.

Heitmann, A. J. *et al.* (2018) ‘Observations and Modeling of Traveling Ionospheric Disturbance Signatures From an Australian Network of Oblique Angle-of-Arrival Sounders’, *Radio Science*, 53(9), pp. 1089–1107. doi: 10.1029/2018RS006613.

Hoppe, D. (1975) ‘The Grayline Method of Dxing’, *CQ*, p. 27.

Hulburt, E. (1927) ‘Ionisation in the Upper Atmosphere’, *Nature*, 120. Available at: http://www.nature.com.ezproxy1.bath.ac.uk/articles/120187a0.pdf (Accessed: 2 September 2018).

Isted, G. (1991) ‘Guglilemo Marconi and the History of Radio - Part II’, *GEC Review*, 7(2). Available at: http://www.trevorwright.com/GEC/Journals/GEC_Review/v7n2/p110.pdf (Accessed: 1 September 2018).

Jones, T. B. and Reynolds, J. S. B. (1975) ‘Ionospheric perturbations and their effect on the accuracy of HF direction finders’, *Radio and Electronic Engineer*, 45(1–2), pp. 63–73.

Karhu Koti LLC (2019) *RF70bw Maidenhead Grid Square - KarhuKoti*. Available at: https://www.karhukoti.com/maidenhead-grid-square-locator/?grid=RF70bw (Accessed: 11 September 2019).

Karia, S. P. *et al.* (2019) ‘A study on Nighttime Winter Anomaly (NWA) and other related Mid-latitude Summer Nighttime Anomaly (MSNA) in the light of International Reference Ionosphere (IRI) – Model’, *Advances in Space Research*. Elsevier Ltd, 63(6), pp. 1949–1960. doi: 10.1016/j.asr.2018.11.021.

Kelleher, R. F. and Röttger, J. (1973) ‘Equatorial spread F irregularities observed at Nairobi and on the transequatorial path Lindau-Tsumeb’, *Journal of Atmospheric and Solar-Terrestrial Physics*, 35, pp. 1207–1211.

Kennelly, A. (1902) ‘On the elevation of the electrically strata of the earth’s atmosphere’, *Elec. World Eng.*, 39(473).

Kurkin, V. I. *et al.* (2000) ‘The features of round-the-world signal propagation over the paths of the russian chirp-sounder network during low and mild solar activity’, *Radiophysics and Quantum Electronics*, 43(10).

Larmor, J. (1924) ‘Why Wireless Electric Rays can bend round the Earth’, *Nature*, 1(1). Available at: https://www.nature.com/articles/114650a0.pdf (Accessed: 3 September 2018).

Malik, R. A. *et al.* (2015) ‘The influence of sunspot number on high frequency radio propagation’, *2014 IEEE Asia-Pacific Conference on Applied Electromagnetics, APACE 2014 - Proceeding*, pp. 107–110. doi: 10.1109/APACE.2014.7043753.

Marconi, S. G. (1922) ‘Radio Telegraphy’, *America Institute of Electrical Engineers*. The American Institute of Electrical Engineers, 8, pp. 561–570. doi: 10.1109/JRPROC.1962.288215.

McNamara, L. F. (1991) *The Ionosphere: Communications, Surveillance, and Direction Finding*.

McNamara, L. F. *et al.* (2008) ‘Nighttime above-the-MUF HF propagation on a midlatitude circuit’, *Radio Science*, 43(2), pp. 1–8. doi: 10.1029/2007RS003742.

Mohler, F. L. (1940) *Recombination and electron attachment in the F layers of the ionosphere.* Available at: https://nvlpubs.nist.gov/nistpubs/jres/25/jresv25n5p507_A1b.pdf (Accessed: 1 September 2018).

Moser-T’, M., Ezque, R. and Jadu, C. (2000) ‘On the critical frequency and height of the e layer peak at noon’, *Adv. Space Rrs*, 75(I), pp. 9–72. Available at: www.elsevier.nl/locate/asr (Accessed: 22 January 2019).

Nichols, S. G. (2002) *Greyline Propagation*. Available at: http://www.norfolkamateurradio.org/Talks/G0KYA Greyline_Propagation.pdf (Accessed: 18 January 2019).

Nichols, S. G. (2005) *The Twilight Zone revisited-recent grey-line research (July 2005)*. Available at: http://oh2aq.kolumbus.com/dxs/. (Accessed: 18 January 2019).

Oryema, B. *et al.* (2015) ‘Investigation of TEC variations over the magnetic equatorial and equatorial anomaly regions of the African sector’, *Advances in Space Research*. Elsevier Ltd, 56(9), pp. 1939–1950. doi: 10.1016/j.asr.2015.05.037.

Pederick, L. H. and Cervera, M. A. (2014) ‘Semiempirical model for ionospheric absorption based on the NRLMSISE-00 atmospheric model’, *Radio Science*. American Geophysical Union, 49(2), pp. 81–93. doi: 10.1002/2013RS005274.

Pederick, L. H. and Cervera, M. A. (2016) ‘Modeling the interference environment in the HF band’, *Radio Science*. John Wiley & Sons, Ltd, 51(2), pp. 82–90. doi: 10.1002/2015RS005856.

Piggott, W. R. (1957) *The measurement of ionospheric absorption*. London: Pergamon.

QRZ. Available at: https://www.qrz.com/ (Accessed: 24 June 2021).

Quaeck, E. (1927) ‘Propagation of short waves around the earth’, *Proceedings of the Institute of Radio Engineers*, 15(4), pp. 341–345.

Radio Society of Great Britain (2014) *International Prefixes - Radio Society of Great Britain - Main Site : Radio Society of Great Britain – Main Site*. Available at: https://rsgb.org/main/operating/licensing-novs-visitors/international-prefixes/ (Accessed: 8 October 2019).

Rishbeth, H. (1967) ‘A review of F region dynamics’, *Proceedings of the IEEE*, 55(1), pp. 16–35. doi: 10.1029/RG013i003p00887.

Rishbeth, H. (1988) ‘Basic physics of the ionosphere: a tutorial review’, *Journal of the Institution of Electronic and Radio Engineers*, 58(6S), p. S207. doi: 10.1049/jiere.1988.0060.

Rishbeth, H. and Garriott, O. K. (1969a) *Introduction to Ionospheric Physics*. New York: Academic Press.

Rishbeth, H. and Garriott, O. K. (1969b) ‘Morphology of the Ionosphere’, in *Introduction to Ionospheric Physics*. New York: Academic Press, pp. 160–189.

Rumi, G. C. (1975) ‘Around-the-world propagation’, *Radio Science*, 10(7), pp. 711–718. doi: 10.1029/RS010i007p00711.

S Chapman (1931) ‘The absorption and dissociative or ionizing effect of monochromatic radiation in an atmosphere on a rotating earth Recent citations NRLMSIS 2.0: A WholeAtmosphere Empirical Model of Temperature and Neutral Species Densities’, *Proceedings of the Physical Society*, 43, p. 26.

Saito, S., Yamamoto, M. and Maruyama, T. (2018) ‘Arrival Angle and Travel Time Measurements of HF Transequatorial Propagation for Plasma Bubble Monitoring’, *Radio Science*. Blackwell Publishing Ltd, 53(11), pp. 1304–1315. doi: 10.1029/2017RS006518.

Stocker, A. J., Warrington, E. M. and Siddle, D. R. (2013) 'Observations of Doppler and delay spreads on HF signals received over polar cap and trough paths at various stages of the solar cycle', *Radio Science*. John Wiley & Sons, Ltd, 48(5), pp. 638–645. doi: 10.1002/2013RS005264.

Symonds, E. J. *et al.* (1924) 'Bridging 12000 miles of space', *Amateur Wireless*, p. 642.

Talbot, A. (2009) *WSPR Coding Process*. Available at: http://www.g4jnt.com/Coding/WSPR_Coding_Process.pdf (Accessed: 29 October 2019).

Taylor, J. (2019) *WSJT Home Page*. Available at: https://physics.princeton.edu/pulsar/k1jt/wspr.html (Accessed: 17 May 2019).

Tilton, E. P. (1947) 'The World above 50 Mc', *QST*, pp. 54–56.

Tilton, E. P. (1957) 'The World Above 50 Mc: What is a contact?', *QST*, p. 55.

Tsunoda, R. T. *et al.* (2016) 'Off-great-circle paths in transequatorial propagation: 2. Nonmagnetic-field-aligned reflections', *Journal of Geophysical Research: Space Physics*. Blackwell Publishing Ltd, 121(11), pp. 11,176-11,190. doi: 10.1002/2016JA022404.

Vilella, C., Miralles, D. and Pijoan, J. L. (2008) 'An Antarctica-to-Spain HF ionospheric radio link: Sounding results', *Radio Science*, 43(4), p. n/a-n/a. doi: 10.1029/2007RS003812.

World Magnetic Model | *NCEI* (2019). Available at: https://www.ngdc.noaa.gov/geomag/WMM/DoDWMM.shtml (Accessed: 15 April 2021).

WSPRnet. Available at: https://wsprnet.org/drupal/ (Accessed: 24 June 2021).

Yadav, S. *et al.* (2009) 'Diurnal and seasonal variation of F2-layer ionospheric parameters at equatorial ionization anomaly crest region and their comparison with IRI-2001', *Advances in Space Research*, 45, pp. 361–367. doi: 10.1016/j.asr.2009.08.018.

Appendix A – Transmitter and receiver activity for WSPR

This appendix shows a number of active WSPR transmitters and receivers in different regions of the world throughout the year 2017 for the frequency 7 MHz.

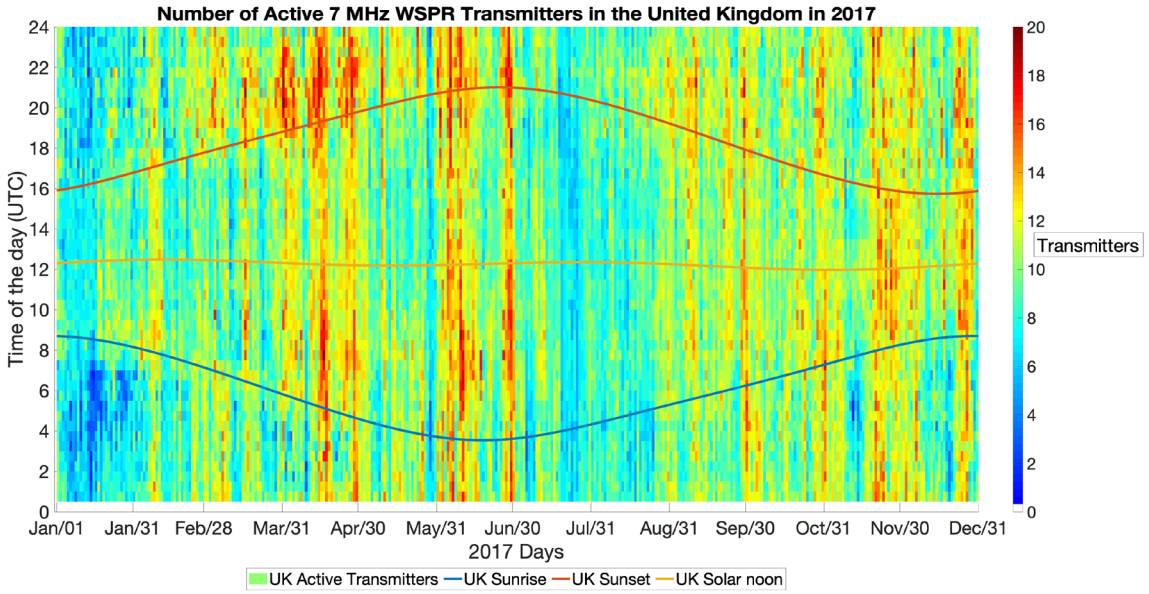

Figure A.1 – Number of active UK WSPR transmitters in 2017. Only transmitters with a proven capability to cover the distance from the UK to New Zealand are shown. The colours indicate the number of transmitters available in each half hour interval

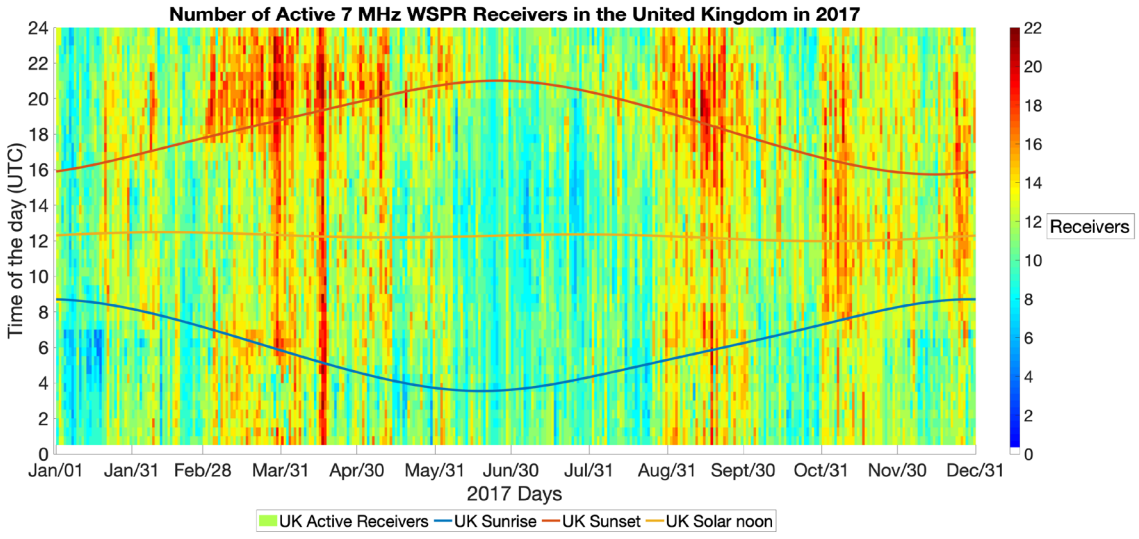

Figure A.2 – Number of active UK WSPR receivers in 2017. Only receivers with a proven capability to cover the distance from New Zealand to the UK are shown. The colours indicate the number of receivers available in each half hour interval

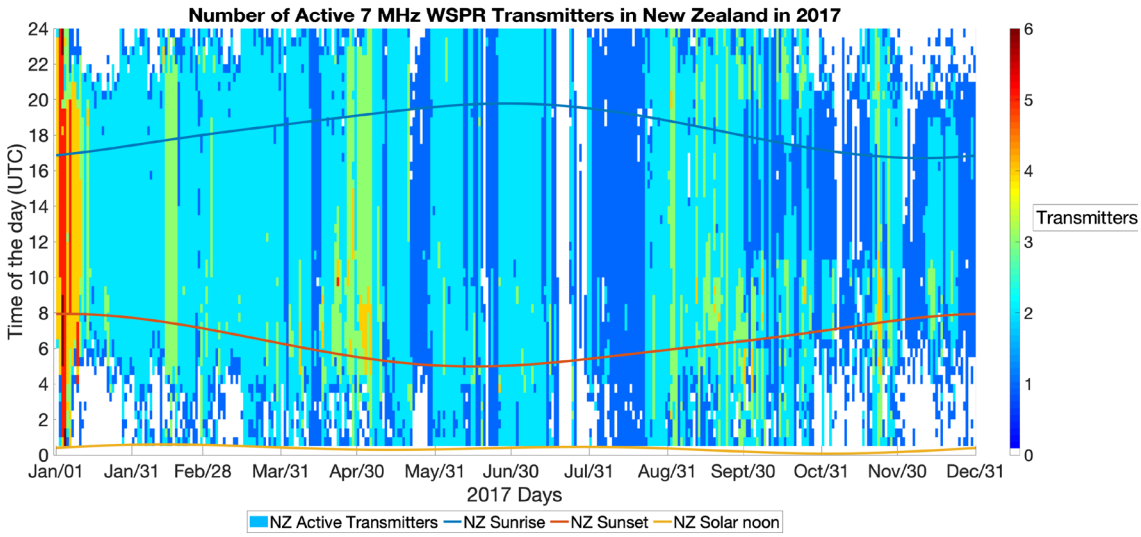

Figure A.3 – Number of active New Zealand WSPR transmitters in 2017. Only transmitters with a proven capability to cover the distance from New Zealand to the UK are shown. The colours indicate the number of transmitters available in each half hour interval.

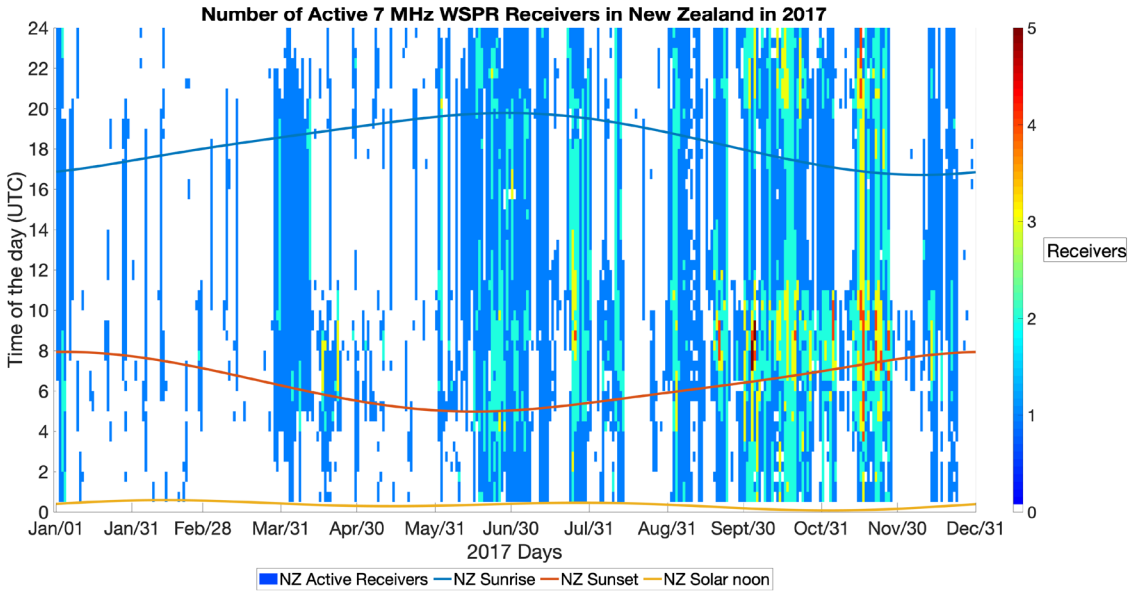

Figure A.4 – Number of active New Zealand WSPR receivers in 2017. Only receivers with a proven capability to cover the distance from the UK to New Zealand are shown. The colours indicate the number of receivers available in each half hour interval.

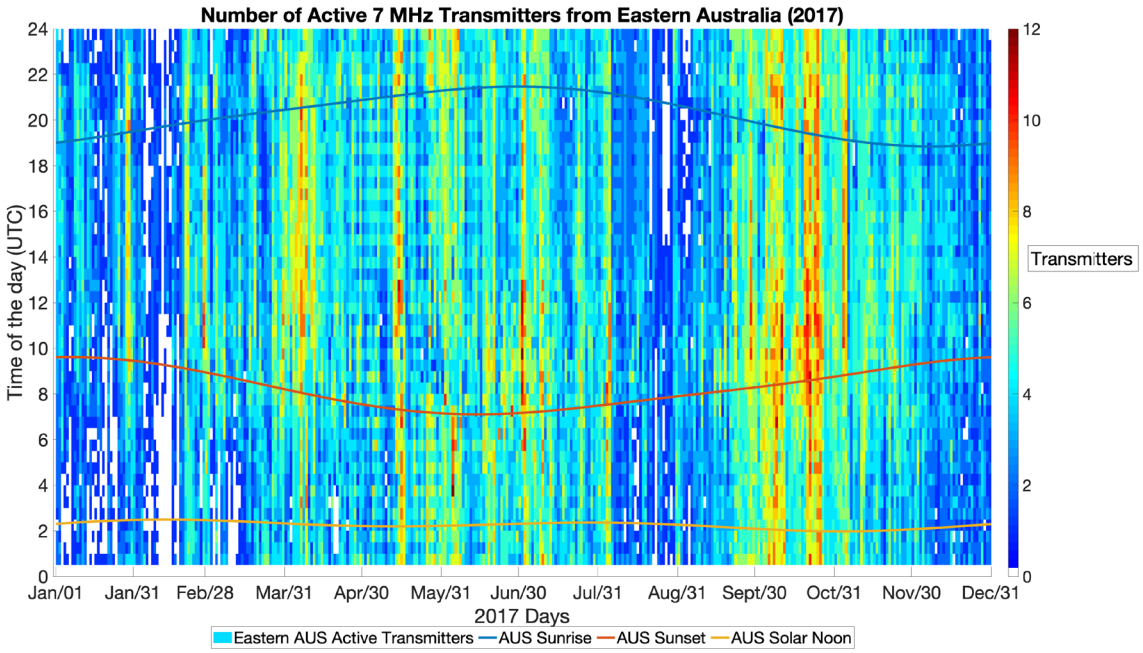

Figure A.5 – Number of active Eastern Australia WSPR transmitters in 2017. Only transmitters with a proven capability to cover the distance from Eastern Australia to the UK are shown. The colours indicate the number of transmitters available in each half hour interval.

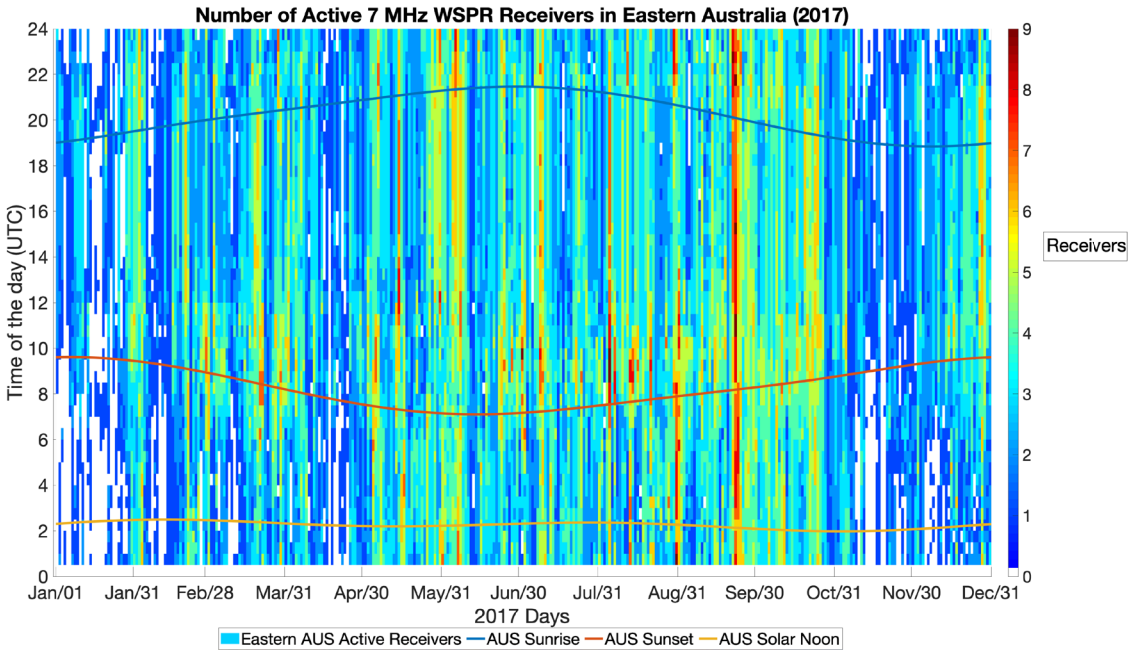

Figure A.6 – Number of active Eastern Australia WSPR receivers in 2017. Only receivers with a proven capability to cover the distance from the UK to Eastern Australia are shown. The colours indicate the number of receivers available in each half hour interval.

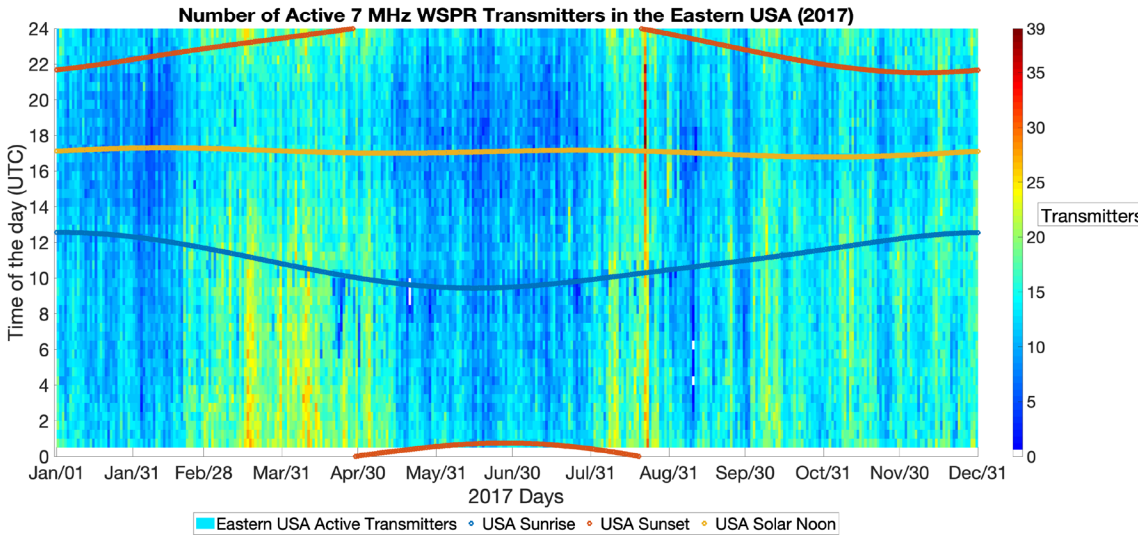

Figure A.7 – Number of active Eastern USA WSPR transmitters in 2017. Only transmitters with a proven capability to cover the distance from the Eastern USA to the UK are shown. The colours indicate the number of transmitters available in each half hour interval.

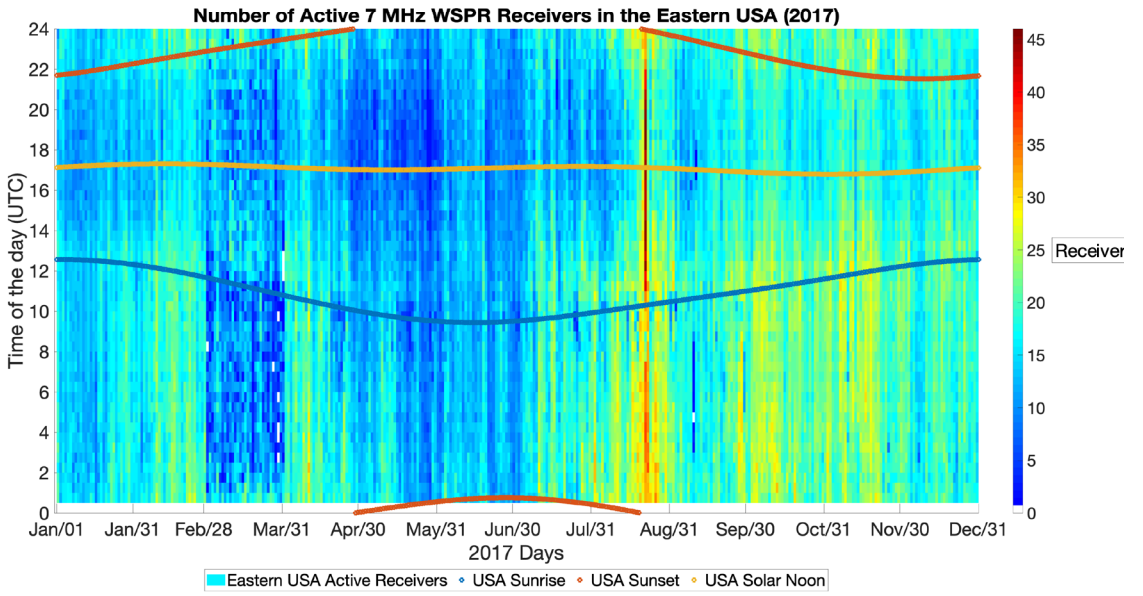

Figure A.8 – Number of active Eastern USA WSPR receivers in 2017. Only receivers with a proven capability to cover the distance from the UK to the Eastern USA are shown. The colours indicate the number of receivers available in each half hour interval

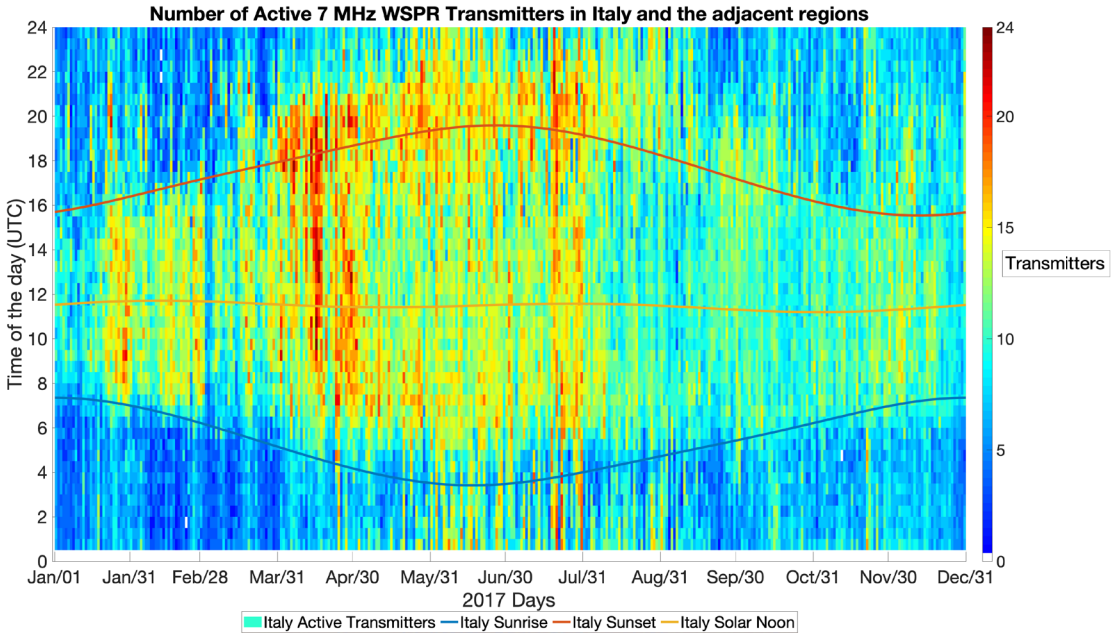

Figure A.9 – Number of active Italy and the adjacent regions WSPR transmitters in 2017. Only transmitters with a proven capability to cover the distance from Italy and the adjacent regions to New Zealand are shown. The colours indicate the number of transmitters available in each half hour interval

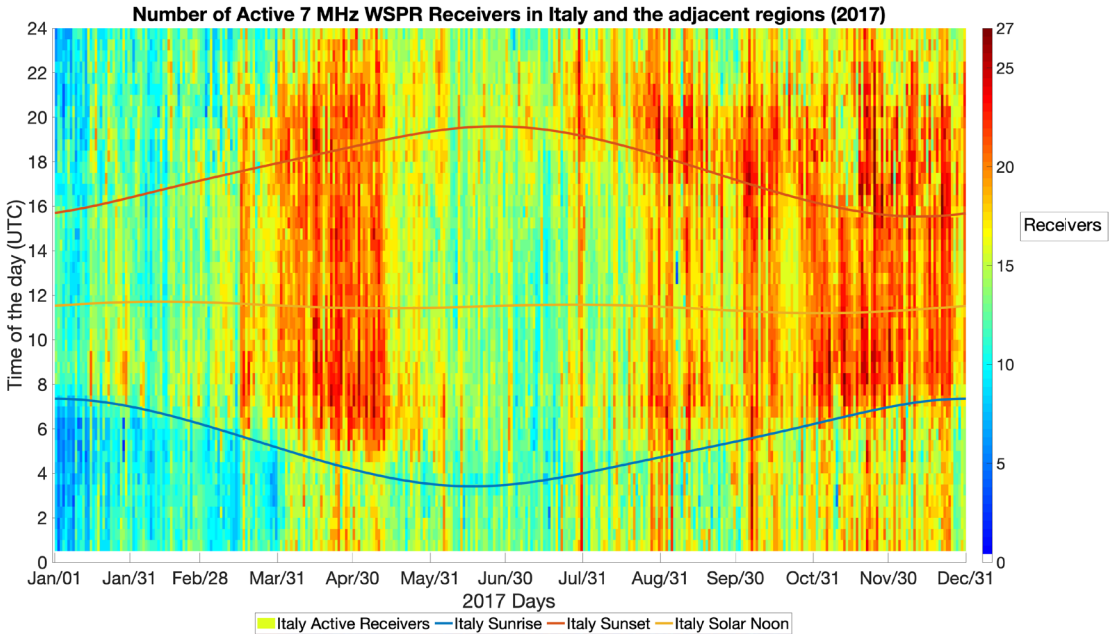

Figure A.10 – Number of active Italy and the adjacent regions WSPR receivers in 2017. Only receivers with a proven capability to cover the distance from Italy and the adjacent regions to New Zealand are shown. The colours indicate the number of receivers available in each half hour interval

Appendix B – Time series of propagation from WSPR and PHaRLAP

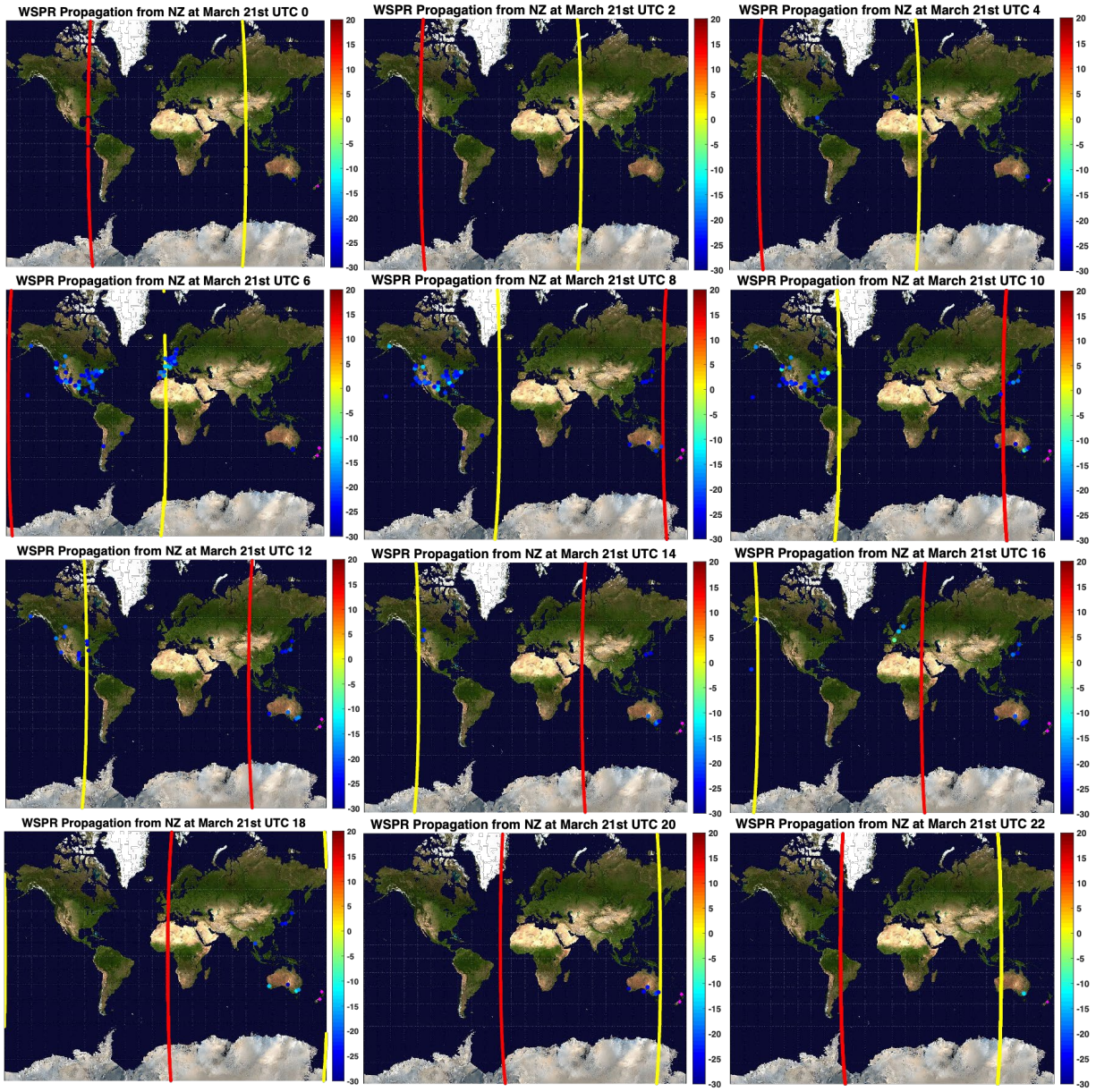

Figure B.1 – Images showing the ground reception locations of WSPR signals transmitted from New Zealand on March 21st 2017. The colours show the SNR in dB.

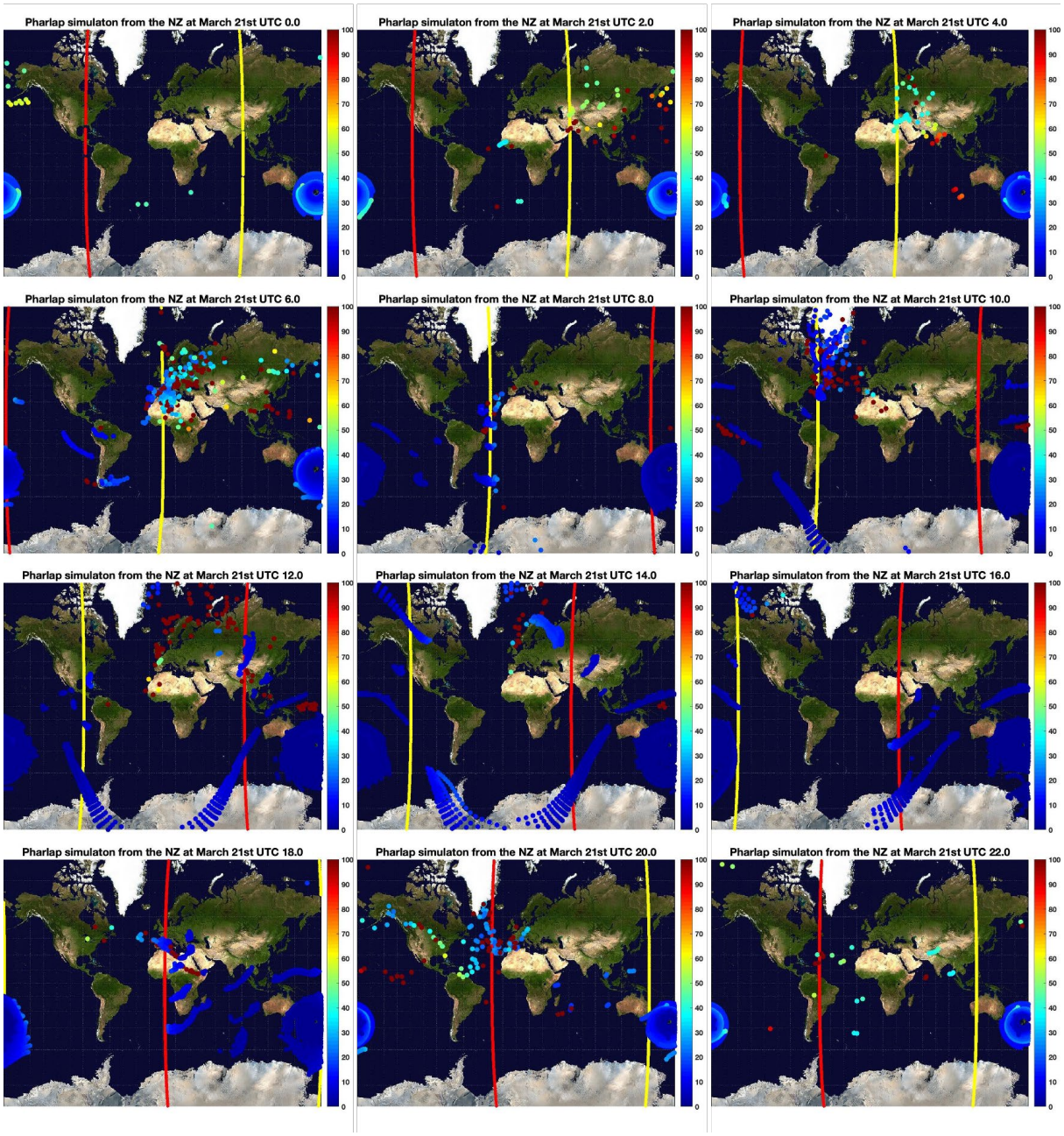

Figure B.2 – Images showing the ground reception locations simulated by PHaRLAP/IRI2016 for a transmitter in New Zealand for March 21st 2017. The colours show the absorption in dB.

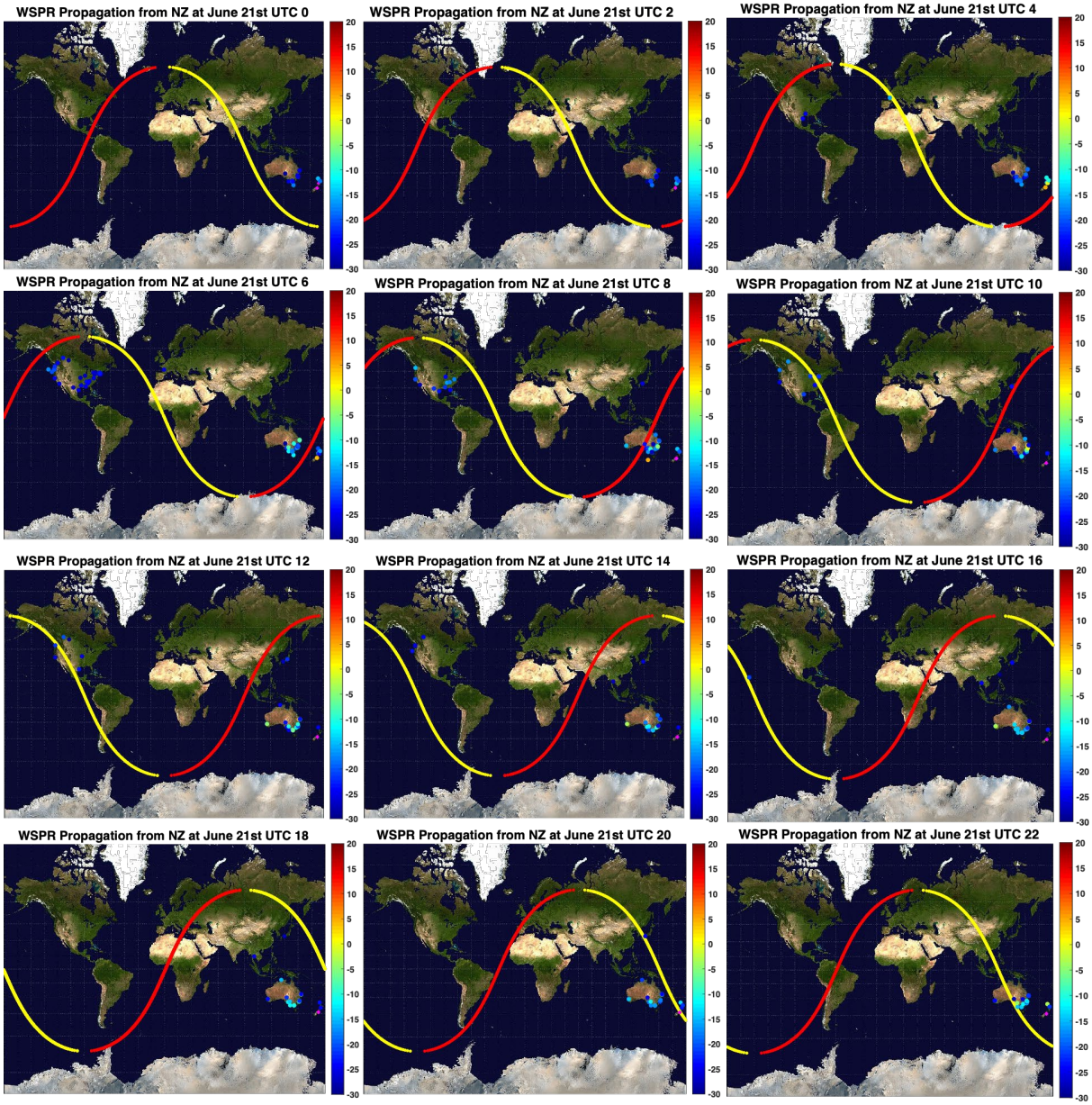

Figure B.3 – Images showing the ground reception locations of WSPR signals transmitted from New Zealand on June 21st 2017. The colours show the SNR in dB.

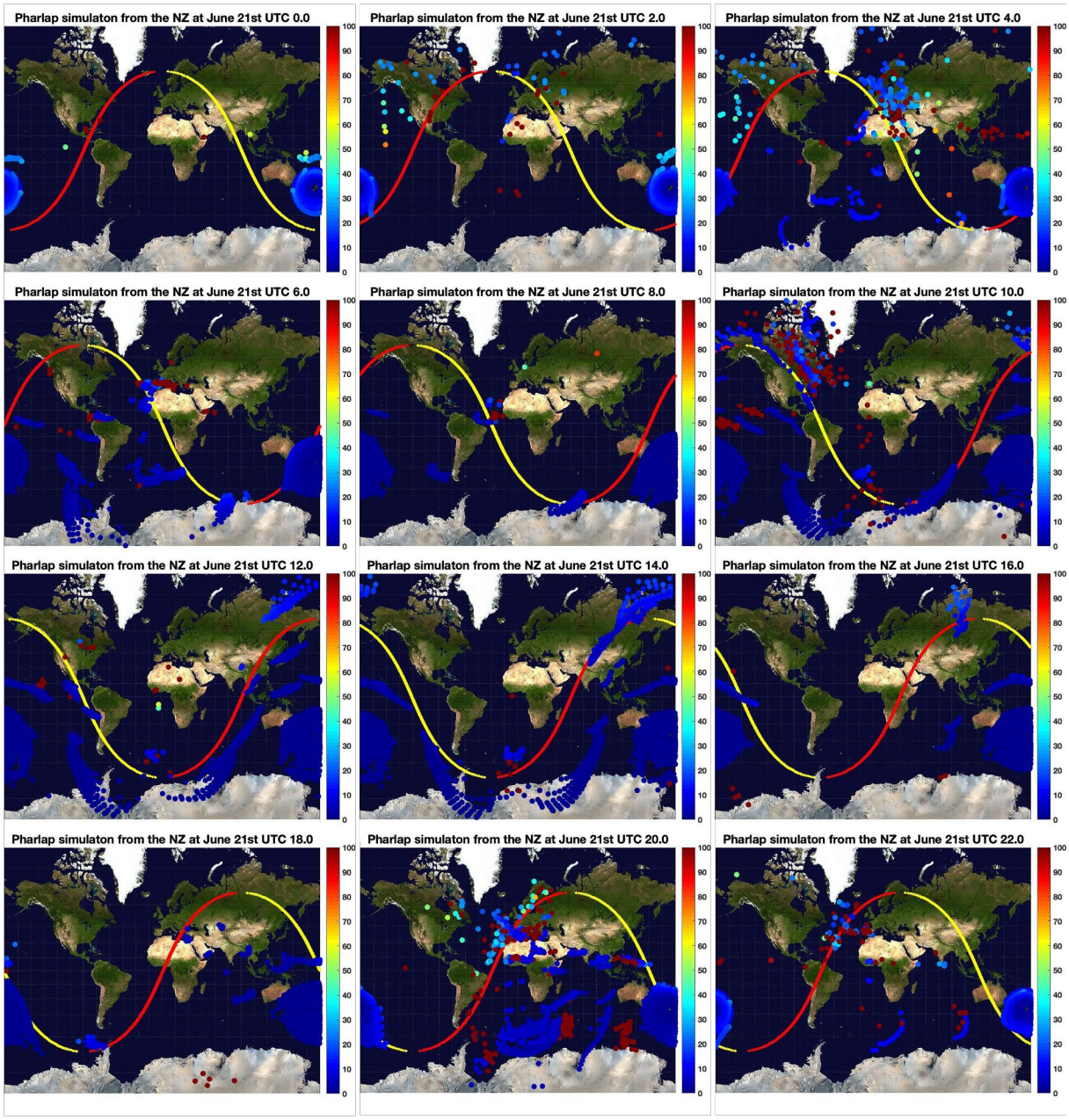

Figure B.4 – Images showing the ground reception locations simulated by PHaRLAP/IRI2016 for a transmitter in New Zealand for June 21st 2017. The colours show the absorption in dB.

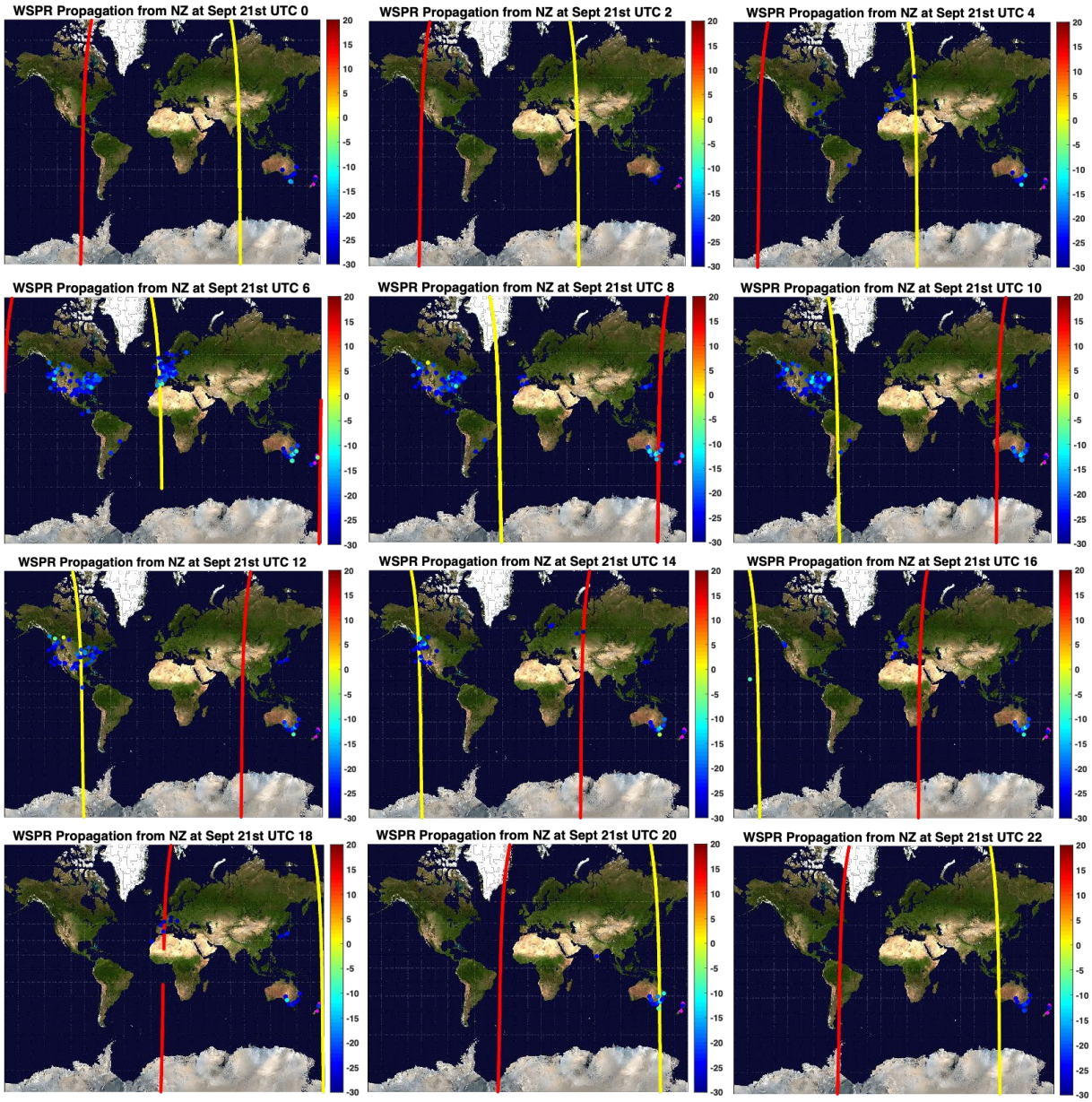

Figure B.5 – Images showing the ground reception locations of WSPR signals transmitted from New Zealand on September 21st 2017. The colours show the SNR in dB.

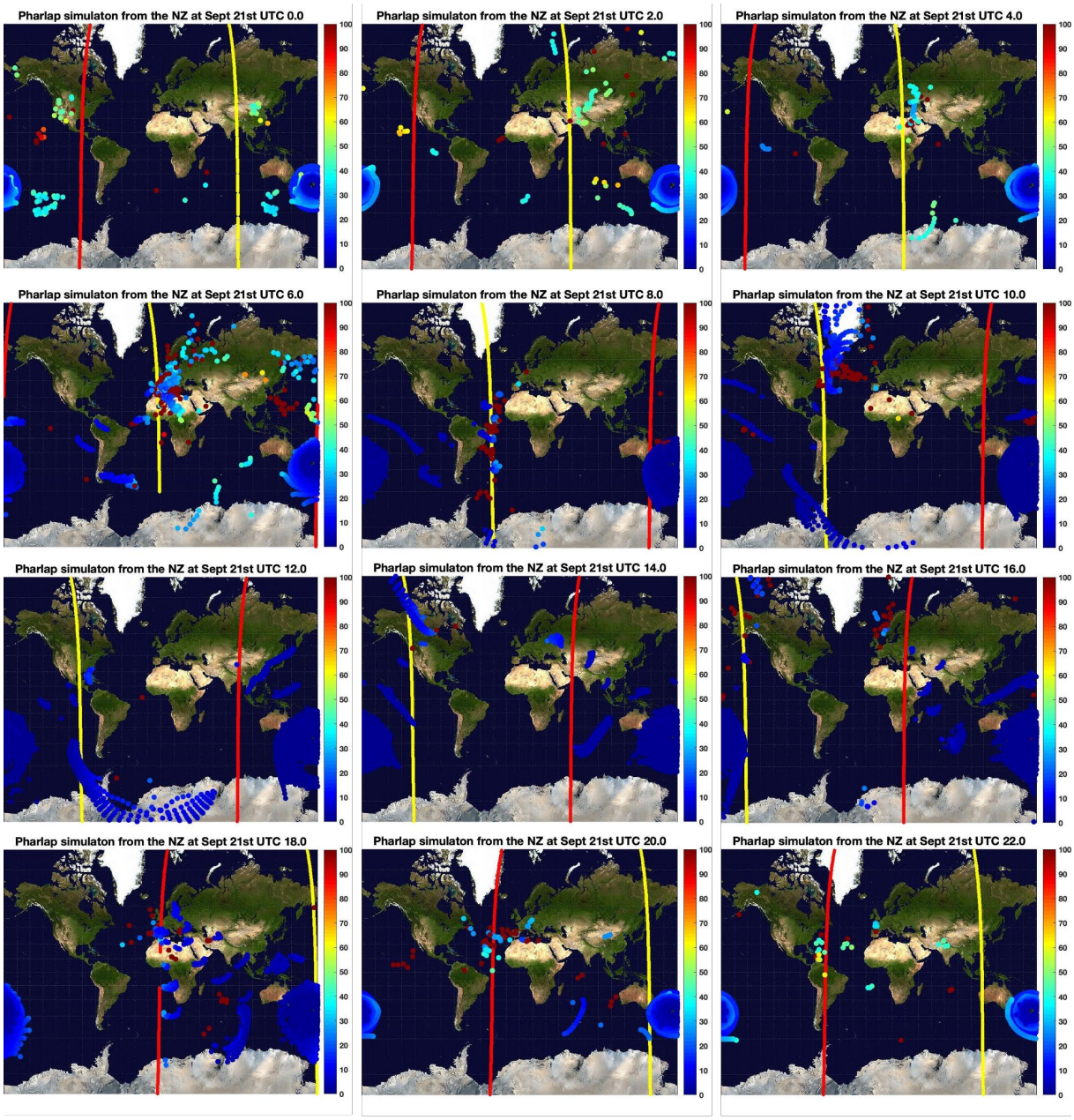

Figure B.6 – Images showing the ground reception locations simulated by PHaRLAP/IRI2016 for a transmitter in New Zealand for September 21st 2017. The colours show the absorption in dB.

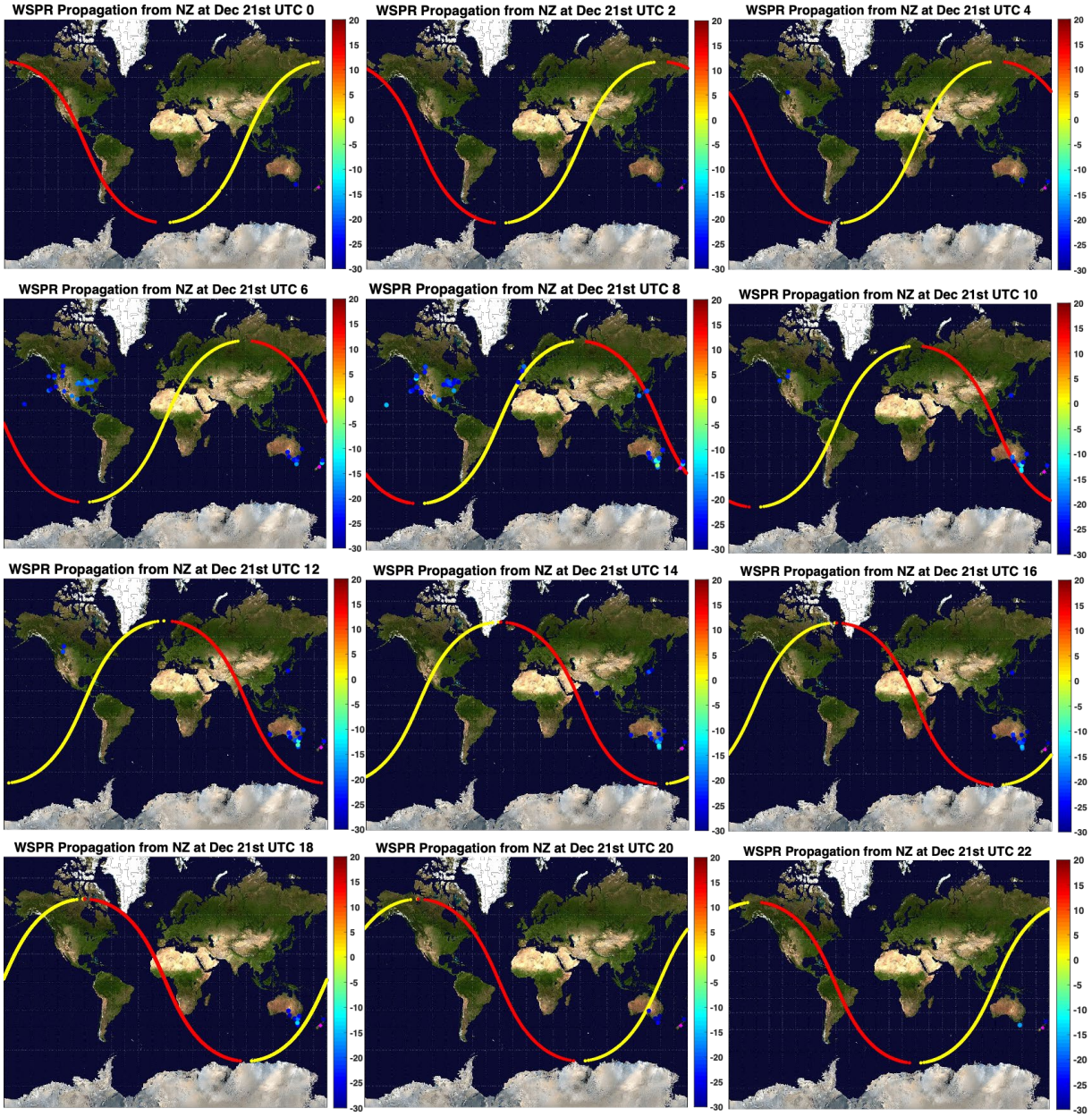

Figure B.7 – Images showing the ground reception locations of WSPR signals transmitted from New Zealand on December 21st 2017. The colours show the SNR in dB.

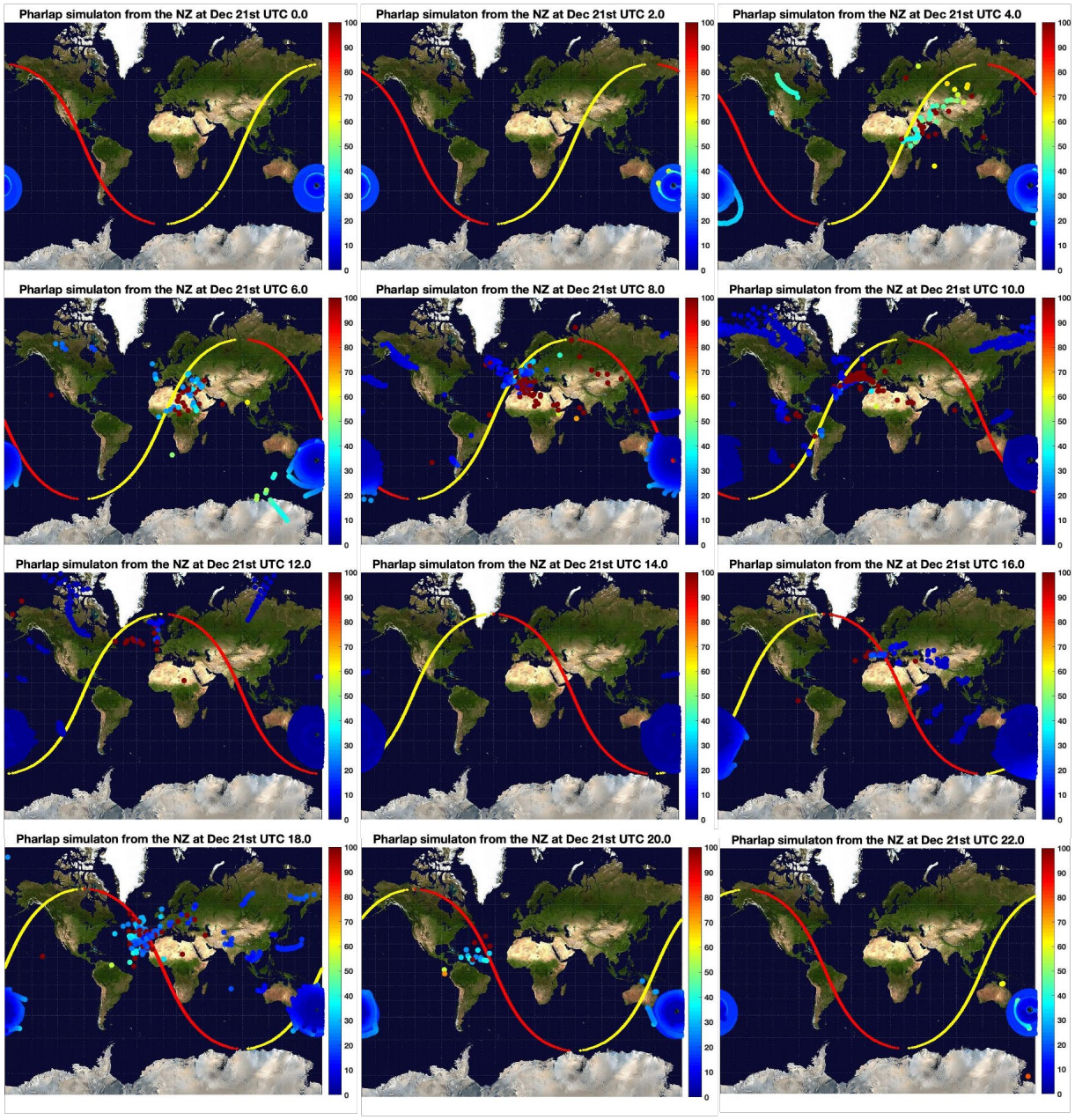

Figure B.8 – Images showing the ground reception locations simulated by PHaRLAP/IRI2016 for a transmitter in New Zealand for December 21st 2017. The colours show the absorption in dB.

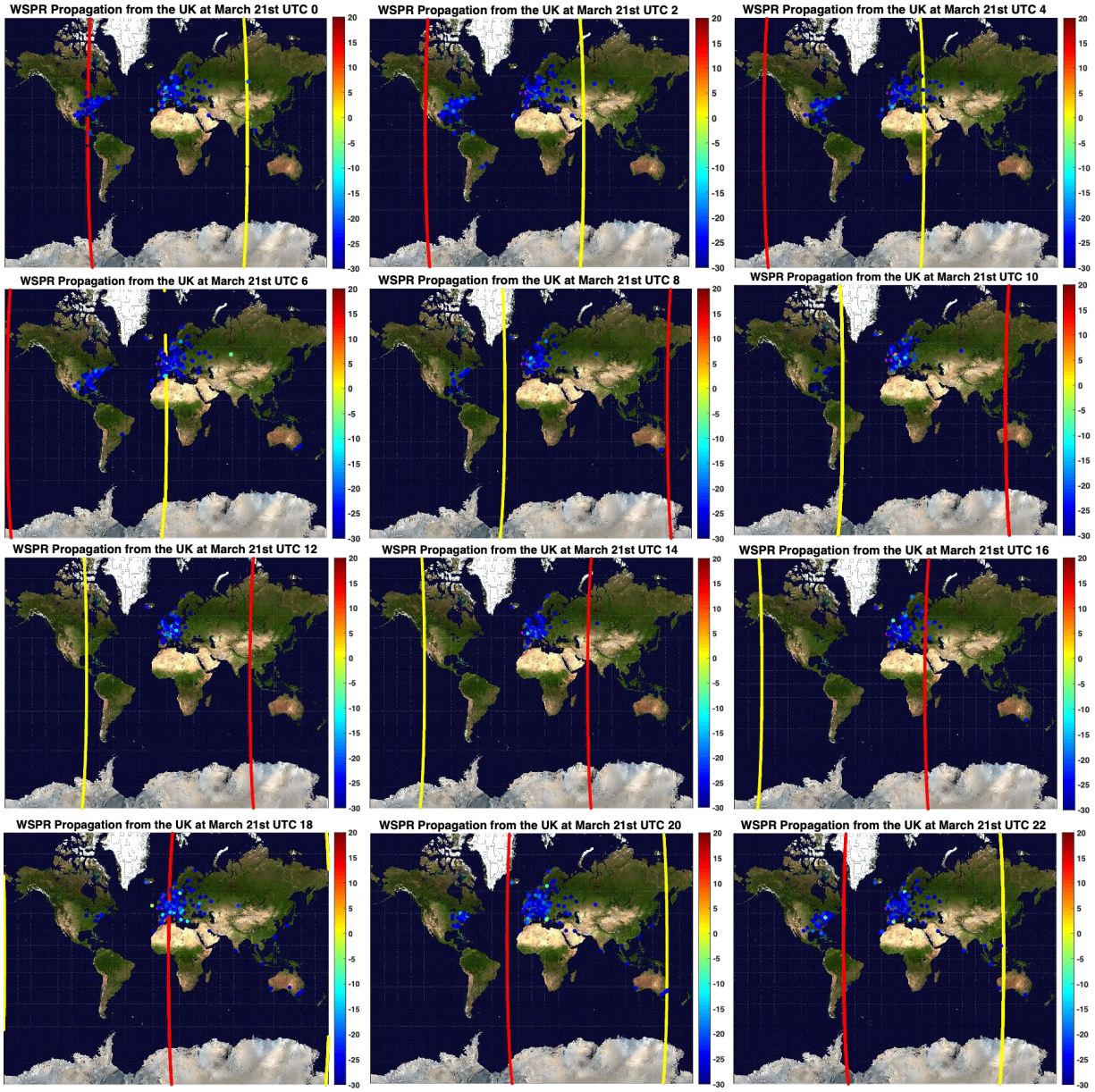

Figure B.9 – Images showing the ground reception locations of WSPR signals transmitted from the UK on March 21st 2017. The colours show the SNR in dB.

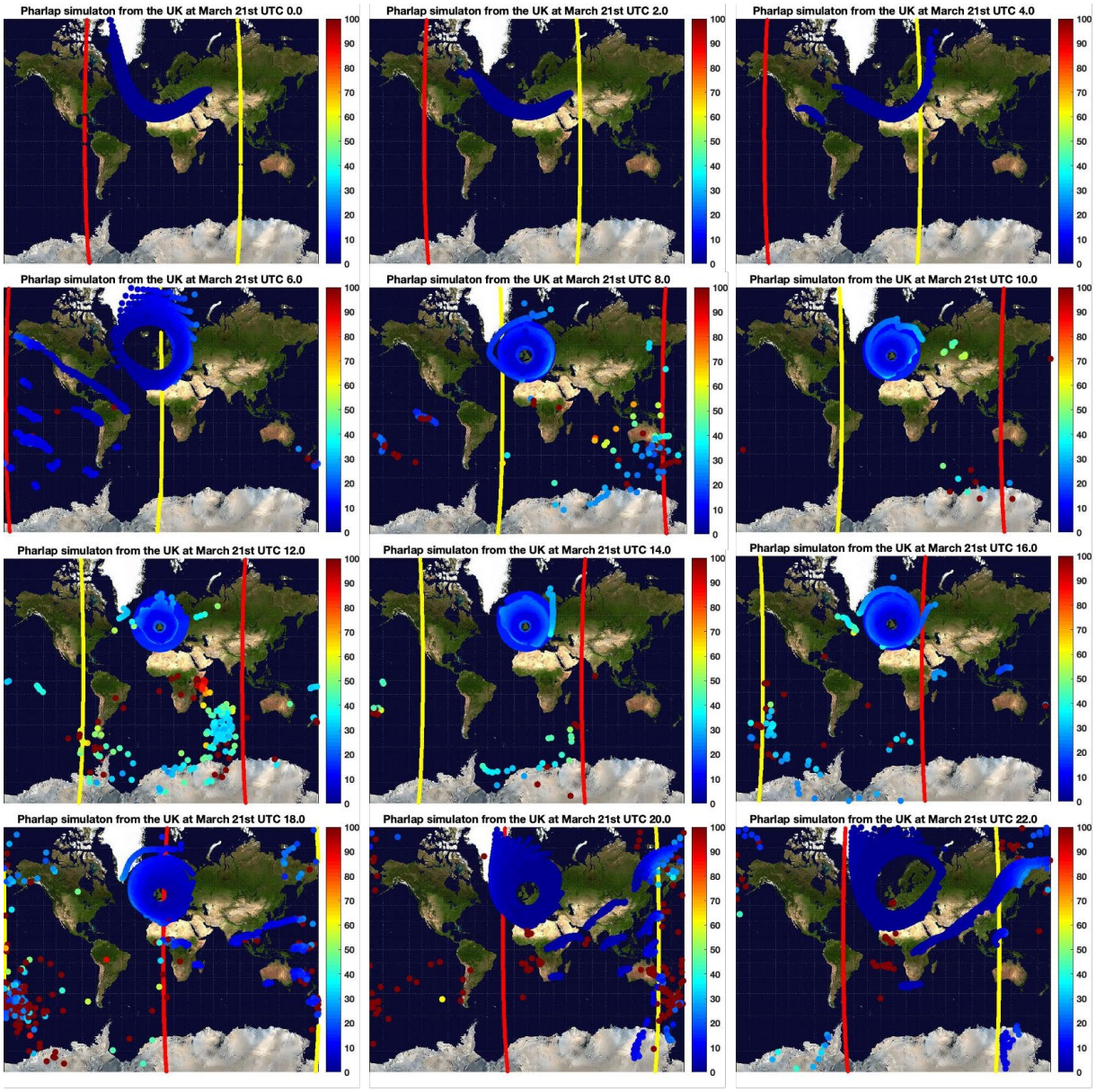

Figure B.10 – Images showing the ground reception locations simulated by PHaRLAP/IRI2016 for a transmitter in the UK for March 21st 2017. The colours show the absorption in dB.

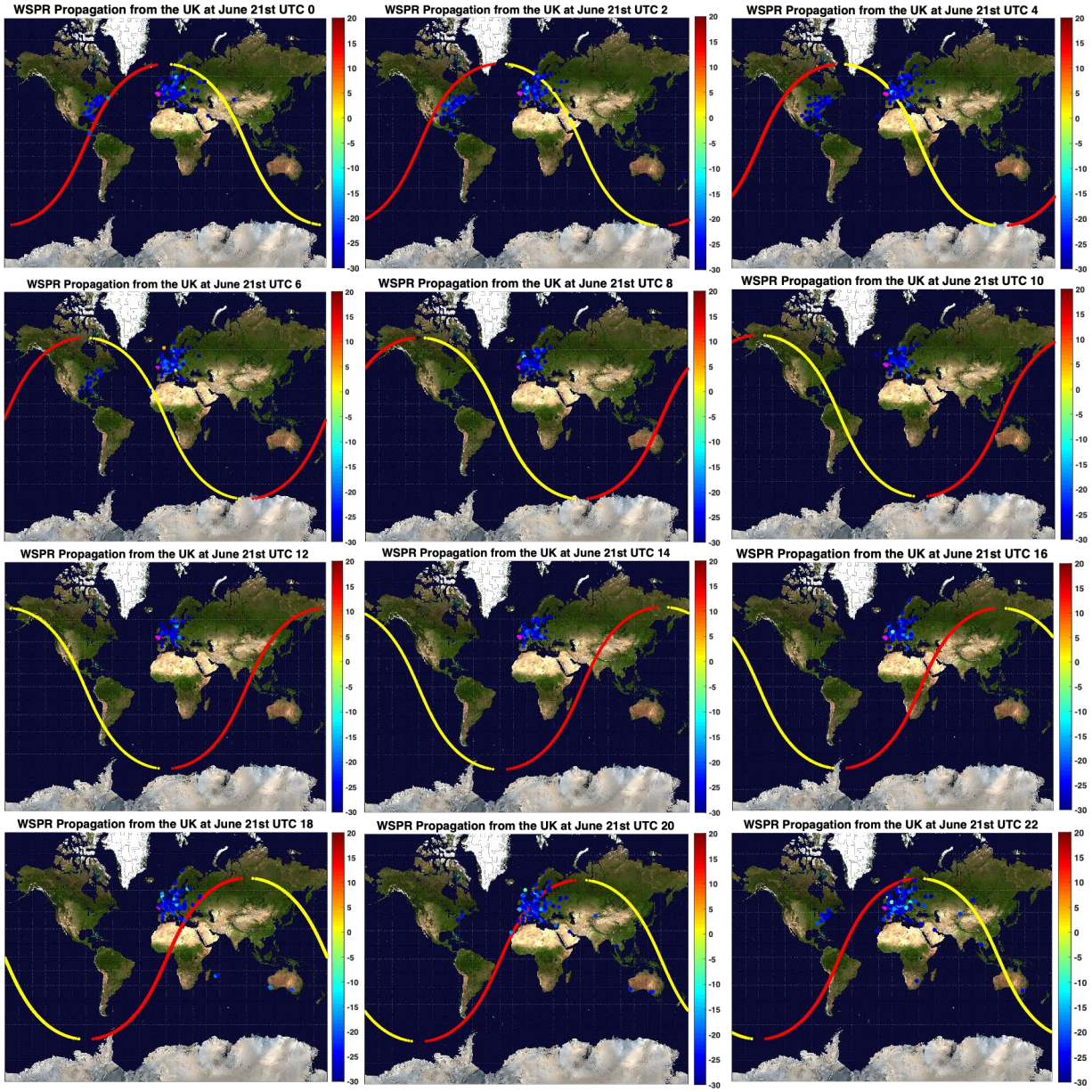

Figure B.11 – Images showing the ground reception locations of WSPR signals transmitted from the UK on June 21st 2017. The colours show the SNR in dB.

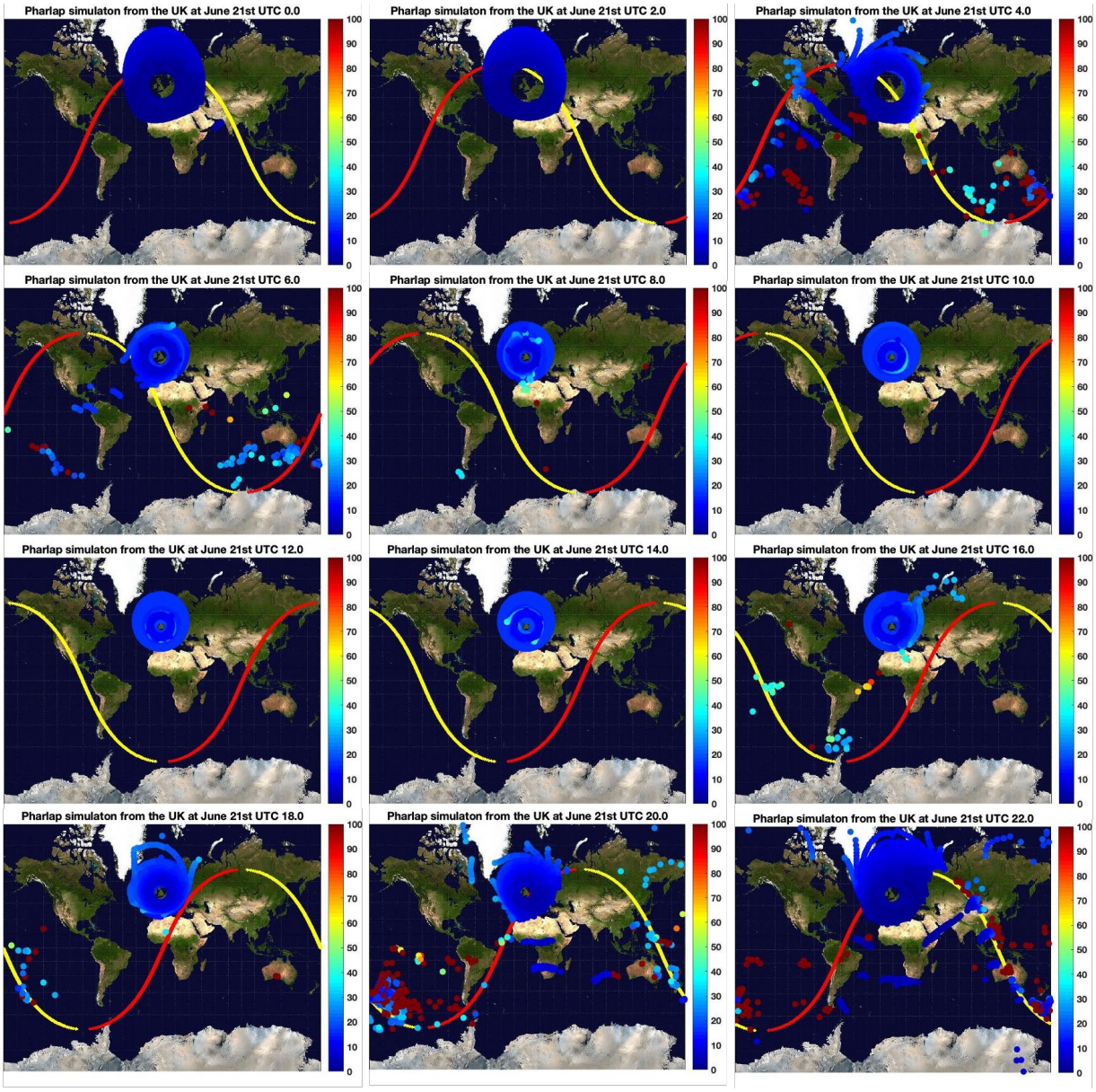

Figure B.12 – Images showing the ground reception locations simulated by PHaRLAP/IRI2016 for a transmitter in the UK for June 21st 2017. The colours show the absorption in dB.

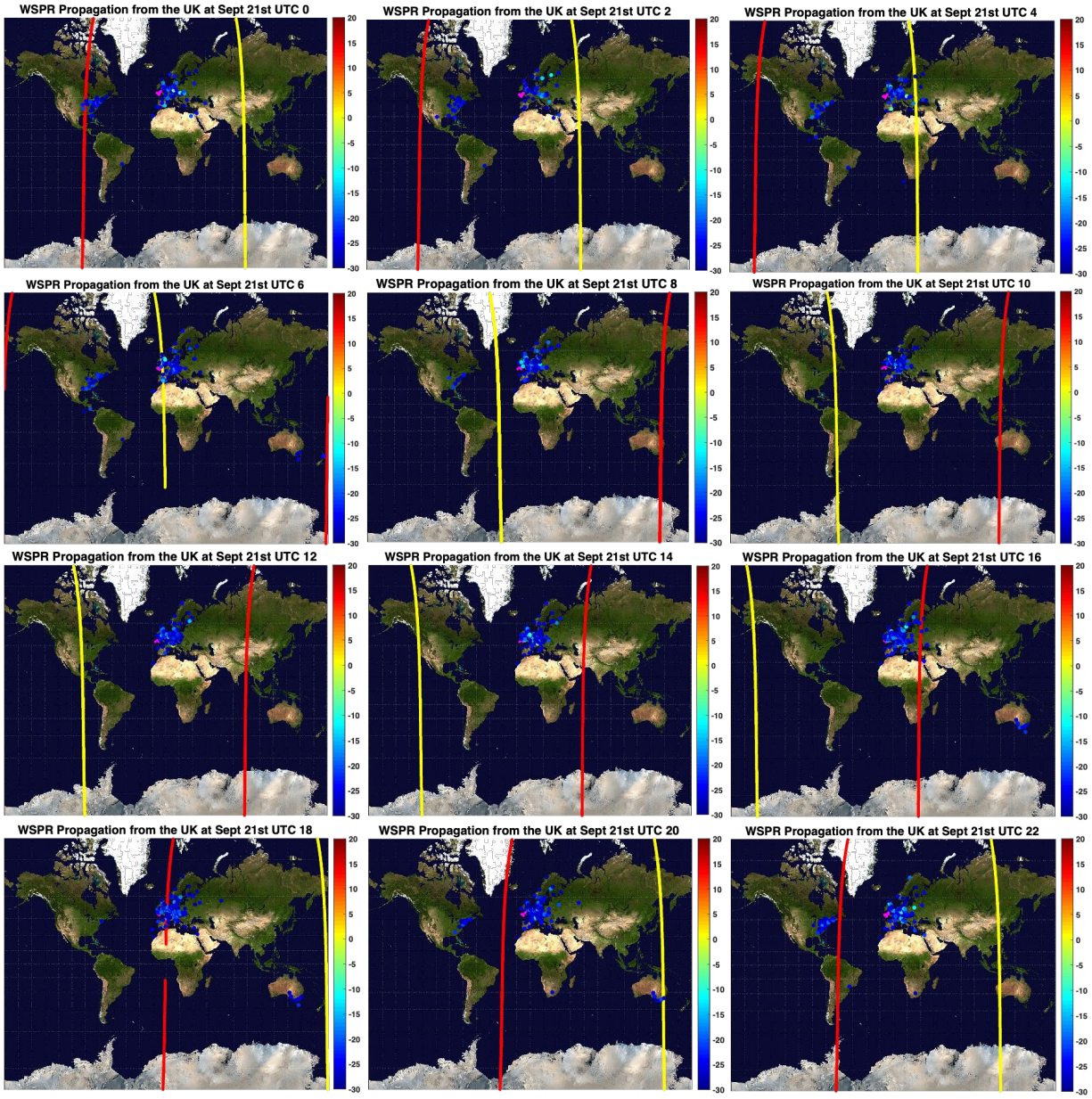

Figure B.13 – Images showing the ground reception locations of WSPR signals transmitted from the UK on September 21st 2017. The colours show the SNR in dB.

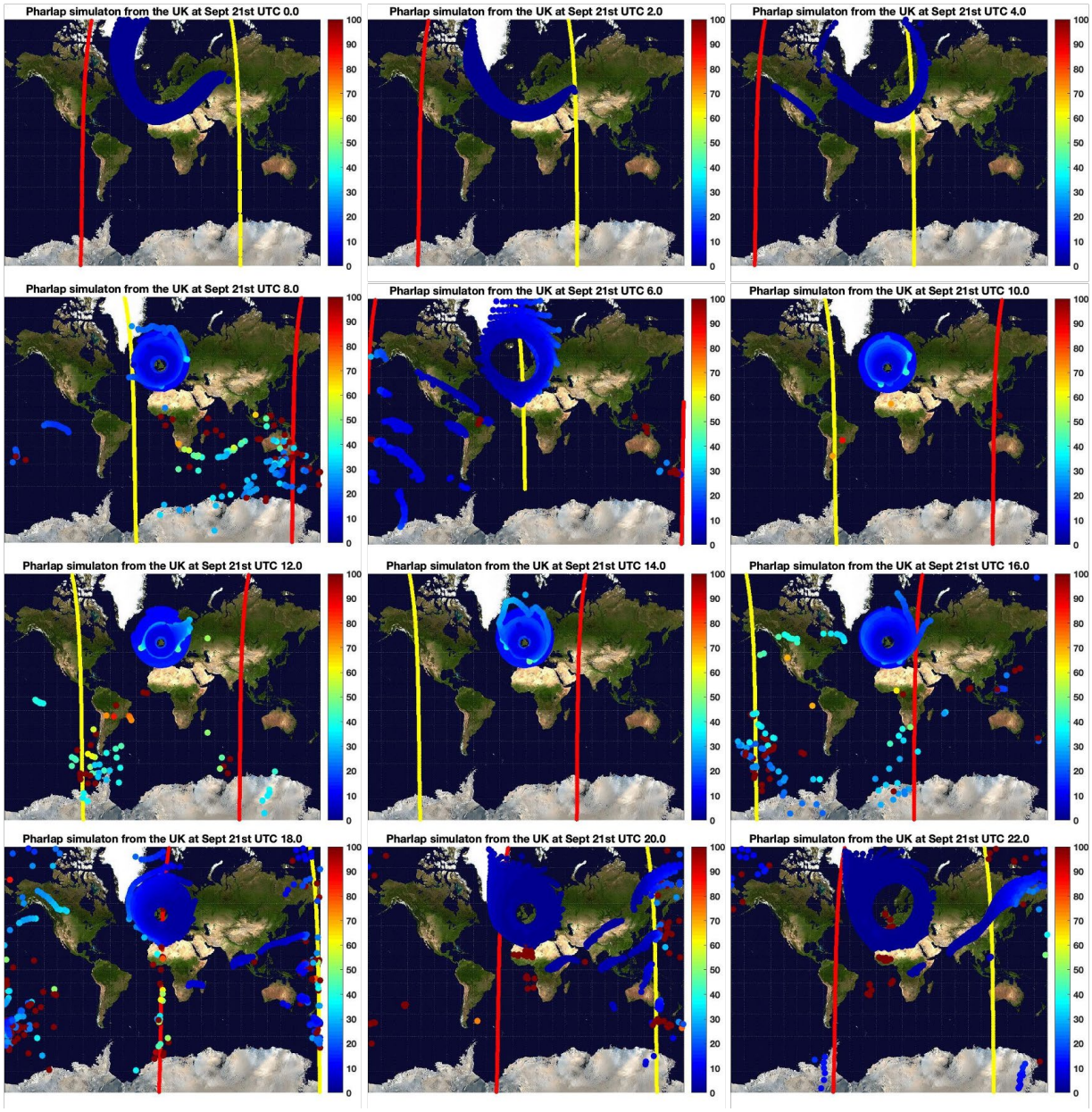

Figure B.14 – Images showing the ground reception locations simulated by PHaRLAP/IRI2016 for a transmitter in the UK for September 21st 2017. The colours show the absorption in dB.

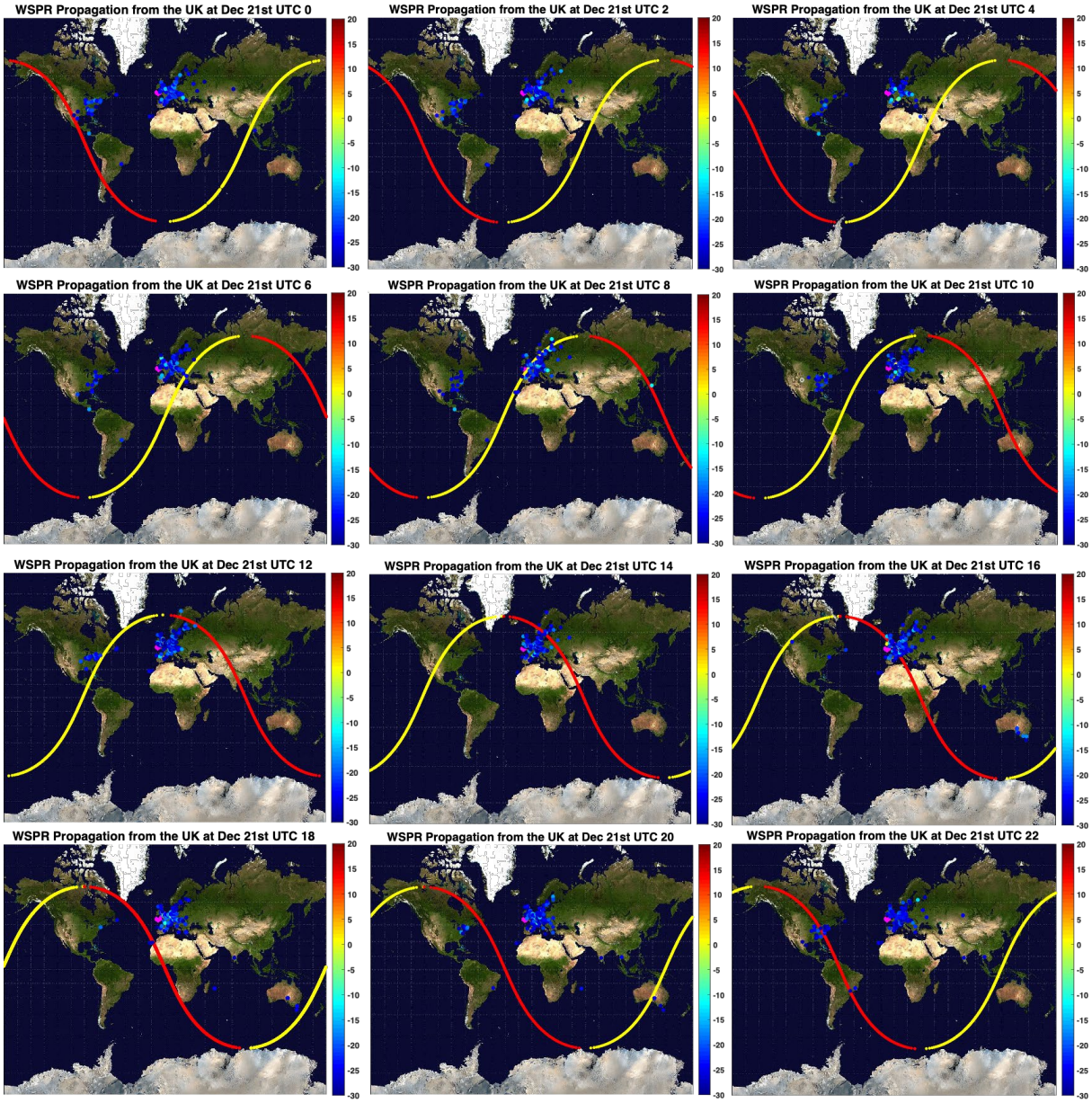

Figure B.15 – Images showing the ground reception locations of WSPR signals transmitted from the UK on December 21st 2017. The colours show the SNR in dB.

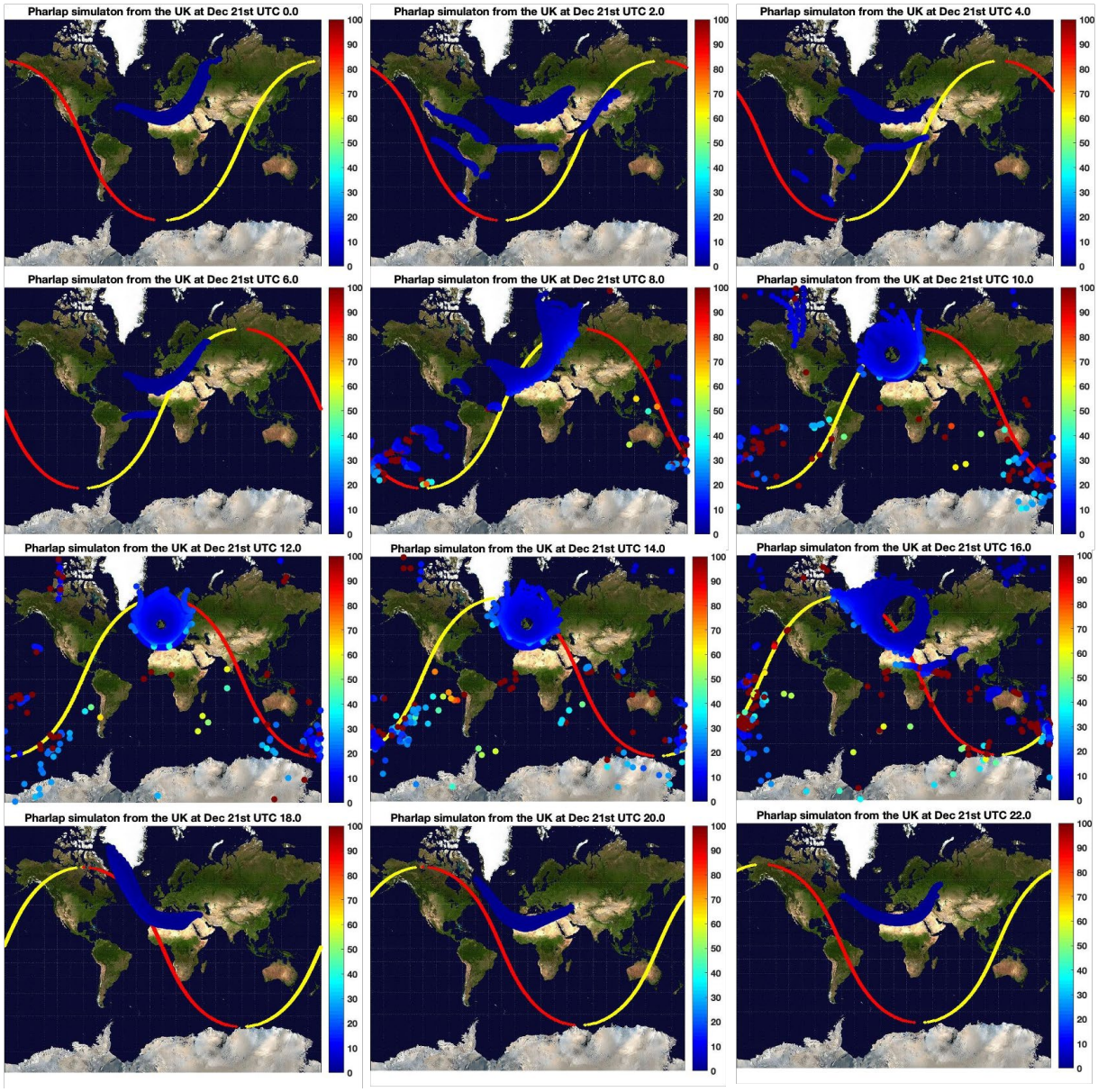

Figure B.16 – Images showing the ground reception locations simulated by PHaRLAP/IRI2016 for a transmitter in the UK for December 21st 2017. The colours show the absorption in dB.

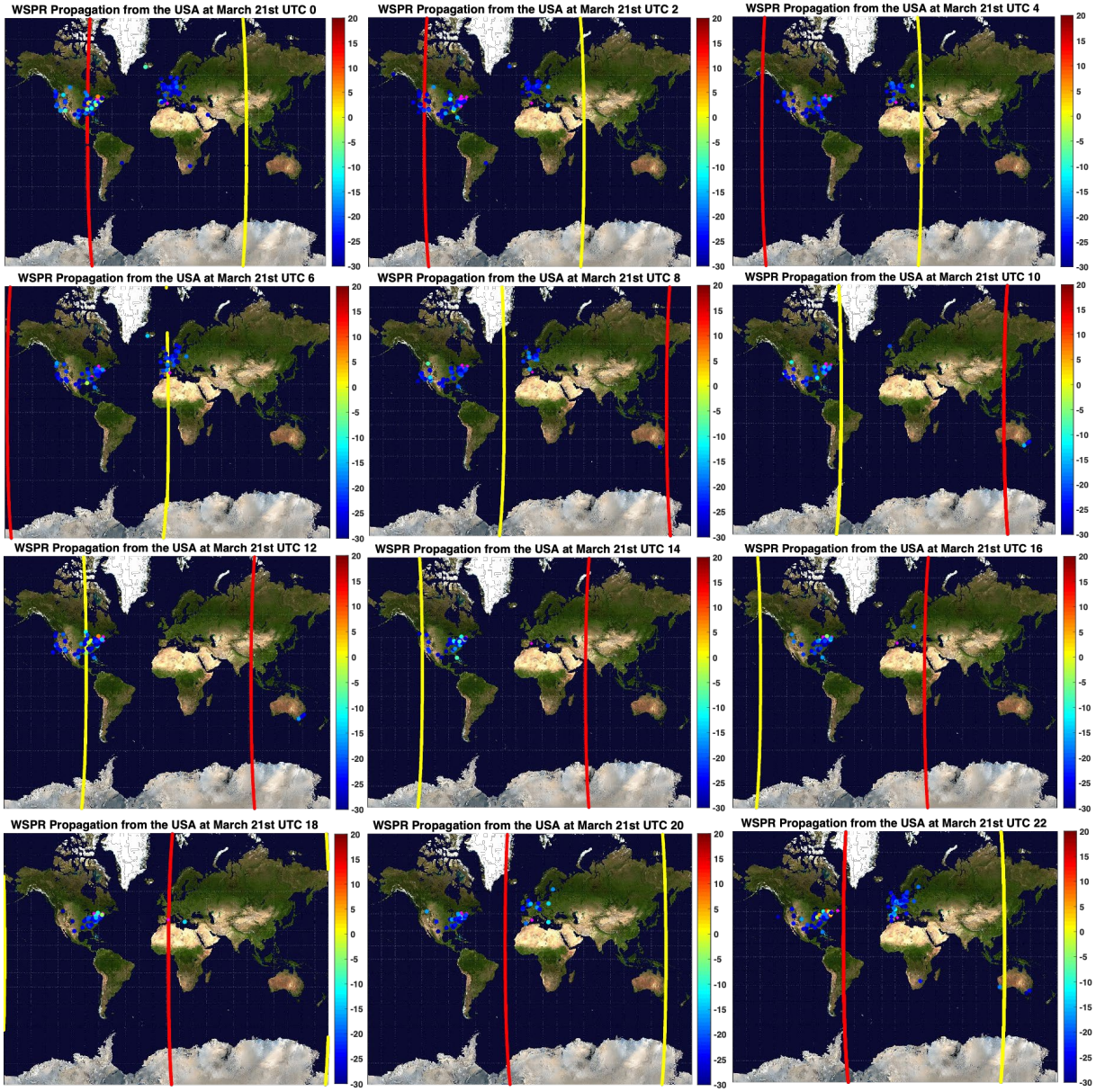

Figure B.17 – Images showing the ground reception locations of WSPR signals transmitted from the Eastern USA on March 21st 2017. The colours show the SNR in dB.

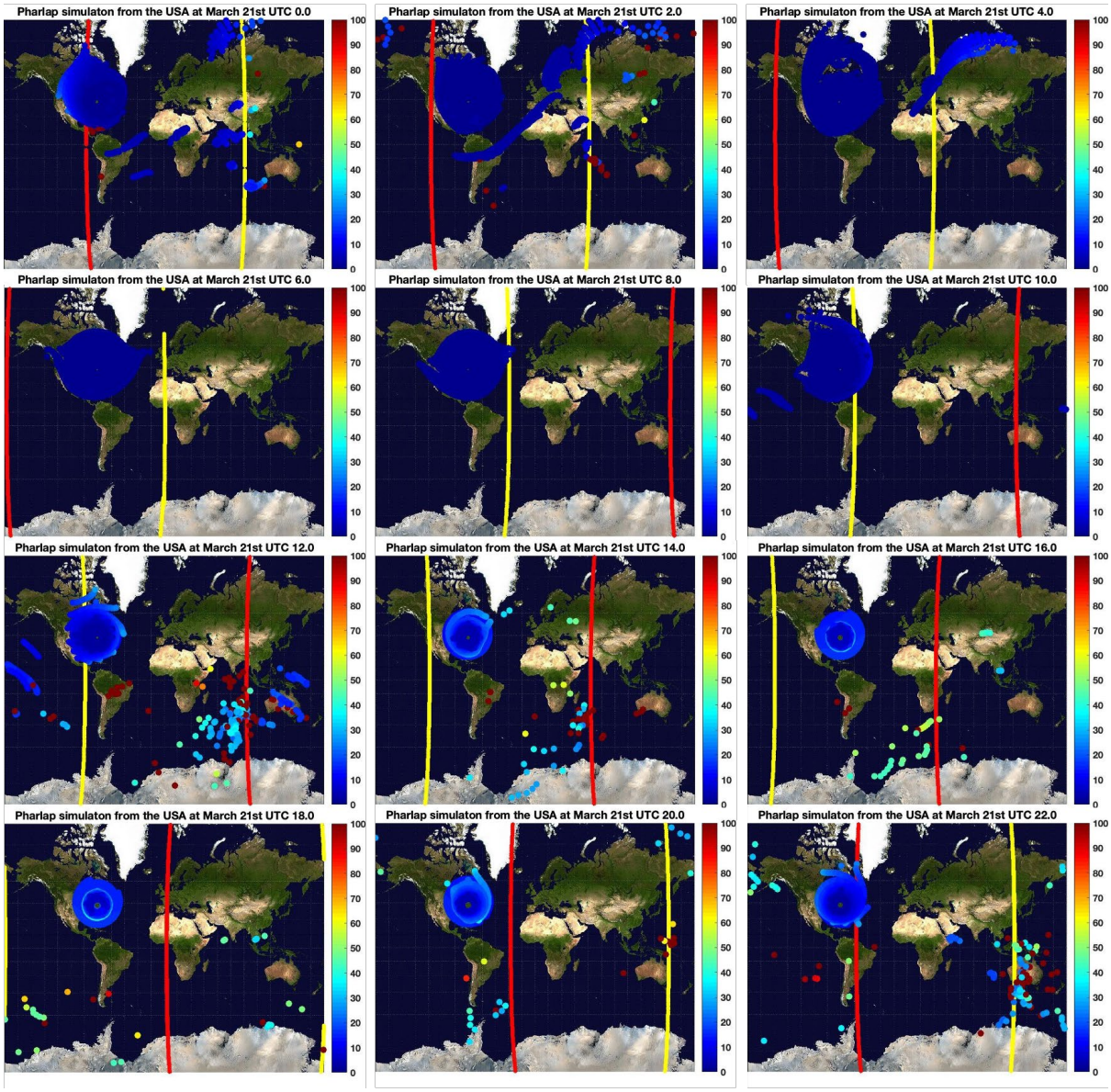

Figure B.18 – Images showing the ground reception locations simulated by PHaRLAP/IRI2016 for a transmitter in the Eastern USA for March 21st 2017. The colours show the absorption in dB.

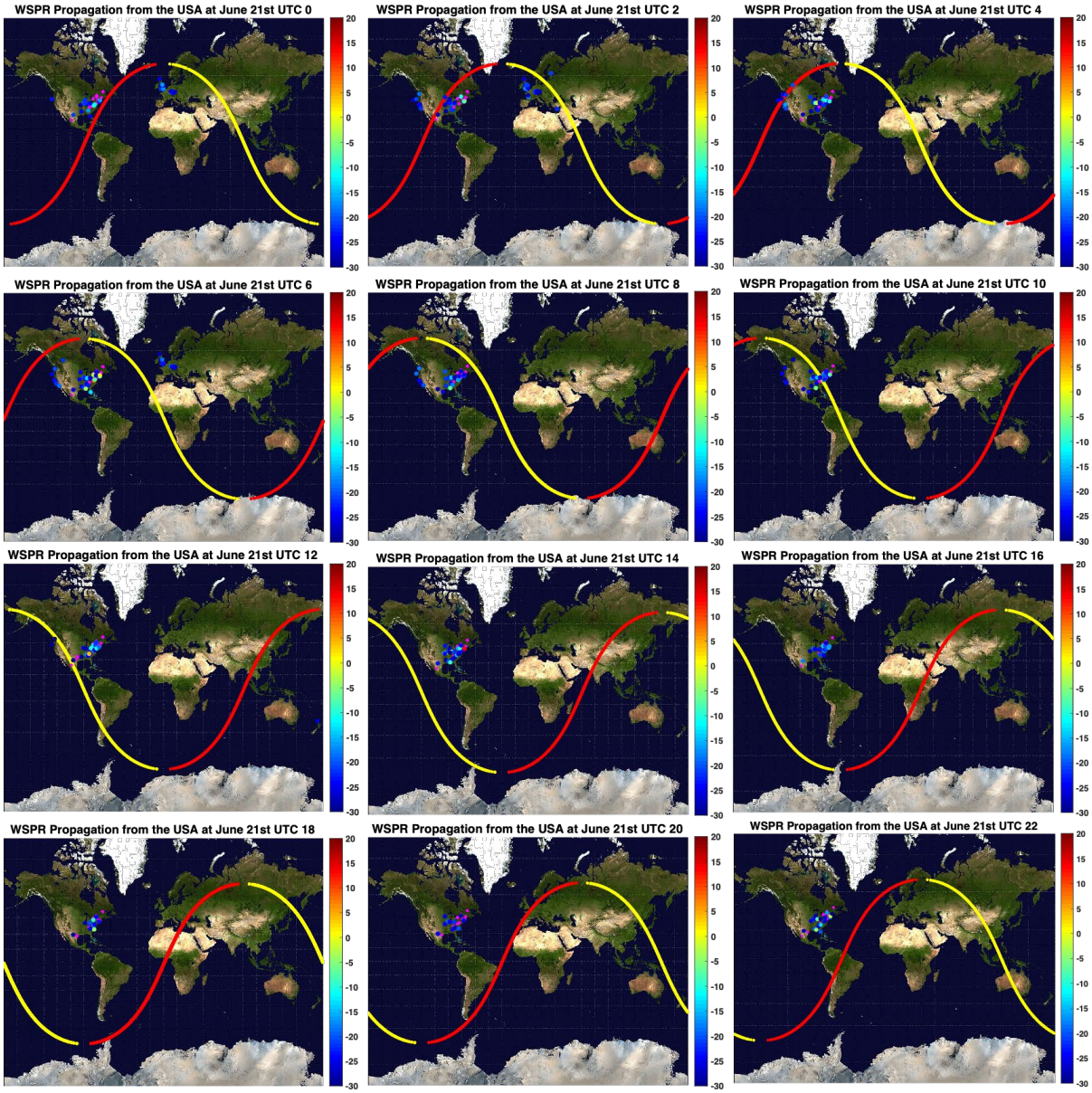

Figure B.19 – Images showing the ground reception locations of WSPR signals transmitted from the Eastern USA on June 21st 2017. The colours show the SNR in dB.

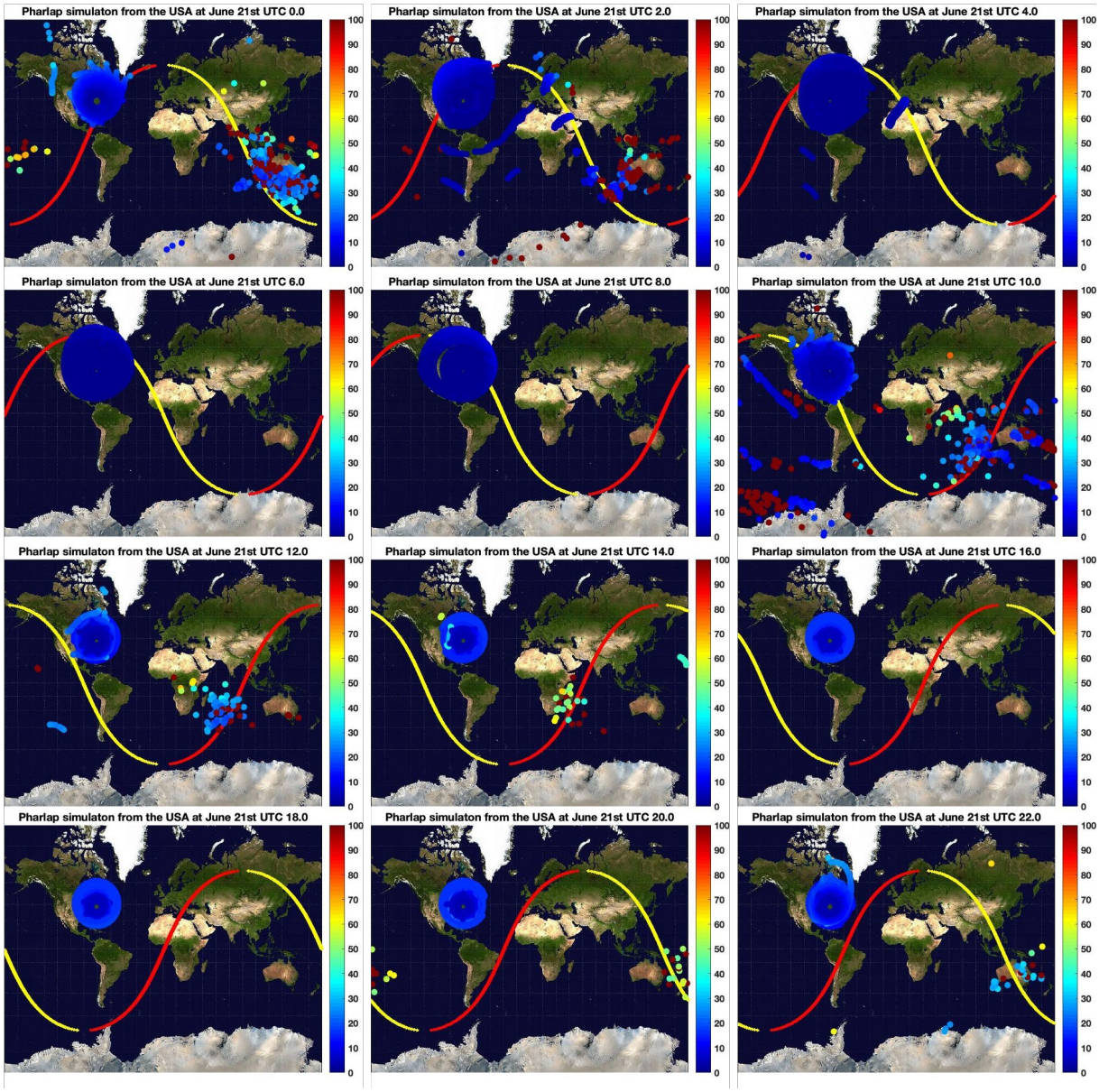

Figure B.20 – Images showing the ground reception locations simulated by PHaRLAP/IRI2016 for a transmitter in the Eastern USA for June 21st 2017. The colours show the absorption in dB.

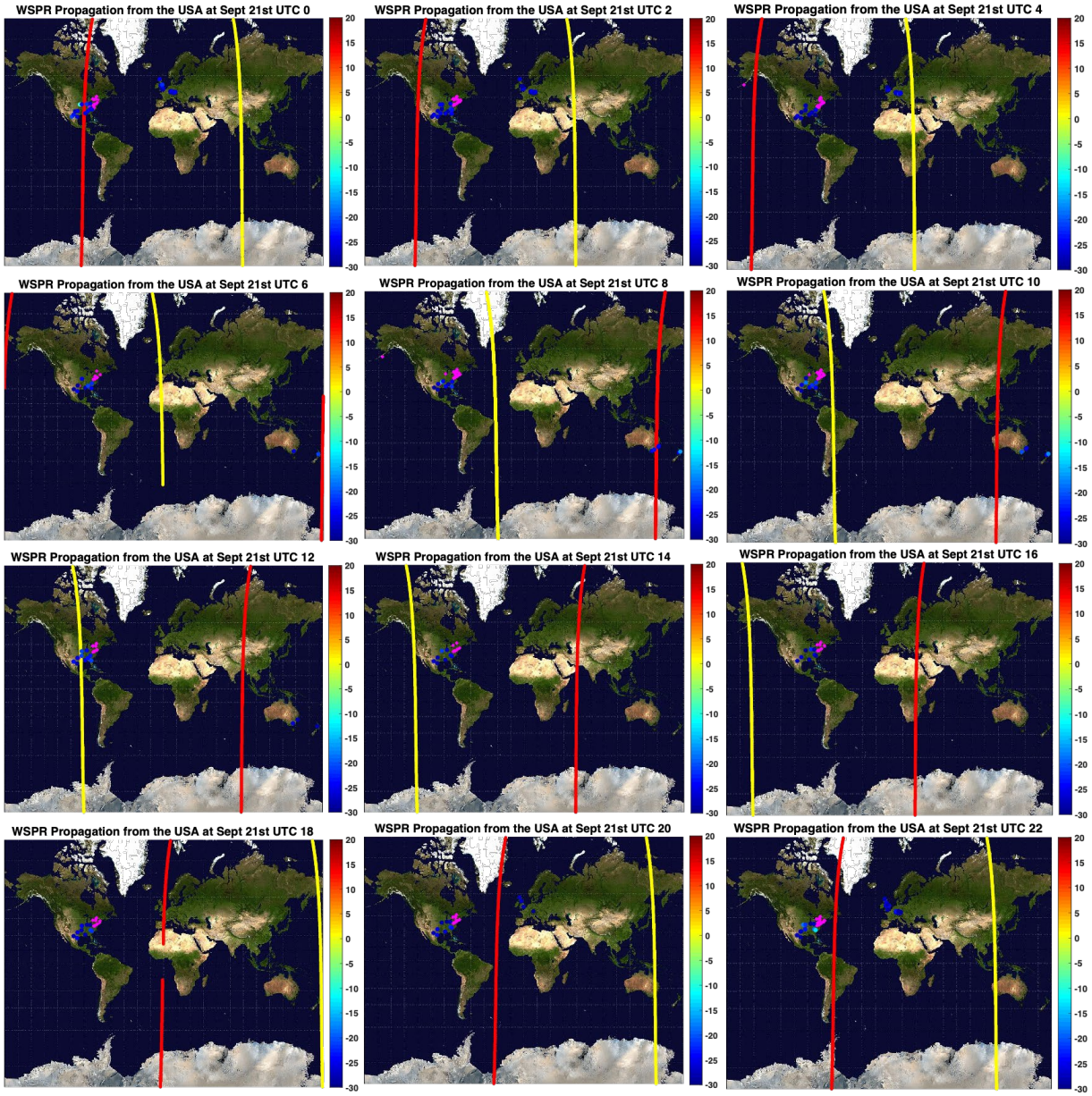

Figure B.21 – Images showing the ground reception locations of WSPR signals transmitted from the Eastern USA on September 21st 2017. The colours show the SNR in dB.

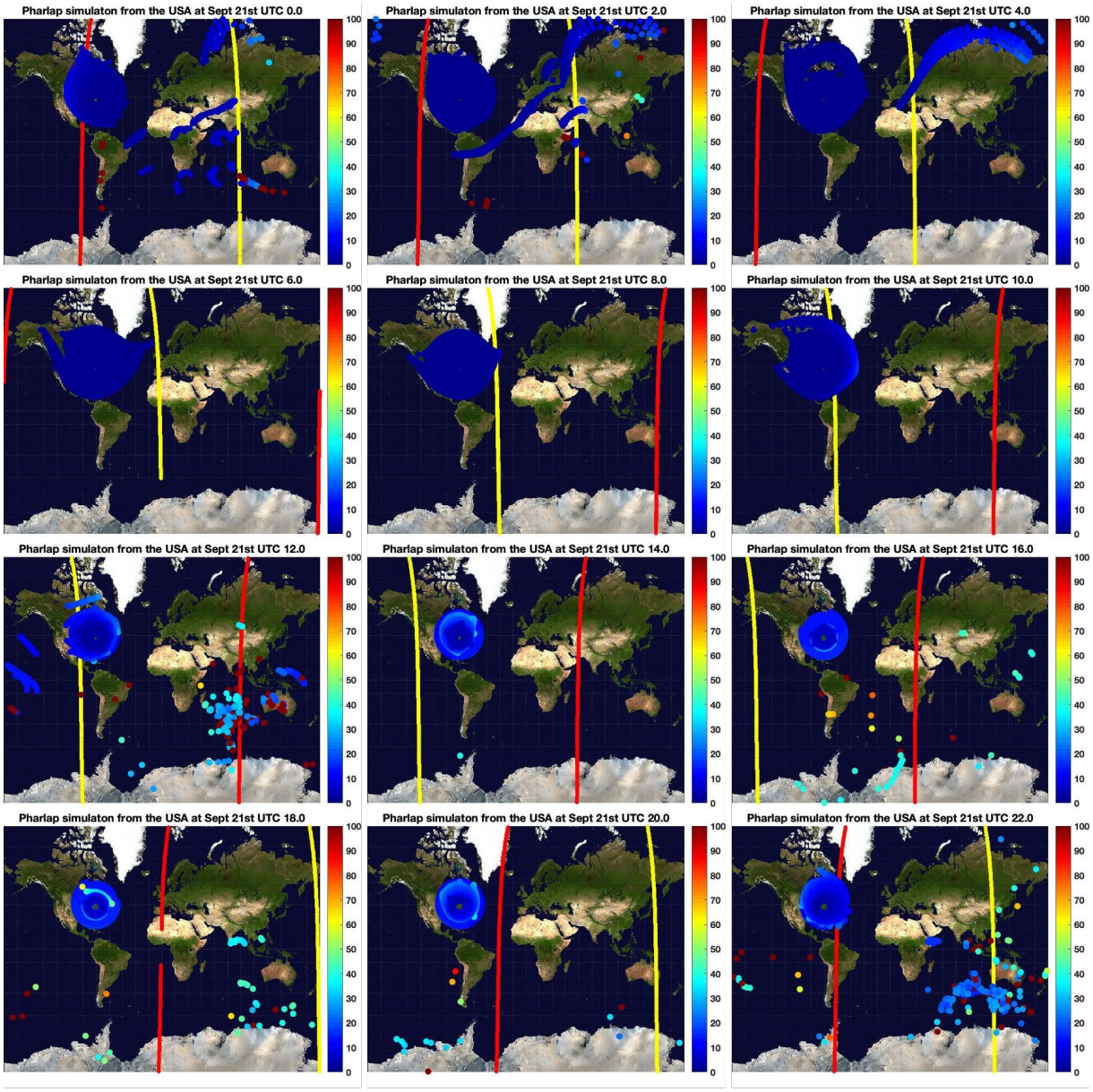

Figure B.22 – Images showing the ground reception locations simulated by PHaRLAP/IRI2016 for a transmitter in the Eastern USA for September 21st 2017. The colours show the absorption in dB.

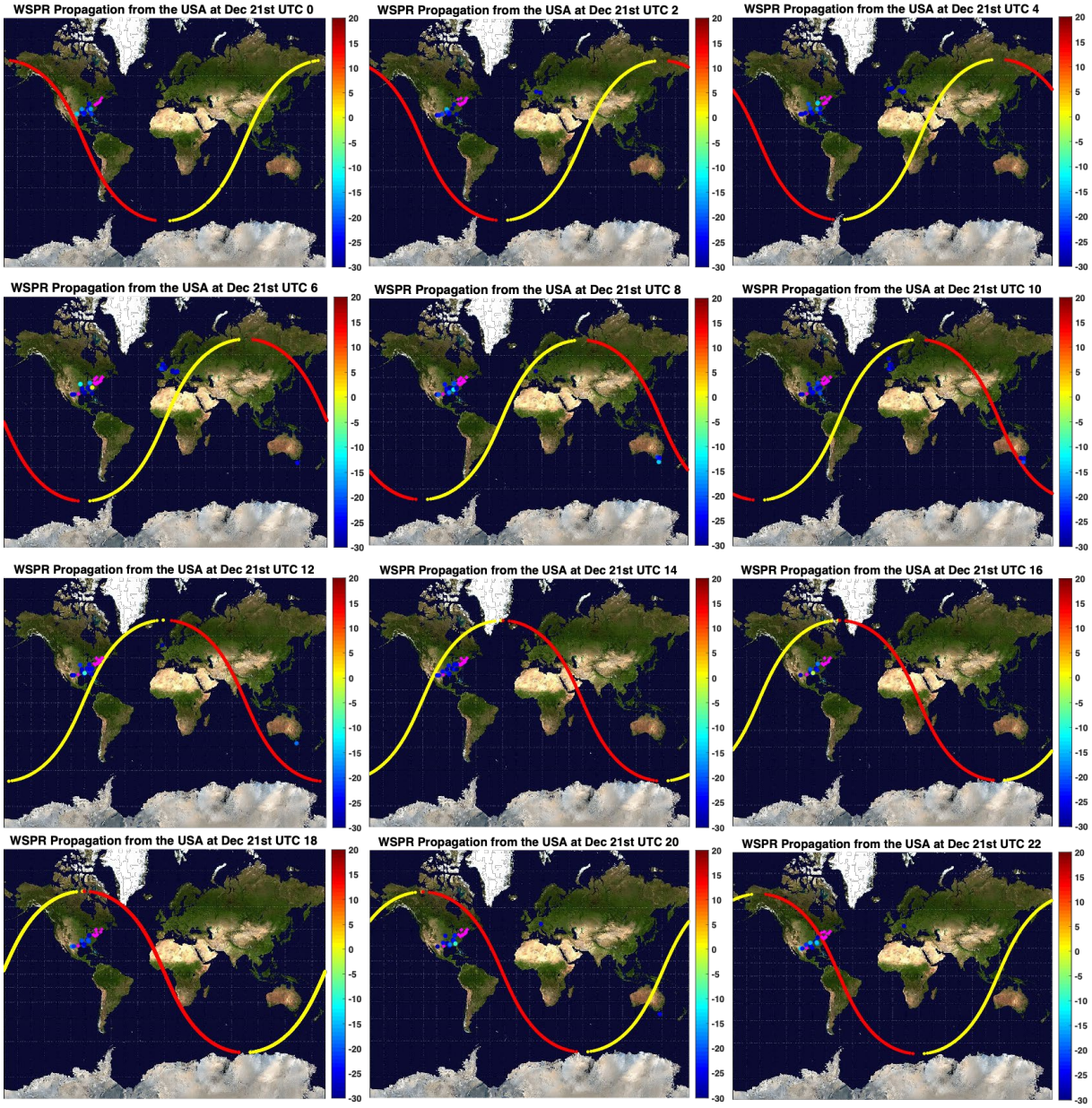

Figure B.23 – Images showing the ground reception locations of WSPR signals transmitted from the Eastern USA on December 21st 2017. The colours show the SNR in dB.

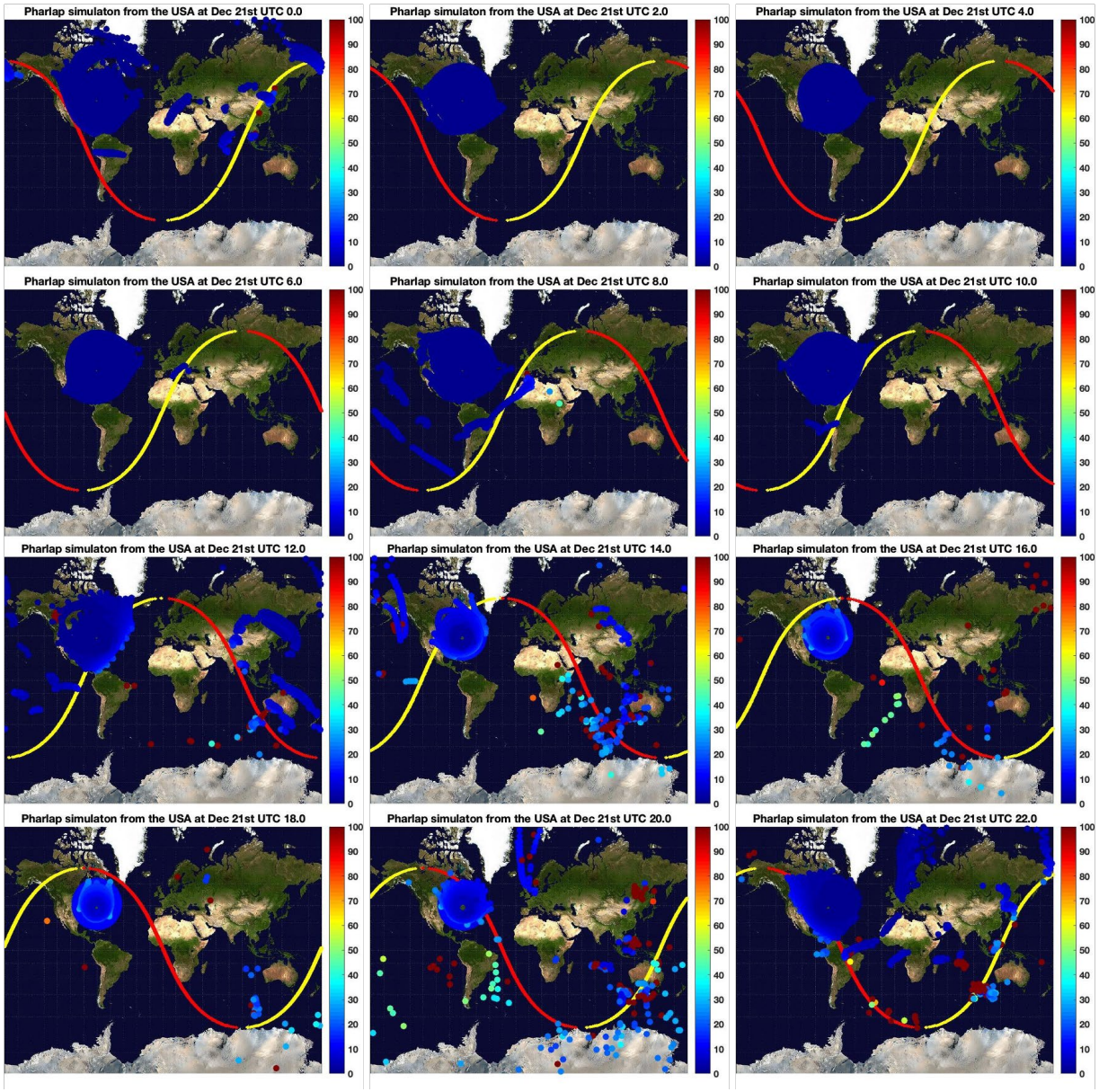

Figure B.24 – Images showing the ground reception locations simulated by PHaRLAP/IRI2016 for a transmitter in the Eastern USA for December 21st 2017. The colours show the absorption in dB.

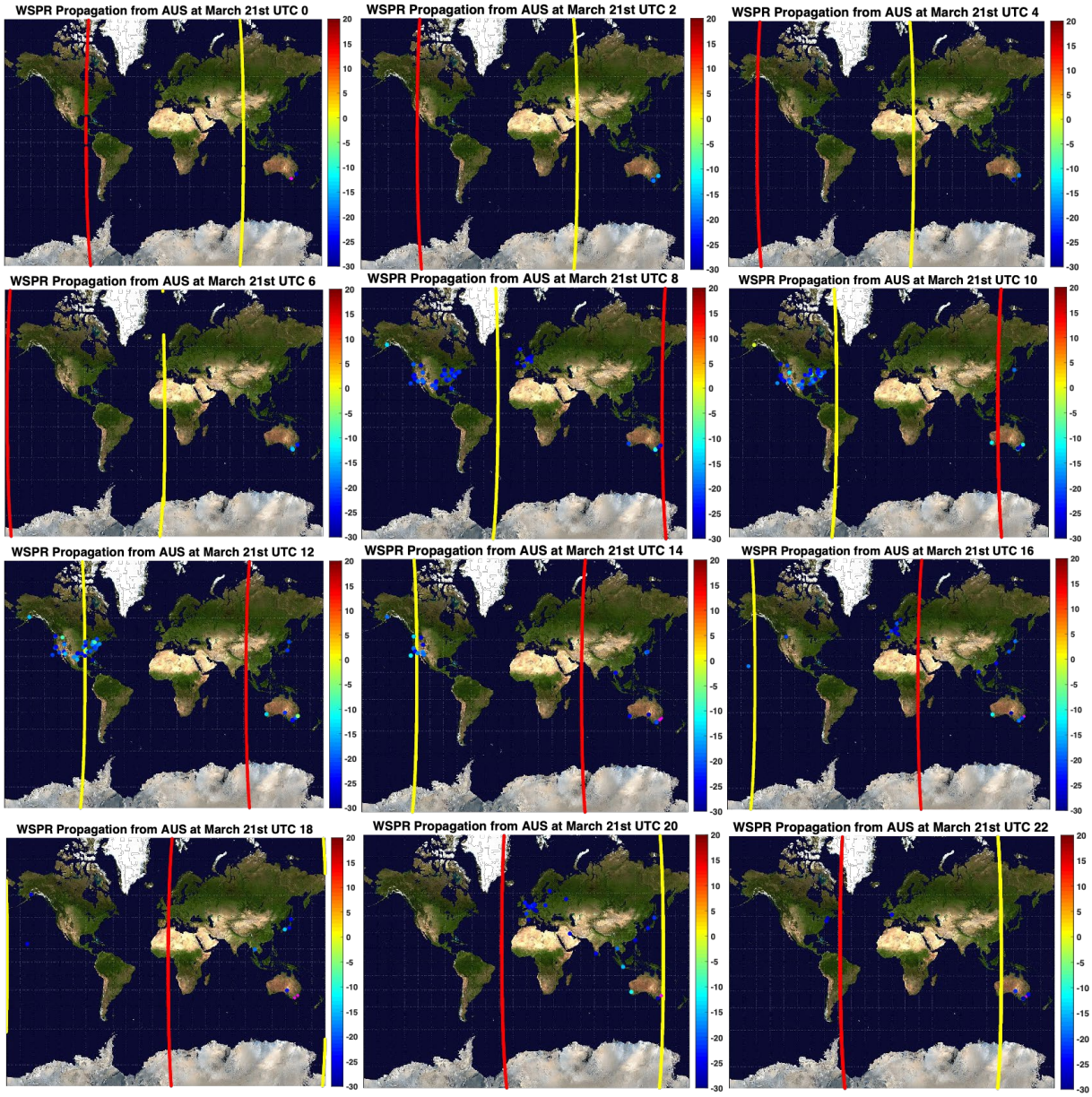

Figure B.25 – Images showing the ground reception locations of WSPR signals transmitted from Eastern Australia on March 21st 2017. The colours show the SNR in dB.

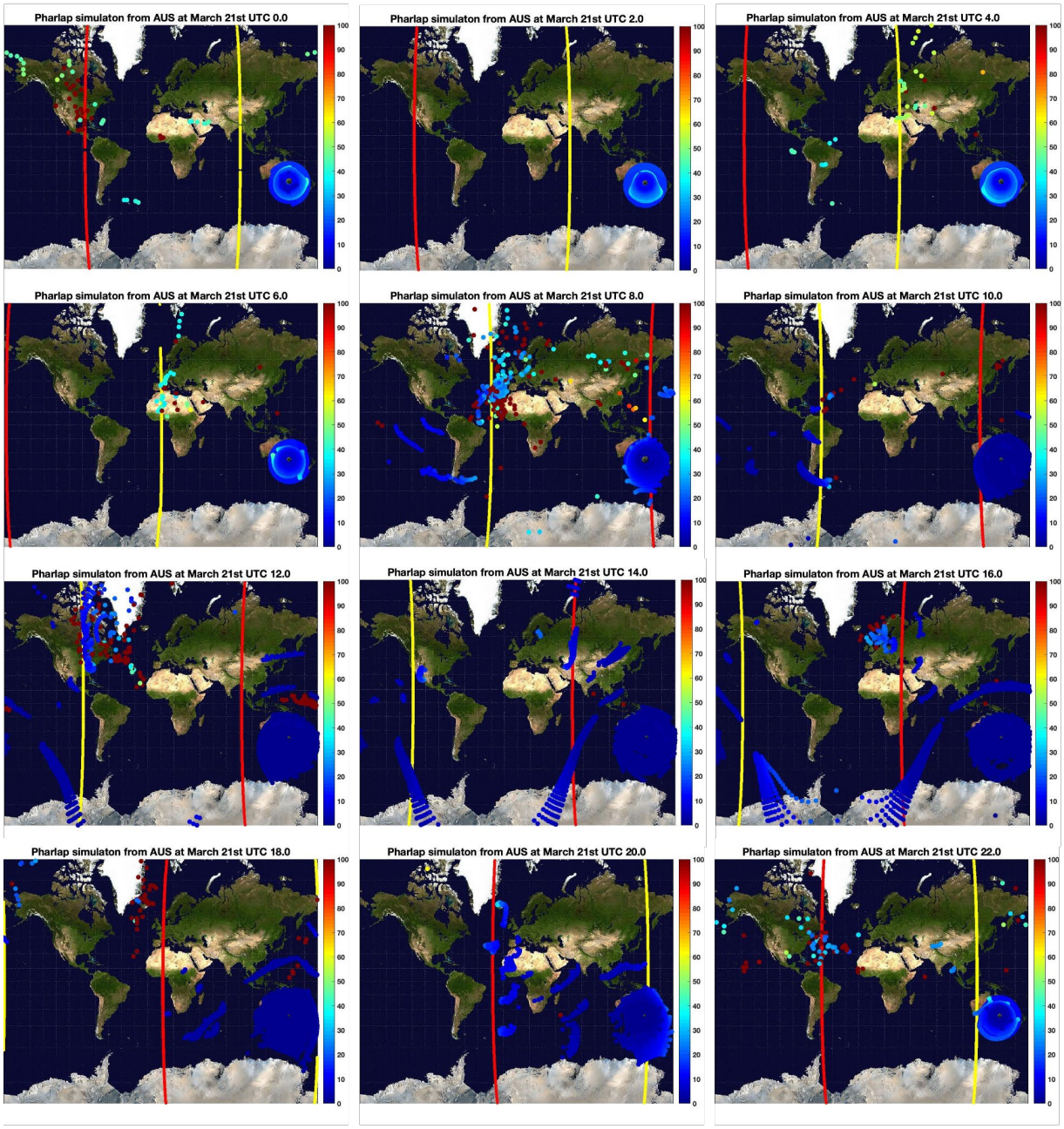

Figure B.26 – Images showing the ground reception locations simulated by PHaRLAP/IRI2016 for a transmitter in Eastern Australia for March 21st 2017. The colours show the absorption in dB.

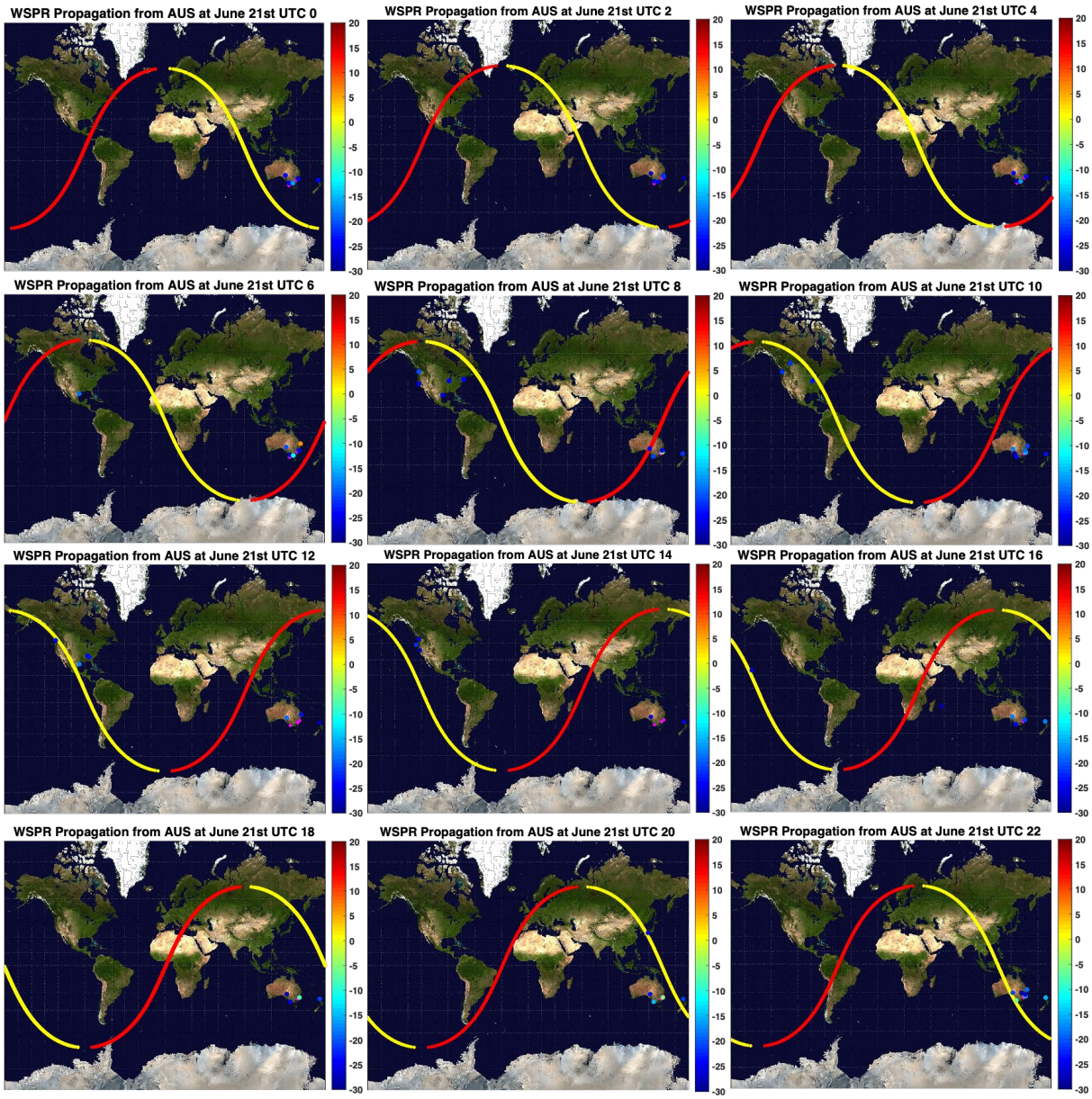

Figure B.27 – Images showing the ground reception locations of WSPR signals transmitted from Eastern Australia on June 21st 2017. The colours show the SNR in dB.

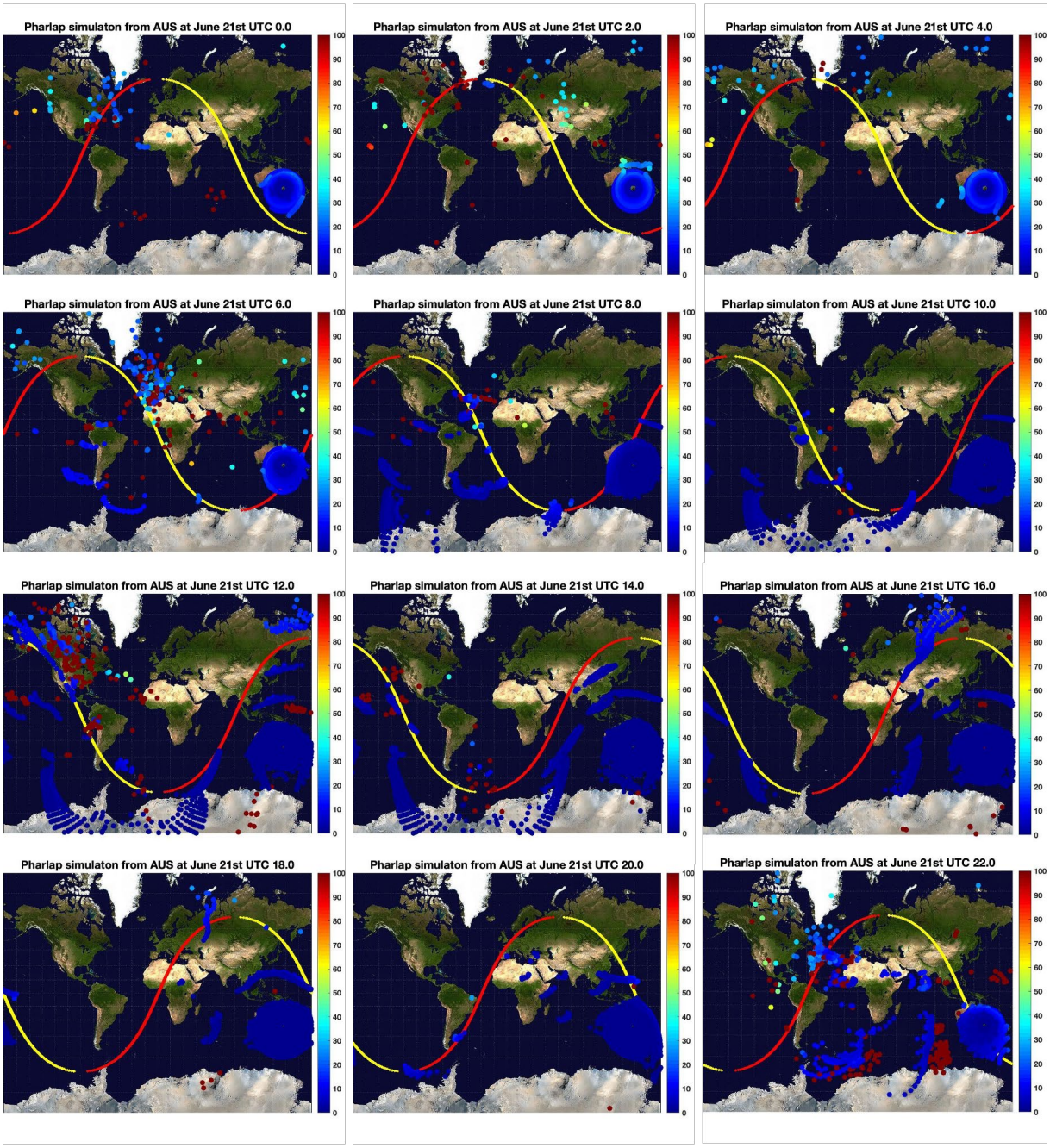

Figure B.28 – Images showing the ground reception locations simulated by PHaRLAP/IRI2016 for a transmitter in Eastern Australia for June 21st 2017. The colours show the absorption in dB.

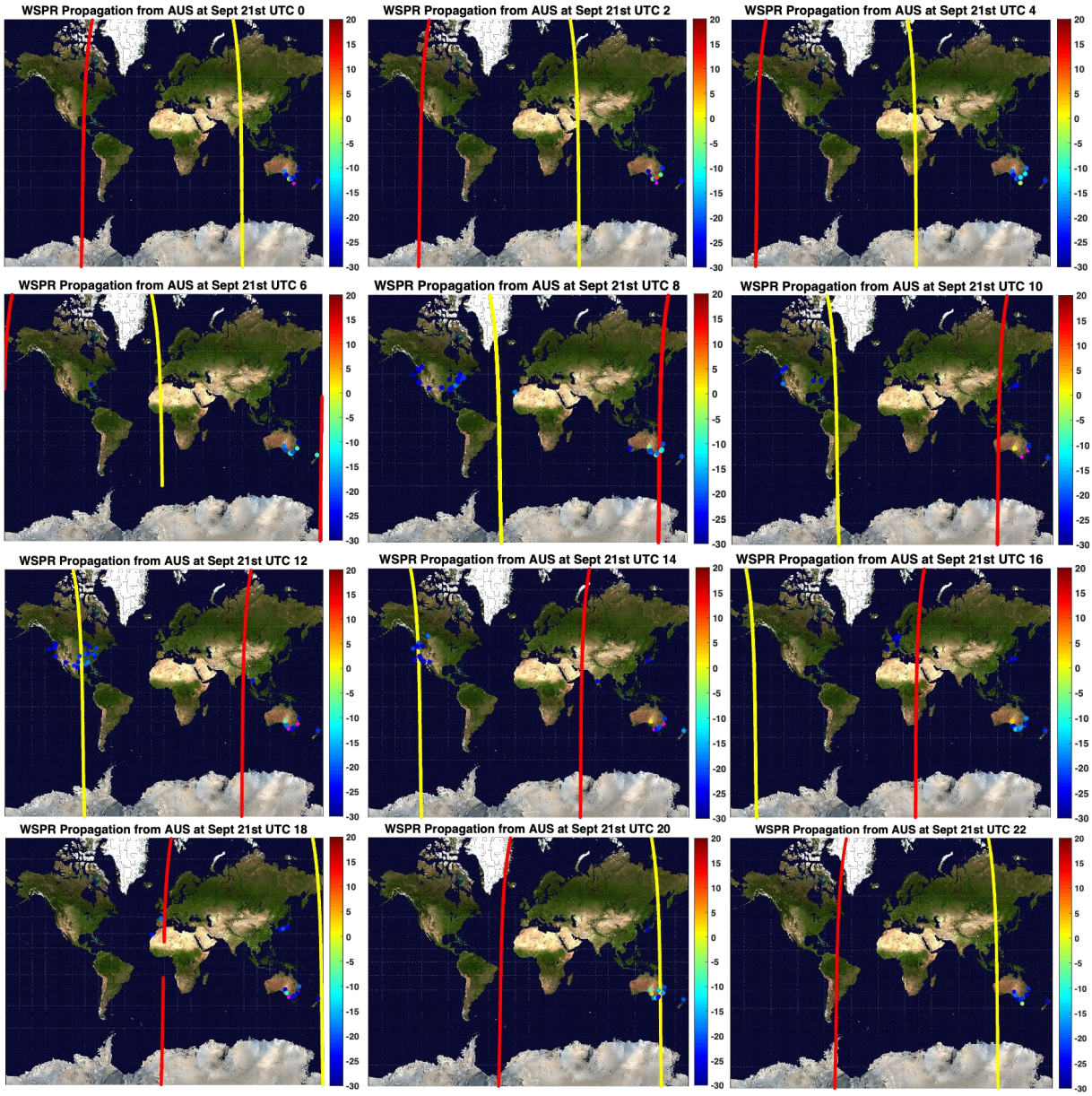

Figure B.29 – Images showing the ground reception locations of WSPR signals transmitted from Eastern Australia on September 21st 2017. The colours show the SNR in dB.

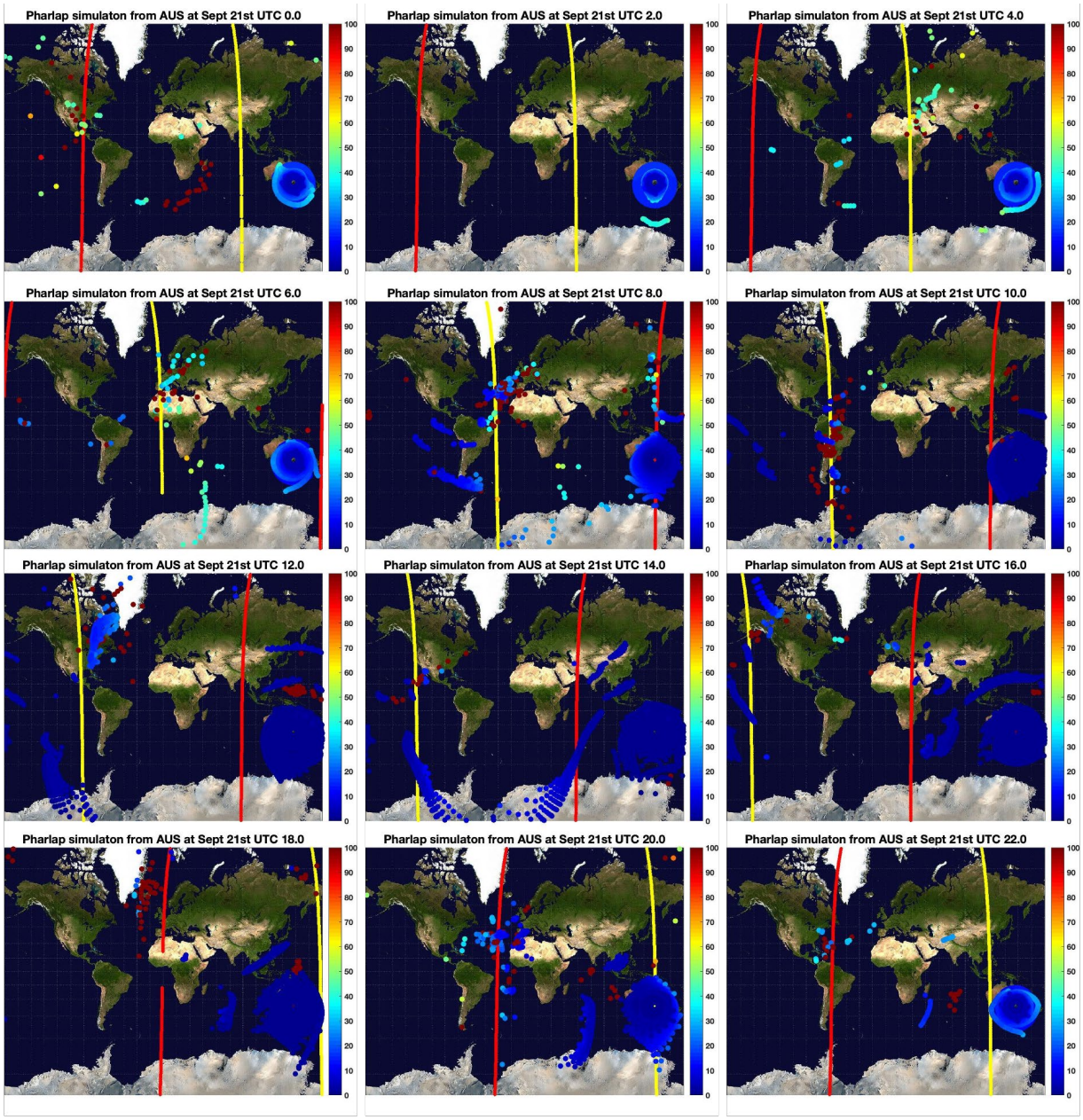

Figure B.30 – Images showing the ground reception locations simulated by PHaRLAP/IRI2016 for a transmitter in Eastern Australia for September 21st 2017. The colours show the absorption in dB.

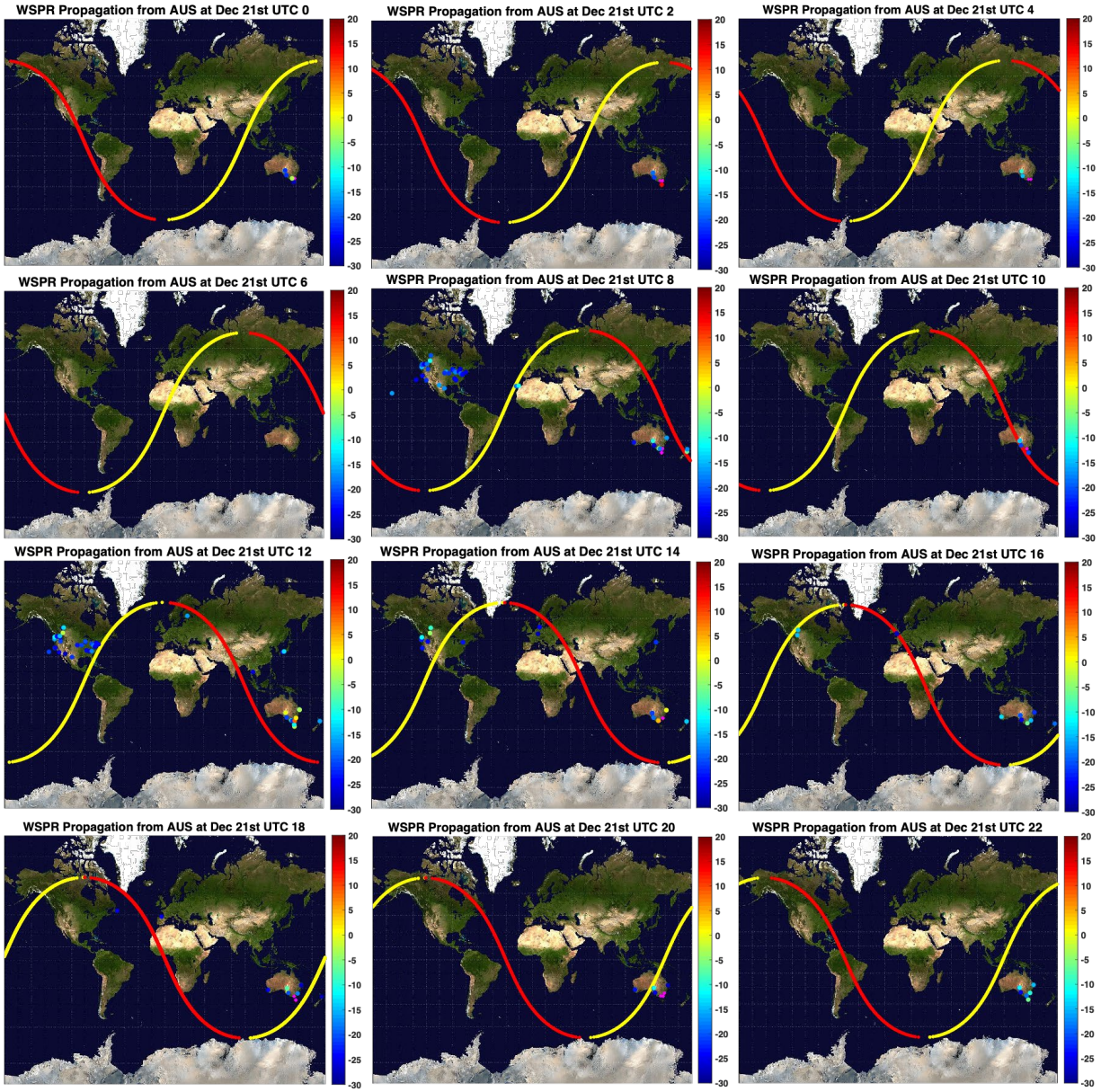

Figure B.31 – Images showing the ground reception locations of WSPR signals transmitted from Eastern Australia on December 21st 2017. The colours show the SNR in dB.

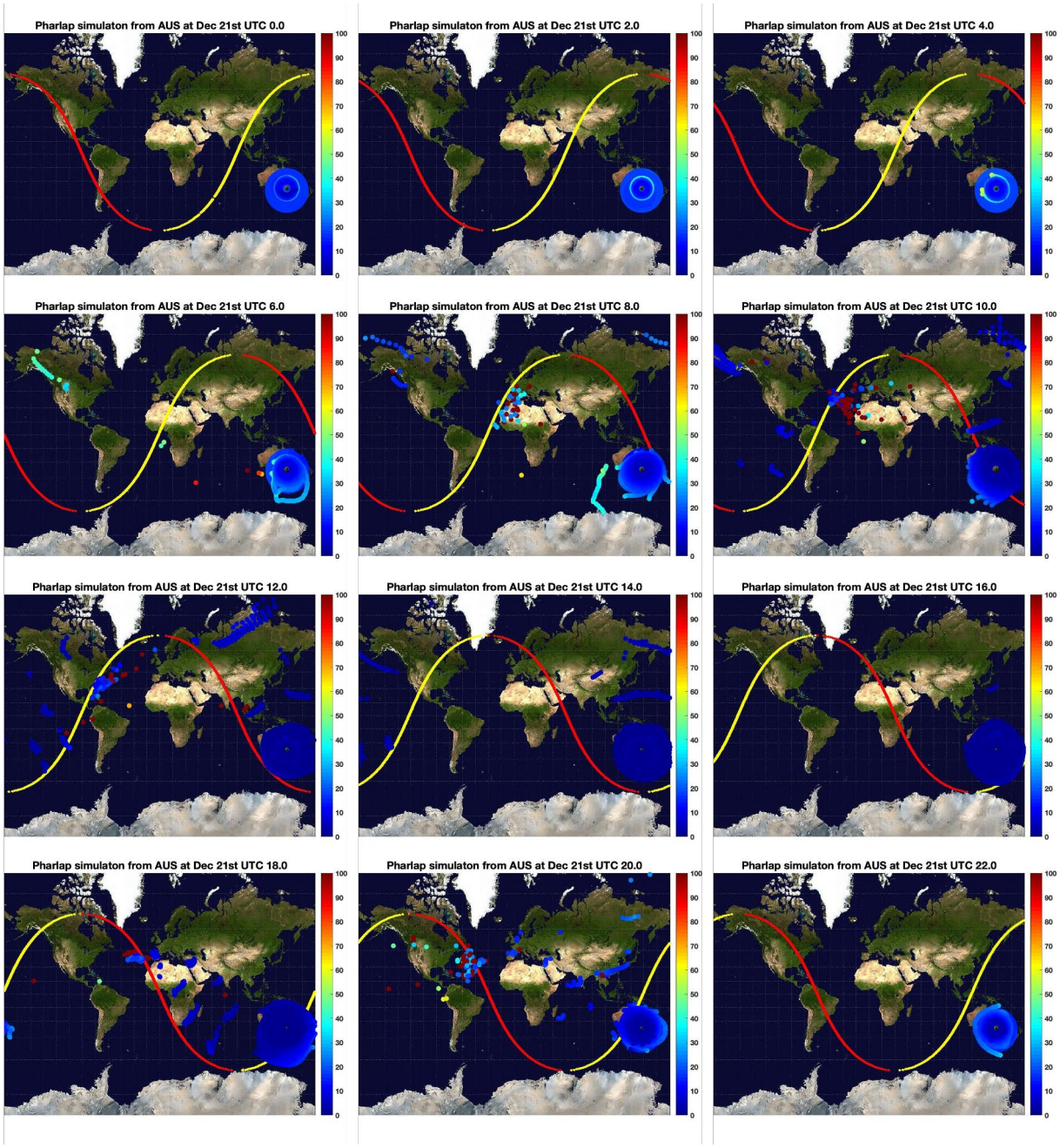

Figure B.32 – Images showing the ground reception locations simulated by PHaRLAP/IRI2016 for a transmitter in Eastern Australia for December 21st 2017. The colours show the absorption in dB.

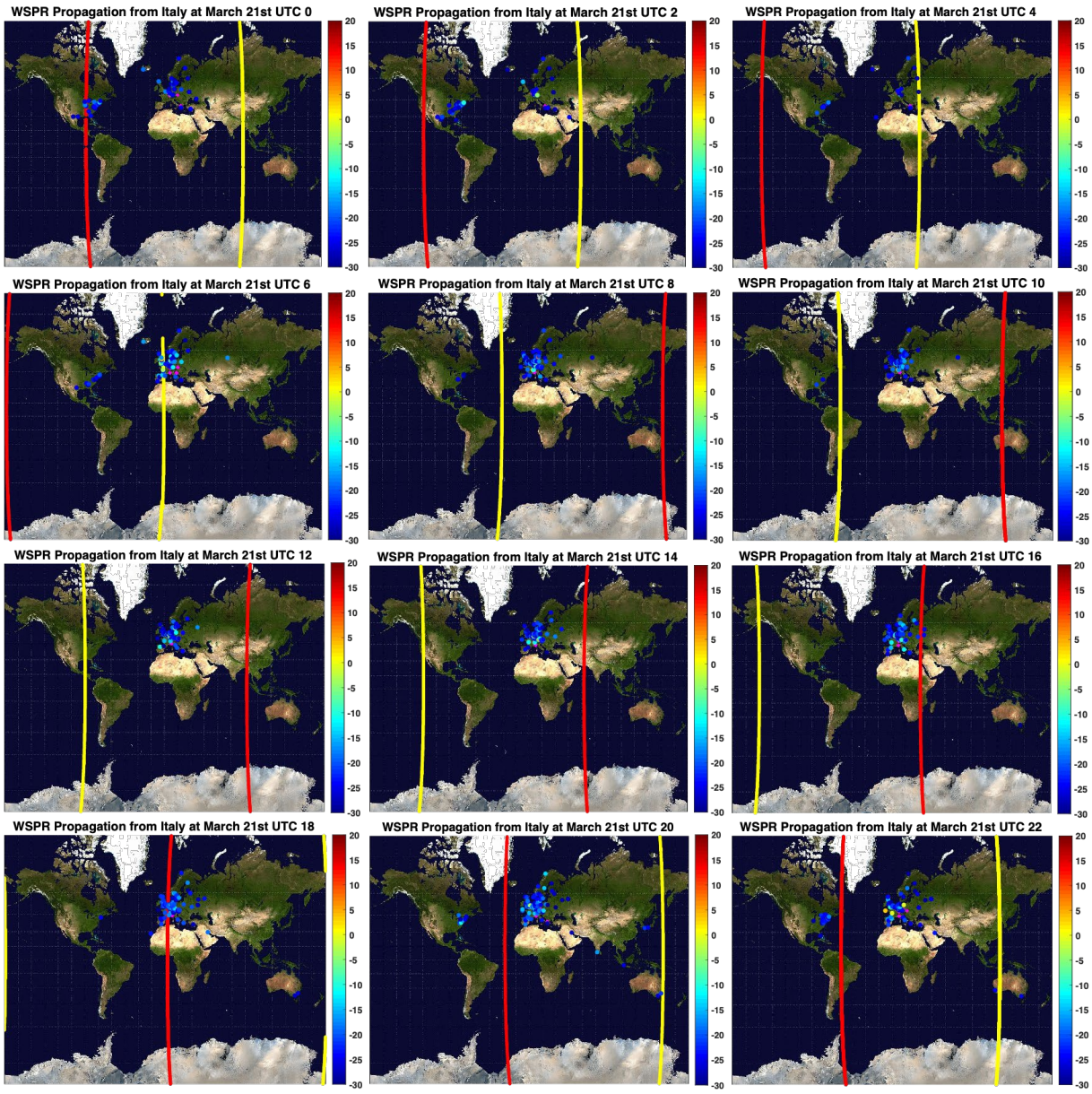

Figure B.33 – Images showing the ground reception locations of WSPR signals transmitted from Italy and the adjacent regions on March 21st 2017. The colours show the SNR in dB.

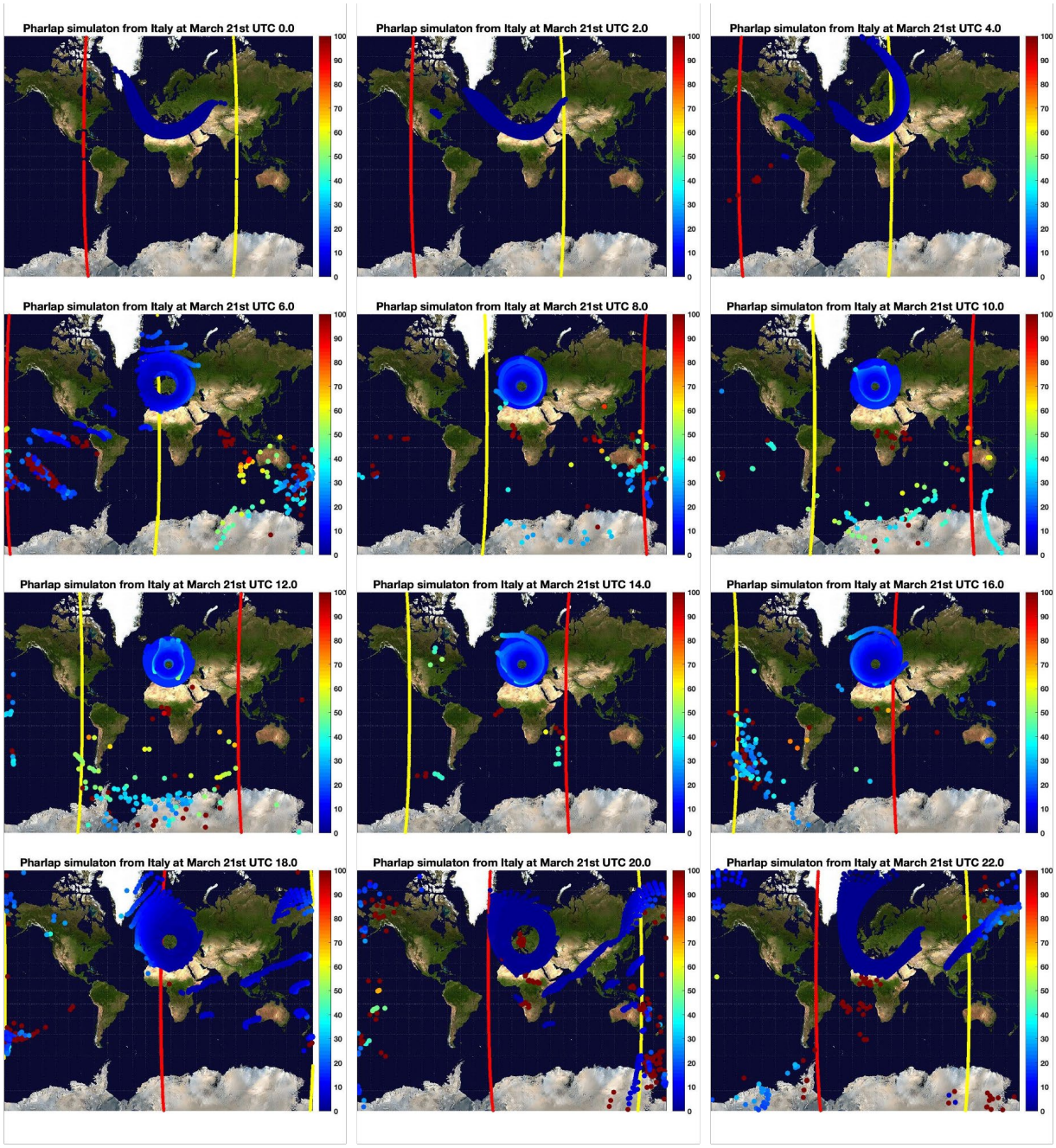

Figure B.34 – Images showing the ground reception locations simulated by PHaRLAP/IRI2016 for a transmitter in Italy and the adjacent regions for March 21st 2017. The colours show the absorption in dB.

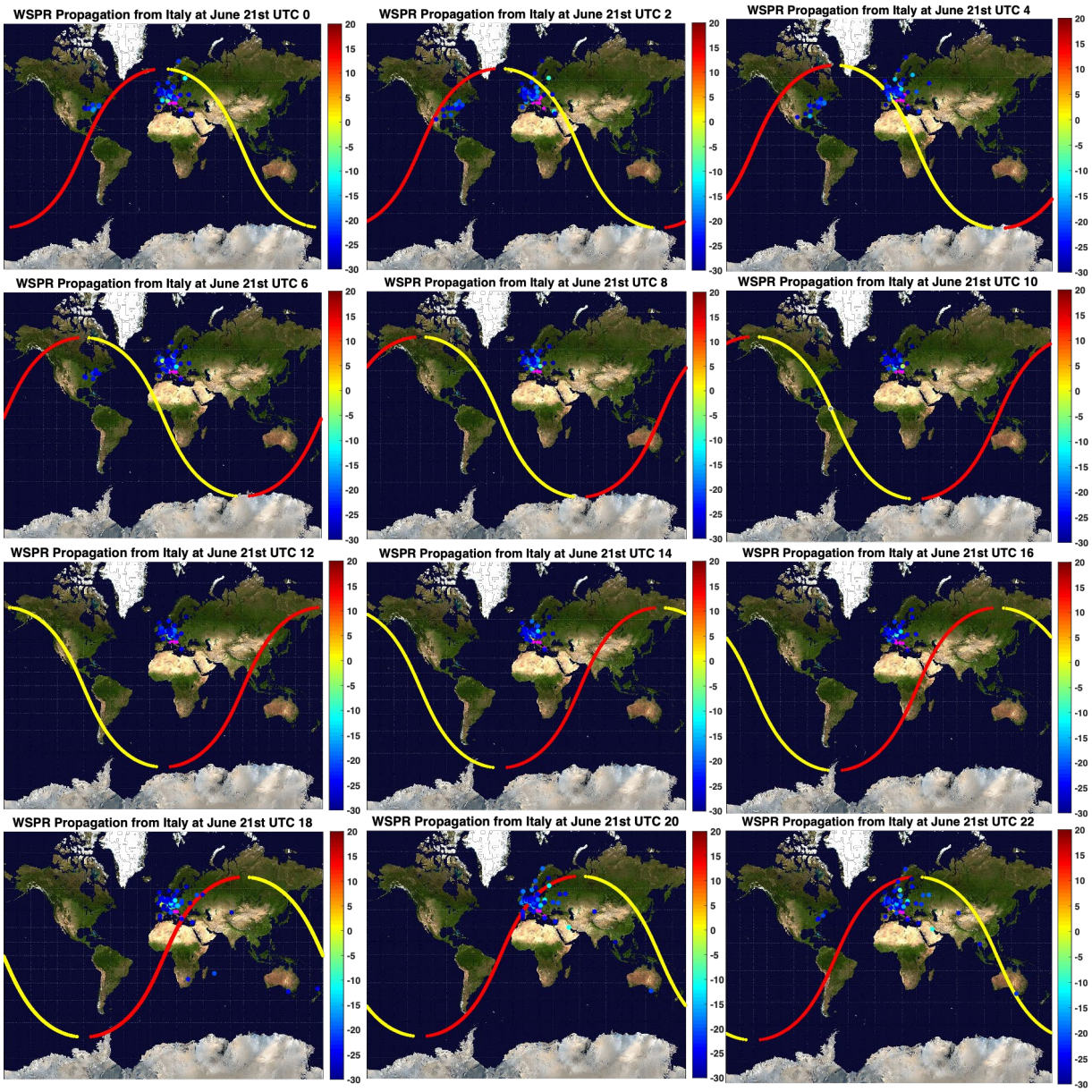

Figure B.35 – Images showing the ground reception locations of WSPR signals transmitted from Italy and the adjacent regions on June 21st 2017. The colours show the SNR in dB.

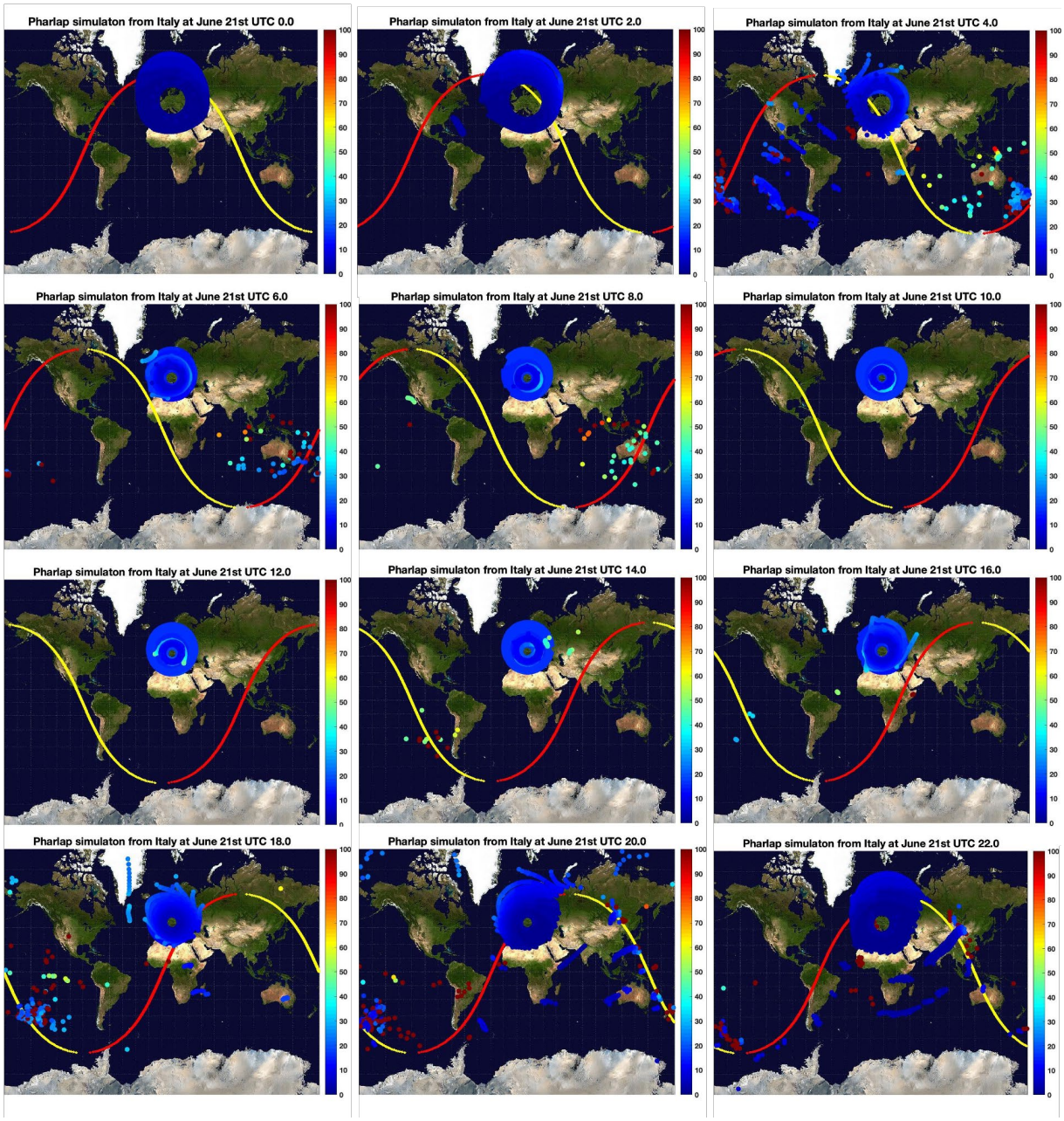

Figure B.36 – Images showing the ground reception locations simulated by PHaRLAP/IRI2016 for a transmitter in Italy and the adjacent regions for June 21st 2017. The colours show the absorption in dB.

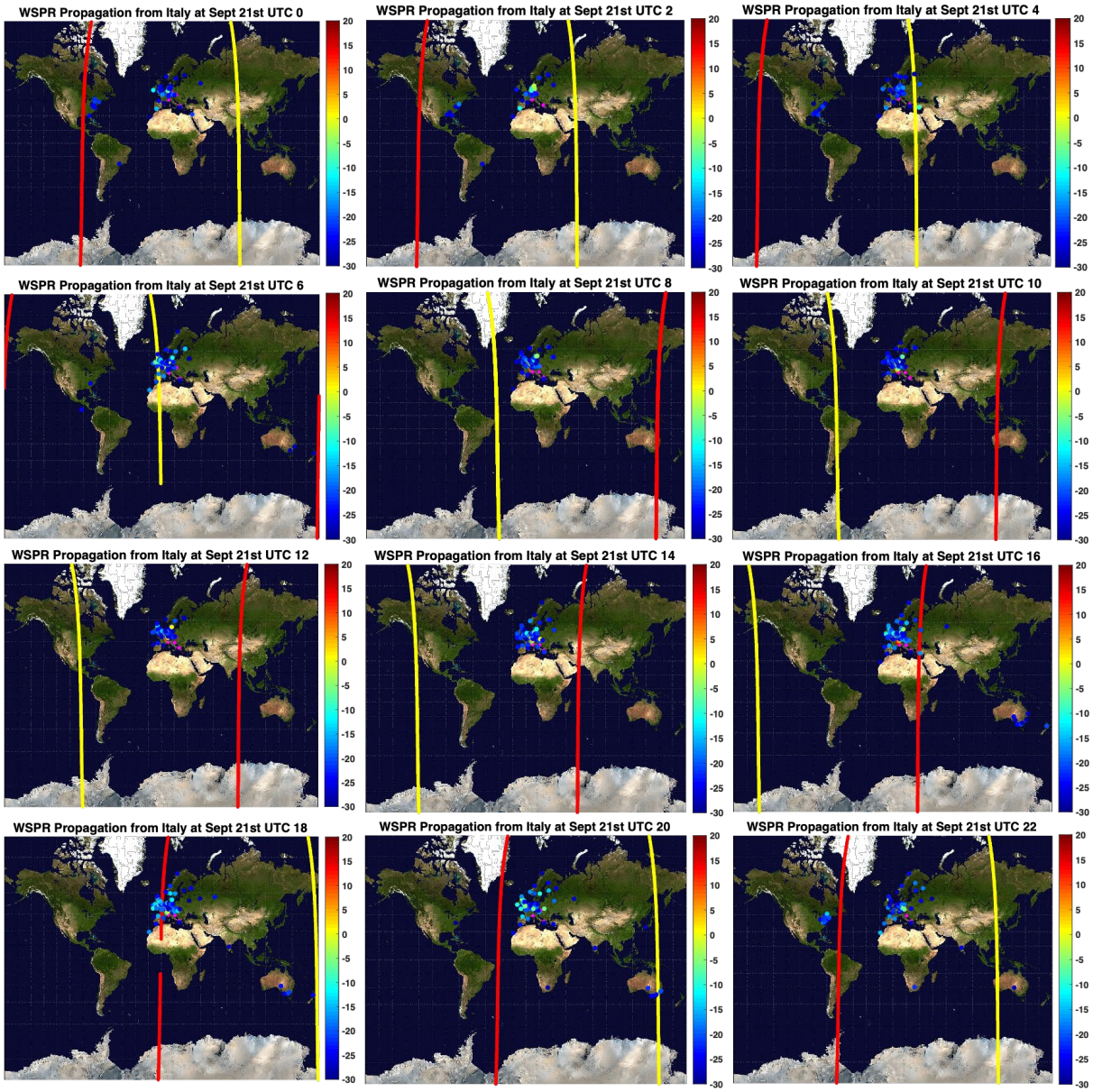

Figure B.37 – Images showing the ground reception locations of WSPR signals transmitted from Italy and the adjacent regions on September 21st 2017. The colours show the SNR in dB.

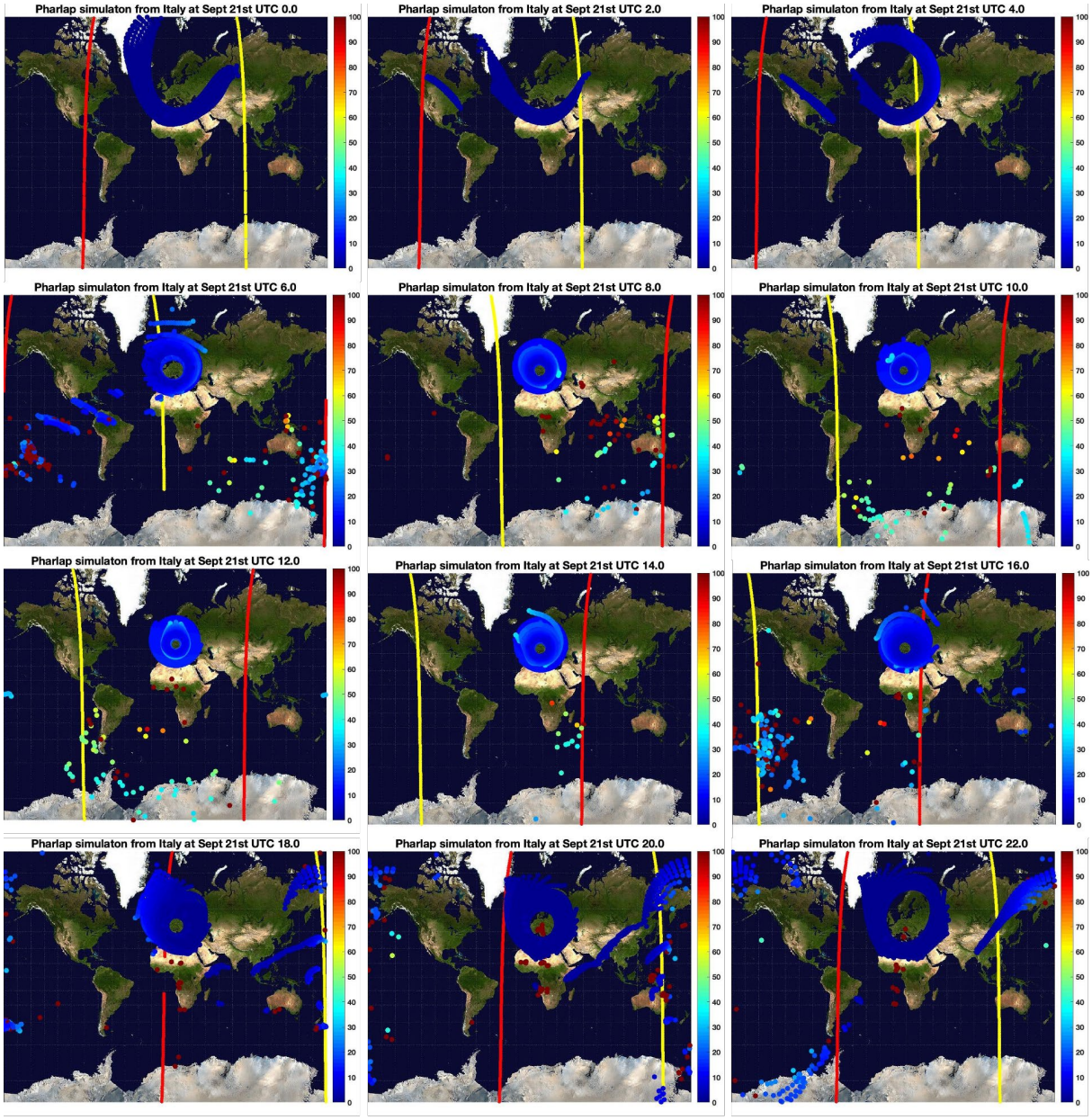

Figure B.38 – Images showing the ground reception locations simulated by PHaRLAP/IRI2016 for a transmitter in Italy and the adjacent regions for September 21st 2017. The colours show the absorption in dB.

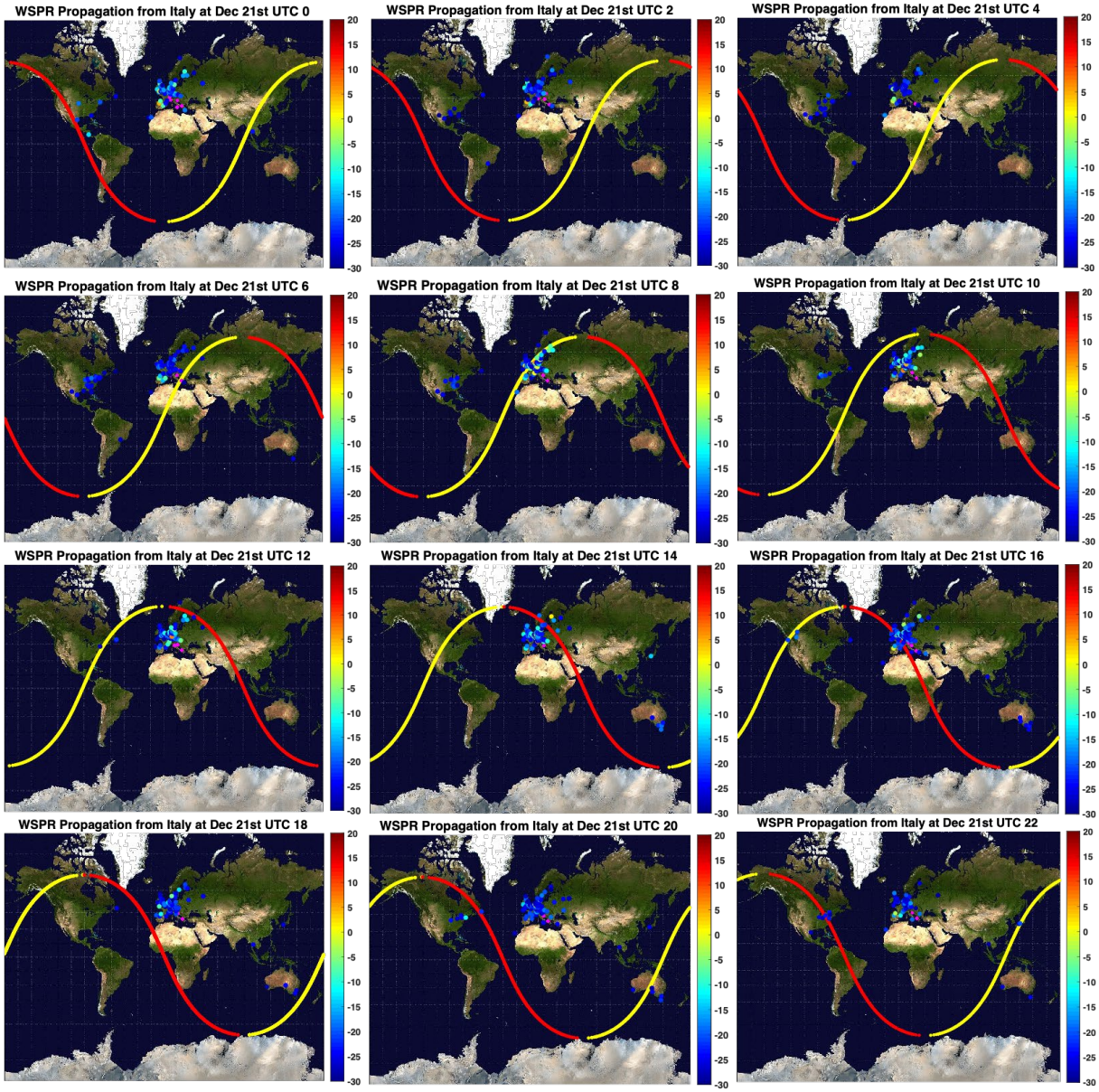

Figure B.39 – Images showing the ground reception locations of WSPR signals transmitted from Italy and the adjacent regions on December 21st 2017. The colours show the SNR in dB.

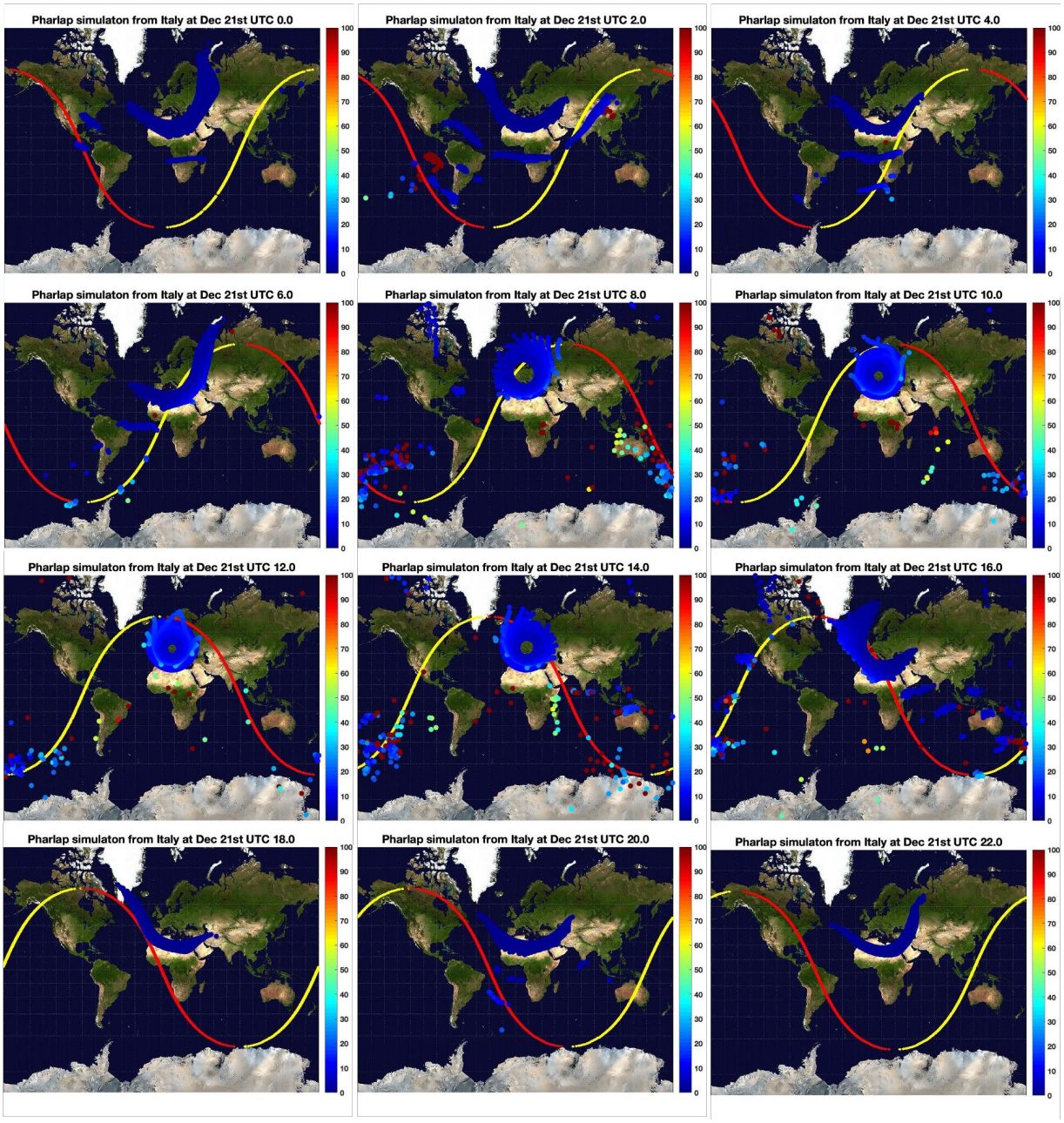

Figure B.40 – Images showing the ground reception locations simulated by PHaRLAP/IRI2016 for a transmitter in Italy and the adjacent regions for December 21st 2017. The colours show the absorption in dB.